USE OF PULTRUDED CARBON FIBER / EPOXY INSERTS AS REINFORCEMENT IN COMPOSITE STRUCTURES

by

Bryan Charles Bundy

A thesis submitted in partial fulfillment
of the requirements for the degree

of

Master of Science

in

Mechanical Engineering

MONTANA STATE UNIVERSITY
Bozeman, Montana

December 2005

APPROVAL

of a thesis submitted by

Bryan Charles Bundy

This thesis has been read by each member of the thesis committee and has been found to be satisfactory regarding content, English usage, format, citations, bibliographic style, and consistency, and is ready for submission to the College of Graduate Studies.

Dr. Douglas Cairns

Approved for the Department of Mechanical Engineering

Dr. Christopher Jenkins

Approved for the College of Graduate Studies

Dr. Joseph J. Fedock

STATEMENT OF PERMISSION TO USE

In presenting this thesis (paper) in partial fulfillment of the requirements for a master's degree at Montana State University, I agree that the Library shall make it available to borrowers under the rules of the Library.

If I have indicated my intention to copyright this thesis (paper) by including a copyright notice page, copying is allowable only for scholarly purposes, consistent with "fair use" as prescribed in the U.S. Copyright Law. Requests for permission for extended quotation from or reproduction of this thesis (paper) in whole or in parts may be granted only by the copyright holder.

Bryan Charles Bundy

December 2005

ACKNOWLEDGEMENTS

I dedicate this thesis to my family: my wife Becky, who has been extremely patient with me as I pursue my education, and my children Kaelyn and Logan, who cannot wait to have their daddy finish school so he can help them grow up right.

I gratefully acknowledge help with this study from my advisor Dr. Douglas Cairns, and my committee members, Dr. John Mandell, and Dr. Ted Lang. This study could not have been completed without the patience, assistance and technical expertise of Dan Samborsky and the other graduate students in the MSU Composites Group.

TABLE OF CONTENTS

TABLE OF CONTENTS - CONTINUED

LIST OF TABLES

Table Page

LIST OF FIGURES

Figure Page

LIST OF FIGURES - CONTINUED

Figure Page

LIST OF FIGURES - CONTINUED

Figure Page

LIST OF FIGURES – CONTINUED

Figure Page

LIST OF FIGURES – CONTINUED

Figure Page

LIST OF FIGURES – CONTINUED

Figure Page

LIST OF FIGURES – CONTINUED

Figure Page

LIST OF FIGURES – CONTINUED

Figure Page

LIST OF FIGURES – CONTINUED

Figure Page

ABSTRACT

As polymer matrix composite based structures such as wind turbine blades get larger in span, the required stiffness is usually supplied by the increasing thickness. The fabrication of current composite thicknesses is expensive in terms of labor, mechanical components and fabrication time. The problems are compounded for very long spans. Thermosetting resins are injected into these fiber pre-forms under very high pressures so the resin can completely encase the fibers before the resin hardens. These pressures can induce waviness into the fibers that significantly reduces the critical compression properties of these large composites.

Pultruded composites are a possible solution to boost the compression properties and enable thinner, more optimized blade designs. The nature of the pultrusion process creates a highly aligned and evenly spaced fiber microstructure that is difficult to move under resin infusion pressures. The issue of efficient load transfer between the pultrusion surface and a secondary resin used to bind the pultrusion in a larger composite structure is the primary focus of this study. The pultrusion surfaces were modified by abrasion, erosion, and wet chemical oxidation techniques.

The interfaces of the rods after treatment were tested in two methods. First, the pullout test consisting of pulling a pultruded rod out of block of epoxy was tried. Second, a pushout test consisting of pushing out a center rod in a representative volume element of a pultruded rod based structure was used. The effectiveness measure of the surface treatments was interface shear strength

The results of the interface tests indicate that erosion surface treatments enable the largest increases in interface shear strength. Chemical surface oxidation had the lowest shear strengths, less than the untreated rod coupons.

Pultruded carbon fiber composites have potential as supplemental reinforcement in larger composite structures. Erosion surface treatments are concluded to be the best at short term interface shear strength boosting, however the untreated rod performed adequately with having surface damage inflicted. Chemical oxidation has the promise of enabling long term interface strength and stablility through carbon fiber energization.

INTRODUCTION

Electricity generating wind farms must generate power at a similar cost to traditional plants to be a competitive alternative for electric power. To increase power output from current wind turbines, the blades that spin the turbine must be longer. However, further development with fiberglass composites is nearing its practical limits and more dramatic changes may be inevitable [1]. Fortunately, more advanced reinforcement materials are working their way into these structures to revitalize and extend their engineering limits. Selective replacement of glass fibers with carbon fibers is enabling more complex hybrid structures that can meet the structural demands in a variety of applications without requiring a massive budget; an example of such an application is explored below.

Case Study: Wind Turbine Blades

Increasing Blade Length Requirements for Power Output

The cost of wind generated electrical power has achieved near-parity with that of energy derived from fossil fuels [1]. The ongoing evolution of the wind power industry is due in large part to successful polymer matrix composite (PMC) development. An example of a typical electric power generating wind turbine is shown below in Figure 1 [2].

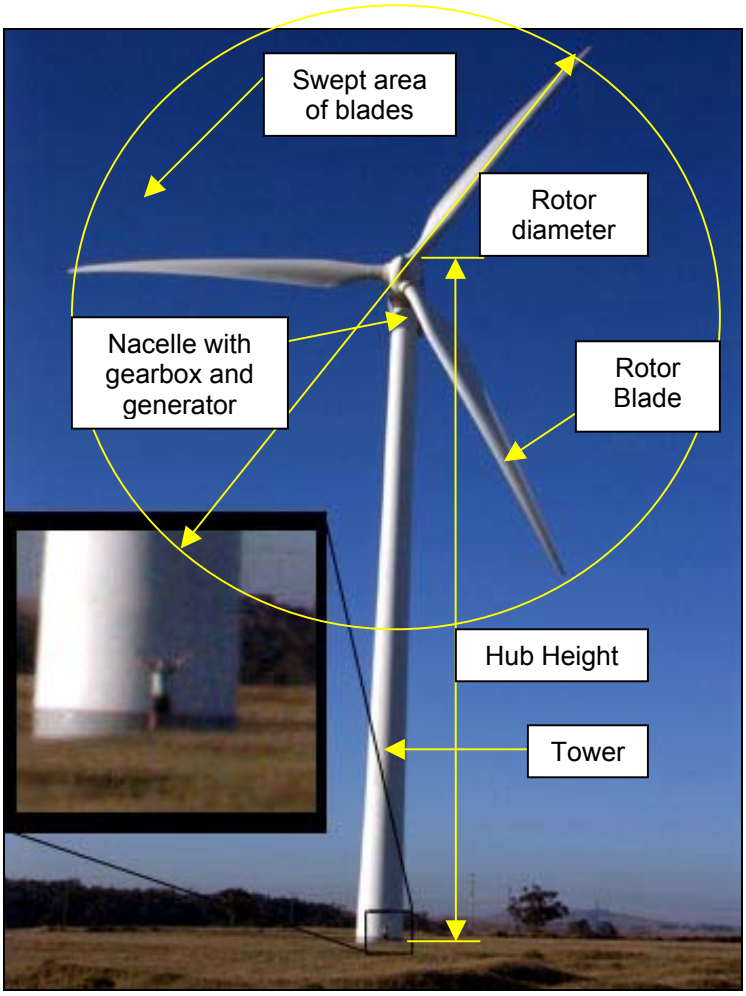

Figure 1: Typical wind turbine with person for scale [2]

PMCs constitute most of the rotor blade except the blade to hub attachment. The hub and nacelle are mostly metallic; primarily steel, to protect the internal mechanisms. The tower is typically all steel or a concrete structure with steel reinforcement [3].

Wind farms designed to output a substantial amount of electricity are employing wind turbines with individual capacities in the multi-megawatt generating range. These generators, housed in the nacelle of the wind turbine, are very large and require a huge torque from the passing airflow to start and

maintain power output. The larger the electric generator, the larger the blades are required to be. Blade lengths of 54 meters are in production and larger lengths have reached prototype stage [1]. The resulting increases in length also increase the weight of a blade by an exponent between 2 and 3 [1]. The additional weight is becoming more difficult for blade manufactures to design with available fiberglass material systems. Building lightweight blades of greater length remains a primary focus for utility-size turbine manufacturers because investment in blade technology has a trickle-down effect on the rest of the turbine systems. At about ten percent of the overall capital expense for a wind turbine, spending on blade innovations is a relatively small factor in energy production costs. A lighter, more structurally efficient blade decreases the demands on the hub components and tower structure, decreasing capital and operating expenses for the entire turbine [1]. However, the increasing sizes of these blades are reaching the cost-effective engineering limits of current fiberglass PMC materials used in wind turbines today [1].

Fabrication of Wind Turbine Blades

A typical blade shown in Figure 2 is frequently assembled to the final form by smaller components. The top and bottom blade skins are made separately as well as the spar. The spar itself can be assembled from the separately made caps and shear webs. The majority of the structural loads are handled by the spar caps within the blade and the blade roots. The spar caps also contribute to most of the mass of a blade. The final assembly is done with high strength

adhesives to bind the elements together into a rotor blade. As blades get longer to increase their power generation capability, the main spar reinforcement must also keep pace by increasing in length, width, and thickness.

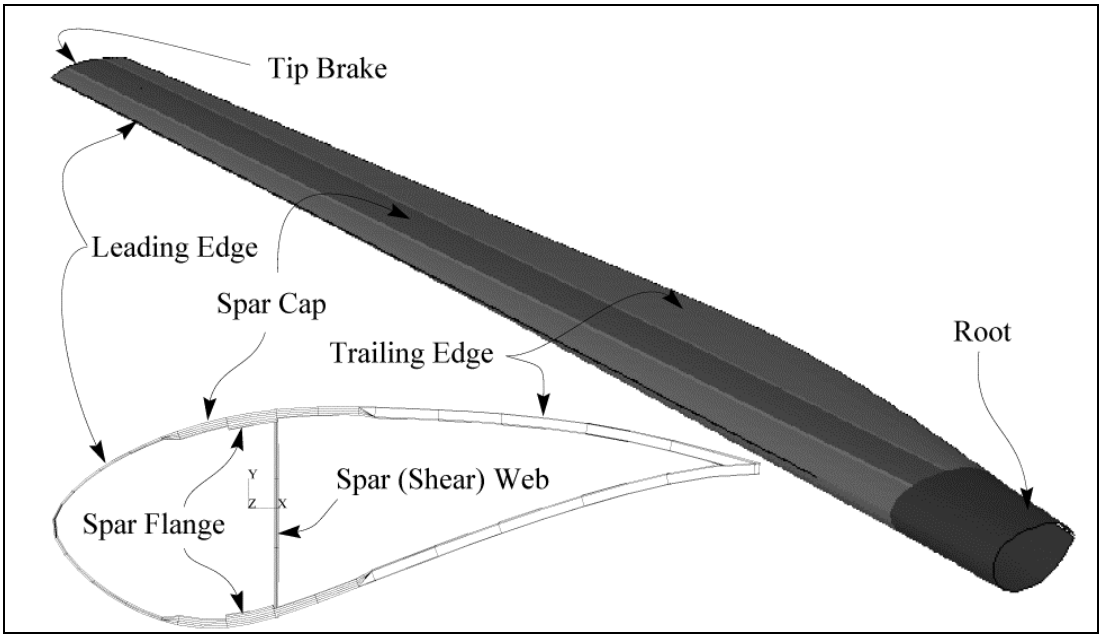

Figure 2: Wind turbine blade schematic showing interior parts and cross section [4]

A photograph showing laborers physically laying up a wind turbine blade skin is shown in Figure 3 [5]. The fabric schedule is placed layer by layer until the desired thickness is reached; between layers polymer resin is poured over the new fabric. Wind turbine blade manufacturers primarily use thermosetting resins for their low viscosities in infusing into fabrics and relative mechanical property stability in higher temperatures and low cost [6]. The hand rollers used are to compact the fibers down, push any trapped air to the surface, and push away excess resin.

Figure 3: Physically laying up half a blade skin [5]

Thin elements such as the blade skin can be hand laid-up or resin infused with little technical difficulty and result in low void volume or other defects. Resin infusion or resin transfer molding (RTM) utilizes pumps or other mechanical devices to push resin into and through fabric and mold. Thicker elements such as spar caps are significantly more difficult; hand laid up elements can suffer inconstancies from part to part in many areas and large defects can be unintentionally created. Infusing resin in thick or multiple layers of fabrics at high pressures can lead to internal defects such as fiber washouts [7]. Washouts are fibers which are pushed out of position by the fluid flow.

Figures 4 and 5 [8] show large structural skin members being infused with resin by use of vacuum pressure (vacuum assisted RTM) to pull resin through the fabric rather than push the resin. Figure 4 shows a 20 meter long rotor blade. Figures 5a and 5b show a 16.4 m long by 4.5 m wide by 2.5 m high fiberglass

boat hull being vacuum infused. The thicknesses of these parts were not given in the reference. Due to increasing understanding and successes of resin infusion processes in thicker laminates, manufacturing methods for wind turbine blades are turning away from hand lay-up methods and towards the various forms of resin infusion because of the advantages in production time, labor, and materials [1, 7, 9].

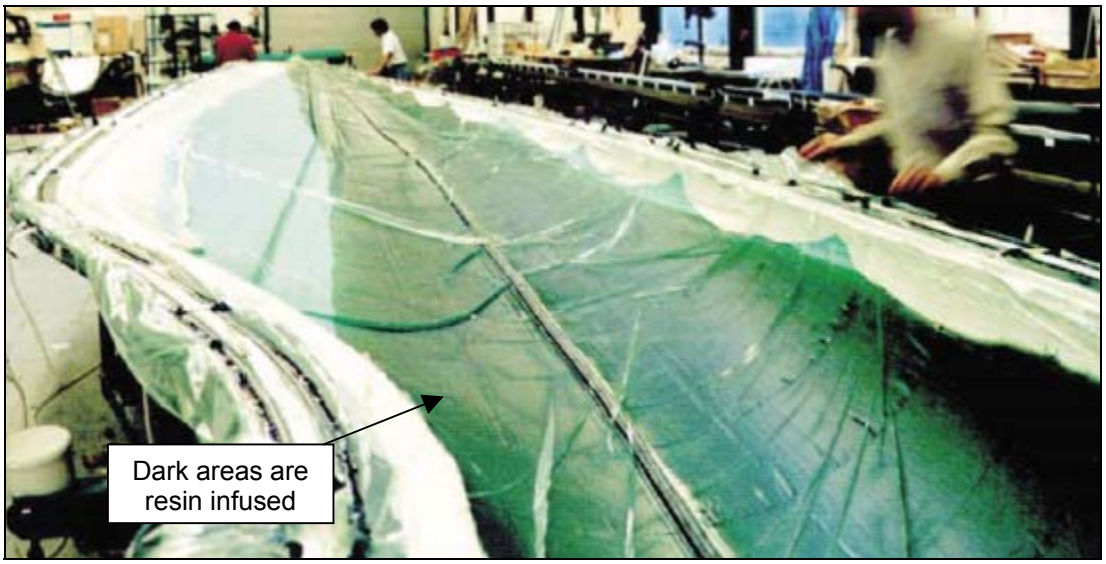

Figure 4: One half outer rotor blade skin during vacuum injection [8]

However, washout-type defects have not yet been eliminated. A possibility to avoid defects like washout is the use of composite elements that already have the matrix cured and thus the fibers are fixed in place. This is the idea behind composites that use pre-impregnated ('pre-preg') fiber reinforcement. The pre-preg has already been infused and the matrix only partially cured to allow some compliance in handling, cutting and part forming. The pre-preg is then fully cured by use of heat and pressure to finalize the part. The drawbacks with pre-preg lay-up include the cost of manufacturing pre-preg itself and the expensive laborious

laying-up of pre-preg either by hand or by automation [10].

Figures 5a and 5b: 54 ft long fiberglass boat hull under vacuum resin injection [8]

The manufacturing of the blade factors into its eventual performance in the field. If a blade of sufficient quality is made, why are more advanced forms of reinforcement needed? In the next section, the forces a wind turbine blade experiences will be explored.

Need for Higher Performance Fibrous Reinforcement

Possible Blade Failures - The external loading on a wind turbine comes from non-periodic cycles of random wind loads in conjunction with the inertial motion of the blade while in operation. Some major concerns about the reliability and performance of wind turbine blades exist in the bending, local area compression, fatigue and a combination of these characteristics throughout the blade structure during operation.

Since rotor blades are essentially unevenly loaded cantilever beams, there is a significant concern regarding end tip deflection as the blades get longer. The rotor must remain close to the nacelle; otherwise there are large eccentric forces at the top that require a larger and more reinforced tower and possibly a redesigned nacelle.

This edgewise blade bending can be caused in part by the weight of blade near the end, wind gusts, and stiffness loss within the blade structure due to material fatigue, various forms of damage or environment factors. Large deflections of the blade tips could strike the tower and wear away the tip of the blade, blade skin and the tower surface, if not causing significant damage to both structures immediately. A wind turbine displaying noticeable bending of its blades is shown in Figure 6 [11].

The resulting damage opens up the structure to environmental factors that could further compromise the performance of the local material or structure. An example of the damage sustained by a 7.5 ft long wind turbine blade after a tower strike is shown in Figures 7, 8, and 9 [12]. It appears from the preceding figures that damage from the strike to the blade weakened the local structure. The loads on the compromised blade tip caused delaminations around the damaged area. The damaged material then cracked too much and finally snapped off.

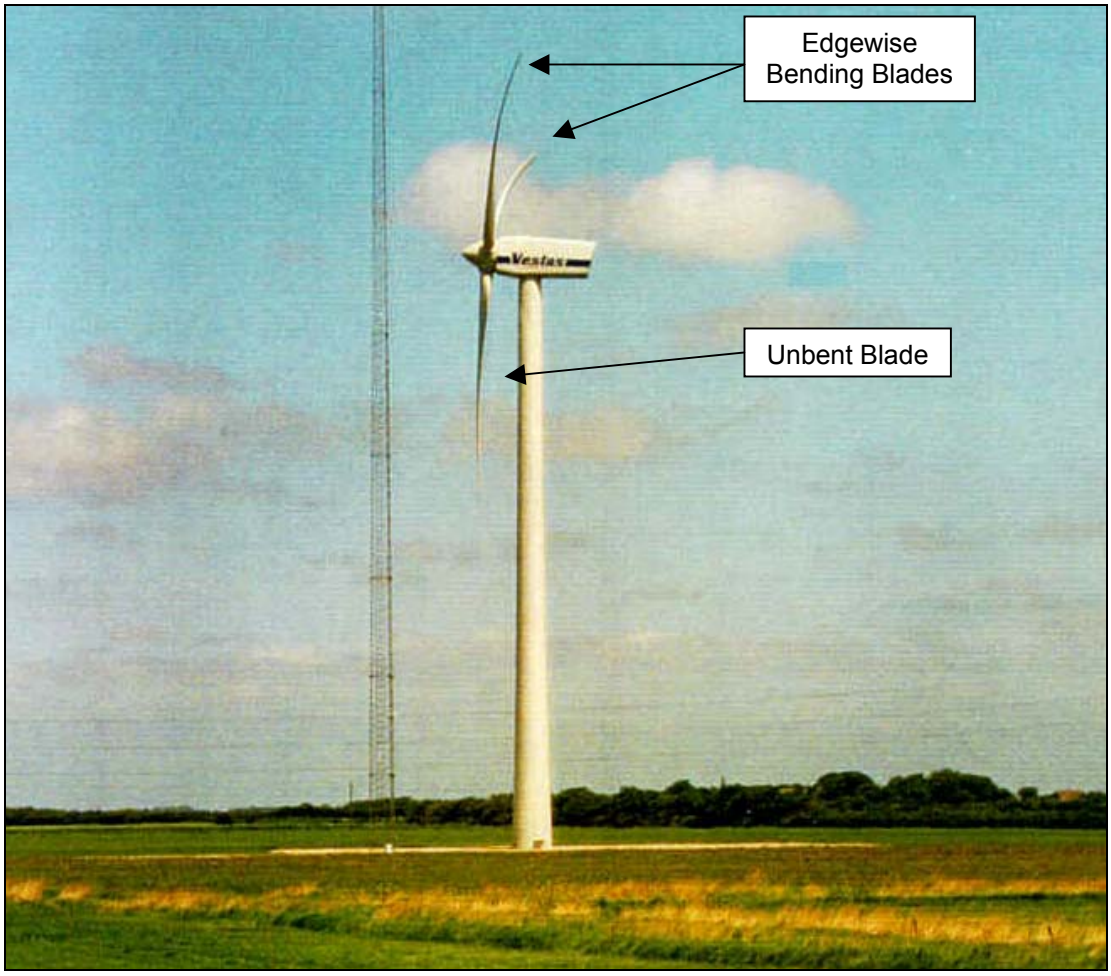

Figure 6: Blades with noticeable bending curvature [11]

Compression aspects are involved in the bending of a blade. As blades get larger in length, width, and depth, local stresses in load carrying members are subjected to pure tension and compression loads during bending action. Some PMC materials used in blade substructures are weaker in compression than tension as will be discussed later.

Figure 7: Damaged blade after tower strike compared to undamaged blade [12]

Figure 8: Same damage, view from trailing edge [12]

Figure 9: Straight on view of damaged blade [12]

Glass vs. Carbon Fiber Reinforcement - Some large-scale wind power developers have been looking into incorporating carbon fibers into the blade structure in varying capacity with the intent to replace the existing glass fibers, specifically in the spar and spar cap regions [1]. However, there are some basic concerns to investors in increasing the carbon fiber content of their designs.

The first concern to a for-profit business is cost: Carbon fibers are typically at a minimum five times the cost of glass fibers. The processes involved with manufacturing carbon fibers from raw materials to final product are much more expensive than the comparative process manufacturing glass fibers [13, 14]. Another related concern is availability. Demand from military aerospace and civilian aeronautical companies are increasing again due to advancements in carbon fiber performance [15]. This increased demand is depleting manufactures stockpiles and contributing to an increase in prices.

The second area of concern in choosing fibrous reinforcement is performance. In structures subjected to dynamic loads such as wind turbine blades, the structure can suffer due to the low fatigue durability and large deflections exhibited by glass reinforcement in highly loaded components. Generally, carbon fiber is stiffer, stronger, and more fatigue resistant than glass. The properties of carbon fiber under tension loads are excellent and fatigue strength losses are nearly negligible compared to glass fibers as seen in Figure 10 [16]. The only concerns about unidirectional carbon fibers are its bending and compression properties. However, carbon fiber and associated fabric and plies are a very anisotropic material and have very weak properties anywhere out of the axial direction of the fiber [17]. The optimal orientation is when the direction of the fiber is parallel to the loading direction for maximum effectiveness. Compression on carbon fiber laminates is more of a concern as the compression strength is very fiber orientation sensitive [9, 18]. The strain to failure is lower

than that of glass fiber in both tension and compression demonstrating excellent stability but little flexibility. Static compression comparisons between carbon and glass fibers are displayed in Tables 1 [18].

Table 1: Static Compressive Strength of Glass Fiber, Carbon Fiber, and Hybrid Laminates containing varying amounts of waviness in 0^0 layers [18]

Database Designation	0^0 Layers	% 0^O	V_F %	Resin	Compressive Strength, MPa	Compressive Strain to Failure, %	Remarks
Glass Fibers							
DD5P	D155	72	37	Polyester	574	2.4	stitched straight strands
DD8	D155	72	44		582	2.1	
DD11	A130	68	30		319	1.6	woven strands
DD12	A130	68	43		302	1.1	
DD13	A130	68	46		314	1.1	
DD27A	Ahlstrom	76	32		381	1.9	siticched to mat, wavy strands
DD27B	Ahlstrom	76	42		321	1.2	
Carbon Fibers and Hybrids							
CGD4	ACM-13-2	76	51	Vinyl Ester	588	0.71	carbon, stiched fabrics, low waviness
CGD4E	ACM-13-2	76	51	Epoxy	684	0.81	
UNI25A	UNI25	100	45	Vinyl Ester	535	0.61	woven large tow carbon
CGD5E	Fortafil 652	71	35	Epoxy	565	1.15	bonded carbon
CGD5E2	Fortafil 652	71	51	Epoxy	546	0.73	
CGB4	SE84lv/hsc	72	43	Epoxy	828	1.0	prepreg
CGB5	SE84lv/ sc300c	63	49	Epoxy	831	1.2	prepreg
CGB6	SE84lv/hsc	80	65	Epoxy	1027	1.0	prepreg with glass 45's

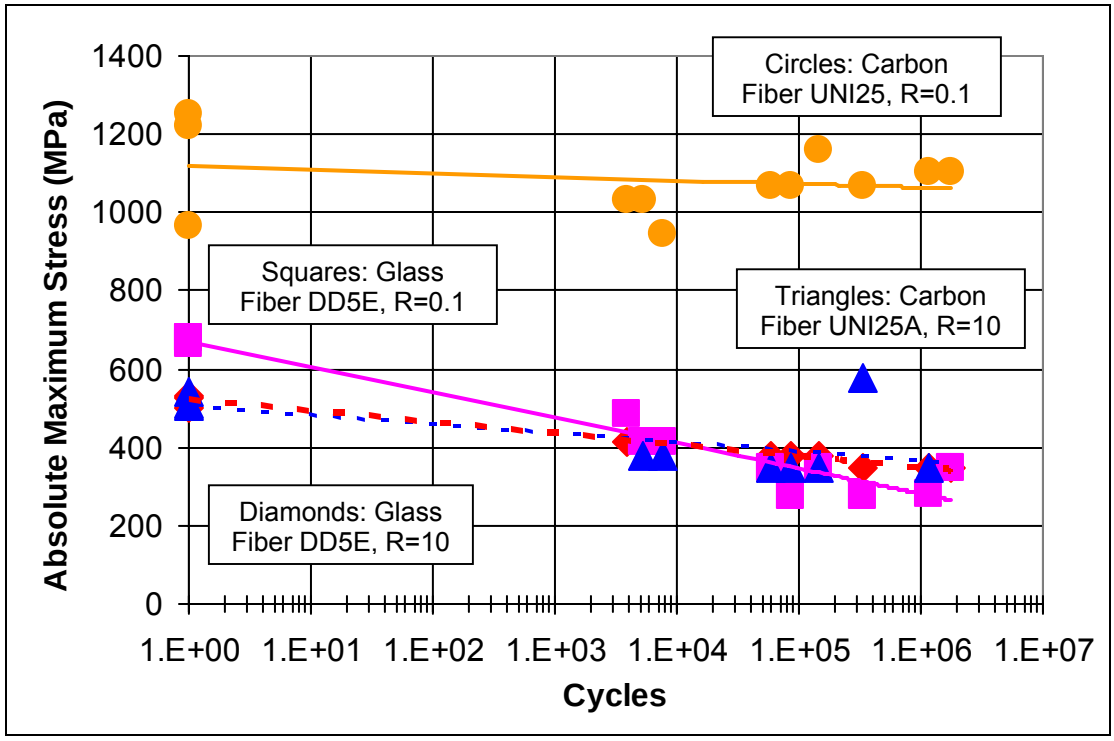

Figure 10: S-N Curves for fiber laminates in tension and compression fatigue [16]

An ideal wind turbine blade is a hybrid where glass and carbon fiber can be used in locations where their respective properties function best. Carbon fiber can be placed where there is a need for both high load carrying capacity and fatigue resistance. The abilities of carbon fiber enable the use of less material resulting in thinner laminates. Optimization is an issue here; the monetary cost associated with carbon is too expensive to over design in areas where it may not give any benefits.

In many ways carbon fiber laminates can out perform glass laminates of a similar fiber volume fraction. The carbon fiber laminate is also usually thinner than the glass fiber laminate. However, working with carbon fibers is more difficult than with glass fibers in laminate processing. Alignment inaccuracies and

void content have a much higher impact on the mechanical properties of a carbon laminate than they do on a glass laminate [1].

Unfortunately, alignment inaccuracies, sometimes called fiber waviness, can be introduced inadvertently and easily. Fiber waviness can be inherent in the fabric architecture, created during resin infusion, or be a consequence of the residual thermal stresses caused by the different thermal expansion rates between fiber and matrix materials while curing. There are two types of waviness: in-plane or fiber waviness, or out of plane or layer waviness.

An example of fiber waviness in dry fabric architecture is shown below in Figure 11. This low cost glass fabric called A130, commonly used in wind turbine blades [19], has inherent out-of-plane and in-plane waviness. The unidirectional tows go under and over the stitching thread creating the out-of-plane waviness. The fiber tow profile expands over one stitching thread and contracts under the next one creating in-plane waviness.

Recent research done at MSU in investigating fiber waviness suggests that any deviation out of the primary load carrying direction in the fibers of a PMC is a serious detriment to the overall performance of that composite. Waviness is expected to reduce compressive strength due to the two factors 1) fibers may be put into geometry that exacerbates the basic fiber, strand or layer buckling mode of failure, 2) waviness shifts fiber orientation off the axis of the ply longitudinal direction producing matrix dominated failures in plies nominally oriented in the primary load direction [18].

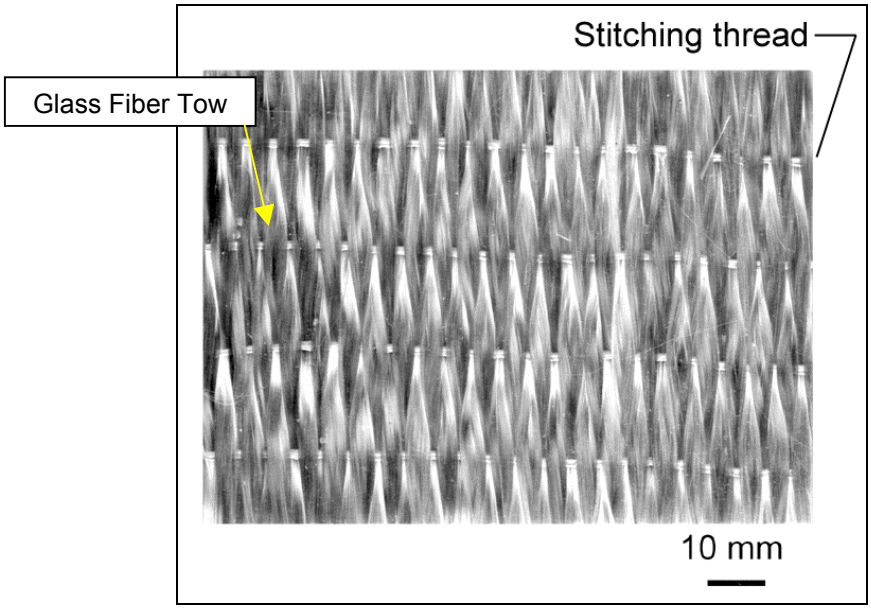

Figure 11: A130 fabric showing fiber strand distortion in the thickness direction [20]

Fiber orientation defects like washouts can exacerbate compression and fatigue related weaknesses in composite materials. This has been shown to be especially true for the compression and compression fatigue characteristics which are known to be sensitive to the straightness of the fibers [18]. Prepregs, where the tows are nominally straight, have higher compression failure strains than fabric based laminates as seen in Table 1.

Intentionally induced fiber waviness in a study by Wang [20] found that conditions where the larger the wave amplitude combined with shorter wavelengths of the displaced fibers worsen the compression strength of a composite both in static and fatigue situations by delaminations between plies. Pictures of tested fiber waviness coupons are shown in Figure 12. The white areas are delaminated damage zones. The results also showed that the more severe the waviness, the larger the damage zone. Even relatively low wave

severities is such as those that occur in A130 fabric in Figure 11, significantly reduce the compressive strength by predisposing the fibers to the buckling geometry that grew the delaminations.

A similar study done by Avery and coworkers [18] intentionally inducing out-of-plane fiber waviness with carbon fiber / epoxy prepregs drew similar conclusions.

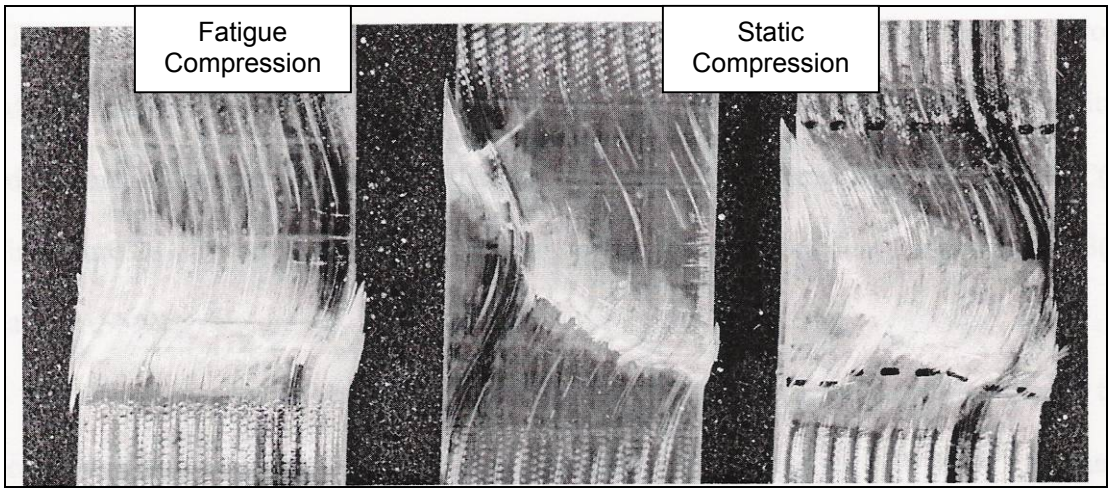

Figure 12: Static compression failure and fatigue compression failure [20]

In low cost structures, composites based on glass fibers have primarily been the norm. However glass, while lighter than steel, can also create heavy structures when the glass reinforcement is present in large quantities. One benefit of carbon fibers is the lower density over glass fiber of similar dimensions. Glass fiber density is around 2.60 g/cm^3 while typical carbon fiber is 1.75 g/cm^3, so moving to an all carbon fiber rotor blade with all other composite components being equal enables a theoretical weight savings up to 33% over an all glass blade. Weight savings of carbon over glass can enable a designer to tailor the mass and stiffness distribution of a blade for more beneficial inertial and

aerodynamic effects and still retain good general performance [1]. However, complete substitution of glass by carbon fiber is very unlikely in the short term [1].

Problem Motivation

As stated earlier, stiffness is a critical issue for wind turbine blades. Blades need to avoid excessive bending under operational loads to prevent tower strikes or fail on the compression side. Stiffness, durability, and dimensional stability are also needed for fatigue damage resistance. The inclusion of carbon fibers to augment fiberglass blades can provide these benefits. However, carbon fibers are getting increasingly expensive with demand still from aerospace markets and raw material costs [1, 15]. During part molding, waste and excessive use of carbon fibers can be issues due to this expense. Studies of defects such as fiber misalignment in composites made with carbon fiber fabrics show that careful manufacturing techniques of such composites are critical. Current wind turbine blade manufacturing processes cannot completely eliminate misalignment problems without costly additions or redesigns to these processes.

The use of pre-cured pultruded carbon fiber composites as reinforcement in place of or in conjunction with traditional fabrics could be an ideal way to get the benefits of carbon fiber using as little carbon fiber as possible while retaining the best alignment configuration during lay-up and infusion. Cured cross-sections such as these could be placed in a structure where they could be used to maximum benefit with minimal use compared to layers of carbon fiber fabric.

An example of pultruded inserts used as reinforcement is in an aircraft fuselage stiffener shown in Figure 13. These stiffeners enabled a fabrication cost reduction between 60 and 80 percent compared to the baseline stiffener [21]. This stiffener will be discussed in the next chapter.

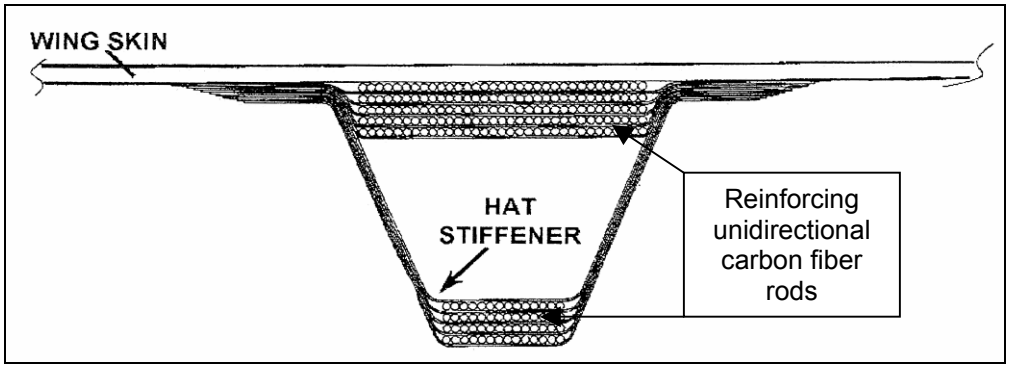

Figure 13: Aircraft stringer using pultruded rods as fiber reinforcement [21]

The nature of the pultrusion process keeps the fibers aligned in a nominally straight direction and theoretically more evenly spaced throughout the pultrusion cross-section. Cross-sections of composites, one having fiber tows and the other fibers in a quarter inch pultruded rod are shown in Figures 14 [19] and 15. The dark areas in both these figures are resin rich areas. The fibers in the pultrusions are more evenly spaced across the composite compared to the fibers confined in the tows.

As pultruded composites are cured as they are manufactured, a possible way of securing pultrusions together is by traditional fabric stitching. Since the fibers within the pultrusion are fixed, multiple pultrusions can be joined together like a fabric. This enables multiple pultrusions to be handled at once and the

fibers within the pultrusion cannot be induced into waviness. A theoretical example of this is shown in Figure 16.

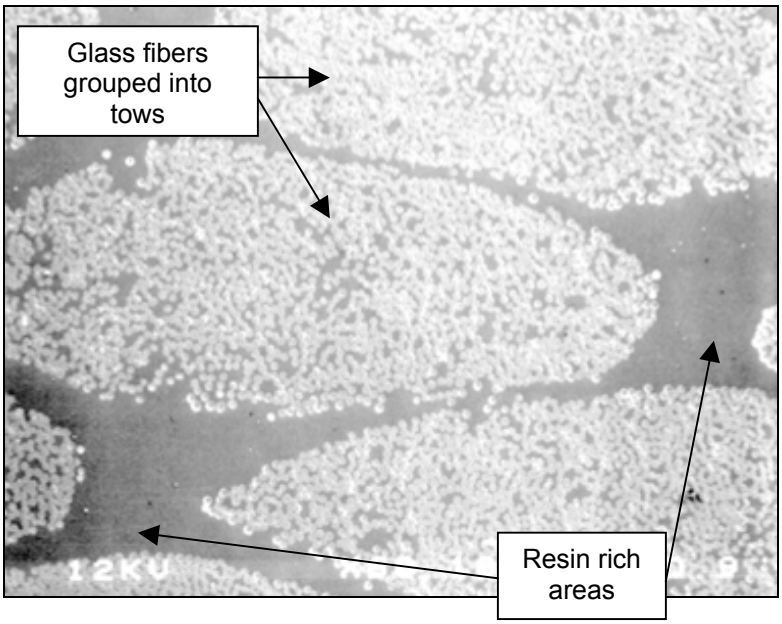

Figure 14: Glass fibers tows in stitched D155 fabric x60 magnification [19]

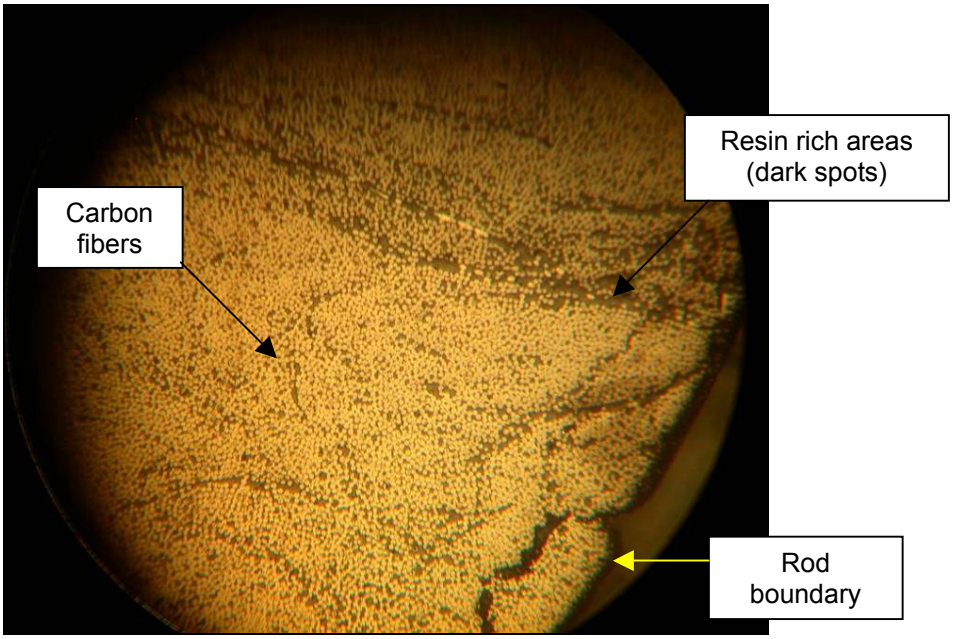

Figure 15: 16x magnification carbon fibers in pultruded rod cross section

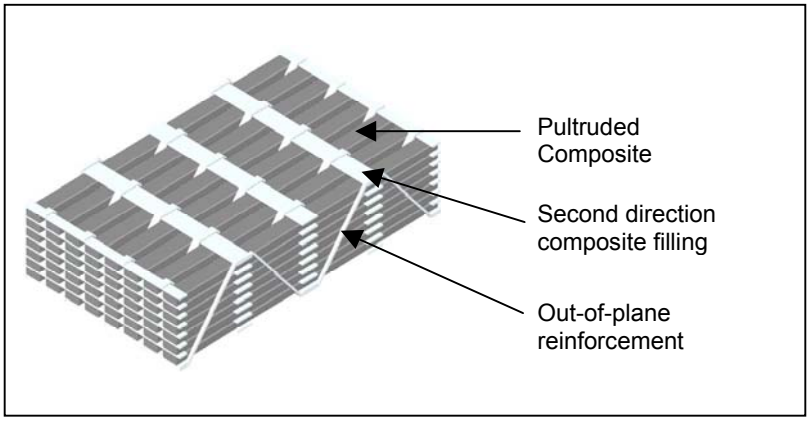

Figure 16: Schematic showing 3-D fabric

As a pultrusion is a cured combination of fiber and resin, encasing a pultrusion in a structural geometry by another secondary, or encasing, resin requires an optimal bond between secondary and primary resins as well as good bonds by both resins to any fibers present on the surface of the pultrusion. The pultruded inserts used in this study have a smooth surface so an additional step for producing an optimal bond may be required for good load transfer capacity. An example of multiple pultruded rods encased in a secondary resin and between two single plies of glass fabric is shown in Figure 17. These rods underwent a hand applied abrasive surface treatment before being cured in a composite.

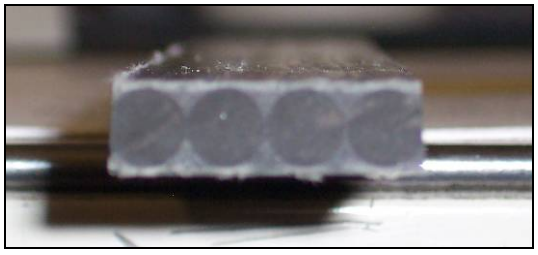

Figure 17: Beam coupon with pultruded rods side by side

The motivation for this research is to determine if pultruded carbon fiber sections perform as well as composites made from unidirectional carbon fiber fabric in compression and bending.

Problem Statement

The objective of this research is to explore advantages and disadvantages of applications using carbon fiber pultruded sections as primary structures. Issues of surface treatment for bonding the carbon fiber/epoxy pultruded rod to secondary epoxy and spacing between rods will be addressed. Also, properties of the individual sections will be tested, reported, and discussed.

BACKGROUND

For long span and thick sections of structural elements, both the hand lay-up and resin infusion methods are very labor intensive and/or expensive in different ways. The optimization of both methods to minimize fiber washouts or other defects can also take time. The use of fully pre-cured structural elements that are already fixed in the desired shape and fiber configuration can be an inexpensive solution to important aspects of these problems. Polymer matrix fiber reinforced composites manufactured by the pultrusion process have existed since the 1950s but in the last ten years have built up and intriguing and promising history in high performance composites.

Pultruded Composites

Pultrusion Process Description

The pultrusion process is a cost effective automated process for manufacturing continuous, constant cross-section composite profiles [22]. Fibers in tow or fabric form are pulled from mat creels and/or rovings into a specific path through either an open or enclosed formulated resin tank. The impregnated fibers are then pulled through a heated pre-former that also strips away excess resin. The pultruded composite is given its final shape as it is pulled through the die and cured. Pultruded composites using thermosetting resins are cured by a heat-activated catalyst that fully cures the pultrusion as it exits the die. After traversing an open span meant for cooling, the pultrusion is then physically grappled and

pulled into a cutting tool where it is cut to a desired length. The pulling force and rate are optimized according to the resin reactivity and fiber reinforcement. Multiple streams of pultrusions within one machine can achieve a high effective output. A block diagram of this process is shown in Figure 18. Surfacing veils help the pultrusion surface through the performer and die and also prevents the reinforcing fibers from contacting the die surfaces.

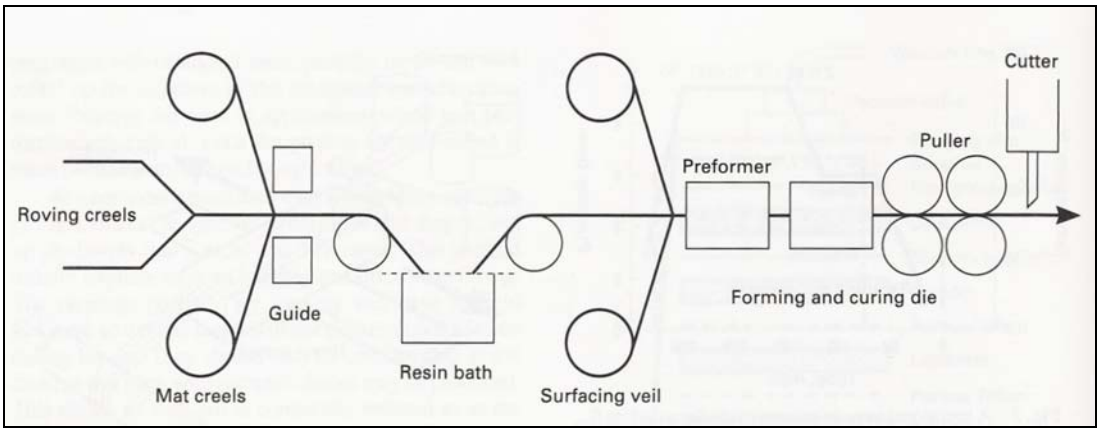

Figure 18: Schematic of fiber composite pultrusion process [23]

Process Advantages and Disadvantages

One of the most visible attractions to pultrusion is in geometric shape availability. Some of the geometric shapes the pultrusion process can perform are shown in Figure 19 below. Abilities such as varying wall thicknesses of constant hollow cross-section pultrusions, multiple hollow sections within a pultrusion, the addition of wire, foam, or other materials as inserts in pultrusions, and cross-sections that can be as large as desired [22] could be of use in large composite structures such as wind turbine blades. Currently thickness tapering and other in situ cross-section changes and length-wise curvatures in

thermosetting pultrusions are in developmental phases [24, 25], but these could also be of interest in turbine blades for long sections that can follow a blade profile to minimize gaps and joints where pultruded sections end. A wide variety of reinforcement fabrics, fibers, pre-pregs, and matrix styles can be used in the pultrusion process.

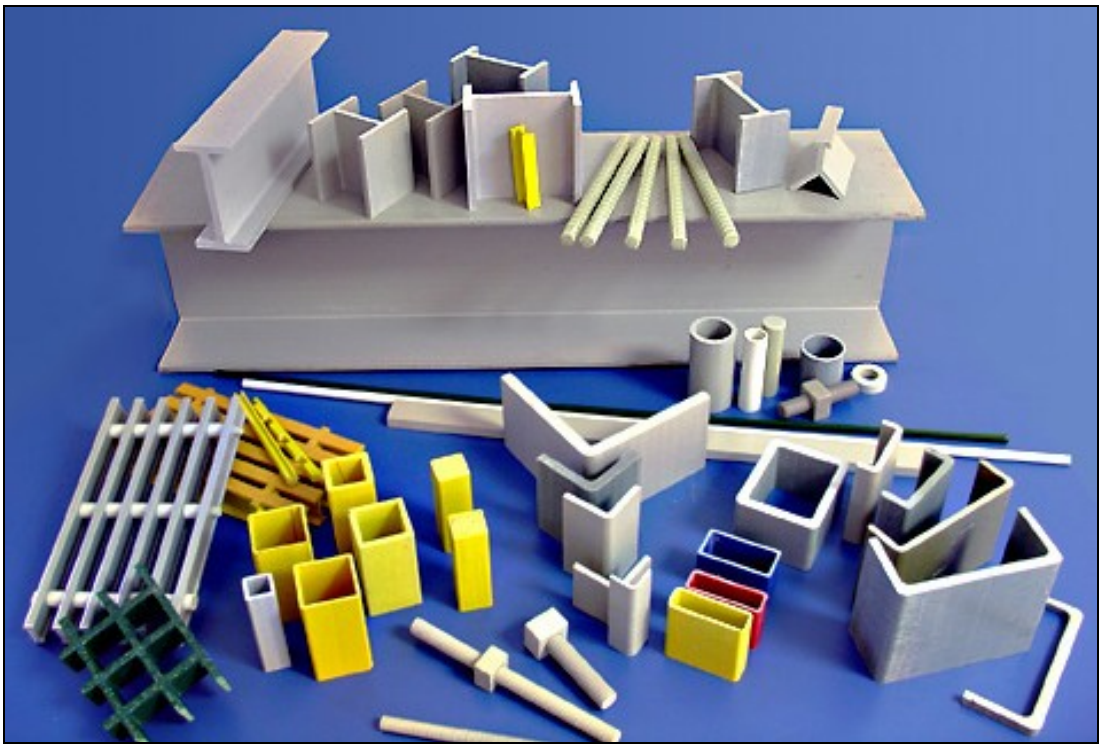

Figure 19: A variety of pultruded shapes are available [26]

Since the fiber reinforcement is pre-tensioned by pulling it through the process, the fibers tend to be straighter overall and have more uniform spacing and distribution within the finished composite in the pulled direction compared to other processes [22]. This can reduce much of the waviness unintentionally introduced during manufacturing. The fiber volume fraction of pultruded composites can be maximized in the high 70 percent range. For tension loads

where performance is fiber dominated, this highly aligned microstructure can be very beneficial. Lengths of any size that can be transported commercially can be made.

Once the pultrusion is cured, the fibers are protected from accidental damage during handling and they cannot be moved during structure lay-up or infusion. If the pultruded shape makes up a large portion of the substructure, placement of these shapes may be easy and speed up processing times. The shelf life of pultrusions is also unlimited once cured.

Thermosetting resins limit the forming abilities of the pultrusion process [22]. Pultrusions having large wall thicknesses are difficult to produce due to the exothermic reactions and shrinkage effects of curing thermosetting resins. These effects can induce matrix cracking and fiber delamination in the walls [22]. Currently, the maximum diameter of solid unidirectional fiber reinforced rods has been 75 mm.

Current Pultruded Composite Research and Applications

Pultruded composites are most successful when they provide corollary advantages that are not available with traditional competitive materials [22]. Market penetrations by pultrusions have come in general places like constant profile stairs, walkways, and hand rails in industrial environments, window and door frames in buildings, and luggage racks in mass transit vehicles. In these

areas the primary advantages have come from the light weight and environmental resistance characteristics of PMC pultrusions.

The use of pultrusions has been expanding to fill needs in more demanding applications. Civil engineering structures have been making increasing use over the last decade of PMC pultrusions to supplement or even replace current materials with encouraging results. High performance aerospace applications have been more theoretical and confined to prototype vehicles thus far but inroads have been made in commercial and personal aircraft [27, 28]. While more published research has been done in composite pultrusions for construction than for aerospace structures, some parallels to potential wind turbine blade applications are worth noting in the following discussion.

Civil Engineering Structures

Fiber reinforced materials in civil engineering structures are enabling engineers to optimize their structural designs in many ways that approach the limiting capabilities of these materials. Fiber reinforcements are seeing increasing use due to their greater durability and higher strengths compared to steel, light weight, and electromagnetic neutrality [29]. These advantages are apparent in different degrees and situations. Pultrusions used in civil engineering structures fall into three application categories: exterior post-strengthening of existing structures, inclusion in concrete as reinforcement, or the pultrusion as the primary structure.

Exterior Strengthening - Pultruded strips, sheets, and shells can be applied externally to deteriorating bridge substructures such as the undersides of bridge decks or support columns. These composites can have their lifetimes extended by strengthening in flexure and shear at a fraction of the associated costs of classical rehabilitation concrete structures. The light weight of carbon PMC composites translates into easier handling, fewer laborers and lifting devices and fast executions needed as seen in Figures 20 and 21 [30, 31, 32]. Most joining is accomplished by high performance epoxy adhesives. The best bonding environment is accomplished by increasing the surface area of both adherends. Sandblasting the concrete and abraiding the surface of the composite is typically done. Mechanical fastening methods are also occasionally employed [32]. The high strength of the composite allows less material to be used compared to traditional steel plate rehabilitation and pultrusions do not corrode like steel.

Figure 20: Column Strengthening [33]

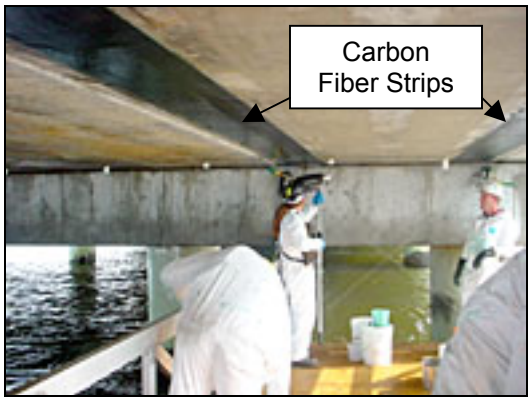

Figure 21: Bridge Strengthening [33]

The bonded composite is more effective if it is prestressed before attachment. Prestressing is more effective with carbon fibers as they can hold a greater tensile load for much longer than other fiber reinforcements [31, 32].

Internal Reinforcement - Similar pultruded composites shapes are replacing or augmenting steel rebar as tensile reinforcement within concrete. This is due in part to the long-term durability offered over traditional steel rebar [34]. The durability is related to the corrosion resistance of composites compared to steel in aging concrete structures, which corrodes easily when moisture from the environment seeps in through cracks. Glass based reinforcement is generally confined to non-stressed concrete; carbon fiber tendons are generally prestressed to take advantage of their high tensile stress support over their design life [32]. Vinyl ester and epoxy matrices in these PMCs are primarily used due to their good environmental resistance. Pultruded rods have been accepted as the optimal shape for internal reinforcement [35].

Bonding and load transfer between concrete and a pultruded tendon are facilitated by increasing the surface roughness of the tendon. With internal composite reinforcement, the bond is solely dependent on the shear properties of the tendon surface. The radial compressive forces of the concrete are the primary load transfer point on the tendon, so the surface has to be able to maintain contact with the concrete [34]. For concrete applications, this is done generally by additions to the surface. Techniques include wrapping fiber tows around the tendon surface, molding continuous positive or negative surface

variations into the pultrusion, having a textured peel-ply on the surface that is removed before use, and bonding fine aggregate particles to the surface of the tendon [32]. Some of these rods are shown in Figures 22 and 23 [35, 36]. Small diameter pre-cured rods can be twisted around other rods to make a cable tendon similar to steel. The surface area is increased due to the grooves between the many twisted rods. Up to 37 12.4 mm rods have been combined [36].

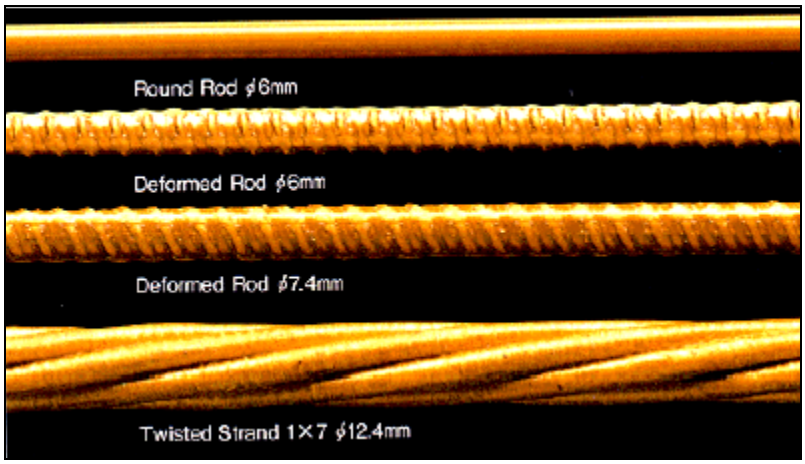

Figure 22: Pultruded composite tendons with molded in surfaces [36]

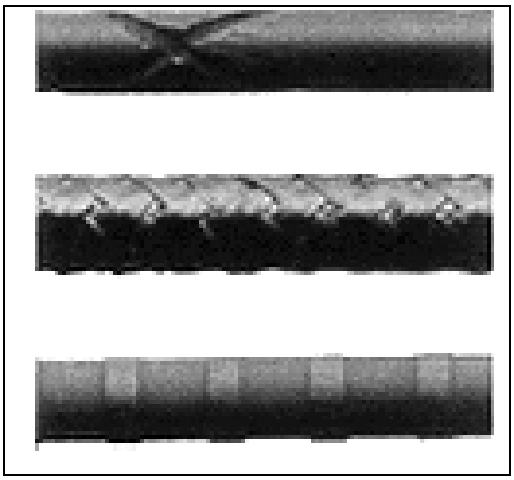

Figure 23: Leadline pultruded tendon surfaces [36]

Bridge structures have been the largest beneficiaries of pultruded rod reinforcements. Prestressed carbon fiber based reinforcement has been used in most of these designs.

Pultruded Structures - Significant bridge and building structures have been designed and constructed using large PMC pultruded profiles as the primary load carrying members [32]. Some examples include short and medium span pedestrian bridges, small highway bridges, and a large causeway structure [32, 37]. A five story office building, a six story stair-tower, and several other small buildings have been constructed in Europe using PMC pultruded shapes [32].

Pultruded bridge deck components have received the greatest attention in recent years due to their inherent advantages in strength and stiffness per unit weight compared to traditional steel reinforced concrete [32]. The light weight of these composites allows rapid replacement of unrepairable bridges and a reduction in the dead load compared to a concrete bridge. Many pultrusion producers supply custom profiles based on customer designs or market directly to engineers with previously used shapes in bridge decking. Some of these profiles are shown below in Figure 24 [38]. The individual cells of these pultruded composites can either be joined by application of adhesives or mechanical fastening. The lightweight of the pultruded PMC components allows easy transportation to the construction site as seen in Figure 25. Joining the composite components together can also easily be done on site.

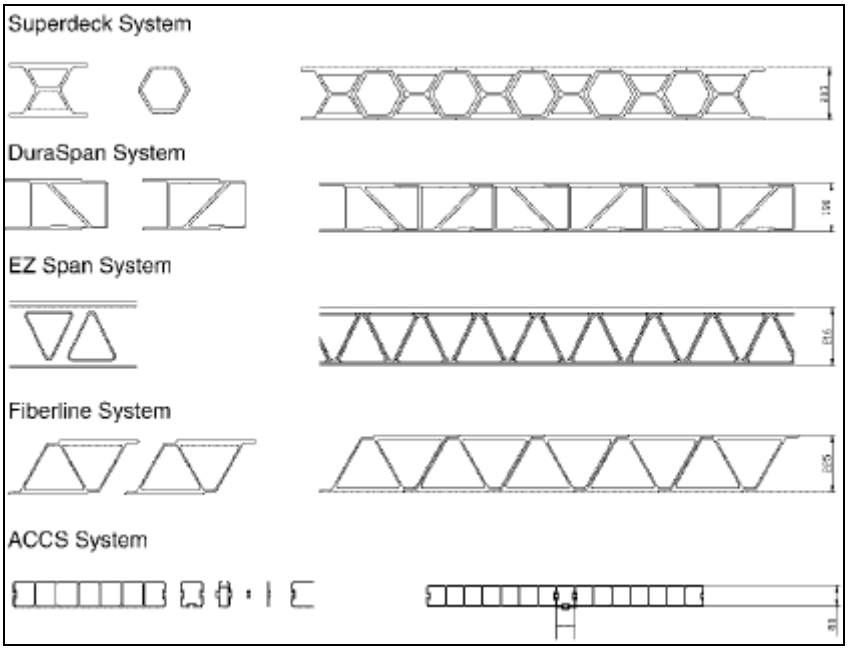

Figure 24: Various PMC bridge deck designs [38]

Figure 25: Element of composite bridge deck transported into position [38]

An example of pultrusions assembled in a box girder for a marine environment causeway structure details how easy it is to assemble a pultrusion based structure. The composite structure shown below in Figure 26 was

assembled from several multi cell pultrusions as shown in Figure 27. The assembly was done by a couple of laborers and a light crane. Each square beam in Figure 27 was mechanically fastened at its corners to a girder along the top and a T-beam connection at the bottom. The completed structure in Figure 26 was loaded by 14 1-m^3 containers filled with water for a total of 132.7 kN for 7 days. The structure deflected 6 mm at the center and recovered half of that after unloading [37, 39].

In terms of rough costs, an average pultruded bridge deck is about \$700/m^2, which corresponds to \$7/kg. Although more than twice the amount of bridge deck with steel reinforcement (\$322/m^2), the cost can theoretically be made up in labor and transportation savings among other things [32].

Figure 26: Completed causeway structure element under load [39]

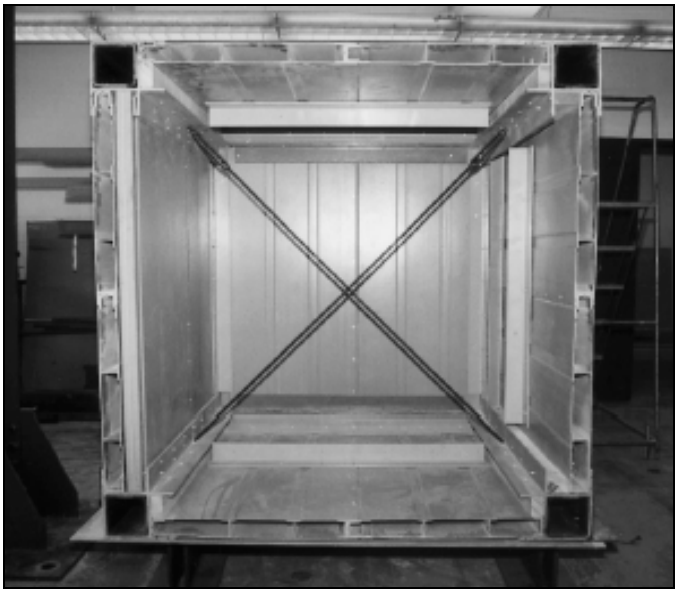

Figure 27: Single completed causeway element [39]

While pultruded products in civil engineering construction are making inroads and showing promise, it is important to note that they are not overwhelmingly superior to conventional steel reinforcement. PMC pultrusions use is best justified when the secondary characteristics such as weight and corrosion resistance are very important [29]. The building codes based on steel reinforced concrete are inadequate concerning uses of composite pultrusions, especially as internal reinforcement. Much work still is needed to qualify pultrusions for more widespread use [29, 32].

Aerospace Applications

With the highly demanding loads aerospace structures experience, the main goals regarding pultrusions is to capitalize on the high fiber content and fiber straightness to maximize the strength and stiffness of these structures

Conceptual Structural Configurations - British researchers have experimented with very small 1.7 mm diameter rods in various anisotropic components as concept composites. The highly anisotropic nature of unidirectional pultruded cross sections allows creation of some novel structural configurations. The composite below in Figure 28 was designed as a concept for a heavy helicopter flexbeam application where a specified low value of torsional stiffness and a high value of compressive strength were required. The composite was able to achieve a 20 degree angle of twist with no apparent damage, and snapped back to the undeformed shape after the load was removed [40, 41]. The measured torsional stiffness was 3.2 N*m per degree at the start to 2.3 N*m per degree at 20 degrees of twist.

The effect was achieved in part by reinforcing a low modulus matrix with 1.7 mm pre-cured carbon fiber reinforced epoxy pultrusions. The middle portion of the composite was 50 by 22 mm. The total number of reinforcing rods in the composite was 332, laid out in 7 rows of 26 rods between 6 rows of 25 rods. The rods on the outer edges of the composite had a curve trajectory from one end fitting to the other, with less than a one percent strain on these rods [40, 41]. The matrix was a special blend of epoxy, polyurethane, and triethylenetetramine hardener. The researchers concluded the low torsional modulus would not be possible without the pre-cured fibers constrained against microbuckling.

This twist capability is useful in blade designs that incorporate some blade twisting for enhanced aerodynamics. A slight twisting with no damage in a spar

that still has high stiffness could be very beneficial to blade spar cap designers [1].

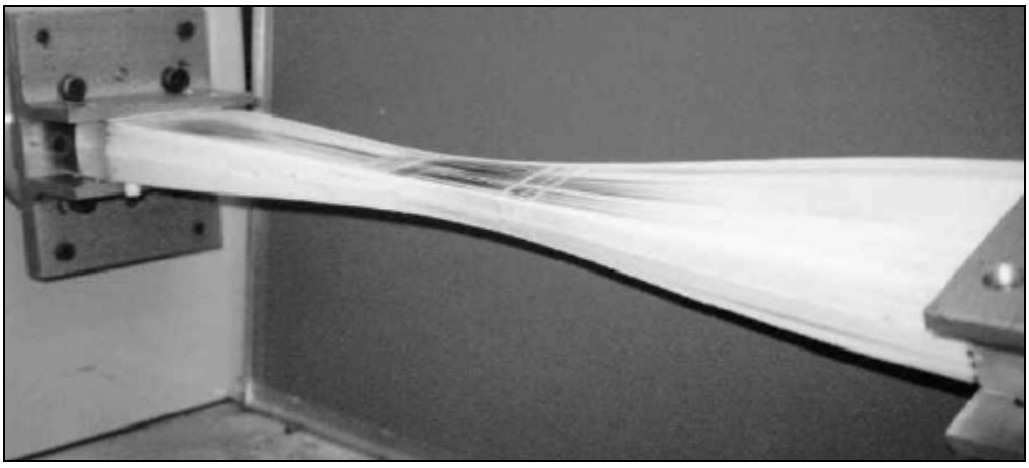

Figure 28: Pultruded rod based composite with 20 degree of twist applied [41]

A damage tolerant design for a pultruded rod-based composite was also proposed. A highly tensioned aramid fiber was wrapped around a 240 count bundle of 0.68 mm (65% V_f / rod) rods after the rod bundle had been infused and cured with epoxy resin. This resulted in a composite rod diameter of 12.4 mm and overall fiber volume of 47 percent. The aramid fiber overwind in the hoop direction induced transverse compression in the rod. Damage to the rod by low energy impact (20-40 J) is inhibited from initiation and subsequent propagation due to the overwind. Also the compressive strength of the rod is minimally affected due to the overwind compared to unwound rods [9, 10]. It was also concluded that the pretensioning of the aramid fiber contributed more to damage resistance than the amount of aramid fibers present [41]. The aramid fibers also permit stable failure under compressive loads in the more heavily wound cases.

As described in the previous section, similar overwinds are done for rod reinforcements embedded in concrete to increase surface area and enhance bonding. Aramid fibers are discouraged in wind turbine blade manufacture due to their susceptibility to degradation by moisture. A glass overwind could accomplish similar impact resistance and the possibility of different resin systems could be used against the glass surface like vinyl ester for increased environmental resistance. This design could reduce the thickness in wind turbine blade skins if the spars below were low impact resistant. The observation that pretensioning of the overwind fibers matters more than amount of overwind could enable a weight savings for wind turbine blades. It was also observed that overwinding suppressed stress concentrations at the end fittings when post impacted rods were tested in compression [41]. This effect could be of interest to wind turbine blade spars using rods near the blade roots and associated attachments. Overwinding the rods in the spars near the roots could suppress fiber kinking failures in the blade root attachment leading to a more efficient use of materials and designs.

Very small tubular elements were also produced using small 0.74 mm carbon fiber/epoxy rods aligned axially around the circumference as seen in Figure 29. This tube has an inner diameter of 10 mm and a wall thickness of 1.5 mm and takes advantage of ideal fiber alignment for low weight, high strength strut applications for structural truss members. A single layer of carbon

fiber/epoxy prepreg was laid on either side of the rod with epoxy film adhesive between the pre-preg and rods [44].

This design could be enlarged and expanded to provide vertical stiffness in a small tower structure if the rods are overwound with off axis strands done by filament winding processes. The small size of these tubes could also allow core inserts. These tubes might also find use in wind turbine blades in the skin strengthening for bending, compression, and tension.

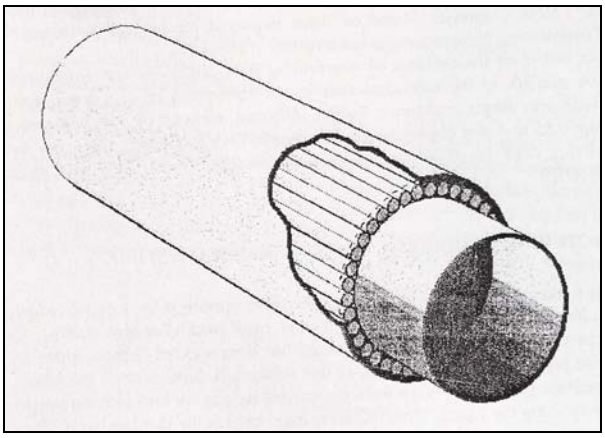

Figure 29: Structural Schematic of a tube manufactured from small rods [44]

Tubes 680 mm long were tested in pin ended compression. Polyester resin filled the core to suppress ovalization of the cross section at the center under very large displacements. Tubes failed suddenly in compression near the center around 1.79 percent strain [40].

Pultrusion Research in a Tilt-Rotor Helicopter Wing - Bell Helicopter has examined unidirectional carbon fiber rod reinforcement for use in next generation helicopter designs, primarily the V-22 Osprey tilt-rotor aircraft. The pultruded rods were incorporated into the wing skin hat stiffeners as seen previously in Figure

13 and below in Figure 30 to carry the axial tension and compressive loads [21]. The minimal fiber waviness exhibited by the pultruded parts was ideal for this design. The use of pultruded rods decreased the manufacture time and amount of materials needed to construct this wing box.

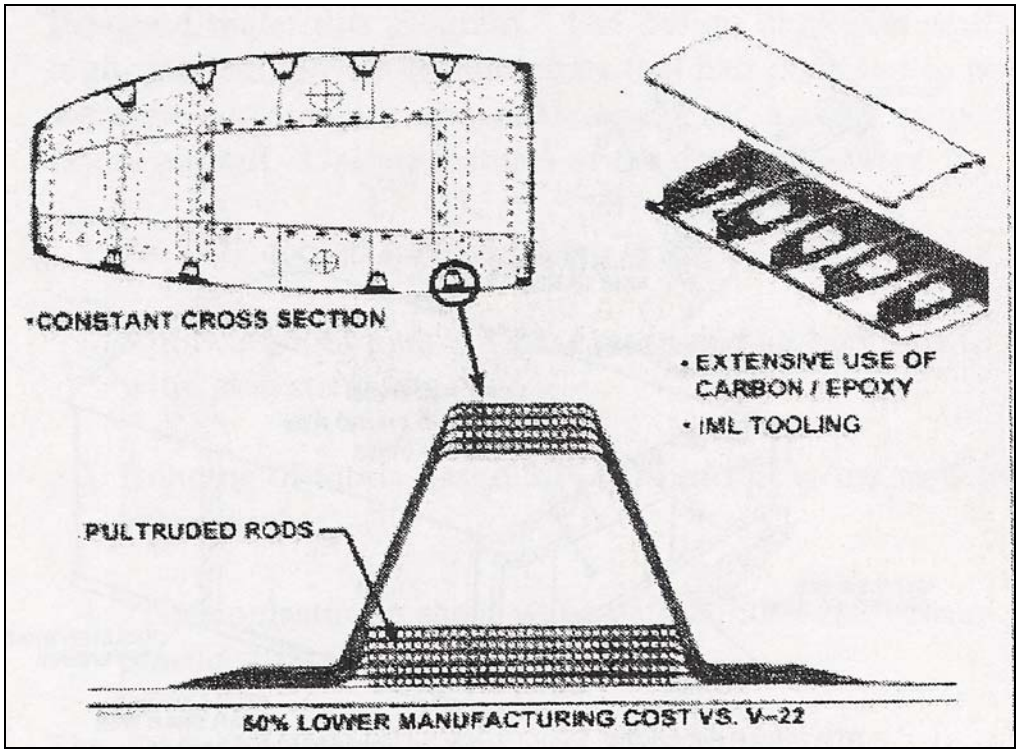

Figure 30: Cross-section of proposed wing with detail of pultruded rod stringer [21]

The rods within the stringers were embedded in a syntactic epoxy resin filled with hollow ceramic microspheres and ±45 degree carbon fiber/epoxy pre-preg on the outside for load transfer. Bending tests on the stringers loaded on the small rod pack side produced failure strains of 1.2 percent [40].

This design was not adopted for use primarily due to the resulting overall average fiber volumes (~50%) in each finished hat stringer [45]. These fiber volumes coupled with the large resin regions were determined unable to meet

the operational performance demands of this stiffener design, even though the load carrying efficiency of the stiffener could be enhanced through pultruded rod reinforcement.

One possible way to improve this design or any composite using pultrusions is to use very small diameter pultruded rods inserted in the regions between larger diameter pultrusions. This could raise the overall fiber volume of the composite structure and reduce the size of the matrix rich regions of the stringer. The performance and financial economics of this approach would need to be compared with using large fiber tow fabrics.

Lower fiber volumes are more acceptable in the wind turbine blade because of the lower design loads. Around fifty percent fiber volume in as laminate is considered passable. The resin rich regions between pultrusions are still problem areas in wind turbine blades.

Braided Rod Structure Research - Multidirectional fabrics are of interest to wind turbine blade manufacturers because of the multiple reinforcement directions present within one layer of fabric. The problem with three dimensional fabrics is their inherent fiber waviness when they are braided together [46]. Research in Taiwan has examined the topology, processing aspects, and mechanical properties of the two-step braiding process for fabrics incorporating small diameter (1 mm) pultruded rods [46, 47, 48, 49, 50, 51].

Using these rods can significantly reduce the level of crimp in both axial and braiding yarns and thus provide better quality reinforcement in orthogonal

directions. Crimp-induced problems such as irregular fabric patterns and localized fiber waviness can be effectively improved as the rods used are already cured and cannot be deformed by the braiding tow tension. Rods that are placed in an orderly way greatly improve yarn compactness [46]. Figure 31 shows that the resulting composite has evenly spaced rods and little braiding tow warpage. The non-axial fiber direction consistency is improved for out of plane damage and this also allows channels for resin infusion through between braid and rod. The resulting fabric is semi-rigid that allows easier handling of large pre-forms with small amounts of fabric deformation [47].

One of the resulting drawbacks of using this kind of composite is the inability to form intricate shapes as the rod reinforcement forms a skeletal structure and is fairly rigid in handling. Also since the rods are incompressible, the fiber volume of the overall composite tends be low but the fibers are more consistently and evenly spaced throughout the composite cross section [50]. Part of this drawback was due to the resin infusion mold not being compressed during infusion to preserve the pre-mold fabric architecture [47]. Rods also cannot be very stiff due to the details of this process. Resin infusion of this fabric architecture is difficult unless done right after stitching as cutting the fabric releases some of the tension out of the braiding. Releasing the tension softens the fabric somewhat and allow some deformation if high viscosity resins and large pressures are used during resin infusion [47].

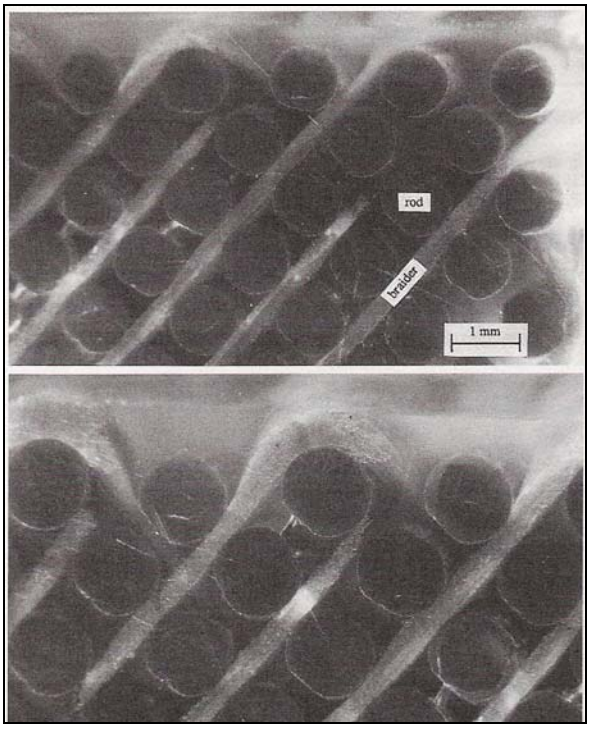

Figure 31: Pultruded rods braided into a large layer [46]

Braided rod composites manufactured with this method were tested in three point bending, short beam shear, and compression [48]. The rods were made from Kevlar fibers and vinyl ester braided in either Kevlar or carbon fiber tows and infused in vinyl ester after braiding. The flexure failure modes consisted of matrix crushing and rod matrix kinking on the compression side. The fibers within the rods were undamaged and still able to perform in axial tension. As the rods buckled the braider tows on the compression side failed in tension. In the short beam shear test, the rods on the tension side pulled into the composite while the rods on the compression side pushed out. This has advantages in energy dissipation as the rods themselves were not immediately damaged and relieved stress by shearing the complete interface. A similar effect was seen in

impact tests of these composites [49]. In compression failure, the main failure was due to fibers kinking the rods that were driven quickly to failure when the kink band contacted the surface loops in the braiding tows [49, 51].

Much of the previous research done with pultruded rods has focused on very small diameters for their flexibility and compactness. Large diameter pultrusions should not be discounted over smaller diameter rods because of the increasing size of the surrounding resin rich area. Large pultrusions can be easier for mechanical and non-mechanical handlers to manipulate for preparing a pre-form for resin infusion. A tougher resin can be used to limit the delamination initiation and propagation. Aerospace researchers have applied syntactic resins around the rods to increase the energy needed for delamantions to grow, thereby keeping cracks to small sizes.

An issue that has not received much attention is the quality and the quantification of the bond between a pultruded cross section and the resin that it is embedded in. As pultrusions and the fibers within the pultrusion are used as reinforcement in a wide variety of geometric configurations and supporting resins, how good is the load transfer between the structure and the pultrusion? The fibers within the pultrusion are typically bonded well to the pultrusion matrix, but any supporting resin of the structure may or may not have an efficient load path to make use of the fibers. In the Experimental Methods section of this paper, some surface treatments to these pultrusions will be employed to observe their effects on pultrusion / secondary resin interface strengths.

EXPERIMENTAL METHODS

Materials Used

The focus of this thesis was on pultruded carbon fiber / epoxy matrix composites. Two kinds of this composite were generously donated by Zoltek Corp of St. Louis, MO [52]. In November 1999, Zoltek purchased Entec Composite Machines, Inc., located in Salt Lake City, UT. Entec manufactures equipment and machines that facilitate the fiber reinforced pultrusion process [53].

The pultruded sections used in this study were primarily 5.91 mm diameter by 1.83 meter rods that employed Zoltek brand Panex® 35 intermediate modulus carbon fiber [54]. The matrix was Epon 826 Bisphenol-A based epoxy manufactured by Shell Chemical Corp. The curing agent used was LS-81K, made by Lindau Chemicals. This epoxy system is specially formulated for pultrusions [55]. The tip of one such rod is shown in Figure 32.

Manufacturers' performance data provided by Zoltek indicated the pultruded rods had a tension break load around 5500 kg, an ultimate tensile strength around 20 MPa, and an elastic modulus around 175 GPa.

Also provided were 1.2 mm x 5 cm flats using Panex 32 carbon fiber [54]. Neither the matrix material nor curing agent were given but assumed to be the same as in the rods. Three types of flats were provided. The first containing 19 tows of Panex 32 with 50,000 fibers per tow, the second containing 20 tows of

Panex 32 again with 50,000 fibers per tow, and finally Toray T-700 carbon fibers having 24 tows of 12,000 fibers per tow. The fiber volume fractions of these pultrusions were investigated and results reported in the next chapter.

Figure 32: Scale of pultruded rods used in this study

The epoxy matrix materials infused over the rods for testing was EPON 862 (diglycidyl ether of Bisphenol-F) based epoxy made by Shell Chemicals Limited [56]. This chemical structure is seen in Figure 33. This epoxy was chosen by the recommendation of Zoltek resin scientists to provide a good bond with the untreated surfaces of the inserts [57]. It is a room temperature curing epoxy with an initial viscosity of 350 cp [58]. The chemical structures of Bisphenol-F and Bisphenol-A based epoxies, seen in Figure 34 [59], are very similar. The curing agent for this epoxy was EPIKURE 3234, an unmodified aliphatic triethylene tetramine (TETA) [59]. This chemical structure is seen in Figure 35. The recommended weight ratio mix was 100:14.5 epoxy to curing agent [57]. Approximately a 7:1 epoxy to curing agent weight mix ratio was adopted in manufacture. Gel time was approximately 30 min at room temperature (18-20 degrees C).

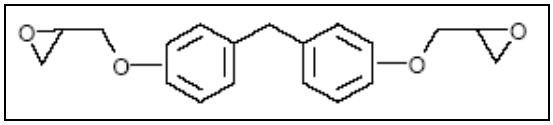

Figure 33: Chemical structure of diglycidyl ether of Bisphenol-F [58]

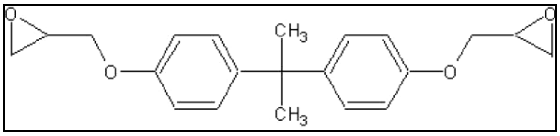

Figure 34: Chemical structure of diglycidyl ether of Bisphenol-A [59]

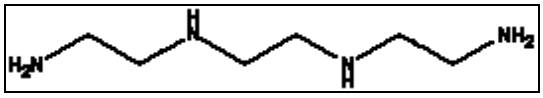

Figure 35: Chemical structure of TETA [61]

Tests Performed and Coupon Manufacture

Pultrusion / Secondary Resin Interface Description

The issue of the adhesion of the reinforcing pultrusion to the embedding matrix is very important. The matrix material transfers the exterior loads to the pultrusion and the fibers within the pultrusion, so excellent pultrusion-matrix attachment is crucial as the load transfer at least must go through two mediums to reach the fibers.

The pultruded rods used in this series of experiments have a very smooth surface to the touch when received from the manufacturer. This might lead to an inadequate bond between pultrusion and embedding matrix that would easily fail under load. Initial three-point bending tests on a rod based beam structure shown previously in Figure 17 showed that the vinyl ester secondary resin around the

pultrusions peeled away under load. Observations of the rod surfaces and resin in Figures 36 and 37 saw that the resin had an imprint of the lightly abraded rod surface. It would be an area of concern if this phenomenon was common. Thus various mechanical and chemical surface treatments were performed on the rods in this study to observe the pultrusion-secondary matrix (Epon 862 epoxy) bond strength change compared to an untreated rod.

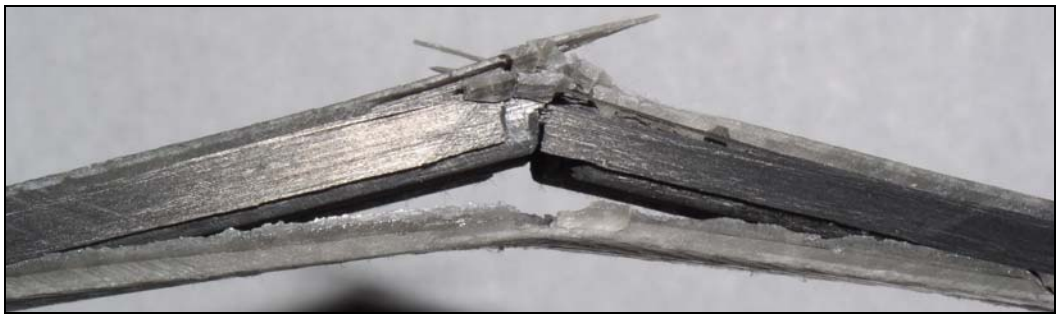

Figure 36: Three-point bending test result showing that the secondary resin had peeled off the pultrusion

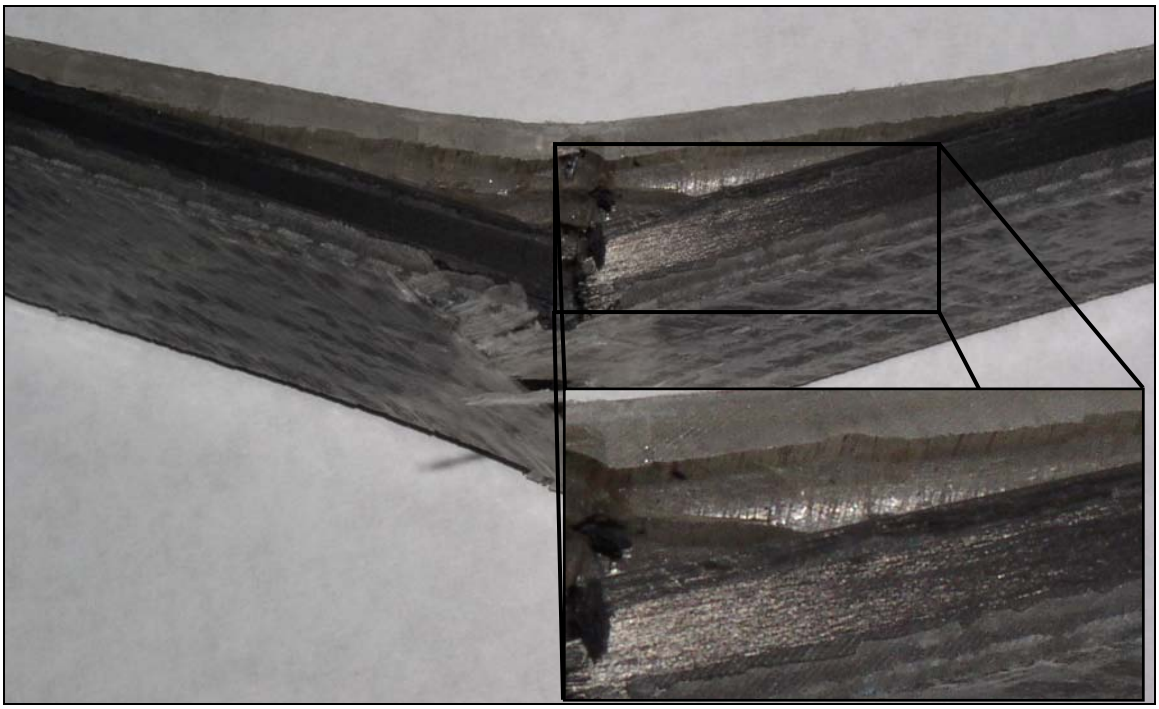

Figure 37: Another view of the three-point test result with detail

Surface Treatment Descriptions

Most surface treatment studies to date have focused on adhesive joining of finished composites in local areas and not wholesale surface treatments of composites for primary reinforcement. The intention of the surface treatment is to modify the chemistry or morphology of a thin surface layer without affecting the bulk properties [62]. The mechanisms that improve bond performance may include the elimination of weak boundary layers at the surface such as loose particles or contaminates, improved wetting of low-energy surfaces, introduction of polar chemical groups that are favorable for bonding to other chemicals, and the increased surface roughness leads to mechanical interlocking sites held together primarily by friction [62]. A summery of the surface treatments used in this study are shown below in Table 2 with associated treatment variables, advantages and disadvantages to each treatment.

Surface Abrasion - These treatments are the physical sustained contact between the abrasive particle and the surface to be sheared away. This treatment was investigated as a low cost method of surface treatment that can be incorporated into a blade manufacturing process either as a step in the pultrusion process after part curing or as a step done before the laying-up of a blade spar by laborers.

A study by Parker and Waghorne recommended some form of surface treatment to remove traces of mold release agents from carbon fiber reinforced composites intended for bonding to other composites [67]. High concentration of

release agents considered contaminates on pre-bonded surfaces lead to extremely low-strength joints. They found that abrasion treatments generally reduced the contamination and greatly increased the strength of the joint compared to an untreated surface. Pultrusions typically have release agents in the form of a surfacing veil or additives to ease the shear stress on the resin when it is pulled past the die [22].

In another study by Matz, carbon fiber reinforced epoxy composites mechanically abraded for a surface treatment for bonding exhibited the best performance in hot/wet conditions [68, 69]. There has been some concern that the heat from the friction between shearing particle and resin surface can increase past the transition temperature and cause local ductile failure [67].

The variables used in this treatment method include hand applied dry sanding by silicon carbide particles of various particle sizes. The time spent abrading in a local area, the general direction of the abraded paths, the pressure used and other minor variables will be detailed later in this chapter.

Surface Erosion - This treatment is the process where high velocity particles impinge on the surface of the composite. The particle impact in thermoset resin composites removes material in a complex process involving matrix micro-cracking, fiber-matrix debonding, fiber breakage and material removal [70]. This method was investigated as a low cost method of surface treatment the can be incorporated into the blade manufacturing process. This

method is possibly an alternative to abrasion or can supplement the abrasion treatment.

Table 2: Summery of Surface Treatments Used

Treatment Type	Treatment Variables	Known & Perceived Advantages and Disadvantages
Physical Abrasion [63]	• Grit Size • Grit Type • # of Passes • Wet/Dry Sanding • Pressure Applied • Hand or Sanding Block Application • Abraded surface temperature	+ Easy to apply by hand or automation + Small amount of materials and equipment needed - Fiber Damage on surface - Sheared resin damage and fiber debonding on composite surface
Particle Erosion without Corrosion mechanism [62, 63, 64, 65]	• Blast Pressure and Particle Speed • Grit Size and Shape • Grit Type • # of Passes • Speed of Passes • Recirculating / Non-recirculating media • Vacuum exhaust in blast cabinet • Exposure Time • Blast Angle of impingement • Distance of blast nozzle to surface • Others	+ More effective at removing surface contaminates than abrasion + Easy to apply by hand or automation +/- Unidirectional carbon fiber / epoxy composites erode very fast [64] - Requires more equipment than abrasion - Fiber Damage on surface - Resin cracking and fiber debonding just below composite surface - Unskilled application can cause variable surfaces and composite deformations
Chemical Oxidation with Aqueous Media [69]	• Acid Type and Concentration • Acid Exposure Time • Acid Temperature • After Acid Treatment Wash System	+ Pitting increases surface roughness for mechanical bonding + Oxidizes and exposes carbon fibers for better secondary epoxy bonding - Need large equipment set up for large pultruded pieces - Long exposure times in acid degrades fibers - Time consuming to remove acid from pultrusion after treatment - Hazardous waste issues

Parker and Waghorne found that erosion by grit blasting as a surface treatment performed much better than abrasion at removing release agents by almost completely removing any contamination [67]. However, composite materials in general have poor erosion resistance and extended erosion treatments can lead to premature composite failure by the nature of the removal process [70].

The variables used in the erosion treatments in this study are time under erosive jet, speed of the particles, the distance between blast nozzle and composite surface, and angle of impingement on the surface.

Surface Oxidation - These treatments on fiber reinforced composites involve altering the fibers surface topology, removal of weak carbon surface layers, and the energization of those fibers [66]. Energization involves breaking carbon-carbon bonds on the fiber to add reactive chemical groups to the carbon atoms that are more thermodynamically favorable for resin compounds to attach to. A chemical bond of resin to fiber is a more stable and stronger bond than a mechanical bond which relies more heavily on friction to maintain contact. The amount and types of different side groups that can be attached depend on the type of chemical treatment. Previous research with various types of acidic treatments directly on carbon fibers has been seen to increase the interfacial shear strength of the fiber/matrix interface up to a point [66]. Prolonged acidic treatments however damage the fibers and significantly reduce tensile strengths [71].

A wet heated chemical type of treatment was investigated as an alternative to mechanical surface treatments that target the outside fibers on the pultrusion exposed and potentially energized by the chemical treatment. This could theoretically lead to more efficient interphase within the larger composite if the embedding epoxy can bond directly and effectively to some of the outer fibers in the pultrusion.

The variables used in this surface treatment method include the temperature of the acid, time of exposure, and after-acid wash method.

Rod Interface Test Coupon Manufacture

Quantifying the traditional fiber / matrix interface is relatively easy but open to a wide range of interpretation [72]. Two methods were used in this study for quantifying the pultruded rod / secondary epoxy matrix interface, the pullout and the pushout test. Both methods have their respective advantages and disadvantages. Table 3 below is a summery of tests conducted in this thesis with a short statement of the motivation behind each test, the information desired from each test and the number of coupons that will be used.

Traditional single fiber pullout tests measures the force required to pull a fiber out of a matrix block in a known geometry. The embedded fiber length must be known and require that the tensile stress of the fiber be less than its tensile strength, otherwise the fiber will break during testing. The typical embedded lengths with this test are less than 0.1 mm [72]. It was safe to assume that the tensile stress seen by the pultruded rod when it would be pulled out of the

embedding epoxy would be much less than its strength, so much larger embedded lengths could be used in this test. The interfacial shear strength was calculated by dividing the largest force by the embedded rod surface area.

The pushout test performed in this study is an extension of the microdebonding test [73] and measures the same interfacial shear strength as the pullout test. One of the primary benefits of this method is that it is done in-situ within the composite. Thus the interface strengths are possibly more representative of in service composites. One of the difficulties in microdebonding is splitting of the fiber under load. Here with the pultruded rods, the center rod of a representative volume composite element is loaded over the area of the rod. The strength of the rod is not needed for this test.

Table 3: Rod Surface Treatment Test Matrix

Test Type	Test Description	Motivation	Number of coupons tested
Macro-fiber rod pullout	1. Surface treat rods 2. Embed rods in epoxy on both ends with middle exposed for flat surfaces that can be gripped 3. Apply tension until interface on one side fails and rod is visibly mobile	Compare calculated critical lengths between untreated and various abraded rods, determine single best SiC treatment for pushout tests Since rods are stiff and strong, embedding lengths can be substantial, compared to fiber pullout testing	3 Untreated 3 each treated with 120, 240, 320, 800, and 1000 grit size SiC polishing paer
Macro-fiber rod pushout	1. Apply same Surface Treatment to all rods 2. Rod hexagonal composite representative element made with different spacings 3. Apply pushing force on center rod until interface fails, load lessens, and rod is visibly mobile	Pullout interface testing not representative of full composite Effect of similarly treated rods with varying proximity to tested rod can be incorporated Coupons easier and faster to manufacture compared to pullout test	5-10 coupons per various treatment

Manufacture of Rod Pullout Coupons - These experiments consisted of conducting macro-scale fiber pull-out tests where the pre-made carbon fiber rods take the place of the fiber in a tension pull out test as an initial attempt to determine the pultrusion / secondary epoxy interface strengths.

Different degrees of surface roughness were induced using silicon carbide (SiC) metallographic polishing paper of different grit sizes manufactured by Struers [74]. There were 18 coupons: three with no mechanical surface treatment, three abraded with 120 grit size, 220 grit, 320, 800, and 1200. The polishing papers have the following average particles sizes: 120:125 microns, 220:68 microns 320:46 microns, 800:22 microns, and 1200:14 microns. Micrographs of the sizes of these particles are seen below in Figures 38 and 39.

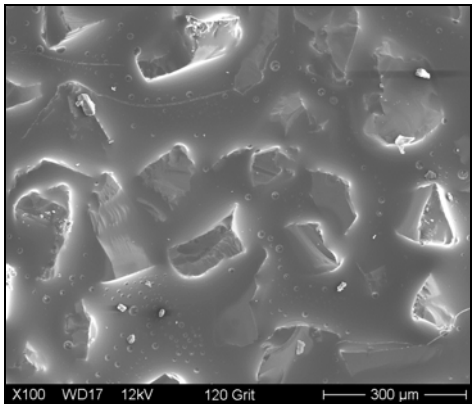

Figure 38: 100x magnification of 120 grit SiC polishing paper

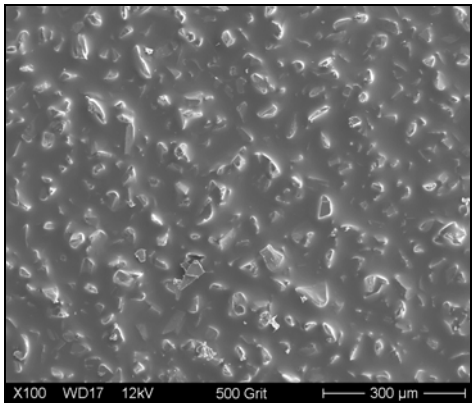

Figure 39: 100x magnification of 500 grit SiC polishing paper

The rods were cleaned with acetone to remove any residue before application of surface treatments. The rods were abraded by securing the rods in a drill press and holding the SiC paper against the rod as it spun at 320 revolutions per minute. The paper was moved up and down the side of the rod at

a low to moderate speed for about 20 seconds. This created a shallow angle cross hatching of grooves and gouges in and across the rod surface. An example of the cross hatching is shown in Figure 40. The carbon/epoxy particulates were washed away with a water rinse and brush scrub, then an ultrasonic bath in de-ionized water for a few minutes. The rods were held in a 1L graduated cylinder for the ultrasonic cleaning.

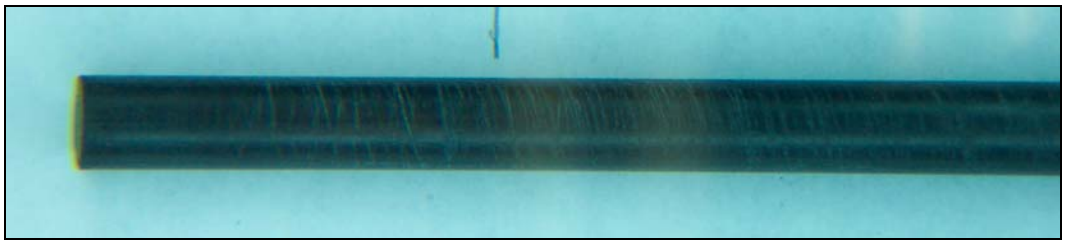

Figure 40: Typical appearance of a surface treatment with SiC paper

Two rectangular molds were made to encase both ends of the rod in epoxy with the middle of the rod exposed. The length of epoxy on the longer end was 76.2 mm long with a depth of 9.525 mm and width of approximately 25.4 mm after cutting the coupons. The shorter end would be 38.1 long x 25.4 x 9.525 mm. Prior pullout tests with just one rod end in resin resulted in premature failure in the free end. Tempered glass was placed over the mold after applying the secondary resin. These molds are seen in Figures 41 and 42.

Custom made flat aluminum grip surfaces with a 6.35 mm diameter notch cut longwise crushed the free rod end before tension could be applied. With the ends of both rods embedded in resin, both ends could be gripped and it did not matter which rod end was pulled out. It was reasoned the shorter side would fail first and all rod surface failure energy would be directed at this side. The smaller

end mold was made separately to encase this end after the crushing problem could not be overcome by other means. The mold was made of 2x4 boards cut lengthwise with the thickness dimension vertical so the thickness of the wood was 9.525 mm. The overall length of the mold was as long as needed to create as many coupons as possible. The mold was held together with gray adhesive tape. This tape did not react with the resin and could be peeled away after infusion. The rod holes were drilled most of the way through with a 6.35 mm drill bit; the last 3.175 mm distance was drilled with a 5.9436 mm bit. This part of the hole fit snugly against the rod and would resist resin leaking through the hole. The wood parts of the mold were bonded to the secondary epoxy instead of the pultruded rod.

Two layers of D155 glass fabric were laid on each side of the rods within each mold. This was done to give the embedding resin some crushing resistance when gripped and tested in an Instron model 8562 [75] and limit the shrinking in the resin rich areas between rods. The innermost fabric layers did contact the rod surface at two locations of unknown area and may have influenced the tests. A schematic of the coupon is shown in Figure 43.

Figure 41: Top down view of the short end mold

Figure 42: Top down view of the long end mold

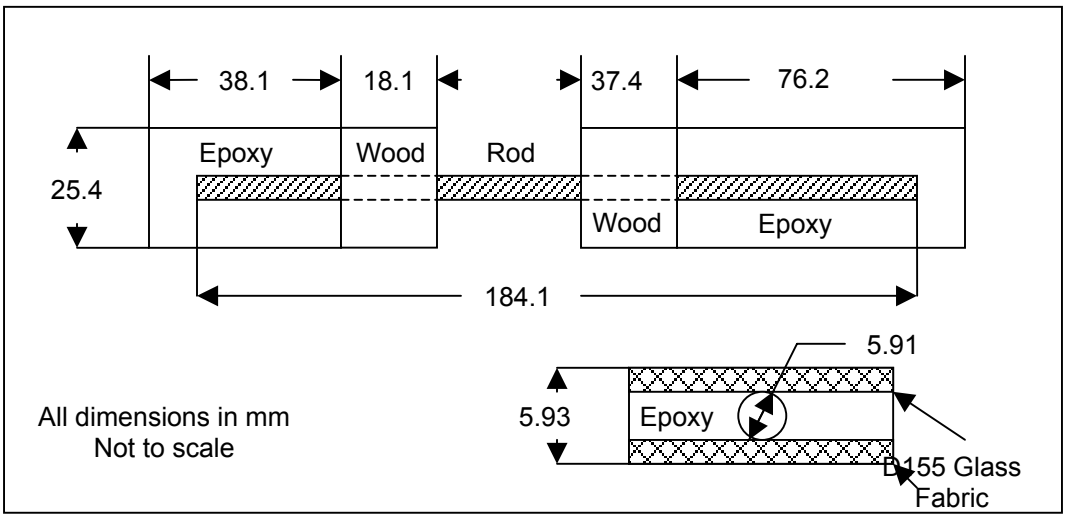

Figure 43: Schematic of a pullout coupon

While the mold was simple in the materials used and construction, extracting the coupons from the mold and smoothing out the coupon surfaces was time-consuming. The resin leaked underneath the mold some during curing, resulting in coupon surface irregularities on the top side against the tempered glass. These coupons surfaces were smoothed by pouring a new batch of the same resin into the irregularities after the original resin had cured overnight at room temperature. After this new resin had cured overnight at room temperature, the entire coupon was post-cured for a few hours at 60^{o}C. This procedure was deemed acceptable as the original curing resin had covered the rod. The post-cured coupons were sanded flat by a belt sander. The embedded lengths of the rods were recorded.

Rod Pullout Test Procedure - Coupons were cut at approximately 25.4 mm width keeping the rod in the middle of the resulting coupon. The coupon was inserted in the Instron model 8562 with the short or long end in the up position

randomly. Figure 44 below is an example of a coupon in the grips for this test. The coupon was then pulled in tension under a displacement control of 1 mm per second. The test was concluded when the rod was visibly slipping as it was pulled out of the coupon. The gripping area did not include any of the wood mold parts attached to the coupon. The maximum load force was recorded from the Instron control panel display. A schematic of the pullout test is shown in Figure 45.

Figure 44: Pre-tested pullout coupon in grips

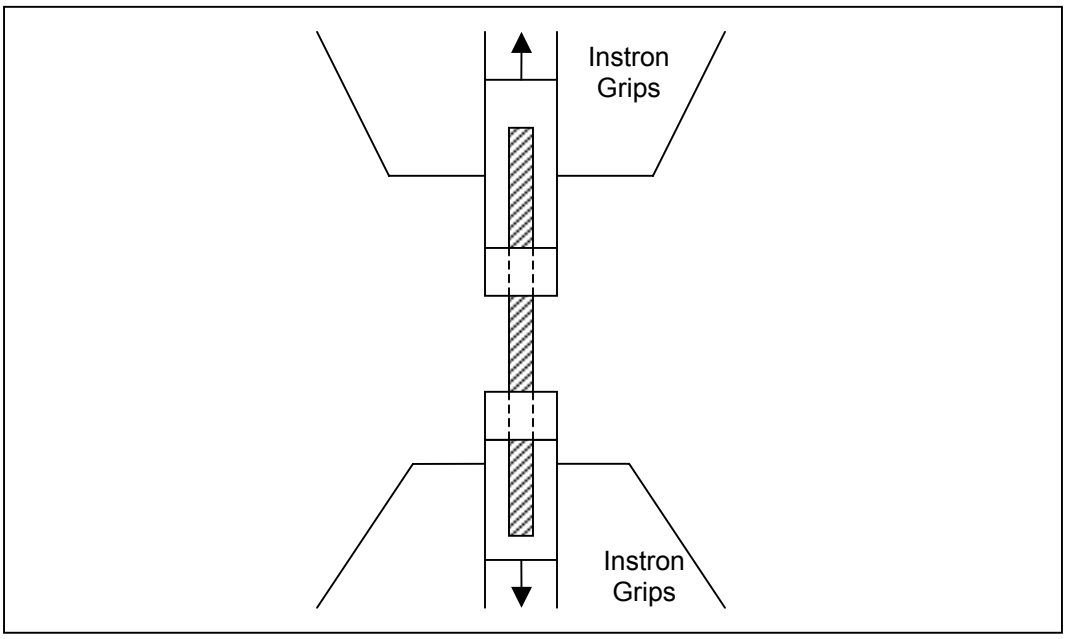

Figure 45: Schematic of pullout test

Manufacture of Rod Pushout Coupons - This type of experiment was conducted as an alternative investigating the pultruded / secondary epoxy interface strengths compared to the pull-out test. Here the effect of the surface finish of a carbon-fiber epoxy insert would be observed in a representative volume element of a larger, pultruded rod based composite. The center rod, surrounded by six other similarly treated rods, would be loaded until the interface failed and rod was pushed out.

For the first three series of pushout coupons: the untreated, abraded, and 'unwashed' nitric acid series, the center rod was cut at 330.20 mm; the surrounding rods were cut at 304.80 mm. For the eroded and 'washed' nitric acid series of pushout coupons, the center rod was cut to 203.2 mm and the surrounding rods at 152.4 mm. The smaller lengths were cut because the larger

lengths yielded more coupons than were actually tested and the limited supply of original rods could be stretched farther.

The mold for the rod packs was 19.05 mm diameter schedule 40 commercial PVC plumbing pipes with 19.05 mm diameter flat end slip caps on the ends. The caps were drilled with a 5.95 mm hole in the center to provide alignment for the center rod. The center rod needed to be aligned vertical for push-out and compression purposes. Not having the rod pack centered in the middle of the PVC tube was deemed unimportant as long as the center rod was vertically straight. Both caps on the mold also had a drilled hole to one side to allow a hose barb for a 6.35 mm silicone tube to allow resin infusion and excess resin and air to escape.

The PVC pipe mold itself was 304.80 mm long for the longer lengths of rod packs; 152.4 mm long for the shorter lengths of rod packs. The slip caps were fitted just enough to engage the center rod into the alignment hole securely and have some space to collect voids that would drift up but could not escape the mold. Plumbers putty was applied around the hose barb threads, the center rod to slip cap interface, and the PVC mold to slip cap interface to prevent resin leakage.

The resin infusion took place with a peristaltic pump through the bottom. The molds were held upright by a stand and finger-type holders. Resin was allowed to flow out the top though the tube and remove as many air bubbles as possible; the resin was drained back into the resin basin. The after test setup is

shown in Figure 46. The molds filled with resin in 10 to 15 minutes at slow pump speeds with an additional 5 minutes to ensure adequate interface wet-out and void escape. The molds were allowed to cure at room temperature then were placed in a convection oven to be post cured for 1-2 days at 70 deg C.

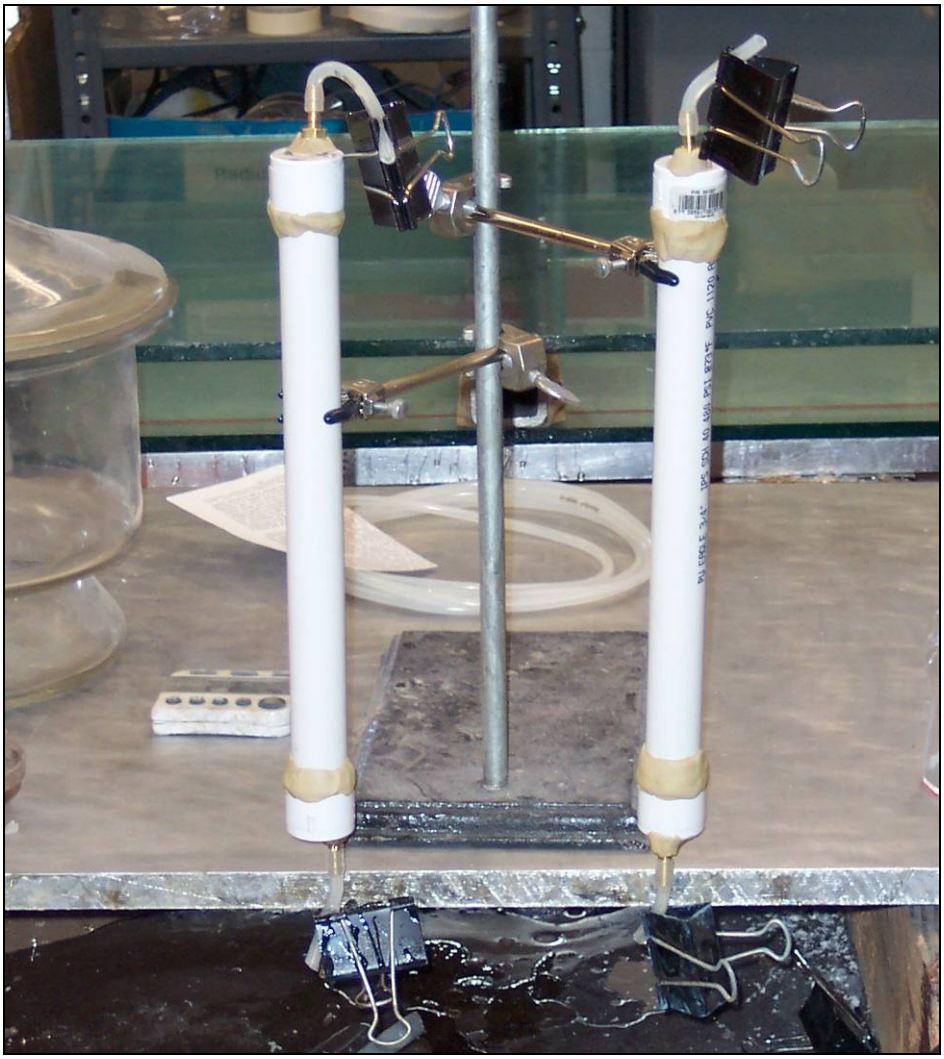

Figure 46: Rod pack infusion setup – after infusion

Two types of spacing between center and surrounding rods were investigated to observe the relationship of the distance between treated rods and determine if it was significant. The first spacing system consisted of a 76.20 mm

by 1.59 mm strip of commercial Teflon thread seal tape was wrapped around the center rod in approximately 50.8 mm intervals starting at 12.7 mm from each end. These ends were left exposed to slip into the alignment holes on the slip caps. This Teflon strip provided spacing from center rod to nearest point of the surrounding rod of approximately 0.127 mm when secured as a rod pack. The second type consisting of orthodontic use rubber bands were placed at the same locations as the Teflon. When secured as a rod pack, the resulting spacing is around 0.762 mm between nearest points on the rods. Small elastic bands bought commercially were wrapped tightly around the outside of the rod pack at the same locations as the spacing elements. The surround rods were spaced from each other to provide a symmetric pattern around the center rod. Gloves were worn throughout the procedure to limit contamination of the treated surfaces. Difficulties in binding the orthodontic (ortho) spaced rod pack were due to the ortho elastic band. This band made it difficult to evenly space the surrounding rods around the center rod and occasionally the elastic band deflected out of position on the center rod. A drop of cyanoacrylate gel between the rod surface and the elastic band was used to secure the band to its position on the center rod. The Teflon spacing arrangement was much easier bundling a rod pack.

During secondary resin infusion for the (ortho) rubber band spacing arrangement, air bubbles tended to collect around the outside elastic band holding the rod pack together because of the small spacing between the mold

surfaces rod pack circumference. Some void collection was seen around the ortho elastic band on the inside of the rod pack as well.

The rod packs were removed by first twisting the hose barbs off with a fitted wrench, then cutting a small slit into the sides of the slip cap. Channel locks then torqued the end cap off. This caused a lot of resin cracking at the ends around the outside of the cured rod pack. Cracks were observed to be limited to around the outside rods and did not extend to the center rod. To avoid this cracking, the PVC mold and caps were removed by using a Dremel tool to cut nearly down to the resin. A screwdriver was placed in the slit and twisted to yield the PVC along the slit and separate the PVC from the resin. The caps were removed in a similar method. The final composite rod pack had the desired smooth surface and slid easily out of the mold.

The resulting cured rod pack in Figure 47 has the following profile with Teflon spacing. Figure 48 is the profile with orthodontic rubber band spacing.

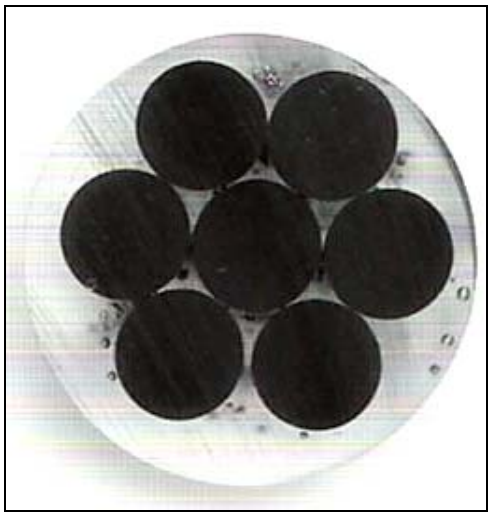

Figure 47: Profile of a generic rod pack coupon with Teflon spacing

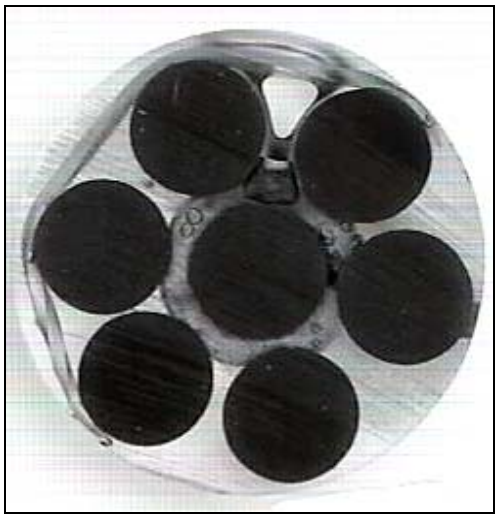

Figure 48: Profile of a generic rod pack coupon with ortho spacing

The mechanical abrasion surface treatment with SiC polishing paper was performed in the same manner described above for the pullout coupons.

For the erosion treatment, the rods were cut at 228.6 mm and fit into a hand-crank fixture that enabled the entire rod surface to be exposed under the erosive stream. These rods were cut down to infusion length after treatment. The rods were rotated by hand at about 0.5 revolutions per second. Three different air stream pressures (2, 3, and 4 kg/cm^2) were selected under which a re-circulating 150 micron spherical glass bead media would flow. Micrographs of the erosive bead medium are shown in Figures 49 and 50. The glass bead media had been used previously and had various unknown contaminates re-circulating during treatment as well as shards of broken glass beads. These pressures had corresponding approximate average particle speeds of 78, 115, and 213 m/s. The particle speeds were determined from a modified spinning disk apparatus described by Ruff and Ives [76]. The nozzle of the bead blasting gun was held away from the rod at about 101.6 to 152.4 mm at a 90 degree angle to the rod surface for maximum erosion capability [64, 65].

Three different exposure times were used with the three pressures. These exposure times were measured in the number of rotations of the rod under the spray. One, two and four rotations were used. Once the number of rotations had been reached under the spray in a local area the nozzle was moved over slightly to a new area of the rod. This action was done to eliminate the difficult to control

variable of pass speed in the coupon manufacture. Seven rods were eroded under each set of conditions.

Figure 49: 16x magnification of glass bead media

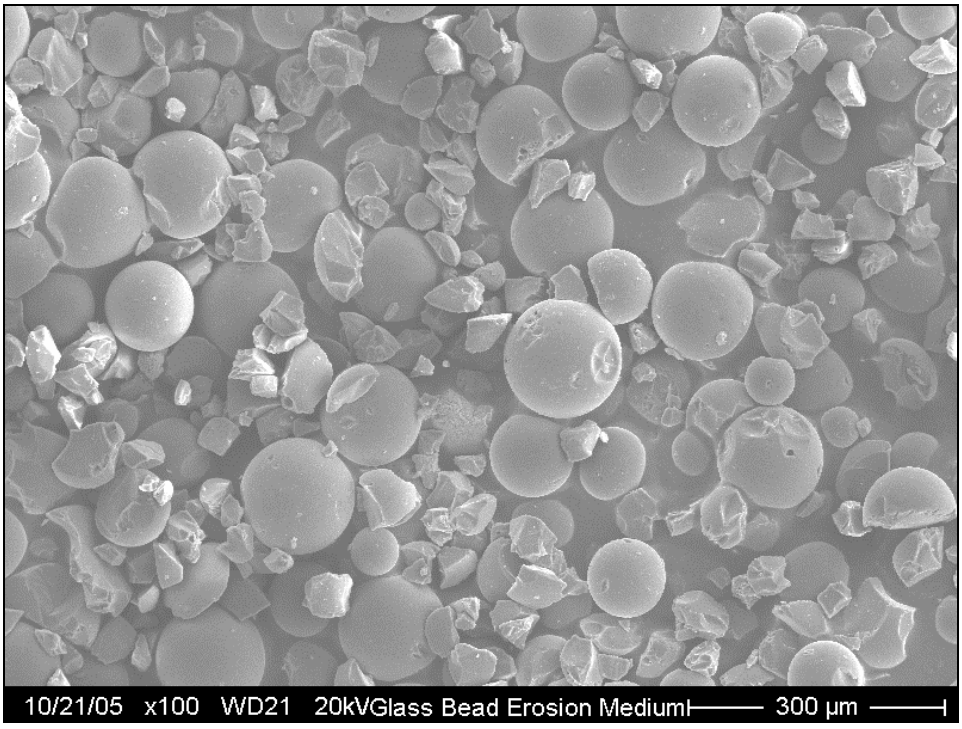

Figure 50: 100x magnification of glass bead media

The typical appearance of an erosion treated rod is shown below in Figure 49 compared to an untreated rod. The eroded rod has a very rough texture and appearance. The rod pack profile of the erosion surface treated rods is similar to Figure 47. Surface profile details are not visible but the eroded rods are all slightly misshapen into ellipses from the circular shape from the treatment.

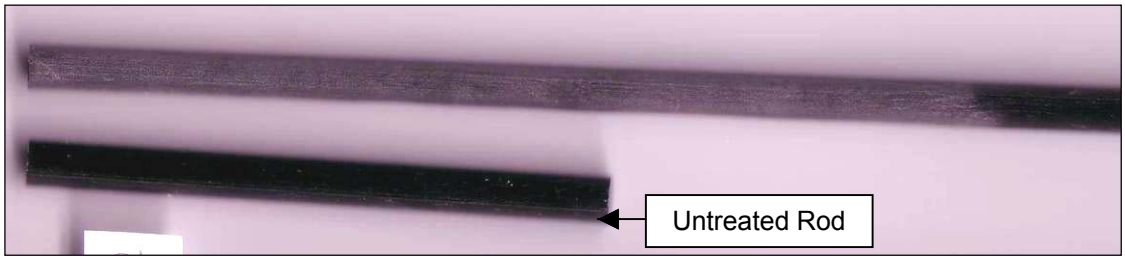

Figure 51: Untreated rod vs. typical erosion surface treatment appearance

For chemical surface treatment, the rods were soaked in nitric acid (HNO_3) at temperatures between 65-75 degrees Celsius for periods of 15, 30, and 60 minutes in the setup seen in Figure 52. Sixty minutes was determined as the point of maximum fiber oxidation; longer times begin to degrade the carbon fiber [70]. The shorter times were investigated with manufacturing process speeds in mind.

The unwashed coupon series was soaked in heated nitric acid for 60 minutes, and washed ultrasonically in distilled water for an arbitrary time of 40 seconds, dried in standing atmosphere for three hours, and bundled into a rod pack for resin infusion. Short test rods receiving no distilled water wash had the same finished appearance when embedded in epoxy compared to rods washed for 40 seconds. To differentiate between other coupon series with more detailed washes, this series was designated ‘unwashed’. These nitric acid treated rods

had a lighter appearance when dried than an untreated rod after the heated acid bath, as if white streaks had been drawn on these surfaces similar to those seen in Figure 53.

Figure 52: Heated nitric acid bath experimental setup

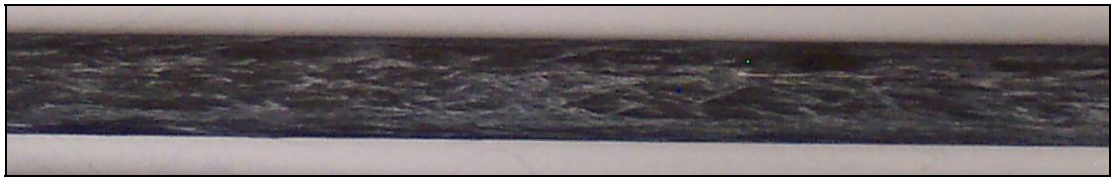

Figure 53: Surface of 60 min HNO_3 treated rod

When infused with secondary epoxy in a rod pack configuration and cured for 4 hours at 70 C, the secondary resin turned a yellow color around the rods and was much more brittle. The resin cracked easily when extracting the rod

pack from the PVC tube as seen in Figure 54 below using applied force that did not cause as much cracking when removing other rod packs. When this rod pack was wet cut for pushout coupons, some coupons fell apart easily from the cutting action.

There was also more widespread porosity in these coupons with unwashed HNO_3 with lots of smaller bubbles around the rod surfaces. The epoxy around the center rod was also black and appeared to be charred as seen in Figure 55 compared to the clear epoxy in non-acid treated coupons seen previously in Figures 47 and 48. This charring was a less dark color in the ortho spaced coupons and concentrated at the rod surfaces as seen in Figure 53. In Teflon spaced coupons, the center rod appears separated from the secondary resin with a thin open space around the rod, probably due to the porosity.

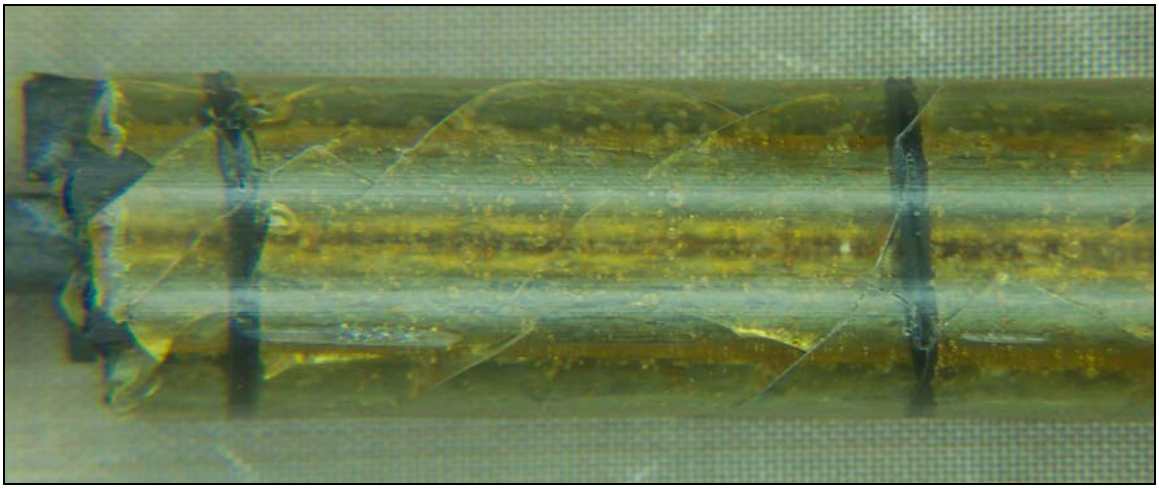

Figure 54: Unwashed HNO_3 treated rod pack after mold extraction

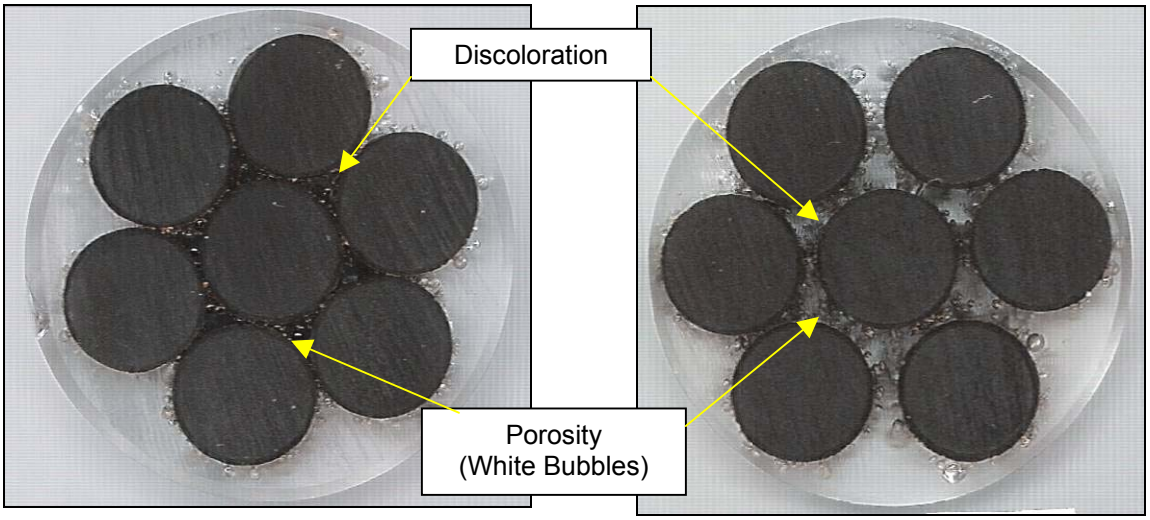

Figure 55: 60 min HNO_3 unwashed rod pack coupon, teflon spacing

Figure 56: 60 min HNO_3 unwashed rod pack coupon, ortho spacing

The charring and discoloring was possibly the effect of nitric acid still present on the rod surfaces. The leftover nitric acid could discolor and embrittle the secondary epoxy molecules in contact with these acid chemical groups. The curing abilities of the secondary epoxy could change when a large quantity of acid is present and concentrated around the rod surfaces. The white residue seen on the pultrusion surface in Figure 53 may be some new chemical compound that causes the porosity, discoloring, and/or brittleness in the secondary epoxy.

Trials with short sections of pultruded rods were done to see what effects acid exposure time and distilled water cleaning had on the secondary resin curing of rods. Partial rod packs were also created to observe the effects in the resin region between the rods. In Figures 57 and 59, the rod(s) with no distilled water cleaning is on the left and the rod with less than one minute water cleaning

is on the right. On and around the surfaces of both rods was a significant amount of bubbles and a yellow discolor as seen from earlier figures.

In Figures 57 and 58 and all HNO_3 only rods, the 'washed' and 'unwashed' rods appear the same, meaning distilled water washed must last more than one minute and possibly longer. Also, the yellow color increased in intensity and distance from the rod in the secondary epoxy as acid exposure time increased. The porosity is already significant even for the short time acid exposure and increases slightly as acid exposure time also increases. The effects appeared the same for coupons that were not post-cured. It was *guessed* that the acid may absorbed into the rod in deep pockets that very short time distilled water cleaning cannot get to. This acid reacts with the secondary epoxy to interfere with the curing process, creating the embrittlement, discoloration and porosity. The exact chemical mechanism is unknown and not explored in this study.

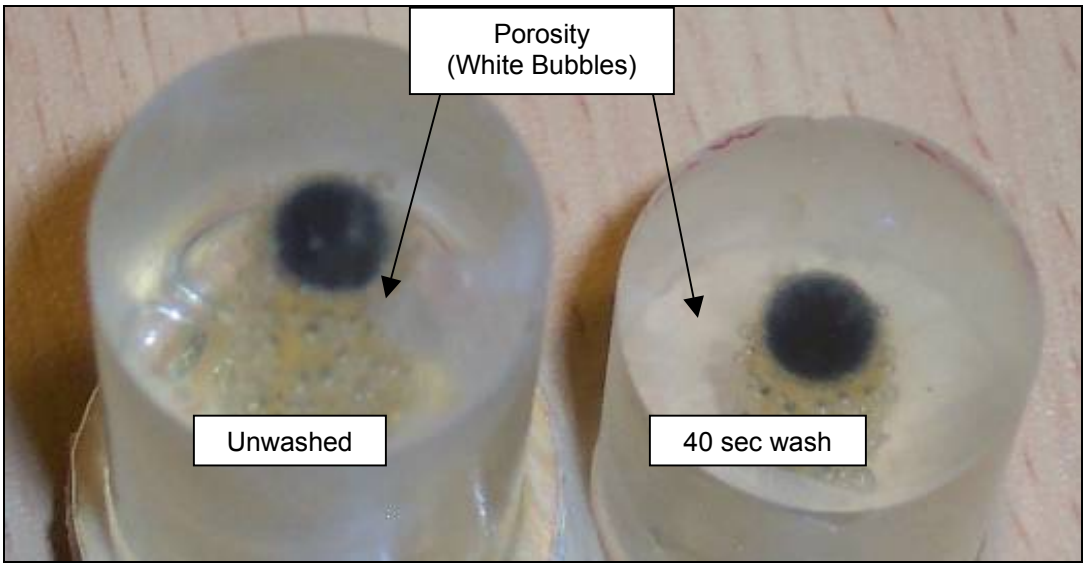

Figure 57: Washed and unwashed 30 min HNO_3 single rod trials

Figure 58: Unwashed 60 min HNO_3 single rod trial

Washed and unwashed 60 min HNO_3 treated rods assembled in a partial rod pack with no spacing between rods in Figure 59 below approach the same porosity and color intensity levels as well as the charring in the resin region between rods seen in Figures 55 and 56.

Figure 59: 60 min HNO_3 partial rod pack trials

With the acid exposure time decided as a key treatment variable, attempts were made to remove as much of the acid as possible from the rods after the acid treatment. Long term attempts such as soak in pH neutral distilled water to dissolve out the acid and short term attempts such as neutralization of the acid with a basic solution were tried.

Again, trials with short rod sections were tried to observe the effectiveness of each proposed solution. The distilled water soak took about five days to reach pH neutrality for the 15, 30, and 60 min HNO_3 only treatments and five days to dry in atmospheric air conditions. When embedded in secondary resin, the porosity was almost eliminated but the yellow discolor remained and the color intensity increased as acid treatment time increased. The resin rich areas between the rods were also clear in all trials. The appearance of the 60 min HNO_3 trial is seen in Figures 60 and 61. The 15 and 30 min trials were all similar in appearance to the Figures below. This distilled water approach, while probably not fit for production environments, was considered a success at neutralizing the leftover nitric acid.

In attempt to speed up the acid neutralization times, after 60 minutes in the heated nitric acid conditions short pultruded rods were placed in 1, 2, and 5 molar concentration solutions of sodium hydroxide (NaOH). After approximately a minute in each solution, the solution around the rods darkens and free carbon fibers and bubbles are observed floating off of the rod surface. It appears as if the rods are ‘bleeding’ and the epoxy holding the rod surface is coming apart and

flowing into the basic solution. This effect is seen in Figure 62 through 64. The higher the molar concentration, the faster the bleeding occurs. Between one and two hours in each solution, the dark color of the solution stabilizes and the bleeding effect seems to stop.

Figure 60: Washed 60 min HNO_3 trial

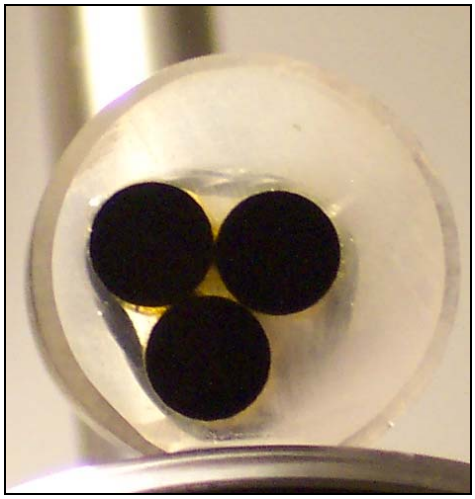

Figure 61: Washed 60 min HNO_3 trial with a clear common region

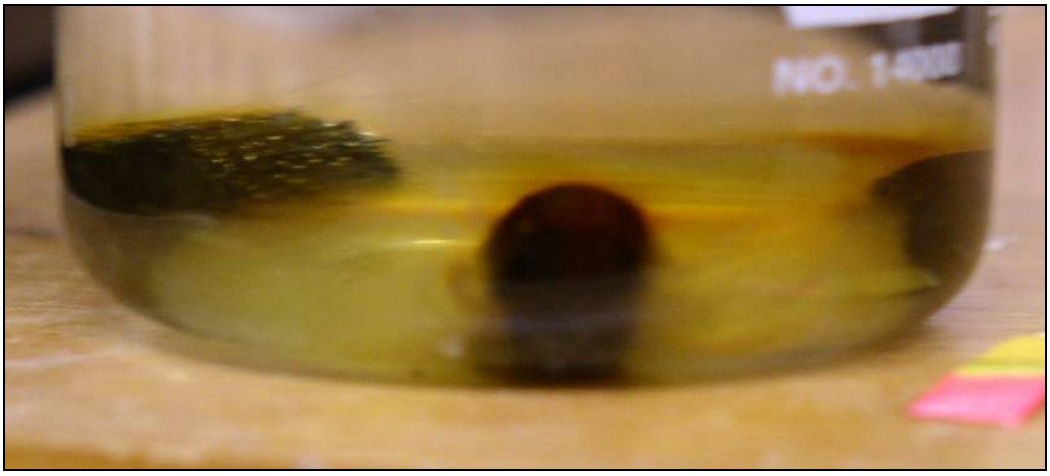

Figure 62: Bleeding effect when acid treated rods are placed in basic pH solution

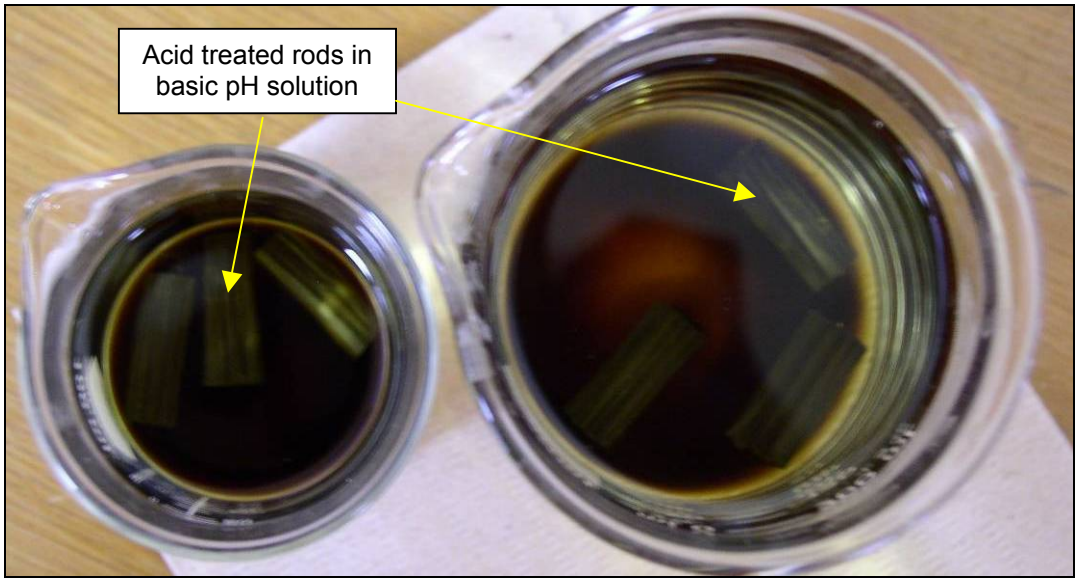

Figure 63: Bleeding effect after several minutes

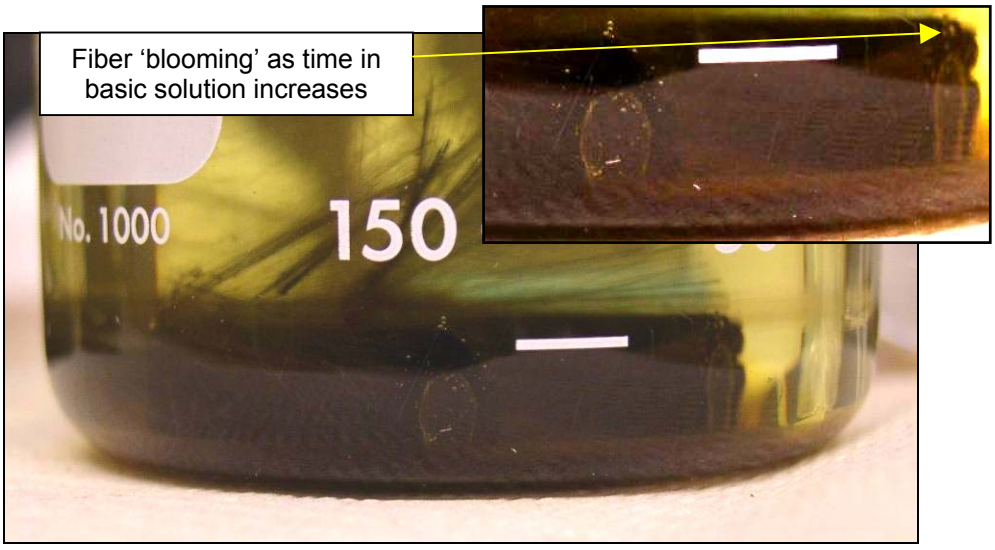

Figure 64: Free carbon fibers on surface of rod in basic solution

After moving these rods into distilled water, the bleeding effect seems to start up again mildly and tapers off. It is possible that the rods are just 'bleeding' epoxy that had not been able to dissolve out into the solution and were doing so in the distilled water. One interesting observation occurred when all NaOH exposed rods were moved into the same large distilled water beaker. The rods

that were just treated in acid already present in the distilled water beaker began to bleed slightly after the NaOH treated rods were placed in the distilled water beaker. It is possible the basic solution adsorbed in these rods migrated over in distilled water solution to the non-NaOH-exposed rods and affected them as well. This interesting effect highlights the powerful interaction between acid and base and cured carbon fiber / epoxy composites and should be investigated further.

Further trials with NaOH solutions suggested that maximum exposure times of 30 seconds or less were enough to treat the surface of the rods. At times greater than 30 seconds, the bleeding effect was visible. Figure 65 below is a picture of three rods after the most severe chemical treatment 60 min HNO_3 / 5M NaOH. The treatment dissolves the epoxy on the surface exposing the fibers down to a small depth. The rods still had a measured diameter of 5.94 mm even though the outer fibers were loose enough to be pulled off by hand. The other treatments involving NaOH solutions had similar rod appearances but slightly fewer exposed fibers at the end of the drying period. Figures 66 and 67 are pictures of short rod trials with the 60 min HNO_3 / 5M NaOH surface treatment. For the 60 min HNO_3 / 1M and 2M NaOH treatments, the yellow color seen on the rod surfaces in earlier figures is still present but with noticeable fading as the NaOH molarity of the surface treatment increases. The 60 min HNO_3 / 1M NaOH treatement produces some loose carbon fibers that are visible on the pultrusion surface that drifted into the resin rich area of the partial rod pack when infused with secondary resin. The resin rich area between the rods remained pretty clear

of fibers when cured. Increasing the concentration of the NaOH solution to 2M produced more loose fibers but the resin rich area still was not completely filled with fibers.

The 5M NaOH exposed rods in Figure 65 are seen embedded in Epon 862 resin in Figures 66 and 67. The loose fibers have filled in the resin rich area completely and have spread away from the rod somewhat. Some of the fibers on the outer surface are now aligned in off axis and out-of-plane directions. The yellow discoloring had disappeared on this trial and little porosity could be seen. After 30 seconds in the various NaOH solutions, the rods were placed in beakers of distilled water to monitor the pH of the water and observe how much acid had been neutralized. This method was considered a success as all beakers with NaOH exposed rods had water pH neutral levels in a slightly faster time than the HNO_3 only counterparts, but this was on the order of a less than a day.

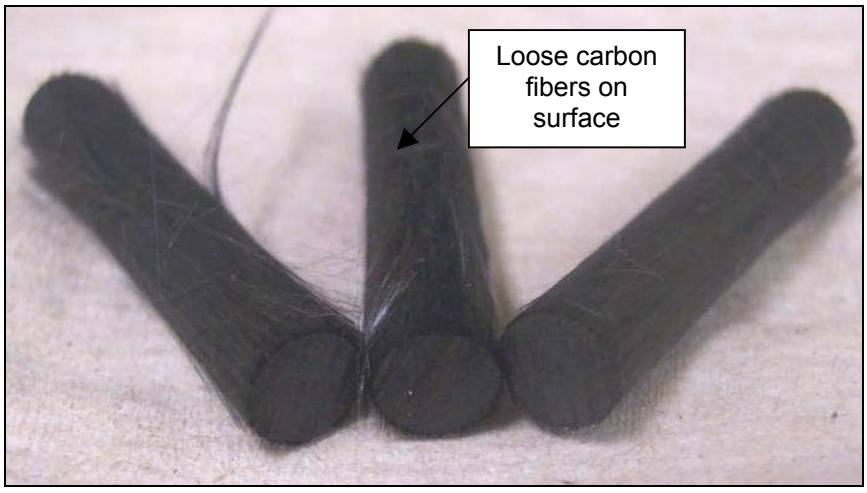

Figure 65: Rods after 30 seconds in 5M NaOH, five days distilled H_2O soak, and atmosphere drying

Figure 66: 60 min / 5M rod pack trial

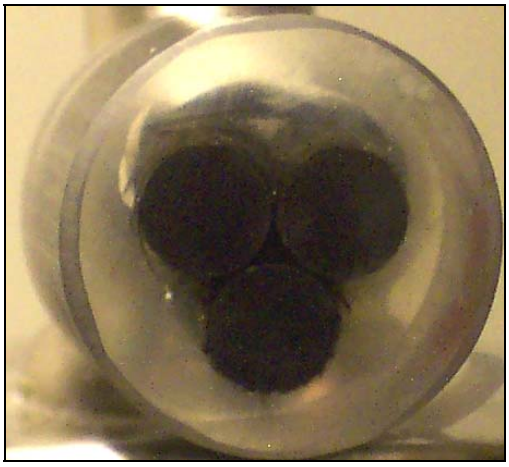

Figure 67: 60 min / 5M trial with filled in resin rich area

The 15, 30, and 60 minute nitric acid only treatment series were soaked in heated nitric acid as previously described for the designated time. All treated rods of these series were then submersed in different beakers of distilled water in an attempt to dissolve out as much nitric acid as possible from the rods before resin infusion. The pH of each beaker of water was monitored and replaced frequently until the water pH reached neutral for several monitoring periods. This procedure lasted 4 to 5 days with shorter nitric acid exposure times needing less time for the pH rising to neutral. The rods were then removed from the water and dried in standing atmosphere for 15 days before bundling into a rod pack for infusion and testing. The appearances of the nitric acid only treated rods after drying are shown in Figures 68 through 70.

Figure 68: 15 min HNO_3 treated rod surfaces before secondary epoxy infusion

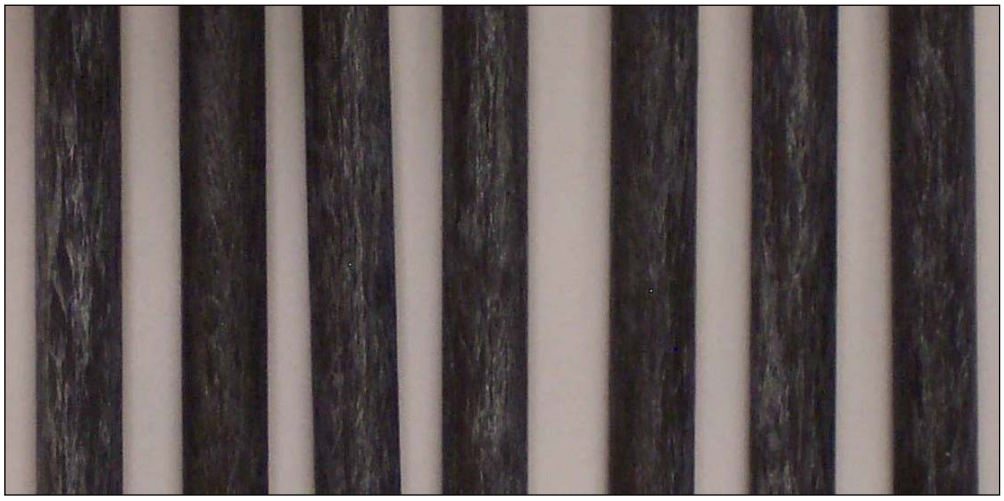

Figure 69: 30 min HNO_3 treated rod surfaces before secondary epoxy infusion

As the nitric acid exposure time increases, the amount of white discoloration on the surfaces of the rods also increases. Free carbon fibers are now visible on the surfaces of the 60 min HNO_3 treated rods and are easily moved out of alignment by handling.

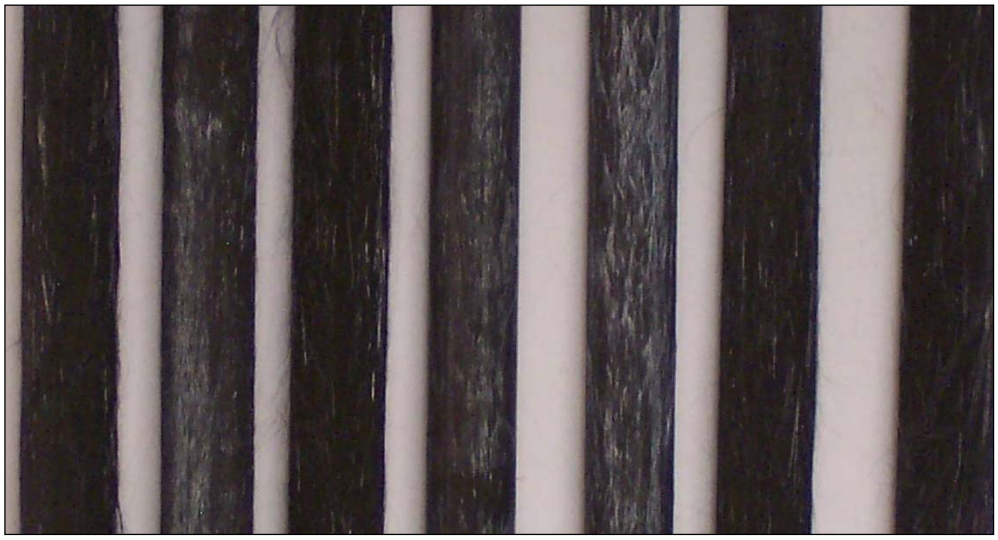

Figure 70: 60 min HNO_3 treated rod surfaces before secondary epoxy infusion

For the test coupon series of HNO_3 plus NaOH exposed rods, the NaOH treatment time was limited to 15-20 seconds in each respective molar concentration. The NaOH exposure was performed in a 1000 mL graduated cylinder over a magnetic mixing plate. The magnetic stirring rod mixed the solution at a medium-high speed. This mixing was performed to allow the NaOH solution to interact with the entire surface of the rod quickly, rather than having an uneven exposure profile when the rod is dipped in. This mixing speed caused the loose fibers to leave the unidirectional orientation and entangle around the surface and freed the smaller loose fibers. This entanglement is seen in Figures 71 through 73 and was exacerbated by the handling of the rods throughout the procedure.

After exposure, the rods were submersed in distilled water and the pH monitored as described previously. The pH of these waters reached neutral in 4 to 5 days, slightly faster than the nitric acid treated only rods. The rods were then

removed and dried in standing atmosphere for 15 days before bundling and infusion. The appearances of the treated rods after drying are shown in Figures 71 through 73.

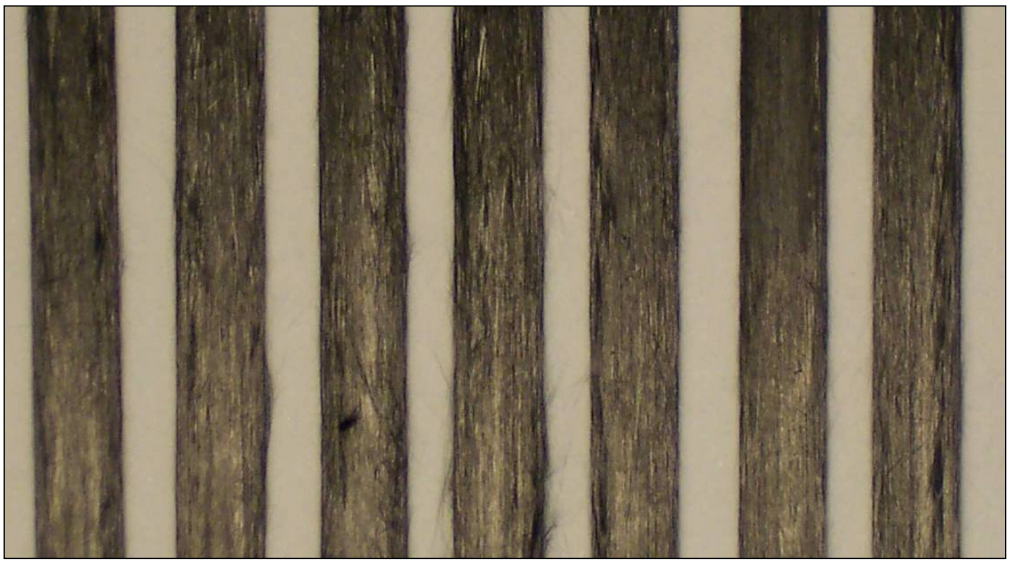

Figure 71: 60 min HNO_3 / 20 sec 1M NaOH treated rod surfaces before secondary epoxy infusion

Figure 72: 60 min HNO_3 / 20 sec 2M NaOH treated rod surfaces before secondary epoxy infusion

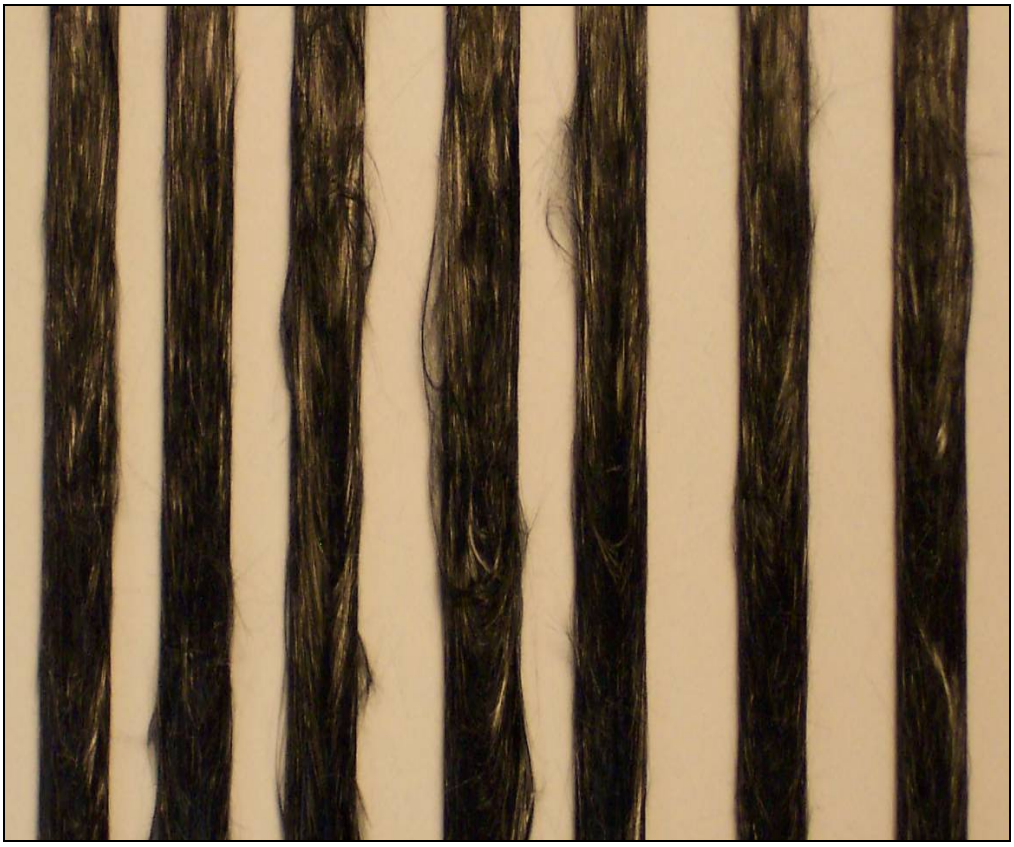

Figure 73: 60 min HNO_3 / 20 sec 5M NaOH treated rod surfaces before secondary epoxy infusion

The rod pack profiles of the 60 min HNO_3, 1M, 2M, and 5M NaOH chemical treatments are shown below in Figures 74 through 77. The 15 and 30 min HNO_3 rod pack profiles look similar to the untreated rod pack shown in Figure 47. The resin rich area between the rods is starting to fill up with loose carbon fibers as the chemical treatment becomes more aggressive. In the 5M NaOH treatment in Figure 77, this region is almost completely filled with fibers.

Figure 74: Washed 60 min HNO_3 rod pack profile

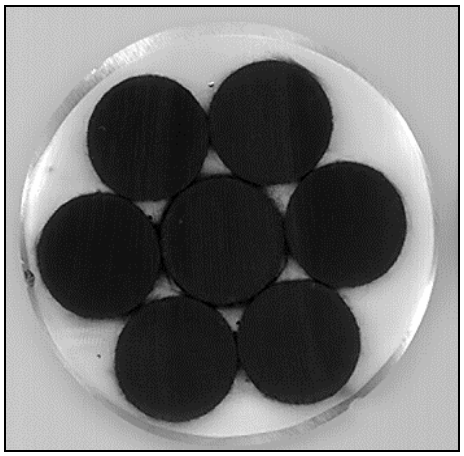

Figure 75: Washed 60 min HNO_3 / 1M NaOH rod pack profile

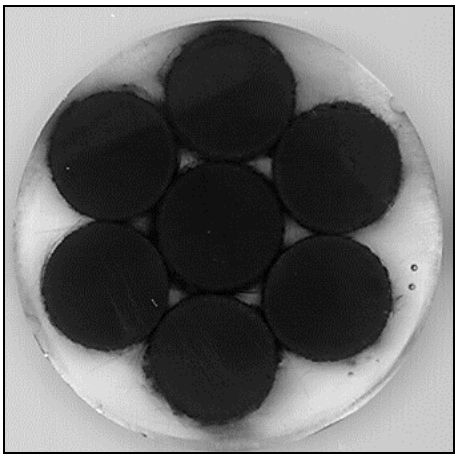

Figure 76: Washed 60 min HNO_3 / 2M NaOH rod pack profile

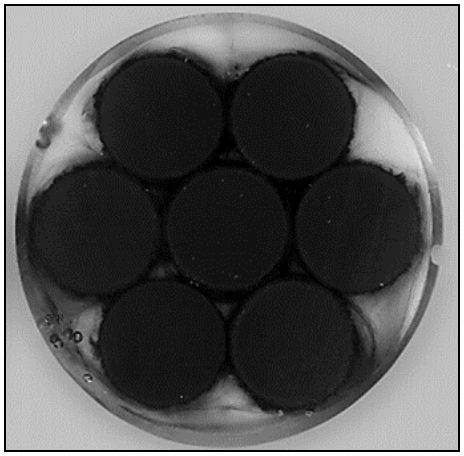

Figure 77: Washed 60 min HNO_3 / 5M NaOH rod pack coupon

The cured rod pack cylinders were wet cut with a diamond saw blade into approximately 12.7 mm thick coupons for pushout testing. The cylinders were cut at the Teflon or ortho band spacing marks to remove as much of the spacing material as possible to minimize its debonding effects during testing. Both sides of all the pushout coupons were wet polished. This was done to get the coupon flat against the aluminum pushout plate and to align the axis of the center rod

with the pushout rod to produce as close to shear loading on the center rod interface as possible.

Rod Pushout Test Procedure - The center rod of the rod pack was directly loaded by 6.35 mm hardened tool steel rod. The loading end was trimmed with a lathe to 5.92 mm for a length of 12.4 mm from one end. The edges on the loading rod surface contacting the rod were slightly chamfered in a polishing wheel. This made the loading rod surface diameter just under the average diameter of the center pultruded rod. The rod pack coupon was secured to a 5.59 mm thick aluminum plate by a drop of cyanoacrylate gel. The center pultruded rod was positioned above a 6.35 mm hole in the plate where the rod could be pushed through without contacting the aluminum.

The test apparatus was the Instron 8562 machine mentioned previously. The loading rod was held by grips designed for holding 6.35 mm to 12.7 mm rounds. The loading rate was 0.01 mm per minute. The loading force was monitored using the Instron control panel. The test was stopped when the load dropped off considerably and an audible pop sound occurred also at this time. The maximum load was recorded from the Instron display. The pushout test setup is shown schematically in Figure 78 with a picture of the in-situ test in Figure 79.

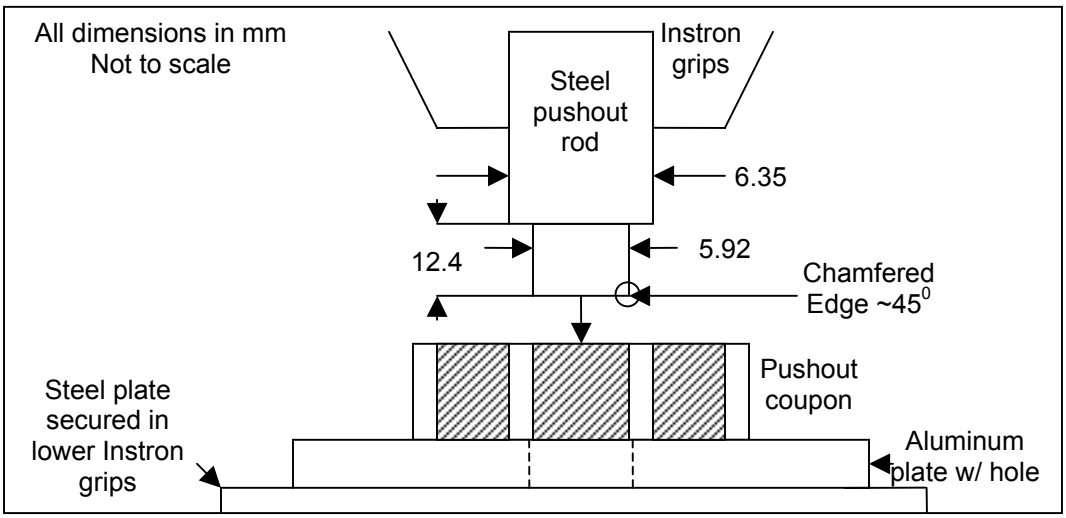

Figure 78: Schematic of pushout test

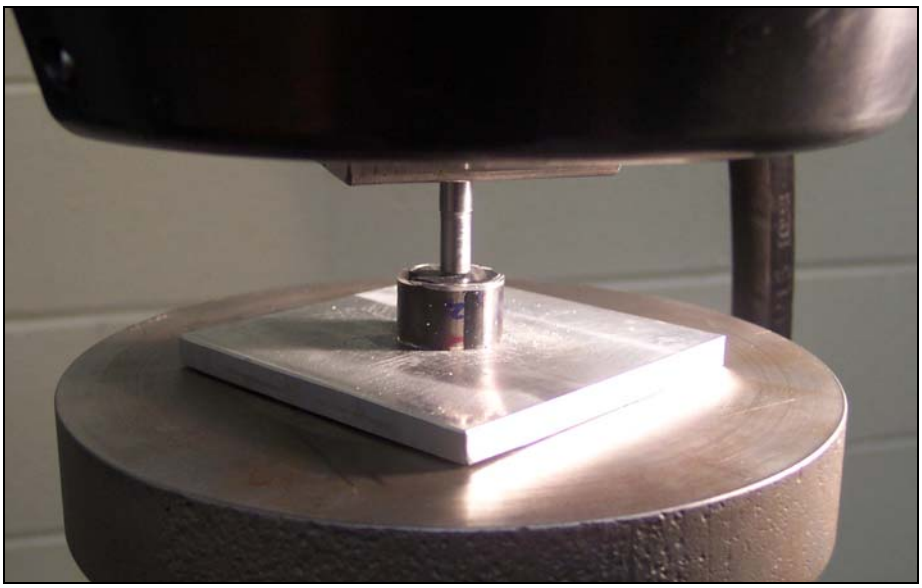

Figure 79: Picture of pushout test setup

Miscellaneous Tests and Coupons

Miscellaneous tests were performed on the other pultrusions provided. Table 4 below is a summery of these tests conducted in this thesis with a short

statement of the motivation behind each test, the information desired from each test and the number of coupons that will be used.

Table 4: Miscellaneous Test Matrix

Test Type	Test Description	Motivation	Possible Information Gained	Number of Coupons
3-pt. Rod Bending	Single pultruded rod simply supported over span, slowly loaded in center until rod fails	Bending deformation of interest in wind turbine blade structures	Determine performance of individual elements in 3-pt. bending loading, observe failure	5
Rod and Flat Short Beam Shear	Small span coupon loaded in center to produce shear failure opposed to bending failure	Determining shear strength of pultrusions, how well they hold together under severe local loads	Shear strength of pultrusions, observe failure locations and crack propagation, understand how pultrusions will hold together if severe deformation seen	5 Flat 5 Rod
Flat Coupon Tension	Flat coupon under tensile force	Find upper bounds on performance in tension	Modulus, break stress and strain-to-failure of small cross sectional area of flat pultrusion	4 Panex Fiber based 4 Toray fiber based
Fiber Volume Fraction Determination	Chemical and Digital Methods to confirm fiber content	Confirm high fiber volume fractions within pultrusion, discover fiber details under magnification	Possible differences in performance between Panex and Toray pultrusions may be explained by constituency	3 rod 3 Panex 19-tow 3 Panex 20-tow 3 Toray

Three-point Bending Tests - Single rods were tested in three-point bending to gauge their elastic modulus in bending. The test apparatus had a support span of 127 mm between contact points. The loading nose was a steel pin with a diameter of 19.05 mm. The support pins were of the same material and diameter. The testing was done with a displacement rate of one mm per second.

The loading was stopped when the maximum load was no longer supported. The maximum load and displacements were recorded off of the Instron 8562 control panel.

Short Beam Shear (SBS)Tests - Single rod and flat coupons were tested in a custom short beam shear apparatus. The rod coupons were 33.02 mm in length. The flat coupons were 12.7 mm by 25.4 mm. The support apparatus for the flat coupons was steel with a support span of 9.61 mm. The support apparatus for the rod coupons was steel with a support span of 19.10 mm. The rod short beam shear support had a 5 mm long by 0.42 mm deep rounded groove in the center that limited the rod movement before loading. Two loading noses were also used. Both were made from steel stock; one contacted coupons of both type on the exterior of a 6.45 mm diameter, 12.65 mm wide half cylinder, the other contacted rod coupons on the inside of a 6.65 mm diameter notch drilled out of a steel flat 3 mm thick by 31 mm wide. This notch was filed into a saddle shape. This loading nose was used for the rod coupons because the other nose was too large for the diameter of the coupon and caused splitting in the rod coupons that traversed the length of the coupon. These fixtures and setups can be seen in Figures 80-82.

The displacement loading rate for both types of coupons was one mm per second. The testing was stopped when the maximum load was no longer supported and/or severe damage was seen in the coupon. The maximum load and displacement were recorded off the Instron 8562 control panel.

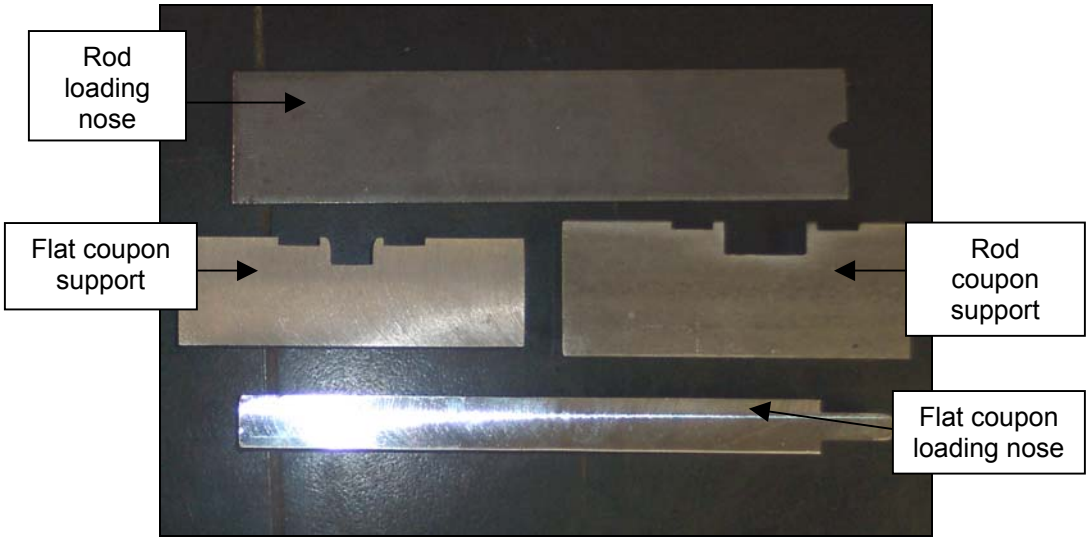

Figure 80: Test equipment used in short beam shear tests

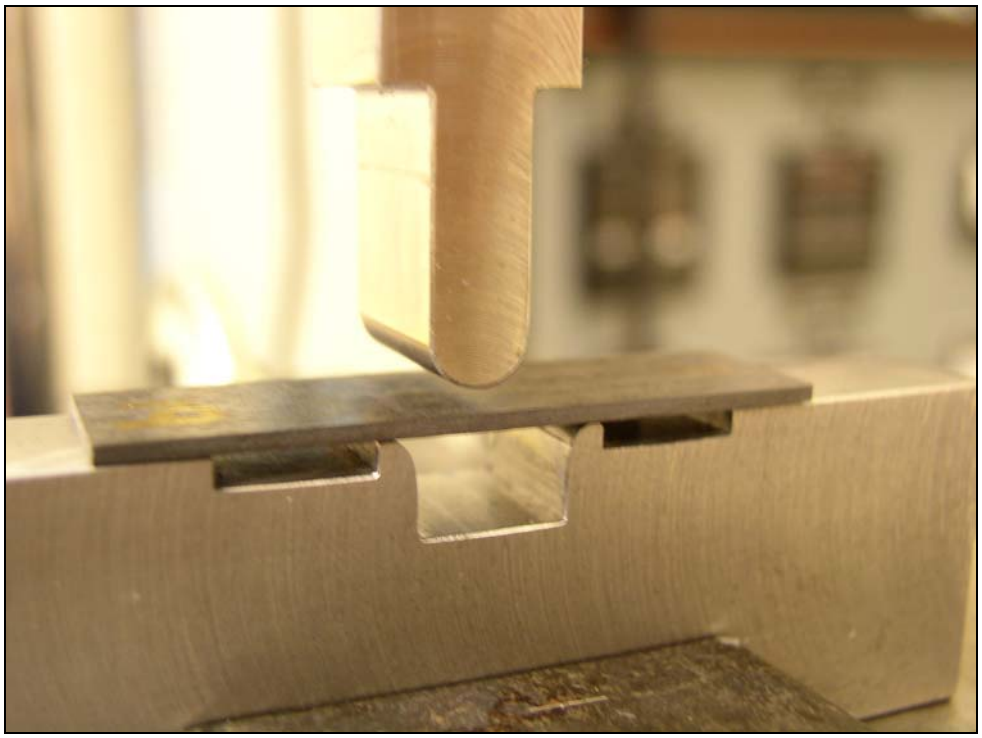

Figure 81: SBS coupon about to undergo loading

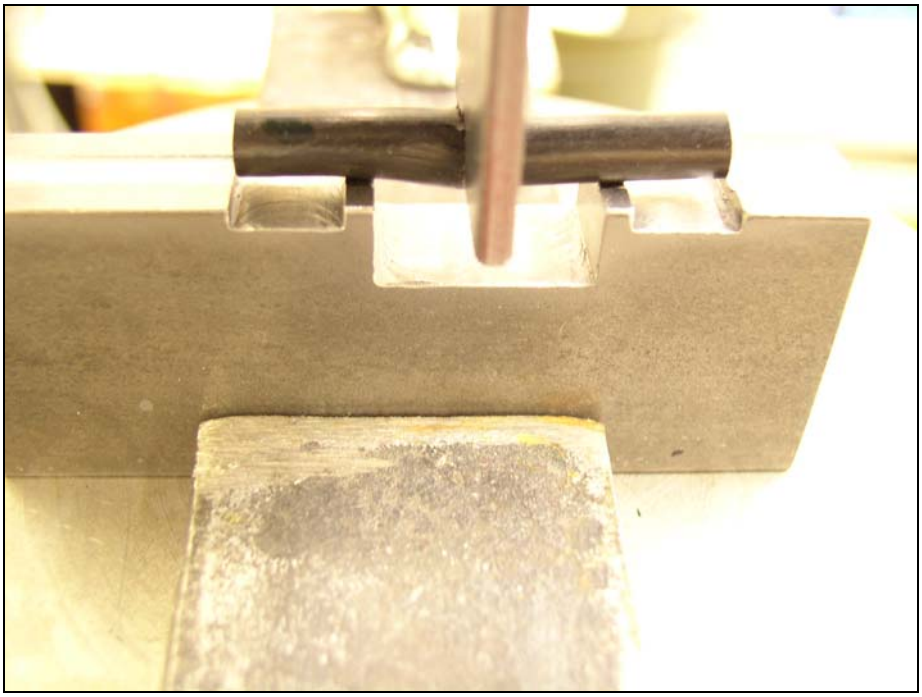

Figure 82: Rod SBS coupon undergoing testing

Flat Pultrusion Tension Tests - The carbon fiber flats were tested in tension for break load and stress, and strain to failure. Because the flats were so wide, wider than the grips that were to hold them, the flats were cut in half lengthwise to a width of 2.5 cm and length of 25 cm. Four coupons each were made from the 19 tow Panex and the Toray fiber reinforced flats. Because they were so thin, the coupons were tabbed by 1.59 x 63.50 x 25.40 mm fiberglass with adhesive epoxy on both sides of either end. Two Panex and one Toray coupon were fitted with strain gages.

Fiber Volume Fraction Determination - The fiber volume fractions of the pultruded composites used in this study were estimated digitally with the following technique. Small sections of the pultruded composites were encased in

polycarbonate appropriate face upwards. The coupons were wet polished to expose the tops of the fibers for better imaging. The polishing schedule consisted of 1200 grit (14 micron average particle size) SiC polishing paper applied with water for a couple minutes, then 2400 grit (10 micron) SiC paper with water for a few minutes. The finishing polish used was a 0.3 micron alumina particle solution.

Images of the fiber ends in the flats and the rods were taken by a JEOL Model 6100 Scanning Electron Microscope (SEM) as part of the MSU Physics Department Image and Chemical Analysis Laboratory (ICAL) [77]. Two pictures of the surface with fiber ends facing the camera were taken of each coupon. These files were imported into Adobe Photoshop [78] and the color was altered to achieve a color disparity between fiber / matrix boundary. A thin line was drawn around the edge of each fiber and save as a separate file. This file was imported into a SigmaScan program [79] and the pixels inside the drawn circles were counted and recorded. The total pixels of the file were counted as well. The fiber pixels were divided by the total pixels to get the fiber volume fraction.

The results of all these tests are reported and discussed in the next chapter.

RESULTS AND DISCUSSION

Results and related discussion of the experiments performed in this study are presented in this chapter. The fiber volume fractions of the carbon fiber pultrusions used in this study is addressed first. Next, the results of the surface treatments are shown in before and after interface testing SEM pictures along with results of the interface tests. Finally, the test results on the individual pultrusions are reported and discussed. Complete data for every test as well as additional SEM pictures of the surface treatments are listed in Appendices A-H.

Carbon Fiber Volume Fraction of Pultruded Shapes

Images of the fiber ends in the flats and the rods used in this study were taken by a JEOL Model 6100 Scanning Electron Microscope (SEM) as part of the MSU Physics Department Image and Chemical Analysis Laboratory (ICAL) [77]. These pictures were then imported into Adobe Photoshop 6 software. The process of determining the fiber volume fraction (FVF) entails counting the pixels that make up each fiber and dividing that number by the total pixels within the photograph. A high resolution photograph taken by the SEM in an uncompressed file format creates a very large number of pixels. With such a large number of pixels, the overall fiber volume error will be low if care is taken in determining which pixels constitute a fiber or matrix material.

Two SEM pictures were taken of each of the following, a Panex fiber based rod, a Panex 19 tow sample, and a Toray fiber sample, each at 1000x

magnification. One photomicrograph of each is shown in Figures 83-85 with a blown up section by scale marker of each picture for a closer view of the individual fiber profiles. The sample size of each Figure is approximately 84 by 111 microns. The .tiff file was imported into Photoshop and the color adjusted to make the fiber boundaries stand out. A layer on top of this image was created for a thin ring about 3 pixels wide was drawn on each fiber in a magnified view. When each fiber boundary was traced, this layer was imported into SigmaScan software. The software counted all pixels outside the drawn boundaries. The total pixels within the image were also determined. The fiber pixels were easily found and divided by the total pixels as determined by SigmaScan. The average total pixels for a SEM file were about four million. As only two pictures were taken of each sample, the accuracy of this method is decent. The results are listed in Table 5.

Table 5: Fiber Volume Fractions from SEM and SigmaScan Determination

Rod A	61.9%	Panex 19 tow A	69.0%	Toray A	71.0%
Rod B	75.9%	Panex 19 tow B	73.9%	Toray B	68.4%
Average Rod FVF	68.9%	Average Panex 19 tow FVF	71.5%	Average Toray FVF	69.7%

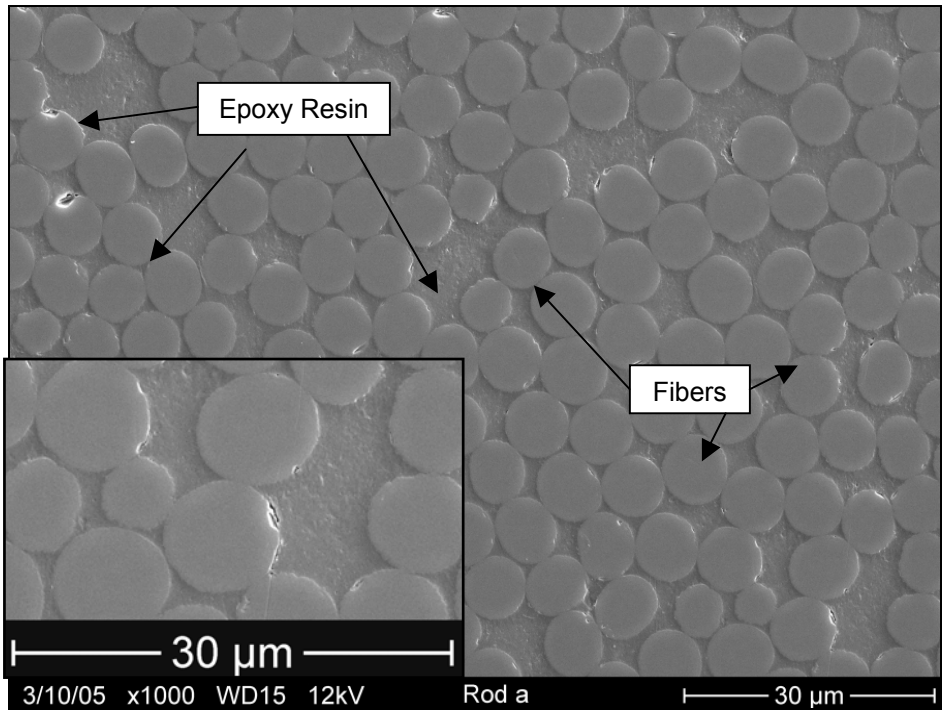

Figure 83: SEM micrograph of the fiber ends in a Panex fiber rod with a magnified view of the fiber profiles

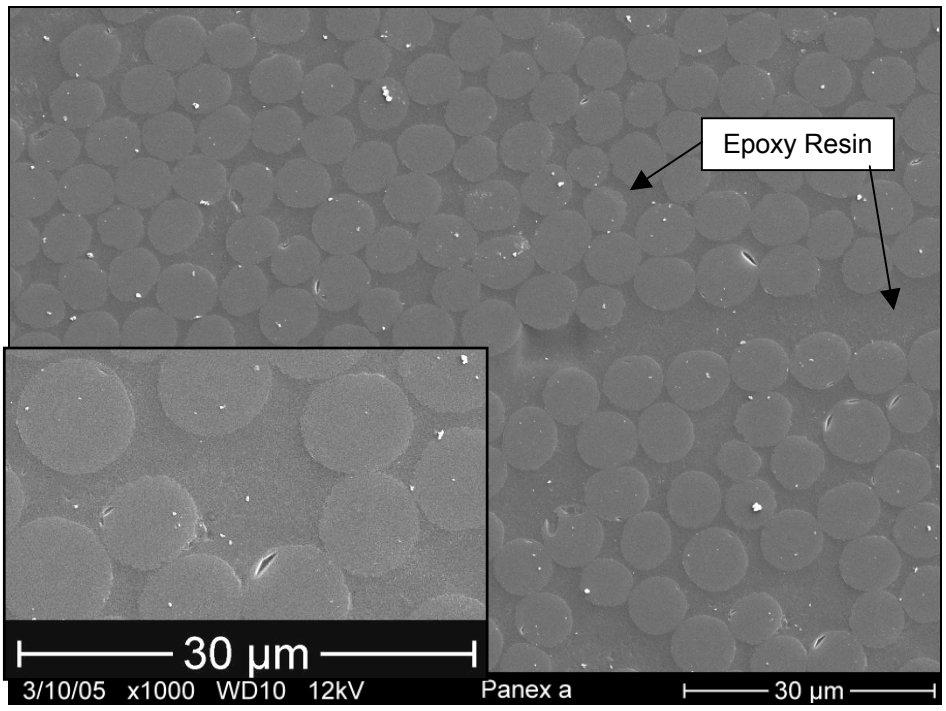

Figure 84: SEM micrograph of the fiber ends in a Panex 19 tow flat with a magnified view of the fiber profiles

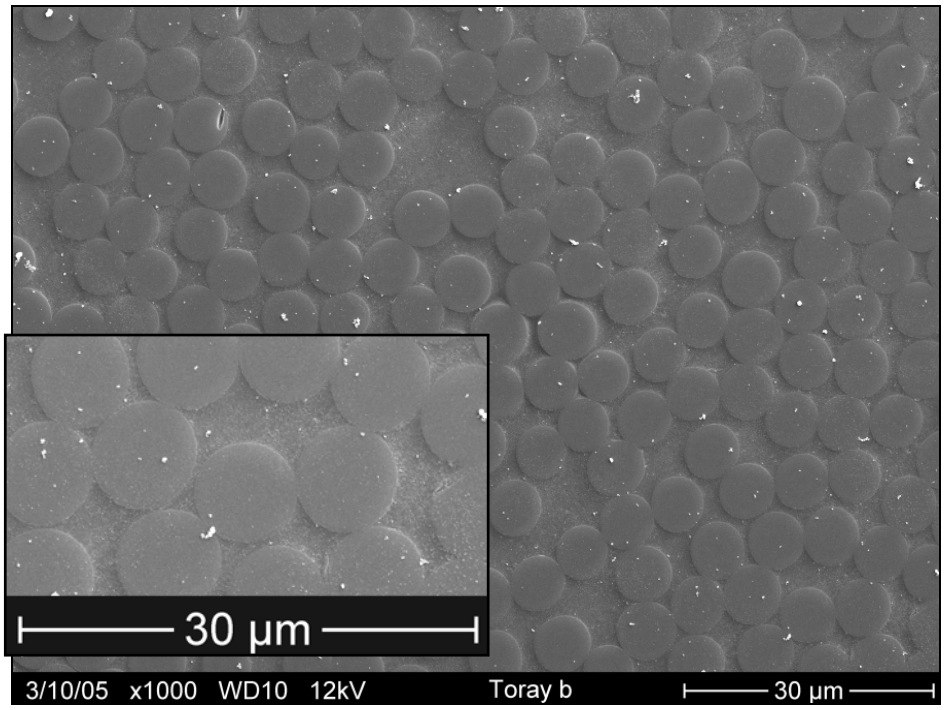

Figure 85: SEM micrograph of fiber ends in a Toray flat with a magnified view of the fiber profiles

As seen from the micrographs and the insets of the Panex based rod and flat in Figures 83 and 84, many of the fibers are slightly misshapen from the circular shape, have variable sizes and appear to have many striations running lengthwise on the fiber making a jagged fiber circumference profile compared to the smoother, much more uniformly circular shape and size Toray fibers as seen in Figure 85. Internal defects and porosity also appear within the Panex fibers that seem less present in the Toray fibers. It is possible that apparent defects and striations seen in the Panex fibers were due to the polishing process for image preparation. If the Toray fibers appear undamaged with the same process, this might suggest that the Panex fibers are less cohesive as a carbon fiber unit and weaker on some levels of performance than the Toray fibers.

Rod Pullout Test Results and Discussion

Pre-test Images and Discussion

SEM micrographs of the pre-tested untreated surface of a pultruded rod before embedding in Epon 862 epoxy are seen in Figures 86 and 87. The only surface preparation done with an untreated rod was an acetone wipe to remove organic contaminates received from handling. The patches of fibers running in off-rod axis directions could be part of the surfacing veil wrapped around the rod tows to assist in the forming process through the shaping die as described in section 2.1 [22]. Another explanation could be that these diagonal fibers are fibers from a carbon fiber tow that came loose from the shearing action between the forming die sidewall and curing epoxy. These loose fibers then were fixed in off-axis directions once the epoxy cured.

From these two figures, some small degree of inherent surface roughness and variability in an untreated pultruded surface is seen due to the fiber veil and/or incompletely epoxy infused areas. These areas are small and shallow but may be enough to help interface strength by providing sites for mechanical interlocking with overlaid secondary resin without the added costs of improvements and surface and fiber damage the other surface treatments cause. These fibers may have become exposed by a few methods. Partially cured, viscous epoxy was sheared away from the outer fibers during the shape forming process, and neighboring epoxy was too viscous to spread to these uncovered

areas. Or rough handling procedures broke off pieces of epoxy that didn't bond well to the outer carbon fibers.

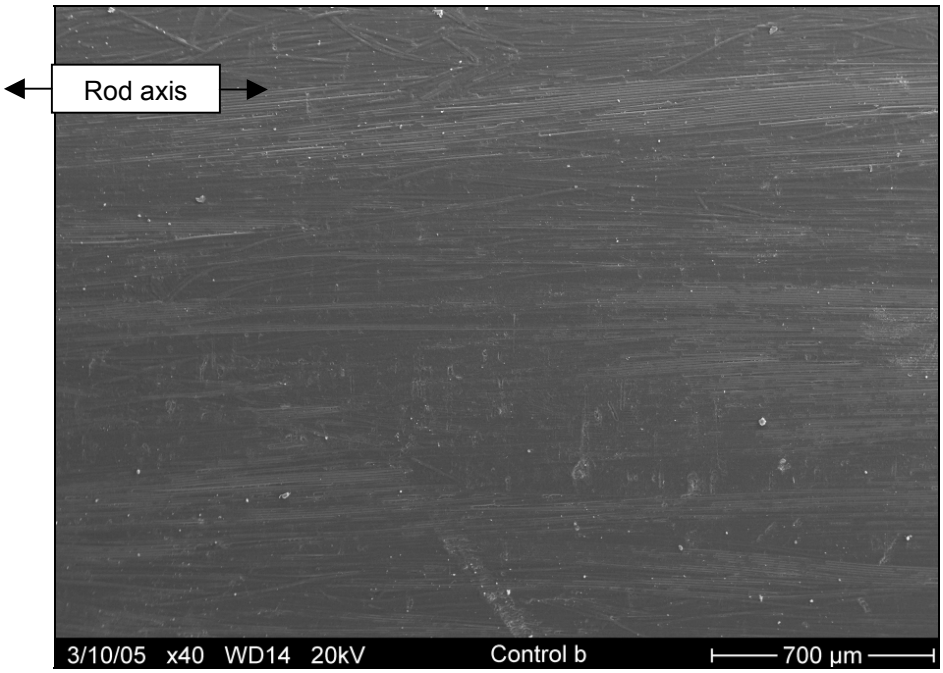

Figure 86: SEM micrograph of a pre-tested untreated rod surface

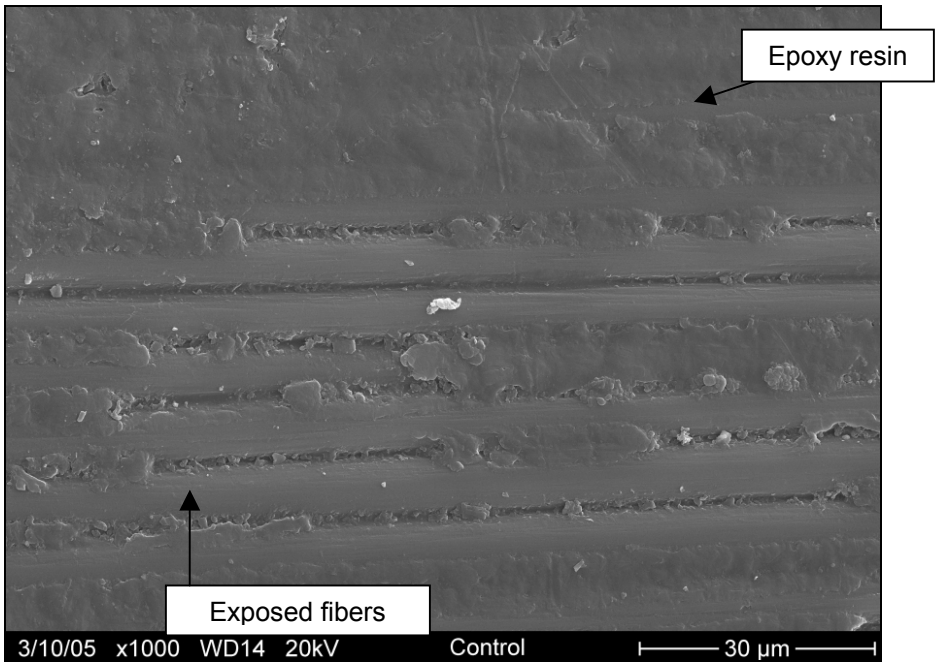

Figure 87: Closer view of the pre-tested untreated rod surface

The following SEM surface images in Figures 88 through 95 are the result of each SiC abrasive surface treatment on a rod *before* embedding in Epon 862. In the coarser grade abrasive treatments (SiC 120 and 220) in Figures 88-91, many deep grooves can be seen in a shallow cross-hatch pattern. As the SiC particles get finer, the overall amount of grooves created slightly increases. The groove quantity also depends on how long the abrasive paper is held against the rod to be treated, but all rod abrasive treatments were approximately equal for application time. The depth of these grooves also decreases as the particles get smaller as well.

In the SiC 120 abrasion treatment in Figure 89, the particles actually break the fibers nearest the surface when a groove is created and some bits of epoxy are still appear loosely attached to some newly exposed fibers. The groove created is fairly wide compared to other abrasive treatments as well as very jagged and some broken surface fibers stick out into the groove. Some of the underlying fibers also appear to be slightly damaged on the exposed surface. Any epoxy allowed to flow over this surface is likely to find many places to form deep mechanical interlocks when forming an interface on this abraded rod.

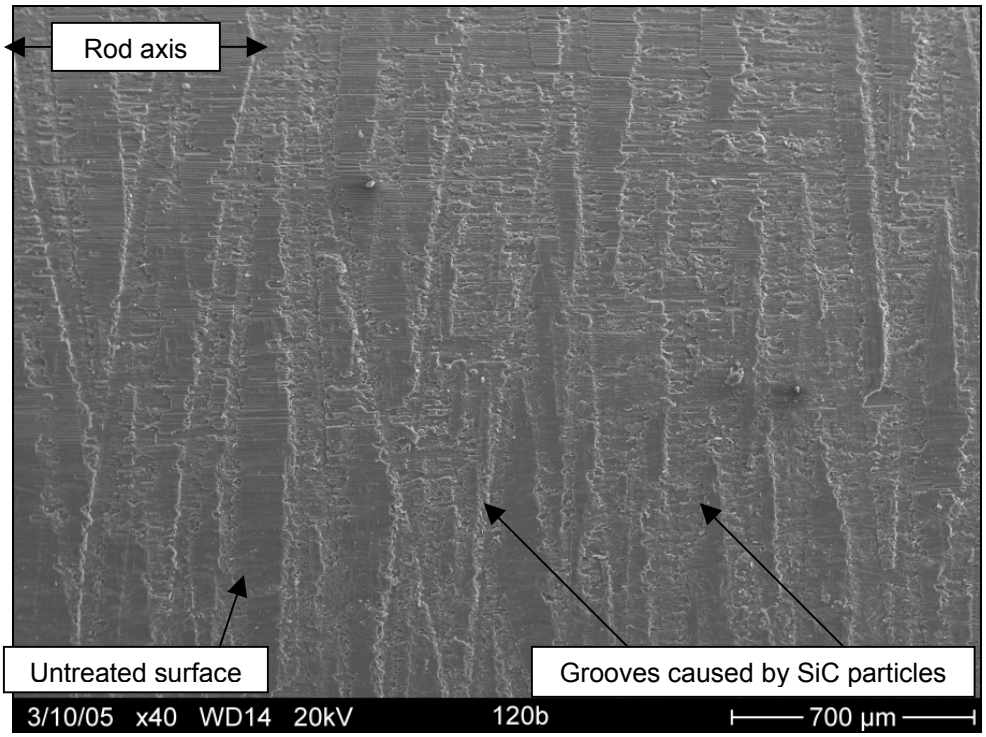

Figure 88: SEM micrograph of a pre-tested rod surface treated with SiC 120 abrasion paper

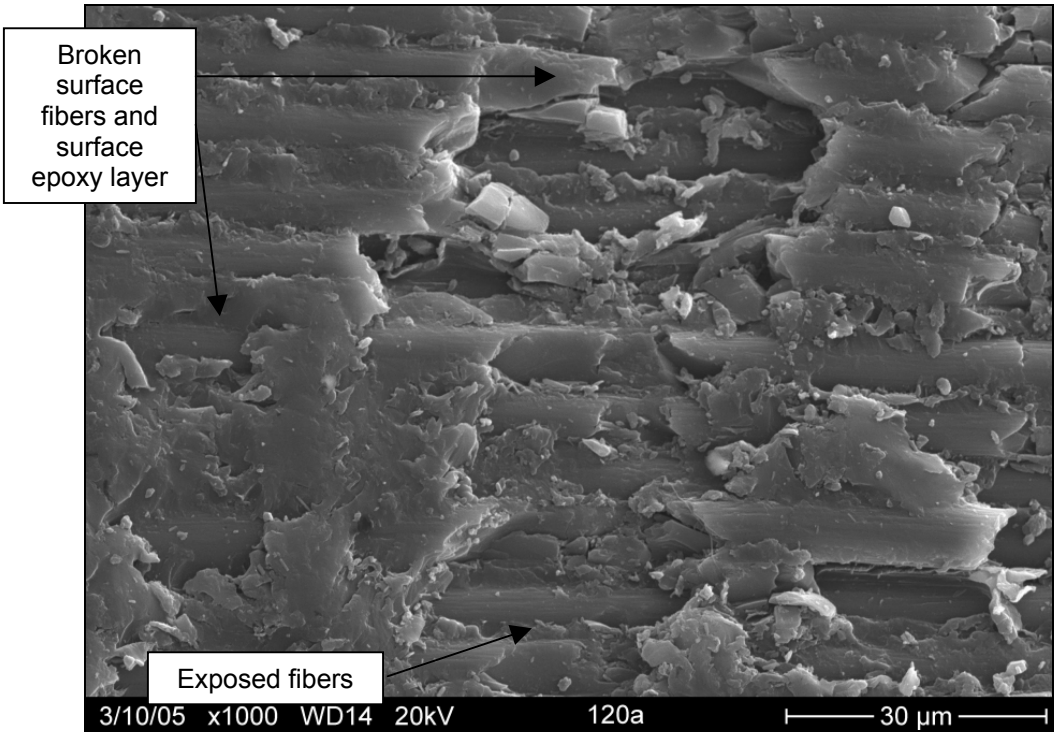

Figure 89: Closer view of a pre-tested surface treated SiC 120

In the SiC 220 abrasion treatment in Figures 90 and 91, the groove appears a little less jagged and narrower and the loosely bonded epoxy particles are smaller and appear to collect on the exposed surfaces of the underlying fibers. The newly exposed fibers also did not appear to be as damaged as the fibers abraded with the 120 grit paper. This bonus will possibly boost the performance capability of the pultrusion as reinforcement compared to the 120 grit abrasion. The new surfaces created by this SiC 220 treatment appear like they could provide as good physical interlocking sites as SiC 120 abrasion for another layer of structural epoxy infusion.

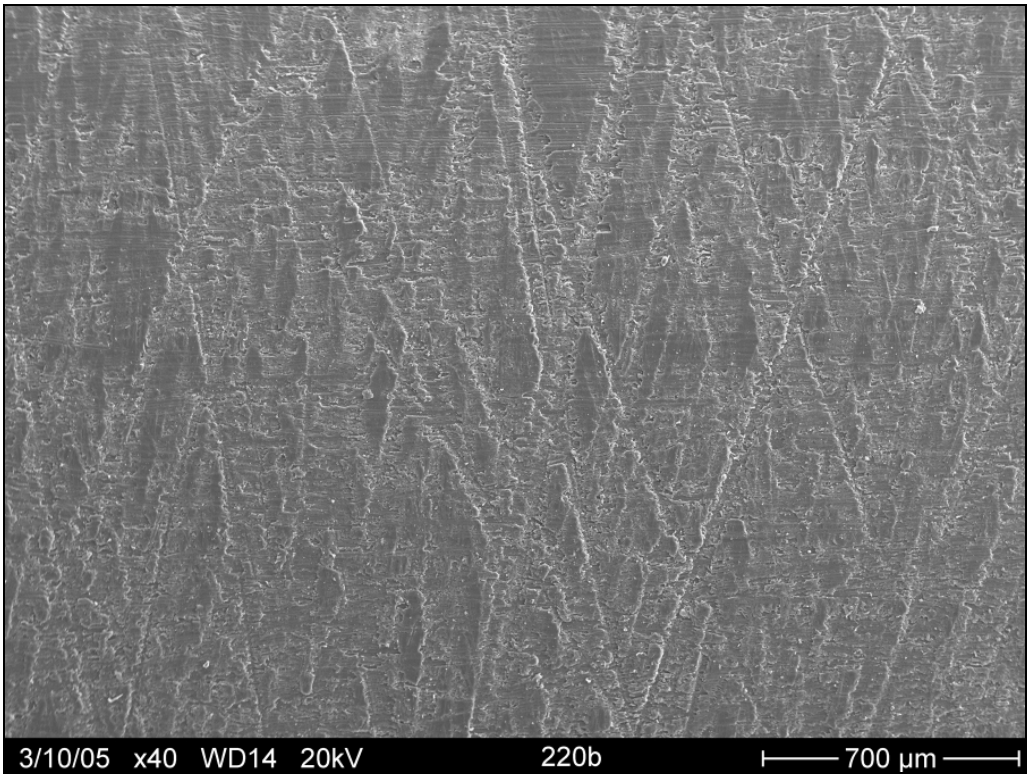

Figure 90: SEM micrograph of a pre-tested rod surface treated with SiC 220 abrasive paper

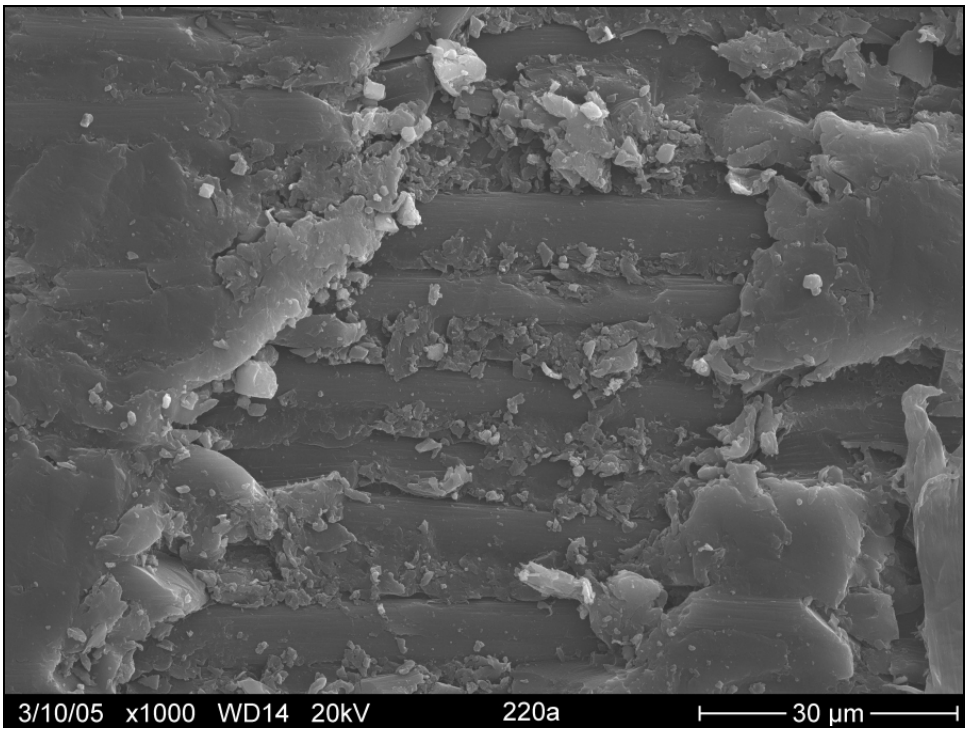

Figure 91: Closer view of a pre-tested surface treated SiC 220

In the SiC 320 grit size treatment, the grooves on the surface below in Figure 92 are still pronounced and their paths are still traceable in the figure, but they do not appear to be as deep as the previous two treatments. In Figure 93, the groove edge appears to be cleaner; more epoxy is left intact on the newly exposed fiber surface and there are few loosely attached particles of epoxy on the new surface. The newly exposed rods under the surface layer do not appear to have any damage inflicted on their surfaces as well. It is not seen in Figure 93, but the outer layers of carbon fibers are broken due to the treatment but many fragments are still present and sticking out into the new surfaces.

Approximately an equal amount of grooves are created in the SiC 120, 220, and 320 grit treatment, but as the abrasive particle size gets smaller, the

grooves become narrower and cleaner, the quantity of overall fiber damage lessens, and the newly exposed fibers have more of the original resin still bonded to them. Judging by appearance alone, mechanical interlocking appears it would be less effective in the SiC 320 treatment due to the smaller grooves created. However, in practice the 320 treatment could be more effective due to less loose surface epoxy fragments for the secondary epoxy to bond with. The large quantity of relatively undamaged exposed fibers is beneficial for the pultrusion performance in service.

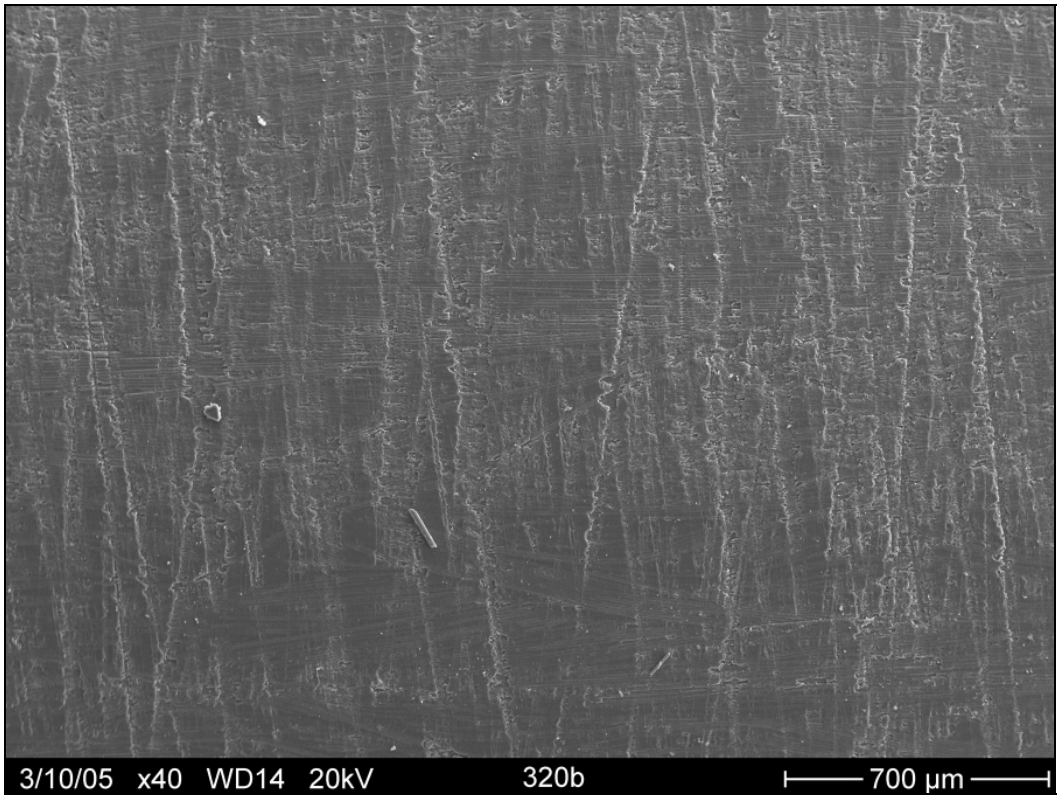

Figure 92: SEM micrograph of a pre-tested rod surface treated with SiC 320 paper

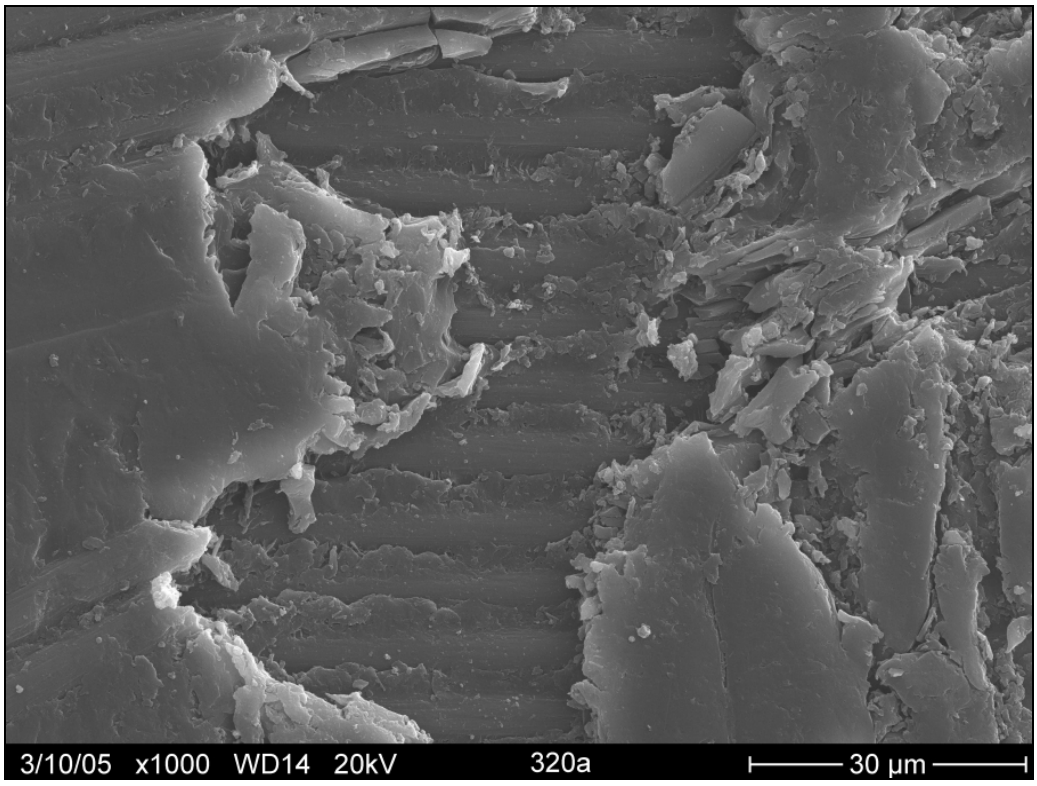

Figure 93: Closer view of a pre-tested SiC 320 treated surface

For the SiC 800 grit size surface treatments in Figures 94 and 95, the grooves are less visible under magnification and appear to barely scratch the rod surface. In Figure 95, the SiC 800 grit surface treatment may have taken off the outer layer of epoxy and just exposed the outer surface fibers as well as damage them slightly, but this is difficult to determine in this figure as there is no obvious groove. The rods treated with the SiC 1200 grit abrasive paper had similar surface appearances to the SiC 800 grit treated rods. The SiC 1200 grit surface SEM images are in Appendix G.

Mechanical bonding would appear to be less successful for these two abrasion treatments compared to the previous three. The appearances of these treated rods look like the untreated rods in many respects. The shallow grooves

created could provide greater interface strength than the untreated rod due to the small contribution of the increased surface roughness, but not much of an increase. An option to increase the surface roughness for abrasion treatments with grit sizes 800 or larger is to increase the exposure time to increase the number of grooves. One benefit to the larger SiC grit size treatments is that for a small increase in interface shear stress resistance, the pultrusion is much less damaged after the treatment, and its maximum load carrying capacity is still mostly intact.

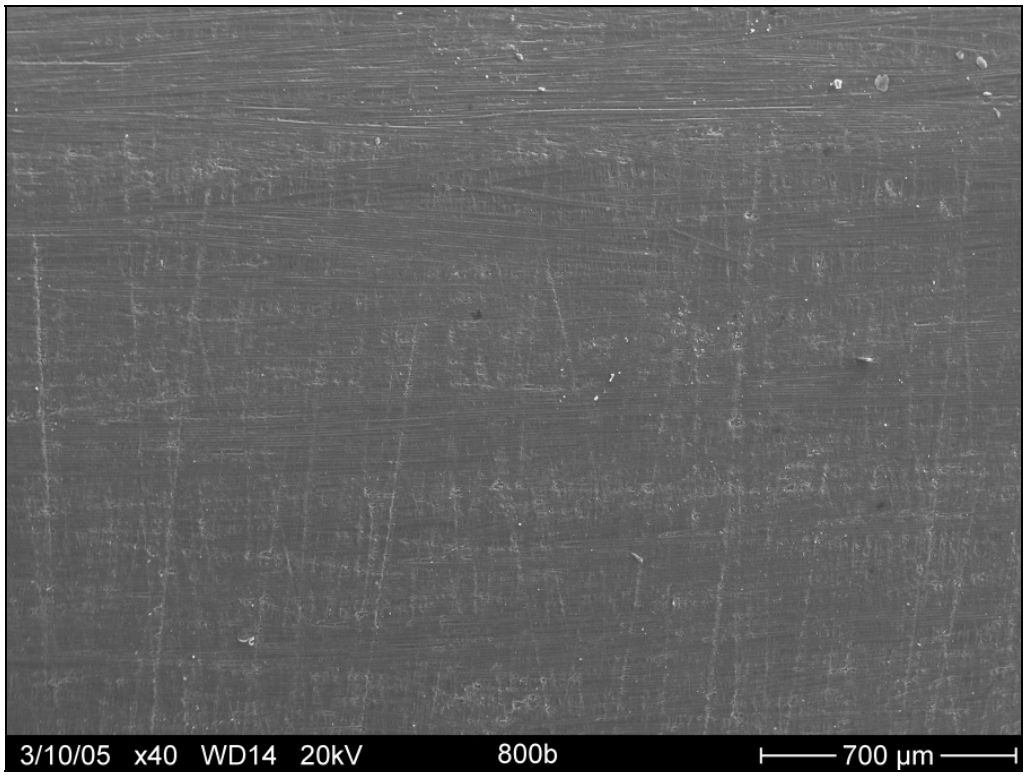

Figure 94: SEM micrograph of a pre-tested rod surface treated with SiC 800 abrasive paper

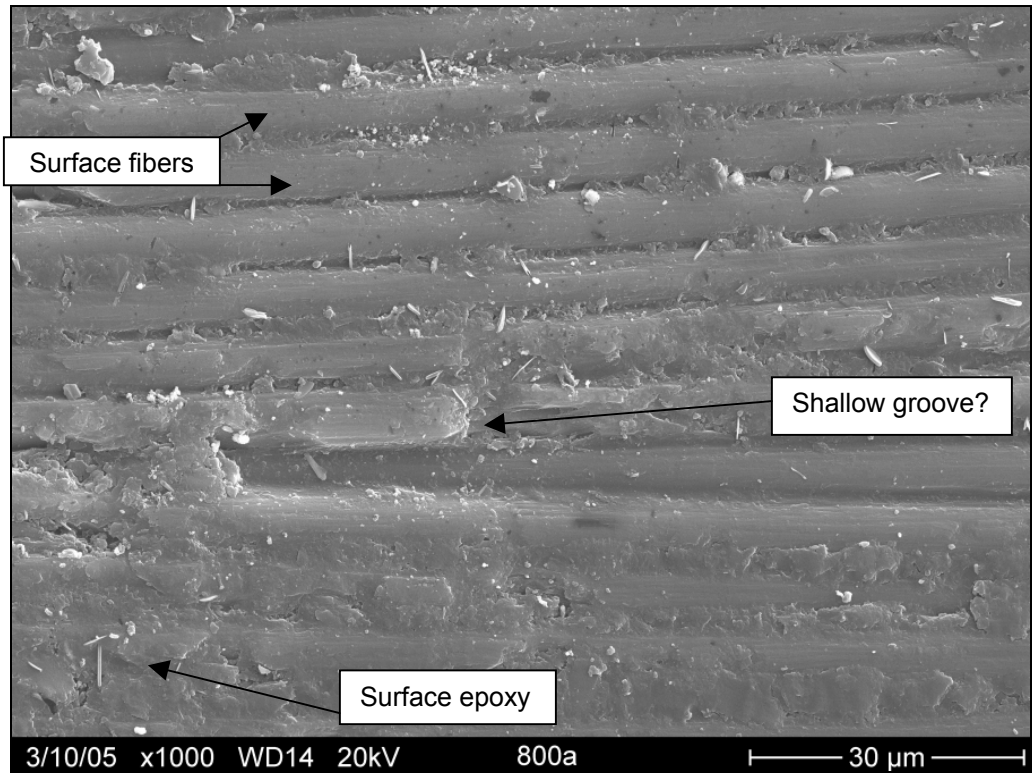

Figure 95: Closer view of a pre-tested surface treated SiC 800

Pullout Test Results and Discussion

The pultruded rod pullout tests were conducted partially to observe if surface area changes have a significant effect on the interface shear strength of a pultrusion embedded in another resin and to determine which surface abrasive treatments would be good candidates for the fiber pushout testing. It was assumed that once one end started to fail and pullout, the other end stopped receiving damage. Pictures of post tested coupons are seen in Figures 96 through 98. Typical short end pullout failure is displayed in Figure 96, typical long end pullout failure is shown in Figure 97, and an inside view of a representative resin end after pullout is shown in Figure 98. The white residue on the rod ends was ground epoxy and glass from the overlaid fabric that stuck on the rod as the

resin end was pulled off the rod. Longitudinal striations can be seen on the ends. These are possibly caused by the weak layers of the pultruded rod surface being separated from the pultrusion in Figure 98 rubbing against the rod surface. The glass fabric on only two sides accounts for the location of the white residue, but not completely its cause. This residue might be indicative of another friction component between the contacting glass fabric and pultruded rod surface.

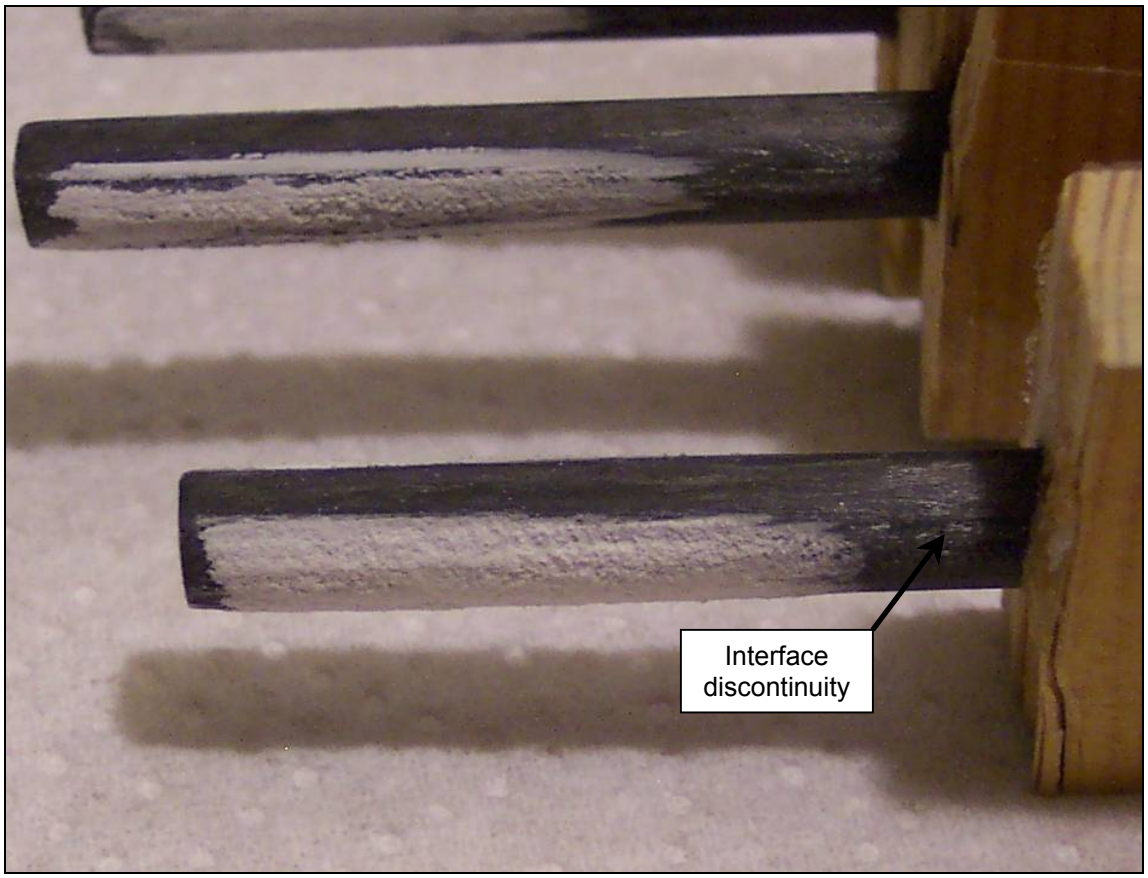

Figure 96: Typical pultrusion appearance after pullout test interface failure

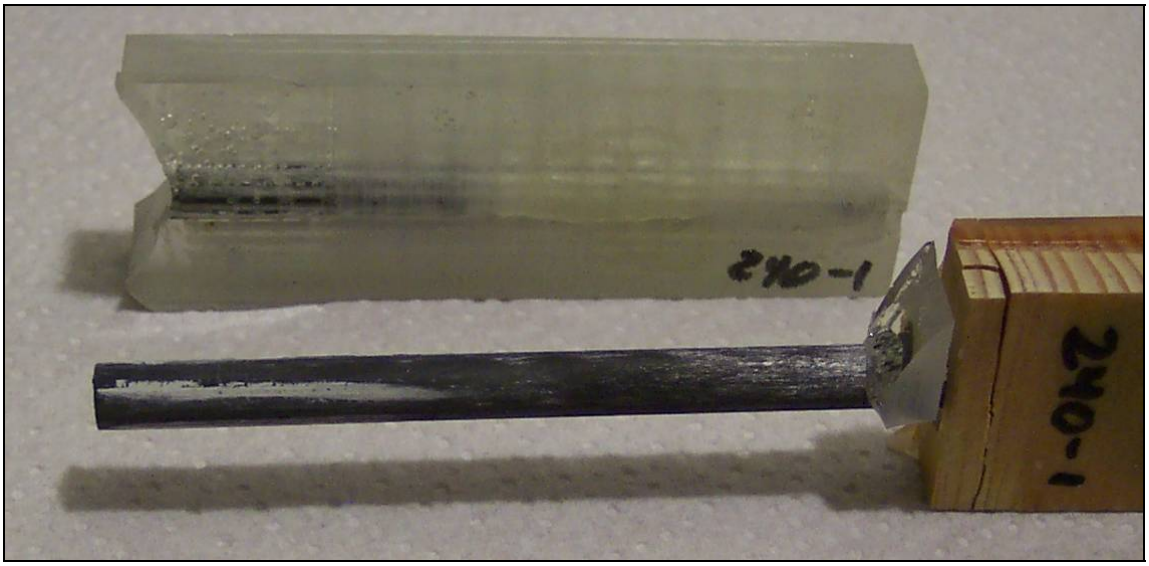

Figure 97: Pultrusion appearance after pullout test interface failure with matching embedding epoxy

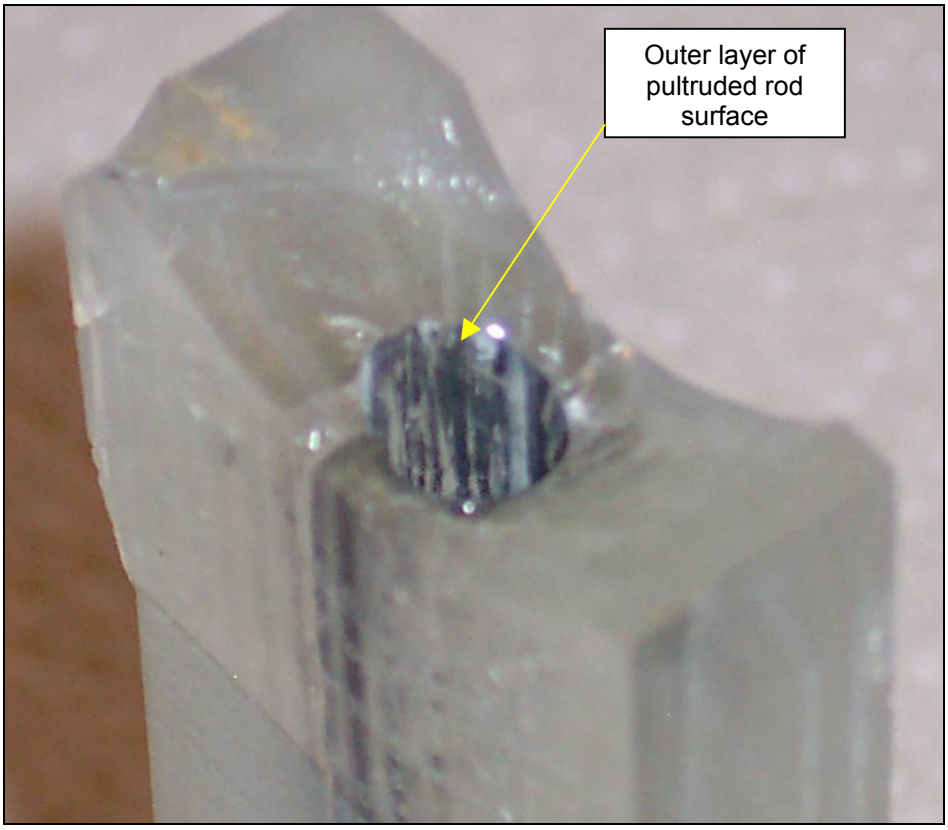

Figure 98: Typical embedding epoxy surface interface failure after pullout

A typical force versus displacement curve for a pullout coupon is shown below in Figure 99. For all pullout coupons there was a steep, fairly linear force/displacement curve for about one millimeter of Instron cross-head displacement. Most coupons had a small jog a small time before the maximum load. This was assumed to be the end of the linear region. This small jog in the curve could indicate that the interface has debonded around the region of the pullout coupon where the embedding epoxy meets the wood attached to the epoxy. This area of the coupon creates a *stress concentration point* at the interface discontinuity between the pultrusion and the embedding epoxy. At the end of the linear region of the curve the stress buildup at this point has debonded the interface from the epoxy. This point is illustrated as A) in Figure 99. The rest of this curve up to the maximum force could indicate the spread of the interface separation crack around the pultrusion surface. As the applied force increases non-linearly after this initial debonding as the interfacial crack grows along the pultrusion surface. This region of the curve is illustrated as B) in Figure 99. At the maximum applied pulling force, the crack has released enough energy to debond the entire interface from the embedding epoxy. This point is illustrated as C) in Figure 99 below.

The other peaks in the curve are most likely indicative of the friction between the pultrusion and embedding epoxy as the pultrusion is being pulled out. The crushed particulate on the pultrusion surface seen in Figure 96 is created from the debonding and friction of the pullout motion. These particulates

have built up during the pullout motion and cause a spike in the applied force as this buildup resists the pullout action and slips when this resistance is overcome. All force versus displacement curves for all pullout test coupons are included in Appendix B.

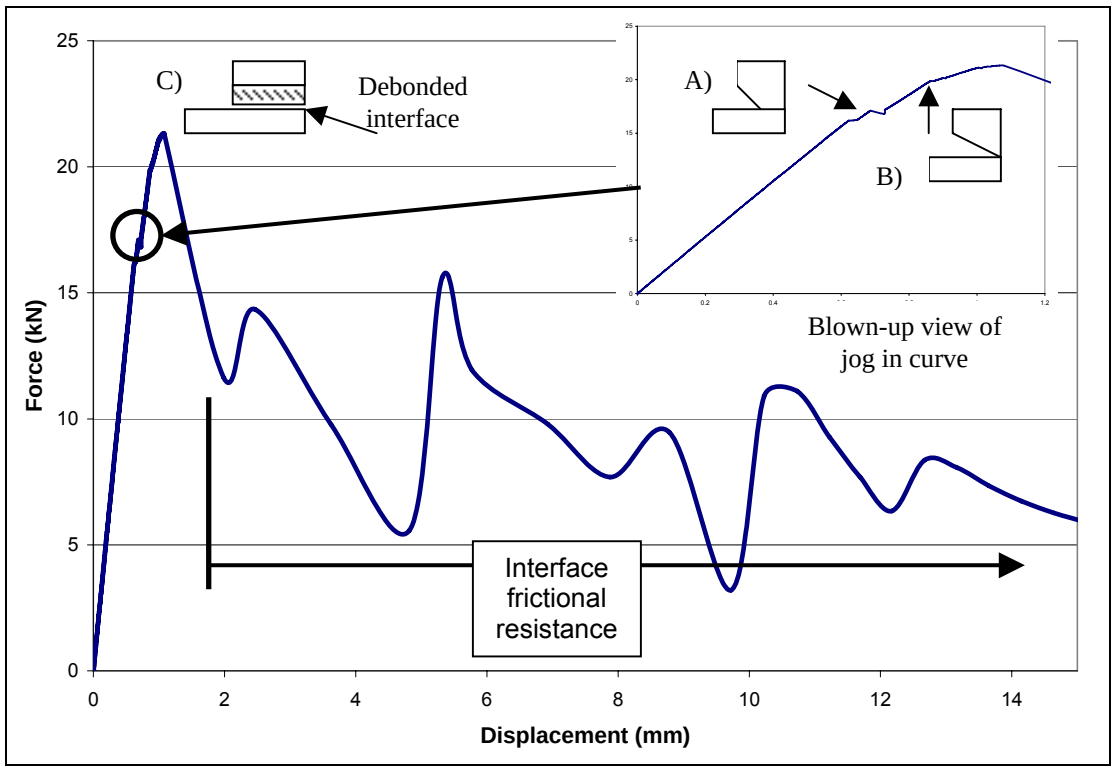

Figure 99: Typical force vs. displacement curve of a pullout coupon

The results in Table 6 list and compare the average maximum pullout force and the average interfacial shear stress (IFSS) from three coupons from each abrasion surface treatment. The IFSS is calculated by dividing the maximum pullout force by the interfacial area of the pultrusion side that pulled out. The average IFSS is based on the assumption that after the debonding at the stress concentration point, it is assumed for the calculation that the shear stress along the interface is *constant* as the interface crack grows.

The highest average interface shear strength shown in Table 6 belongs to the SiC 320 surface treatment with an IFSS value of 36.8 MPa. The untreated rod had an average IFSS of 13.9 MPa. All surface treatments lead to some improvement on the interface shear strength to various degrees over the untreated rods.

Table 6: Pultruded Rod Pullout Test Result Summery

Coupon Surface Treatment	Particle Size (μm)	Average Ult Load (kN)	Average Maximum Debonding Load (kN)	Average Interface Pullout Strength (MPa)
Control	0	19.6	17.1	13.9
120	115	27.3	23.7	26.7
220	58	25.2	19.5	17.8
320	46	24.6	19.4	36.8
800	22	21.3	18.9	22.5
1200	15	20.9	18.0	28.2

The high IFSS value of SiC 320 treated pultruded rods compared to the other abrasive treatments could be due to the fact that the 320 size grit paper produces an average depth of groove and an average amount of grooves compared to the other surface treatments. This gives an adequate amount of interlocking sites balanced with interlocking depth in the epoxy. This correlates with a study done by W.P.W Lam and coworkers on physical grinding with SiC

abrasive papers on metals [80]. Using different grit sizes of Struers SiC paper, they found that best surface area increases on four common metals of various hardnesses came from using the SiC papers with the average grinding particle size.

It might also be possible for the secondary epoxy to bond directly to the exposed fibers if any un-reacted sizing was also exposed, although this might constitute a small fraction of the increase in IFSS. Any damage to exposed fibers could also be beneficial as these fibers are now more opened up to epoxy infusion and an increase in the friction factor during interface loading. As there is a high fiber volume fraction in the rods, and the induced grooves are not deep, fiber damage on the new surfaces may not be a problem during most loading conditions unless the fatigue loads cause the cracks to propagate transversely through the rod quickly.

Rod Pushout Test Results and Discussion

Pre-test Images and Discussion

SEM images of the pre-tested erosion treated surfaces used in the pushout tests before embedding in Epon 862 epoxy are seen in Figure 100-109. Figure 100 below is a surface image of a pultruded rod that had undergone glass bead erosion at an air stream pressure of 2 kg/cm^2 and 1 revolution of exposure time. In short hand these erosion treatments will be referred to by a number pair

with the air stream pressure first and number of revolutions second. Thus the erosive treatment for 2 kg/cm^2 and 1 revolution will appear as (2, 1).

The surface damage seen in Figure 100 is much more widespread than the damage done by the abrasion treatments. The outer layer of epoxy has almost been completely stripped away except for small patches and many broken fiber fragments are visible. The outer layers of carbon fibers are broken in small local areas. These holes are seen in spotty patches on the surface. It is difficult to determine from this figure the amount of the outer carbon fibers that have been removed by the treatment. The surface is very irregular and looks as if it would provide many sites for mechanical interlocking when the secondary layer of epoxy is overlaid on the rod surface.

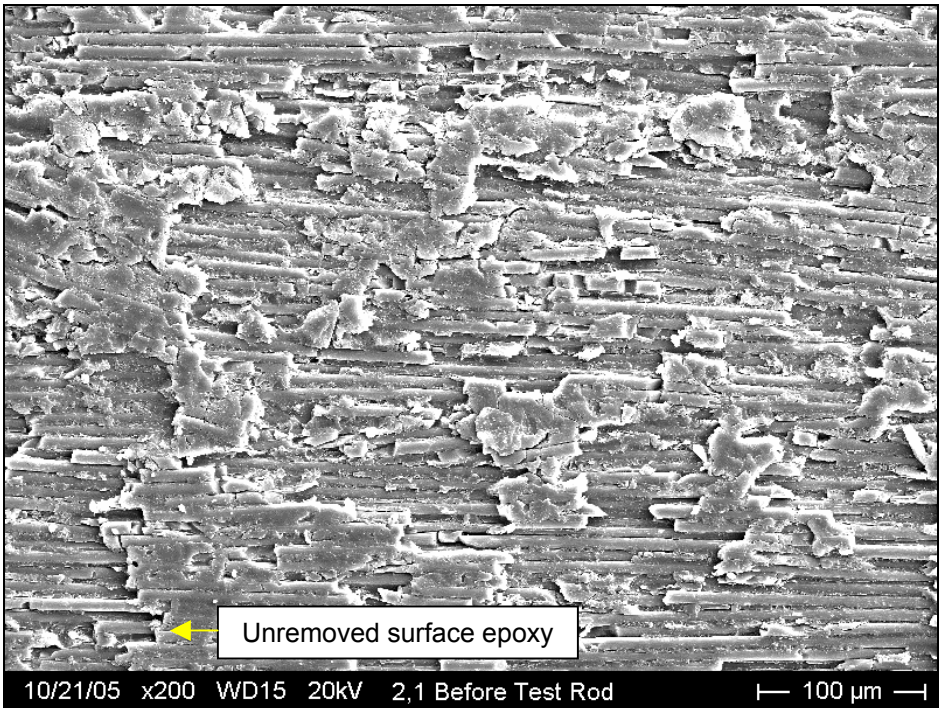

Figure 100: Pre-interface tested rod surface after the 2 kg/cm^2, 1 revolution erosion treatment

In a magnified view of the surface in Figure 100 seen in Figure 101, the outer fibers appear to have clean broken edges. The impingement of the glass bead fragments at an angle normal to the pultrusion surface appears to have crushed a few of the outer fibers. Some of these fiber fragments are pushed into the next layer of fibers. The fibers underneath the outer layer appear to be undamaged for the most part and have the top 180 degrees exposed for secondary resin infusion.

Another detail seen from Figure 101 is that there does not appear to be many loosely bonded carbon fiber particles or loosely bonded epoxy particles that create potential debonding points when the secondary epoxy is cured. It appears from Figures 100 and 101 that the majority of the new surface area comes from the removal of the outermost layer of pultrusion epoxy and exposing and damaging the outermost layer of carbon fibers. A small amount of surface area is created by the particle impinging action that break small areas of the outer fibers and exposes the fiber layer underneath.

The images of the (2, 2) surface treatment are seen in Appendix G. As this treatment had a slightly longer exposure time under the erosive jet, the outermost epoxy layer has been removed a little more than the one revolution treatment. The magnified view of this treatment appears the same as in Figure 101.

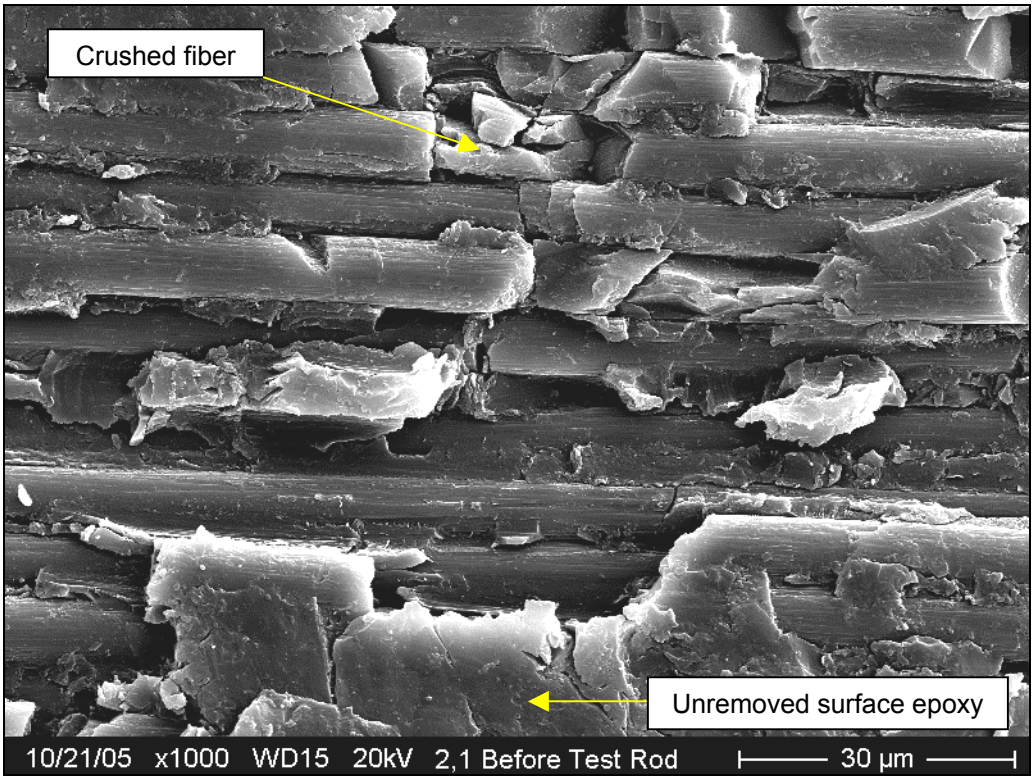

Figure 101: Magnified view of the 2 kg/cm^2, 1 revolution surface treatment

Figures 102 and 103 are SEM images of pultruded rod surfaces that have been eroded by high speed glass beads in an air stream pressure of 2 kg/cm^2 with an exposure time of 4 revolutions (2, 4). The outer layer of epoxy seen in Figures 102 is completely gone due to the increased exposure time and the much of the outer layer of carbon fibers seem to be removed as well. The potential sites for mechanical interlocking do not appear as deep in this treatment due to the relative smoothness of this treated surface compared to Figure 101. However, there appears to be less short chunks of loosely bonded fibers and other materials on the surface, the interface strength could be increased because of this.

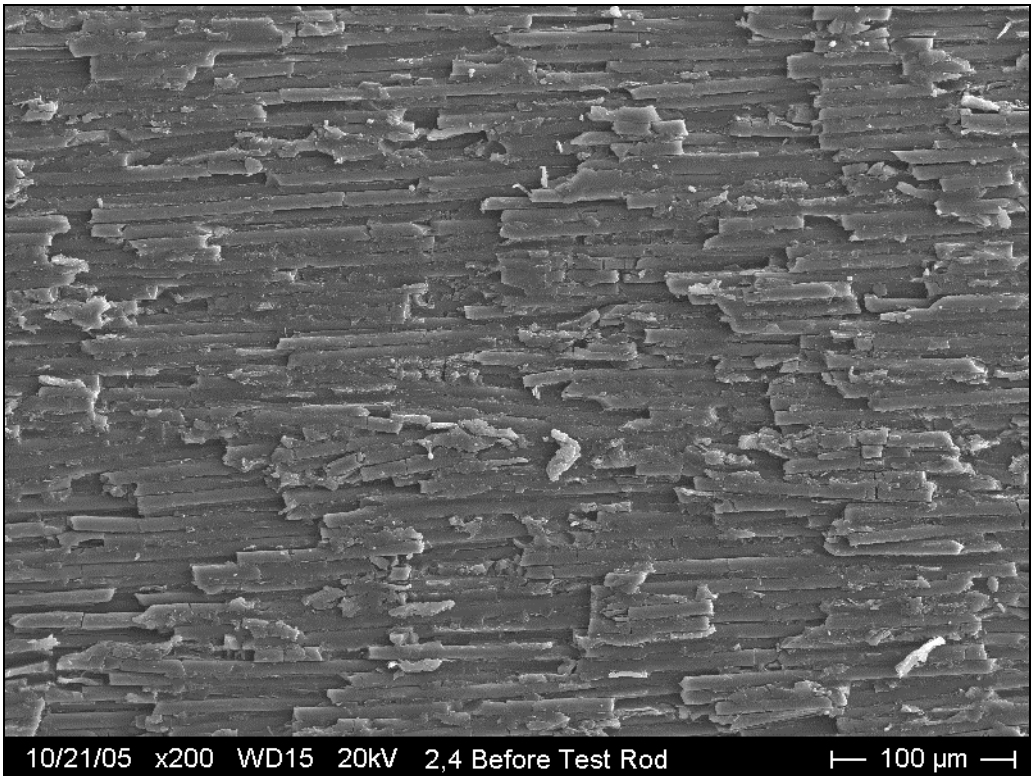

Figure 102: Pre-interface tested rod surface after the 2 kg/cm^2, 4 revolutions erosion treatment

In Figure 103 below, there are many small crevices in the local area of the small fragments of broken carbon fibers. The epoxy between the outer layer of carbon fibers and the layer underneath has been worn down pretty extensively to expose grooves between underneath carbon fiber layer. The mechanical interlocking sites produced by this treatment are smaller than the previous 2 kg/cm^2 treatments, but these sites for the four revolution exposure time seem they would be stronger and more resistant to debonding under load as they are closer to the surface and interlock around more stable sites that consist less of particles loosely bonded on the surface.

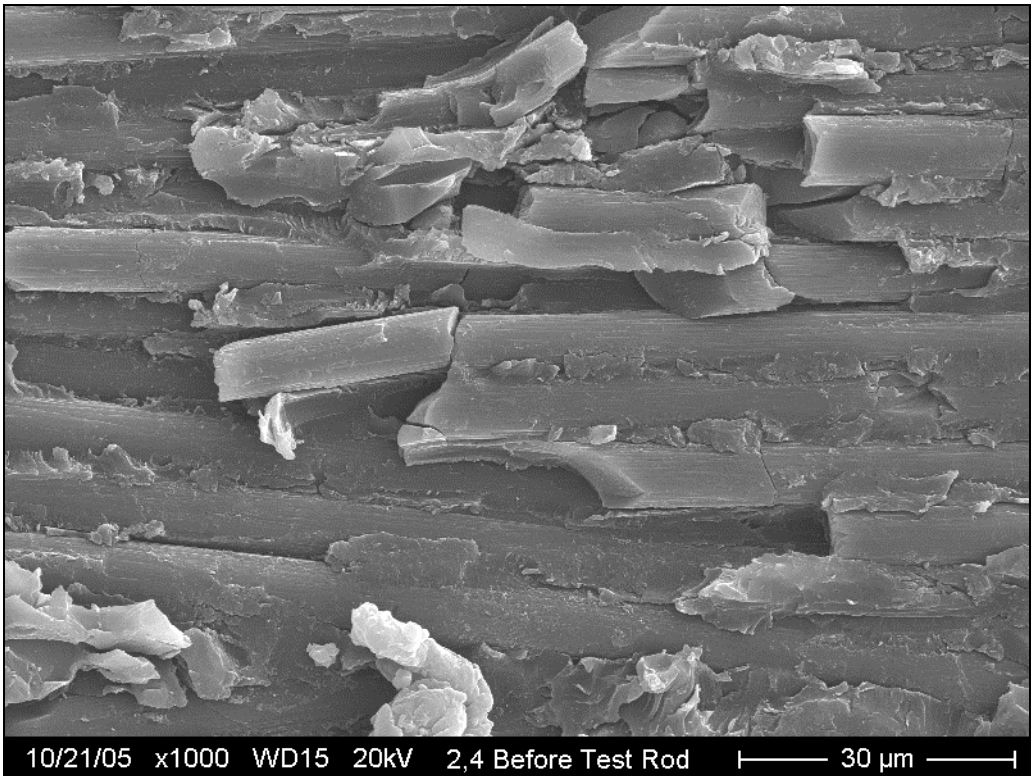

Figure 103: Magnified view of 2 kg/cm^2, 4 revolutions surface treatment

Figures 104 and 105 are images of a pultruded rod surface that had been eroded by the same glass beads under an increased pressure of 3 kg/cm^2 of 1 revolution (3, 1) of exposure time under the air stream. The outer layer of epoxy has been removed from the rod surfaces as well as some of the outer carbon fibers. From this treatment pressure and exposure time to the next higher pressure and similar exposure times, the wide view of the pultruded rod surfaces all share similar appearances. The magnified surface appearance of the rod surface in Figure 105 shows a very fragmented surface and has many crevices of various depths for mechanical interlocking sites for the secondary epoxy.

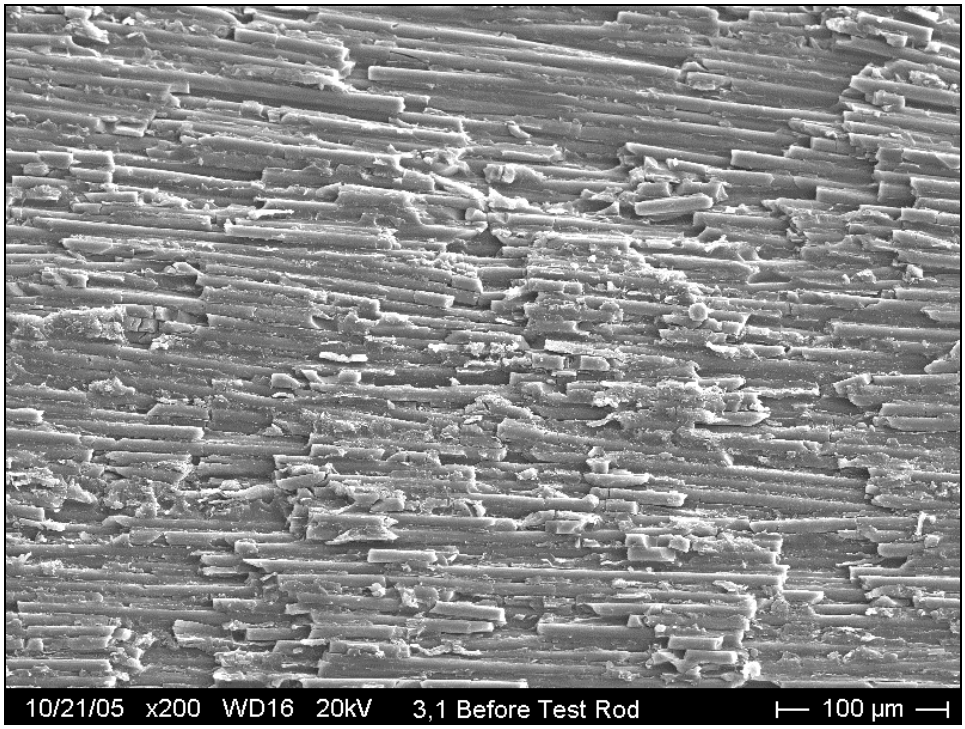

Figure 104: Pre-interface tested rod surface after the 3 kg/cm^2, 1 revolution erosion treatment

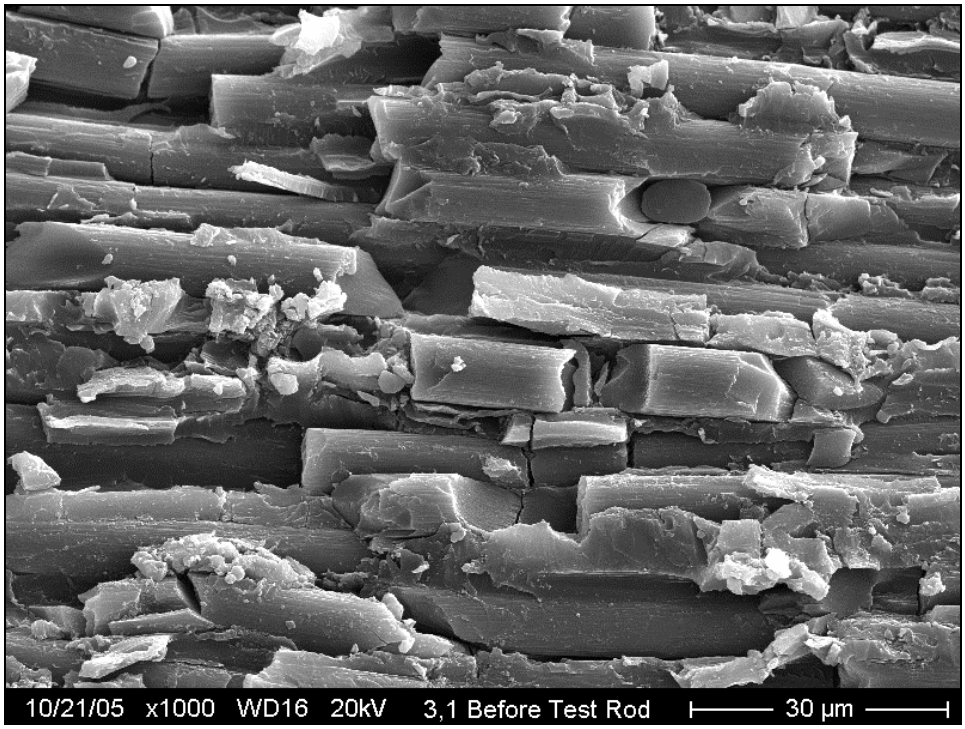

Figure 105: Magnified view of 3 kg/cm^2, 1 revolution surface treatment

The surface of the (3, 2) treated rod are shown below in Figures 106 and 107. The wide view of the surface appears to have had most of the outer layer of epoxy and carbon fibers removed. Some of the underlying carbon fibers appear to have suffered some damage as well. The surface appears sufficiently rough to provide very good mechanical bonding sites.

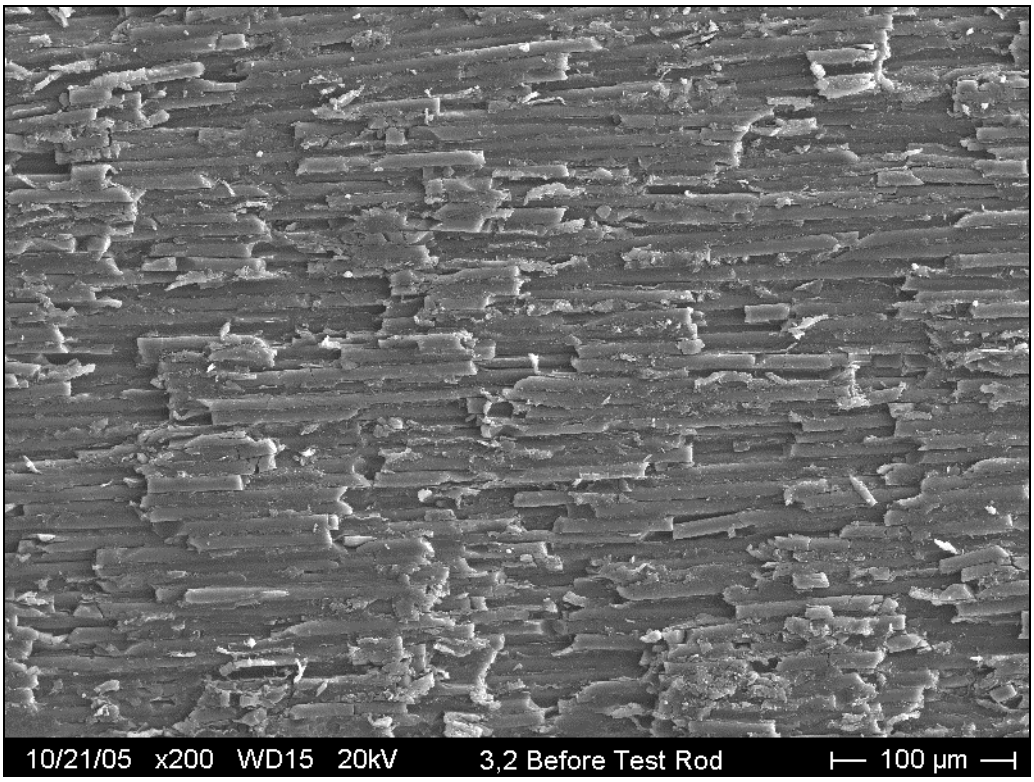

Figure 106: Pre-interface tested rod surface after the 3 kg/cm^2, 2 revolutions erosion treatment

The surface appearance in Figure 107 shows that the epoxy in between some of the second layer of carbon fibers has been removed and would allow the secondary epoxy to infuse into these holes for larger potential interface. Secondary epoxy can get between the outer fibers as well. This could create an interface incorporates some of the outer fibers within the interface instead of just bonding to any available carbon fiber surfaces. The carbon fiber surfaces do not

appear as smooth as in other treatments. This epoxy could be well bonded to the fiber and increase the frictional resistance to pushout loads. The (3, 4) treatment results seen in Appendix G have similar surface appearances to the (3, 2) treatment seen in Figure 107.

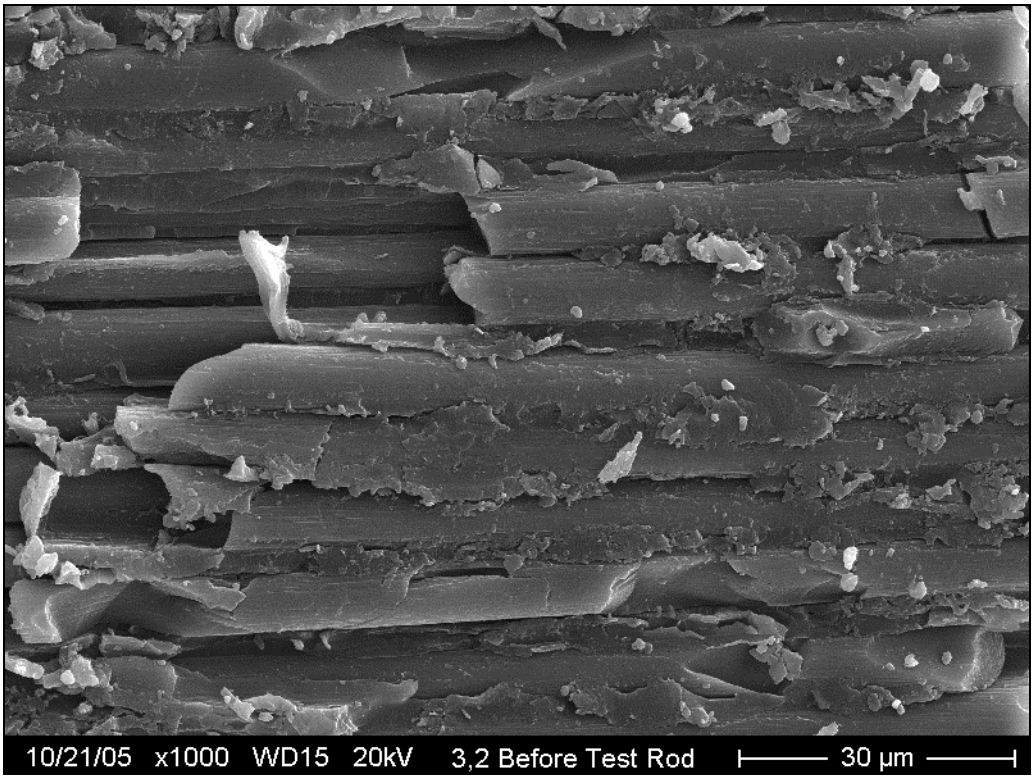

Figure 107: Magnified view of 3 kg/cm^2, 2 revolutions surface treatment

Figures 108 and 109 are images of a pultruded rod surface treated with the (4, 2) erosion conditions. The new surface depth variation appears to be greater here than in the (4, 1) treatment seen in Appendix G. There are many more loose fiber and epoxy fragments on the surface than in the previous treatment. There appears to be a large variety in size and depth of mechanical interlocking sites for good resistance to interface shearing.

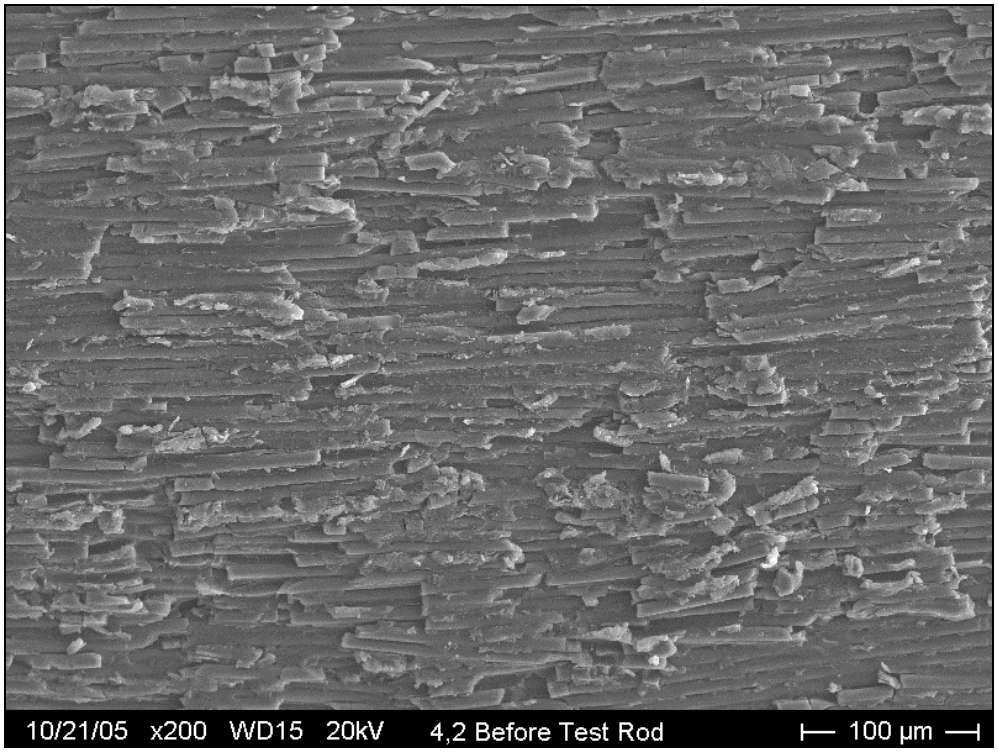

Figure 108: Pre-interface tested rod surface after the 4 kg/cm^2, 2 revolutions erosion treatment

The magnified view in Figure 109 shows some cracks in the epoxy between the exposed fibers. This presents an opportunity for secondary epoxy to flow between the exposed fibers to a decent depth. This may overcome the apparent lack of good potential bonding of the secondary epoxy onto the exposed fiber surfaces, which look fairly smooth. The (4, 4) treatment has a similar appearance to the (4, 2) treatment. With the longer exposure time, the surface has the same heavily eroded appearance with fewer fragments of fibers.

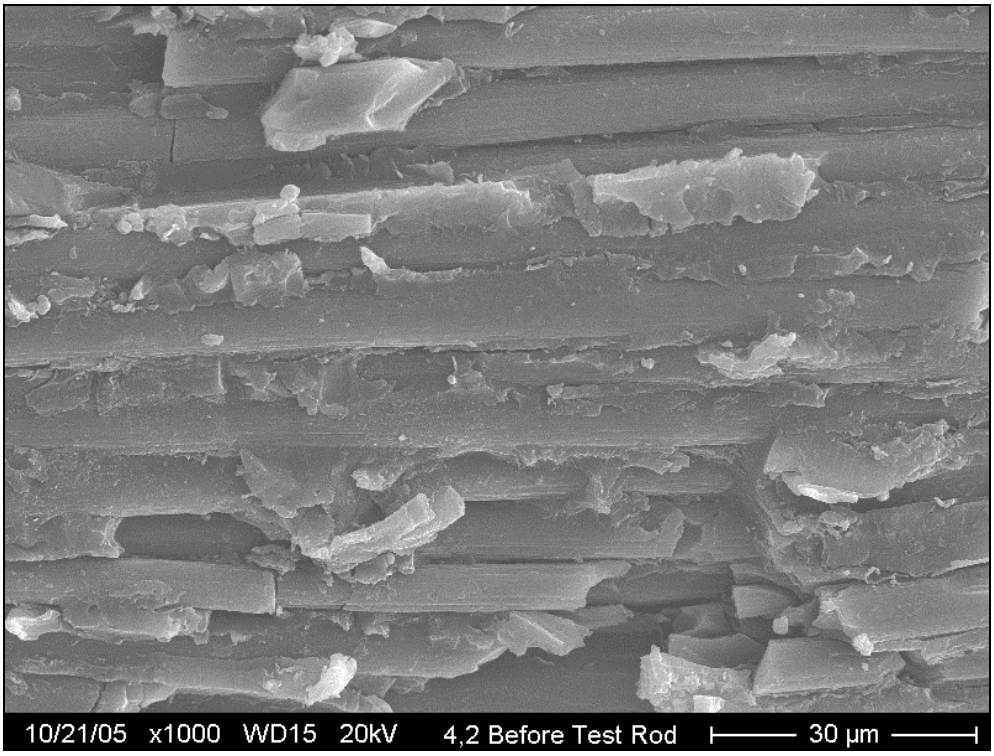

Figure 109: Magnified view of 4 kg/cm^2, 2 revolutions surface treatment

Selected images of the chemical surface oxidation treatments are shown in Figures 110-119. Figure 110 below is a SEM image of a pultruded rod surface subjected to a heated HNO_3 bath for 15 min then soaked in distilled water. The oxidation treatment has dissolved some of the outer epoxy layer making the outer carbon fibers stand out more against the surface compared to an untreated rod surface as seen in Figure 86. Some corrosion pitting of the surface is visible especially around the fibers in Figures 111. The overall surface appearance is smooth although some mechanical interlocking is possible in the corrosion pits around the fibers and in the pultrusion epoxy and from the new surface unevenness created by the treatment. It is unknown how well the secondary epoxy would bond to the oxidized surface chemically.

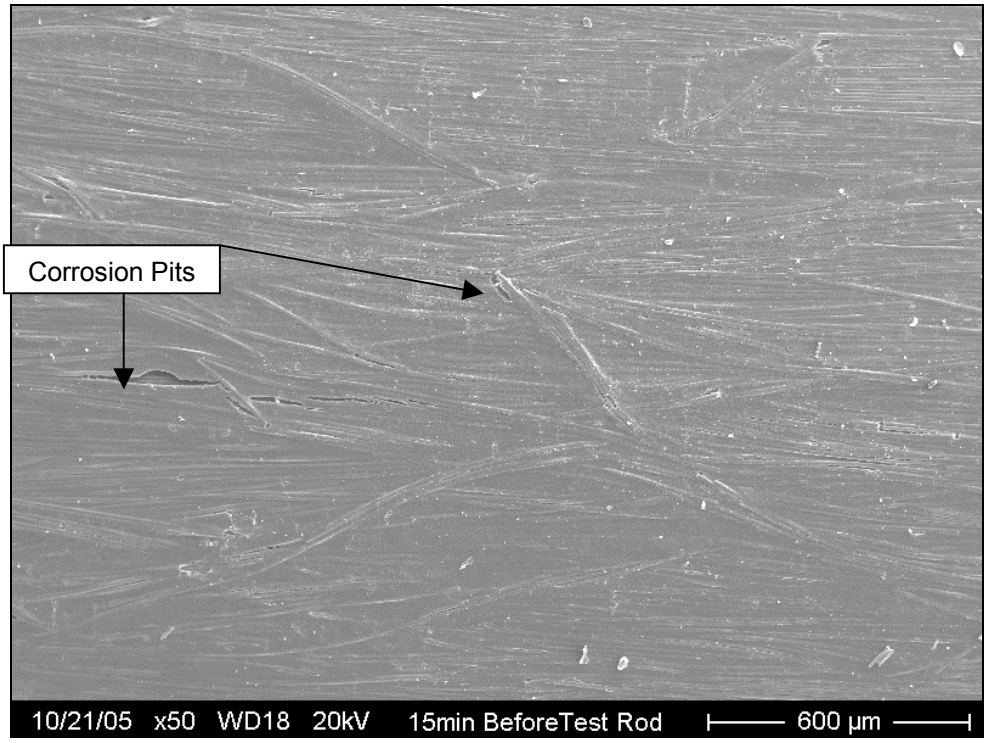

Figure 110: Pre-interface tested rod surface after the 15 min HNO_3 treatment

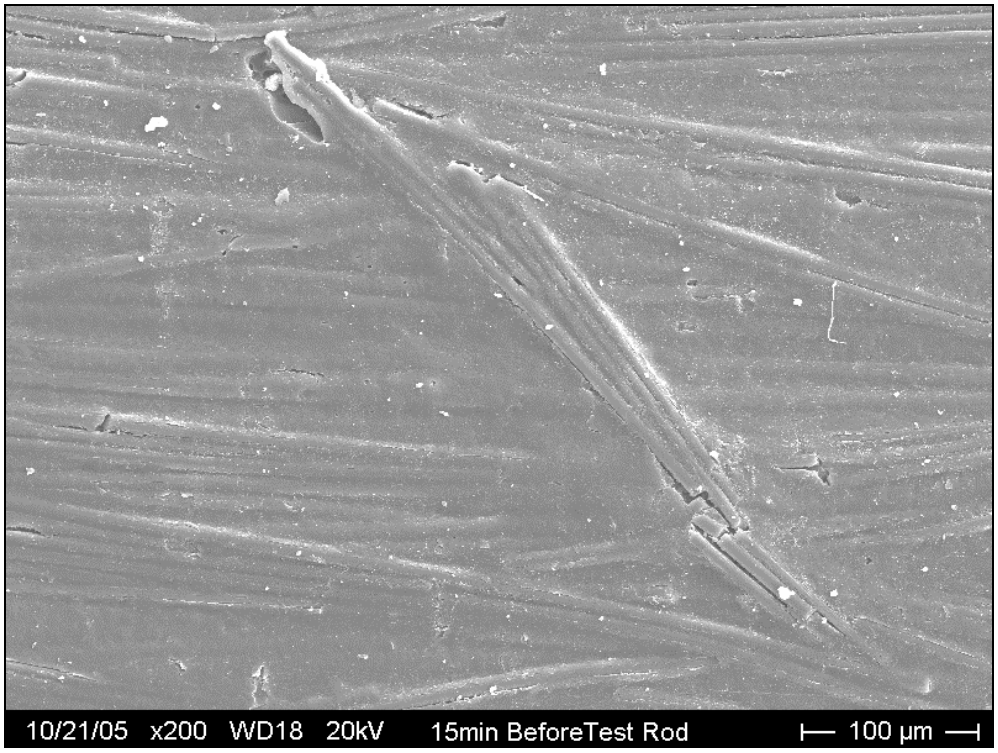

Figure 111: Magnified view of 15 min HNO_3 treated rod surface

Figures 112 and 113 below are images of a pultruded rod surface after a 30 minute heated HNO_3 and then a distilled water soak and atmospheric dry. The oxidation has removed much more outer layer epoxy, exposing more fibers. There are larger corrosion pits present as well as carbon fibers that appear totally free of epoxy. The surface appears rougher than the 15 minute treatment. The pits extend fairly deep into the pultrusion as seen in Figure 113. The fiber surfaces appear free of epoxy and provided a full, theoretically chemically active surface for the secondary epoxy to bond to. The deep pits would provide good mechanical interlocking sites. It is unknown if the broken fibers seen in Figure 113 are from the pultrusion processing or broken off from the chemical treatment and cleaning.

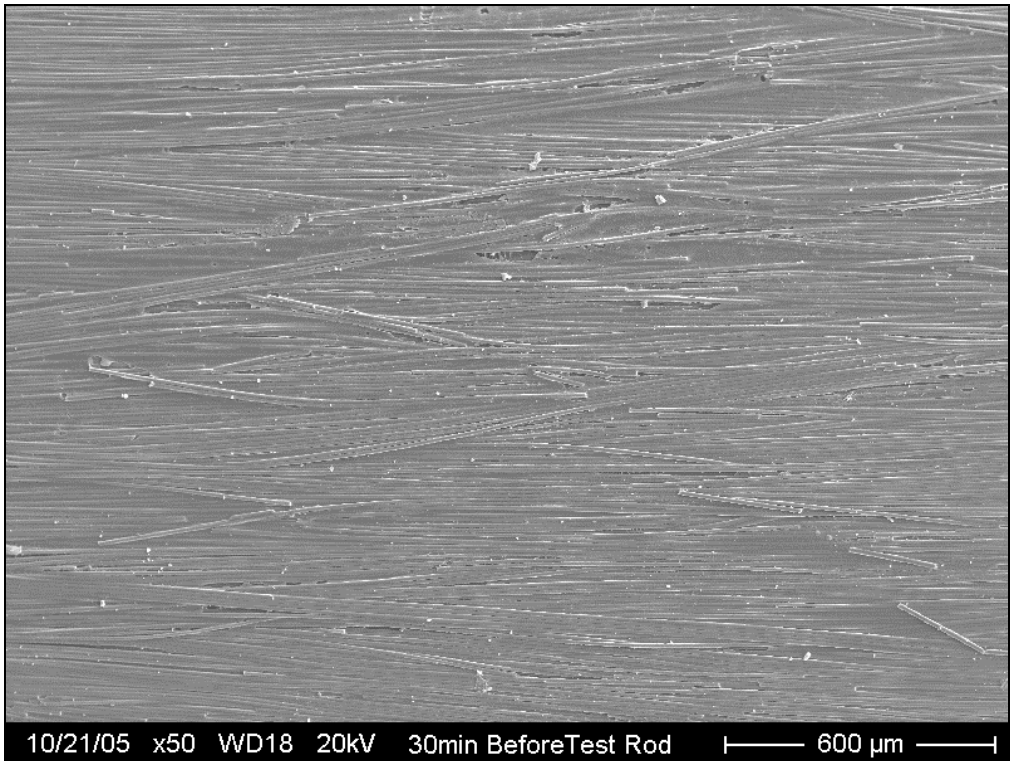

Figure 112: Pre-interface tested rod surface after the 30 min HNO_3 treatment

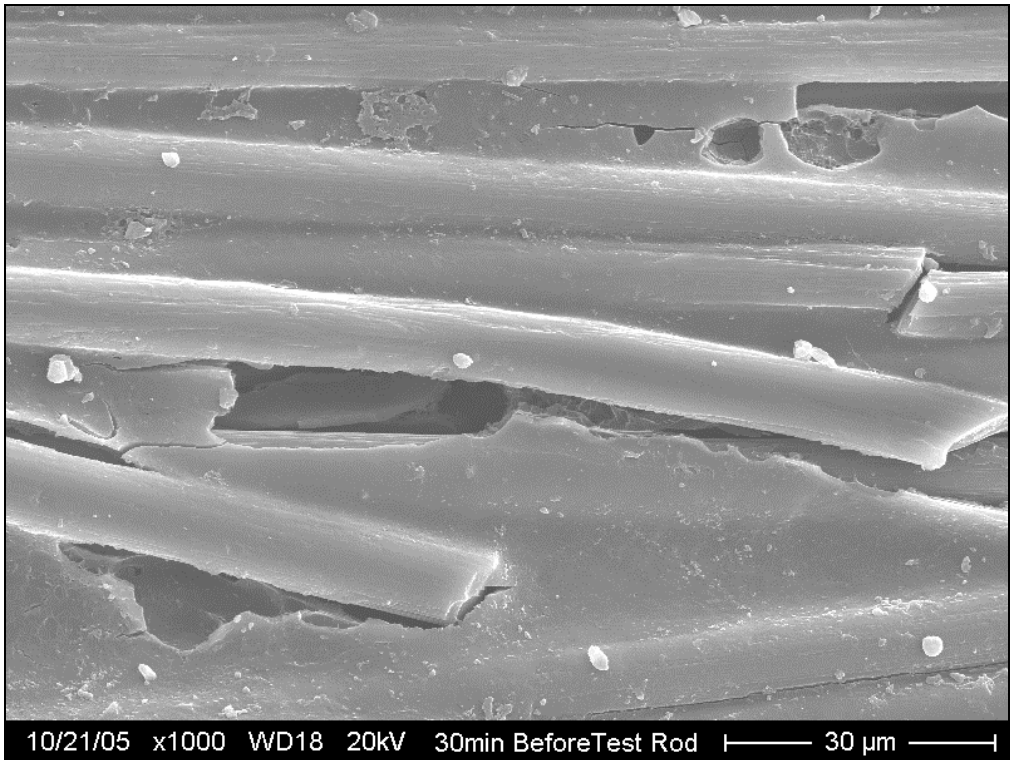

Figure 113: Magnified view of the 30 min HNO_3 treated rod surface

Figures 114 and 115 are images of pultruded rod surfaces subjected to a 60 minute heated HNO_3 bath. The pultruded rod then had a 40 second wash in distilled water before drying in atmospheric conditions. The pultruded rod soaked in distilled water for 5 days before drying in atmospheric conditions seen in Appendix G had a similar appearance to the rod in Figure 112 and 113. The surface in Figure 114 appears to have more exposed fibers and less surface epoxy than the 'washed' surface. The 'unwashed' surface appears to have a more uneven and rough surface than the washed surface although there are more corrosion pitting for a deeper interface. As described in the Experiment Methods chapter, the unwashed HNO_3 rods caused severe side effects in the secondary epoxy. The better surface appearance for interface shear resistance

by the unwashed surface is misleading and the resulting interface is unacceptable.

The SEM images in Figures 116 through 119 are pultruded rod surfaces subjected to 60 minutes in a heated HNO_3 bath followed by 30 seconds in 1, 2, or 5 molar solutions of NaOH. Loose surface fibers resulting from the treatment were peeled off of the 1, 2 and 5 M rods before SEM image preparation to better see the quality of the epoxy still left bonded to the carbon fibers underneath. The rod diameter of the 1M rod after having its fibers peeled off was 0.234 inches, 2M: 0.233 inches, 5M: 0.224 inches.

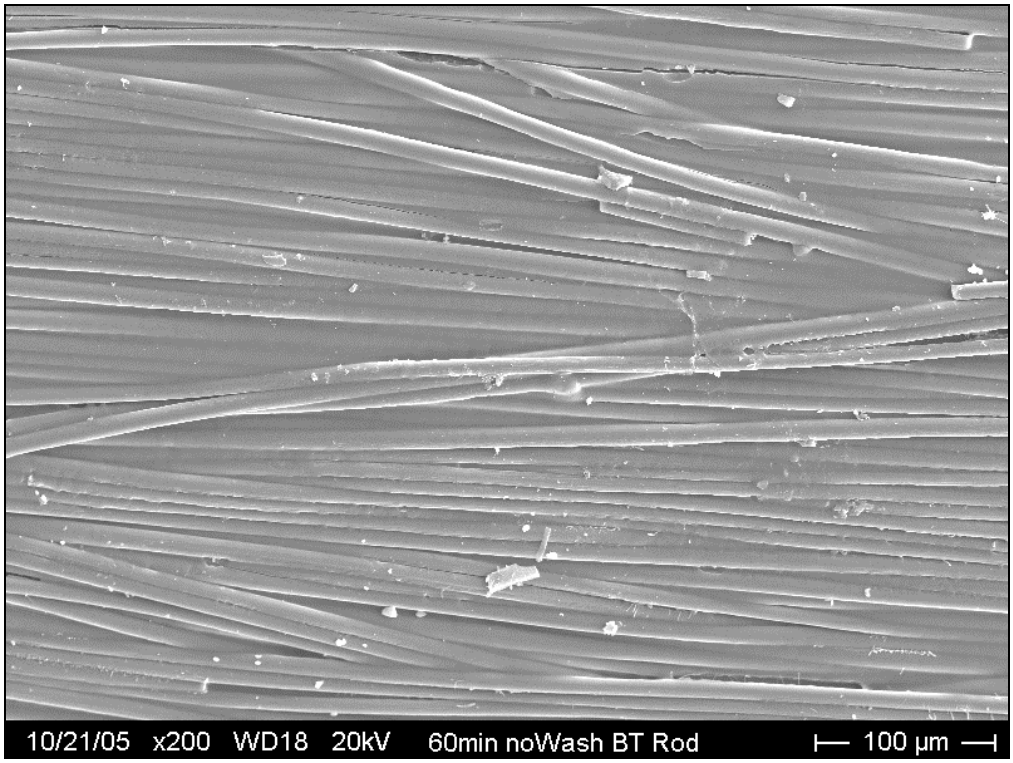

Figure 114: Pre-interface tested unwashed 60 min HNO_3 pultruded rod surface

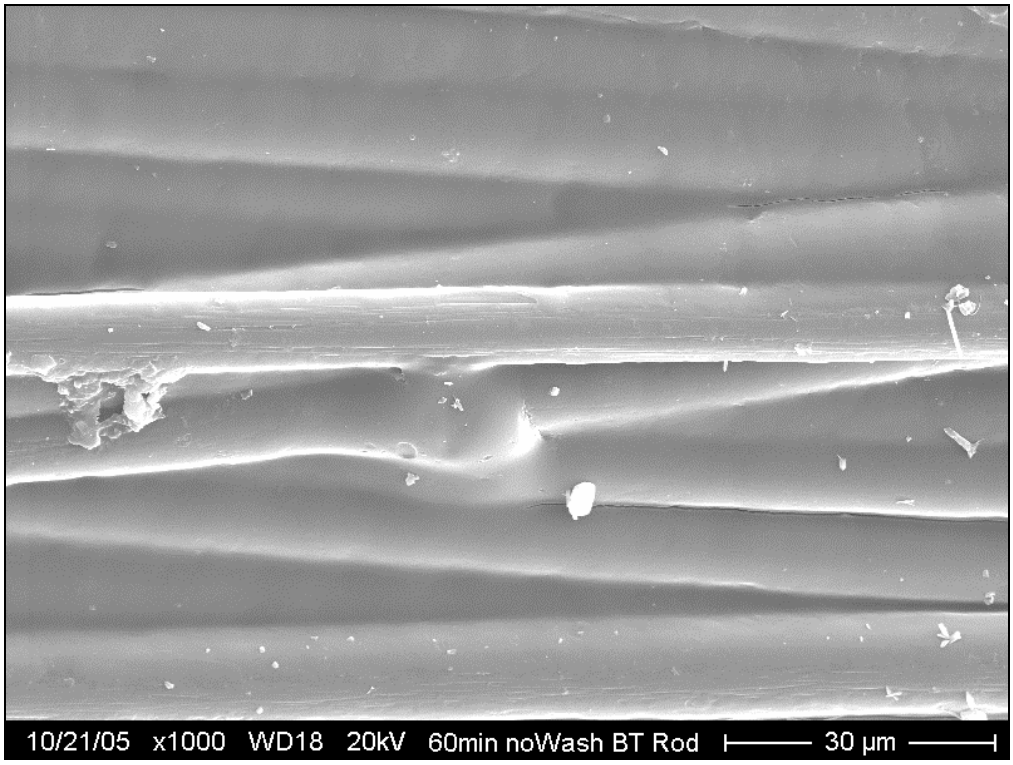

Figure 115: Magnified of the unwashed 60 min HNO_3 treated rod surface

The appearances of these surfaces in Figures 116 and 119 are all similar consisting of loose fibers with little or no epoxy attached to them. The solid surfaces of the pultrusion are difficult to see, especially in the 5M exposed rod image. The loose fibers are in all these cases would create an interphase instead of an interface that consists of misaligned fibers that extends for several microns between the pultrusion surfaces into the bulk secondary epoxy. This tangled interphase could be resistant to shearing forces. The appearance of the rod exposed to 2M NaOH had an appearance similar to the 5M exposed rod in Figure 119 but with bits of epoxy on the fiber surface similar to Figure 116. These images are seen in Appendix G.

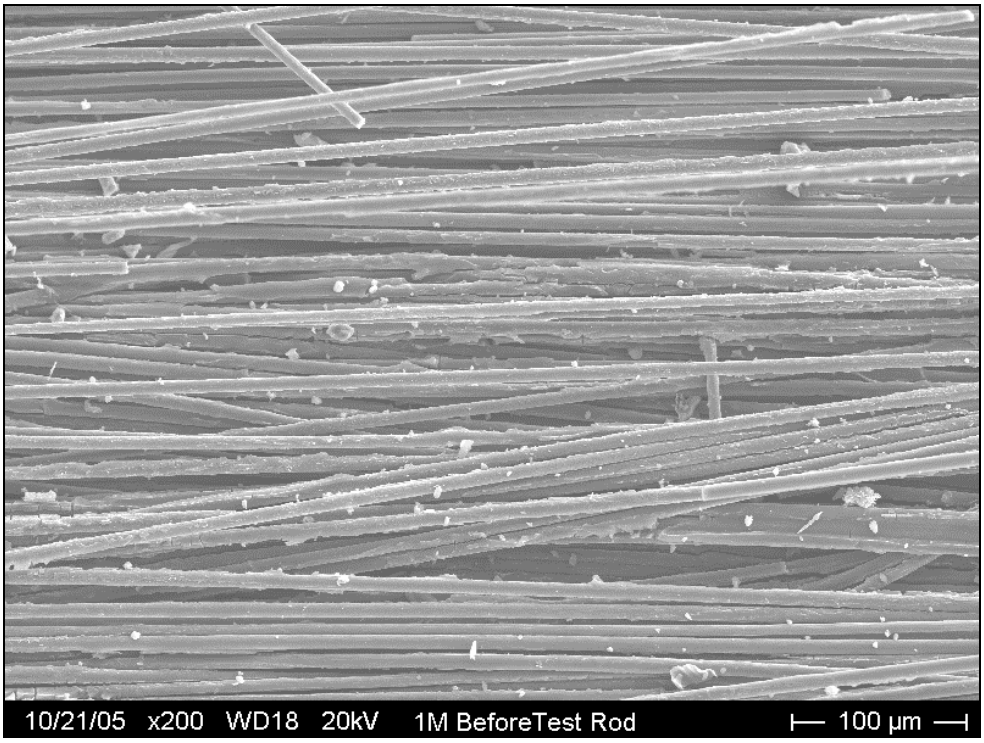

Figure 116: Pre-interface tested 60 min HNO_3 / 1M NaOH treated rod surface

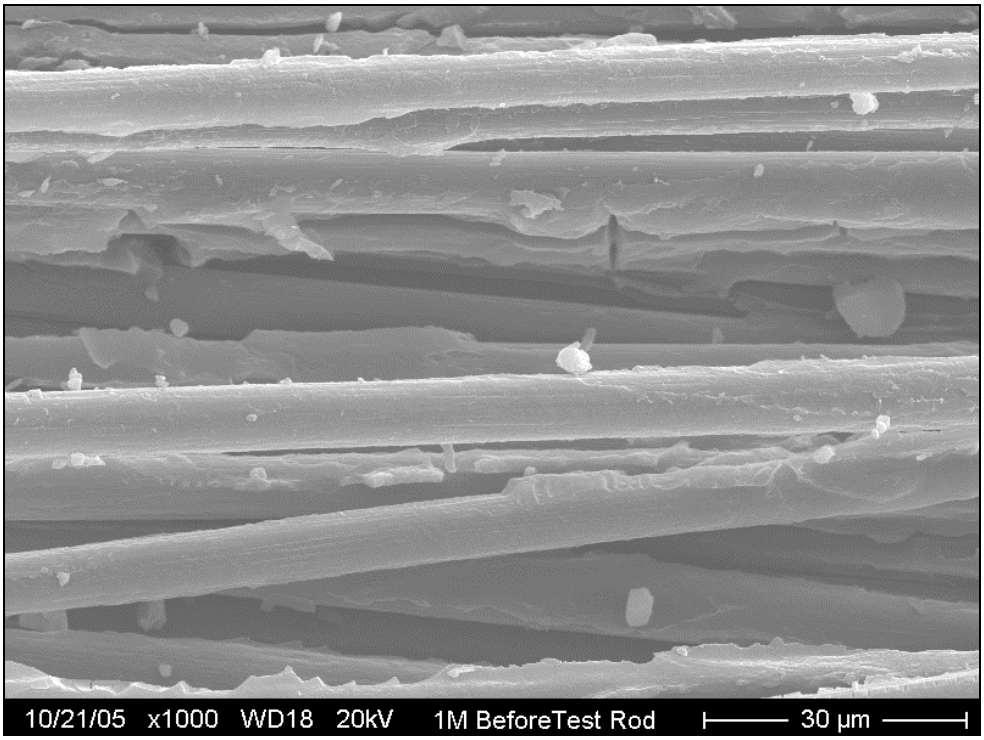

Figure 117: Magnified view of 60 min HNO_3 / 1M NaOH treated rod surface

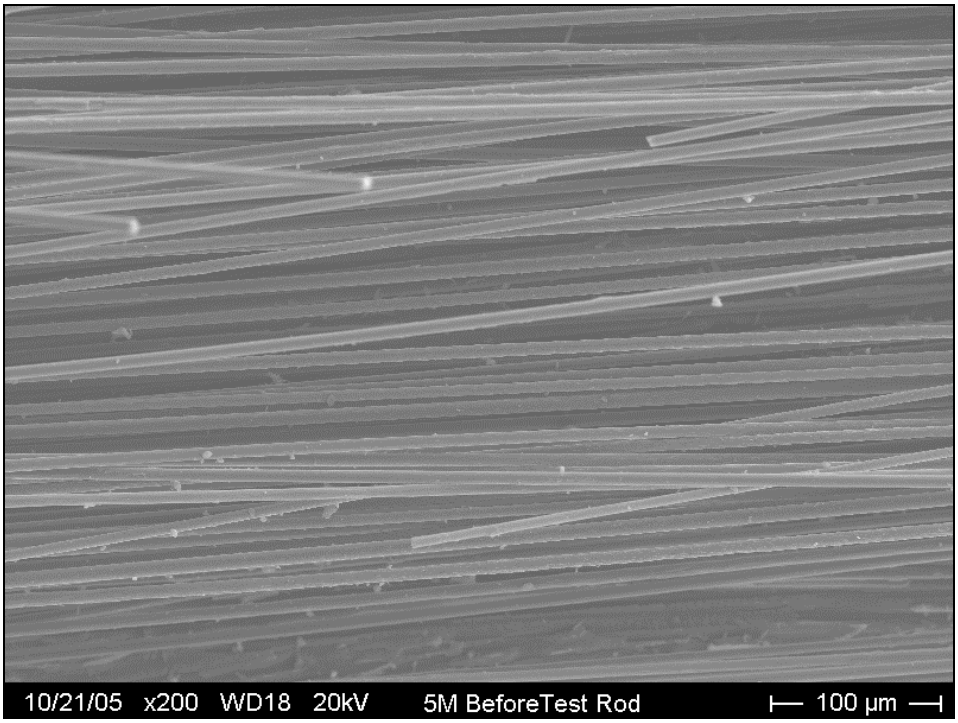

Figure 118: Pre-interface tested 60 min HNO_3 / 5M NaOH treated rod surface

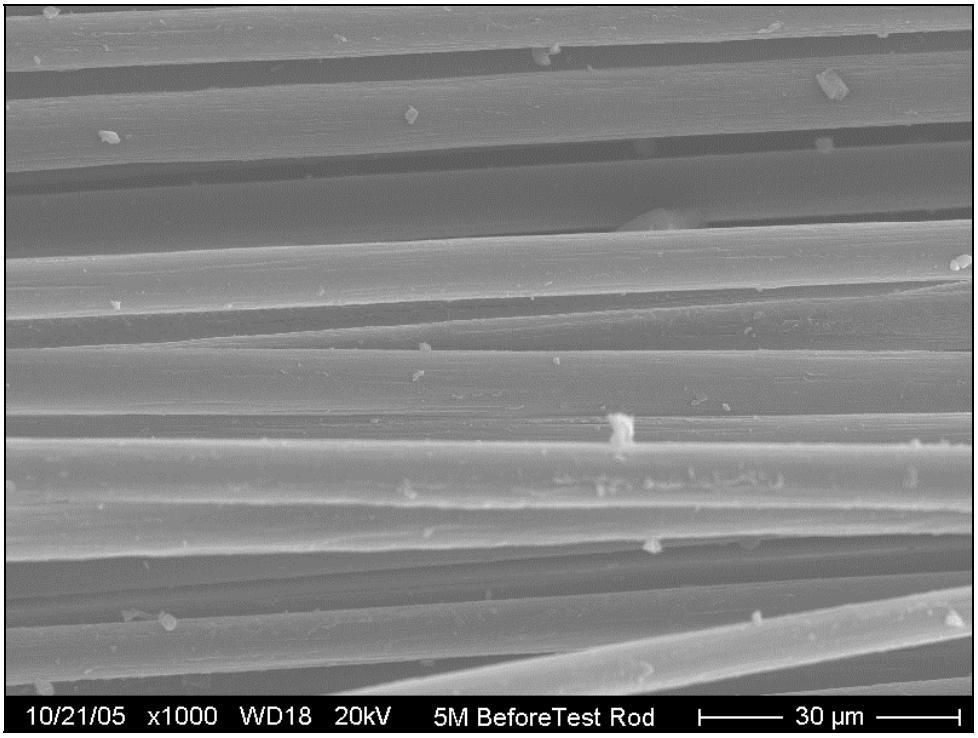

Figure 119: Magnified view of 60 min HNO_3 / 5M NaOH treated rod surface

Pushout Test Results and Discussion

This test is similar to the pullout test in that failure of the interface is initiated at the interface discontinuity where the pushrod contacts the center rod and the embedding epoxy. Once the interface debonds at this location, the interface crack grows around the pultrusion interface by some energy release rate until the crack grows suddenly to debond the final length of the interface. The average IFSS values calculated is based on the assumption described earlier; that the shear stress is constant along the interface after the debonding is initiated. A visual inspection of the failed pushout coupon is shown below in Figures 120 and 121.

Figure 120: Typical pushout coupon interface failure appearance

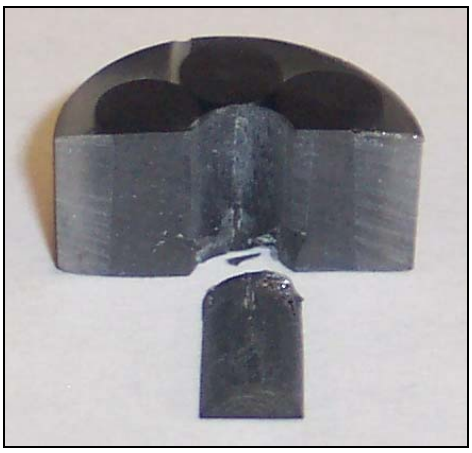

Figure 121: A closer view of the failed interface

A typical force vs. displacement curve for a pushout coupon is seen below in Figure 122. Not shown at the beginning of the curve is a non-linear region where settling and spreading of contact area between the pushrod and the center rod occur. In most cases, there is a small ‘hump’ that is seen before the curve becomes very steep. The hump is roughly analogous to the ‘jog’ described earlier

for the pullout testing; this is where the interface at the stress concentration begins to separate from the embedding epoxy. As the pushout load grows, the interface crack is growing along the interface most likely in a non self-similar growth method. At the maximum load, the crack grows enough to completely separate the pultrusion from the embedding epoxy. After this point, the load drops off considerably and the remainder of the curve is the friction at the new surface between the pultrusion and the epoxy resisting the pushout force. The force versus displacement curves for selected pushout test coupons are located in Appendix C.

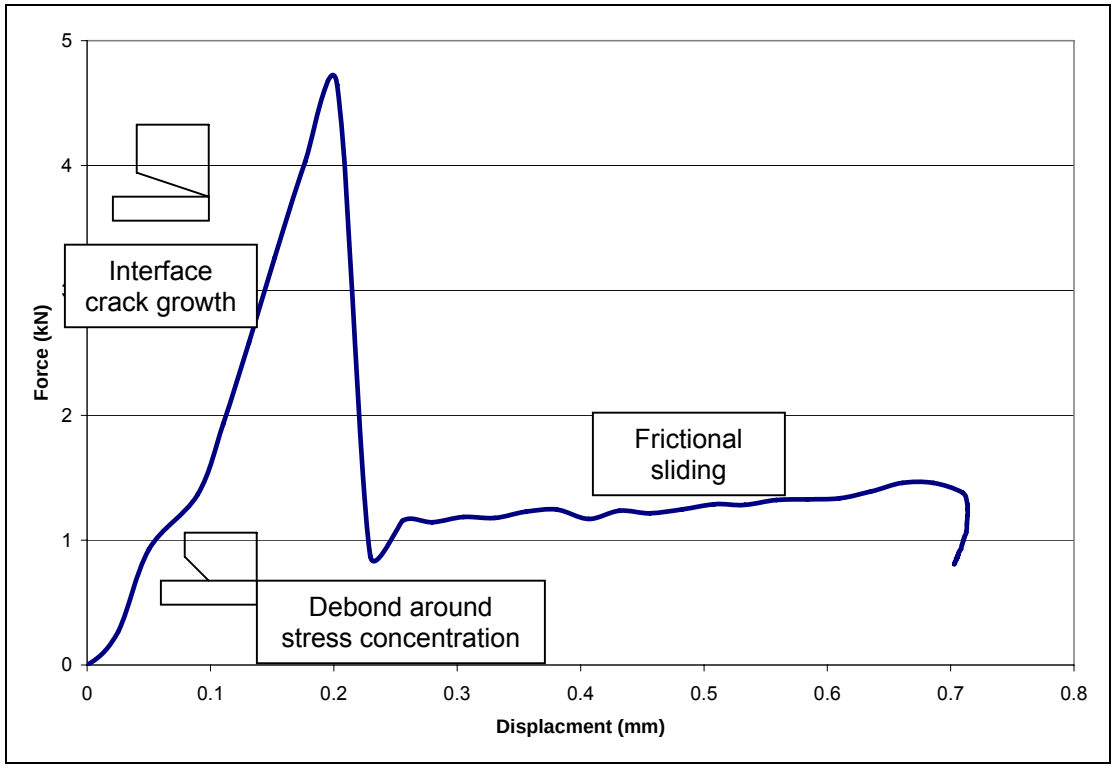

Figure 122: Typical pushout coupon force vs. displacement curve

The interface shear strengths (IFSS) were again calculated based on the assumption that the shear stresses along the pultrusion interface were constant

after the interface had begun to debond as described earlier for the pullout testing. The calculated interface shear stresses on the center rod were highest in all conditions of the erosion treated rods with the (3, 2) case at 58 MPa. Following this, the IFSS was also high in the untreated rod with Teflon spacing with the SiC 320, Teflon treatment right behind. The 5M NaOH rods were next highest followed by both ortho spaced untreated and SiC treated rods. The lowest IFSS were seen in the unwashed 60 minute HNO_3 coupons with less than 4 MPa. The eroded rods also all carried the highest pushout loads, although the untreated rod in both spacings also carried as surprisingly high load as well. The values of the pushout tests are summarized in Table 7.

It is deduced from the table that having the rod elements closer to the center rod also improved the IFSS of the center rod in surface treatments where spacing was considered. The spacing between pultruded elements may affect the buildup of shear stress at the stress concentration point. As the applied force increases, the shear stress profile at the discontinuity encounters the interfaces of the adjacent pultrusions. Faced with another discontinuity, the applied force is now partially being channeled into debonding additional interfaces in more of a crack opening mode (Mode I). The increased energy required to open multiple cracks is guessed as one of the reasons the IFSS of the Teflon spaced coupons is higher than the ortho spaced counterparts.

Table 7: Pultruded Rod Pushout Test Results Summery

Treatment, Spacing	Average Max Load (kN)	Average Max Load Std. Dev. (kN)	Average Calculated Max Shear Strength (MPa)	Average Max Shear Strength Std. Dev. (MPa)	**Rank by Maximum Shear Stress**
Untreated, Teflon	8.95	3.42	41.38	15.20	10
Untreated, Ortho	10.37	3.09	24.51	5.91	14
SiC 320, Teflon	7.76	2.14	36.93	9.82	11
SiC 320, Ortho	4.88	1.96	23.49	7.87	17
2,1 , Teflon	10.51	1.99	50.98	11.30	9
2,2 , Teflon	10.81	2.35	53.07	10.32	5
2,4 , Teflon	11.73	2.19	57.04	9.58	**2**
3,1 , Teflon	10.47	1.57	52.06	8.51	6
3,2 , Teflon	11.86	2.07	57.64	7.48	**1**
3,4 , Teflon	11.41	2.55	55.93	12.18	**3**
4,1 , Teflon	10.31	2.43	51.94	12.53	7
4,2 , Teflon	11.54	2.64	55.55	11.28	4
4,4 , Teflon	10.37	1.32	51.20	7.34	8
60 min Unwashed HNO_3 , Teflon	0.68	0.18	3.24	0.89	20
60 min Unwashed HNO_3 , Ortho	0.50	0.14	2.35	0.61	21
15 min HNO_3 , Teflon	5.00	0.68	24.46	2.10	15
30 min HNO_3 , Teflon	3.98	0.54	19.75	2.33	19
60 min HNO_3 , Teflon	4.49	0.98	22.15	4.05	18
60 min HNO_3 / 1M NaOH, Teflon	4.38	0.65	22.12	3.00	16
60 min HNO_3 / 2M NaOH, Teflon	6.36	0.96	31.58	4.43	13
60 min HNO_3 / 5M NaOH, Teflon	6.58	1.13	32.61	5.59	12

The smaller distances between center and surrounding rods might make a difference in the constitution of the width of the interface off of a rod surface. With smaller distances, the interfaces are closer together and perhaps joined in a way where the interface properties dominate compared to longer distances where

bulk epoxy properties dominate. This might be especially true for the chemical treatments were the loose fibers from each surface could have intermingled in the secondary epoxy infusion.

Some possible errors during pushout testing could be due to the hardened steel pushout rod being slowly bent as the first coupons were being tested. This wasn't noticed until after the untreated othro-spaced rods were tested. This bending might be due to slightly uneven coupon surfaces being tested and the length of the rod being pushed out was too long and the interface damage initiation required large forces. This was mitigated by cutting the remaining coupons in half and re-polishing them. This seemed to work and the rod did not appear to bend afterward. It is unknown how accurate the data for the untreated ortho spaced rods but the data appear to follow the trend where the ortho spaced coupons have lower IFSS than their Teflon spaced counterparts. Also, the small spacing in the Teflon spaced coupons made it difficult to place the pushout rod over the center rod without great care. It is possible that in testing for some coupons, the pushout rod was also pushing on secondary epoxy or clipping an edge of another rod, resulting in skewed higher forces for pushout. This error was believed minimized as severe clipping of any edges was noticeable during the test and could be seen in the tested coupon. The coupon data was then removed from the calculations.

Post-test Images and Discussion

The figures below are selected SEM images of post-tested coupons from the each pushout condition. These are included to observe if any changes in the post-tested center rod and secondary epoxy surfaces can help describe their behavior and the data from Table 7. Other SEM images not included in the body of this study are included in Appendix H.

Figures 123 and 124 are images of post-tested untreated rod with Teflon spacing and the corresponding interface on the secondary epoxy. The hackles from the Mode II component of the debonding interface crack growth are more pronounced in pushout coupons with the Teflon spacing versus the ortho spacing. The hackles extend fairly deep into the spaces between the surface fibers as seen in Figure 124. The large size of the hackles compared to the ortho spacing may be a sign that the shear stresses were higher in the Teflon spaced coupons. With the epoxy in the smaller spacing unable to deflect like the epoxy in the ortho spaced coupons, the secondary epoxy needs to rely on its shear resistance and the tensile component of that resistance created by the mechanical locking of the similarly treated adjacent rods. Thus when the secondary epoxy-outer fiber interface finally gave out, the high stress and load release created the large hackle formation compared to the ortho spaced pushout coupons in Appendix H.

The image in Figure 125 is the secondary epoxy side of the interface. The image has what appear to be deep grooves indented into the epoxy surface.

These grooves look like the carbon fibers exposed on the interface in Figures 123 and 124. The guess here is that the interface failed at *or* just under the pultrusion surface. The fibers are bonded to the pultrusion epoxy stronger than the secondary epoxy.

The SiC 320 abrasion treated rods had similar surface appearances to the untreated rods in both Teflon and ortho spacing. The secondary epoxy side of the interface also appeared the same indicating that the abrasion treated interfaces also fail at the pultrusion surface. These images are in Appendix H.

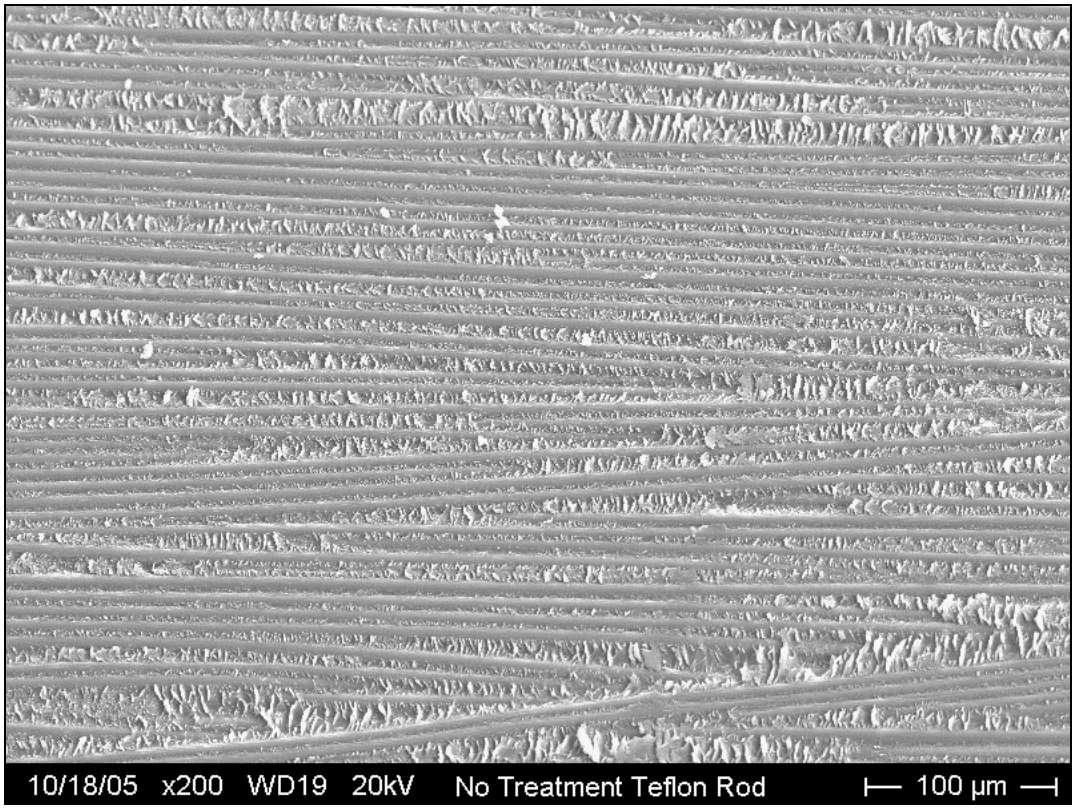

Figure 123: Post-tested untreated rod surface with Teflon spacing

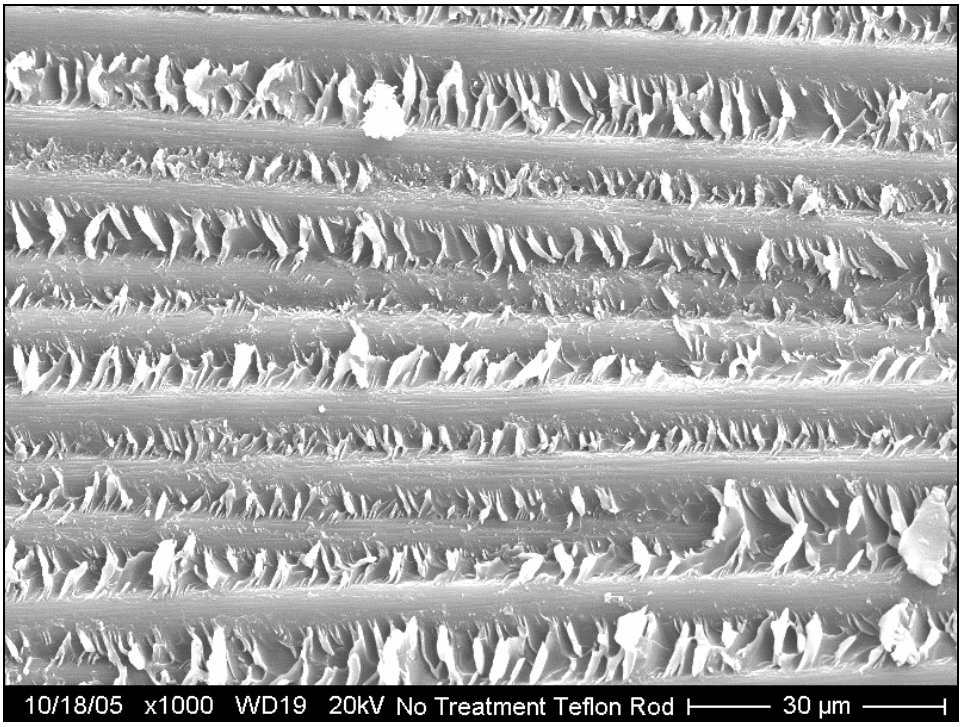

Figure 124: Magnified view of post-tested untreated rod surface with Teflon spacing

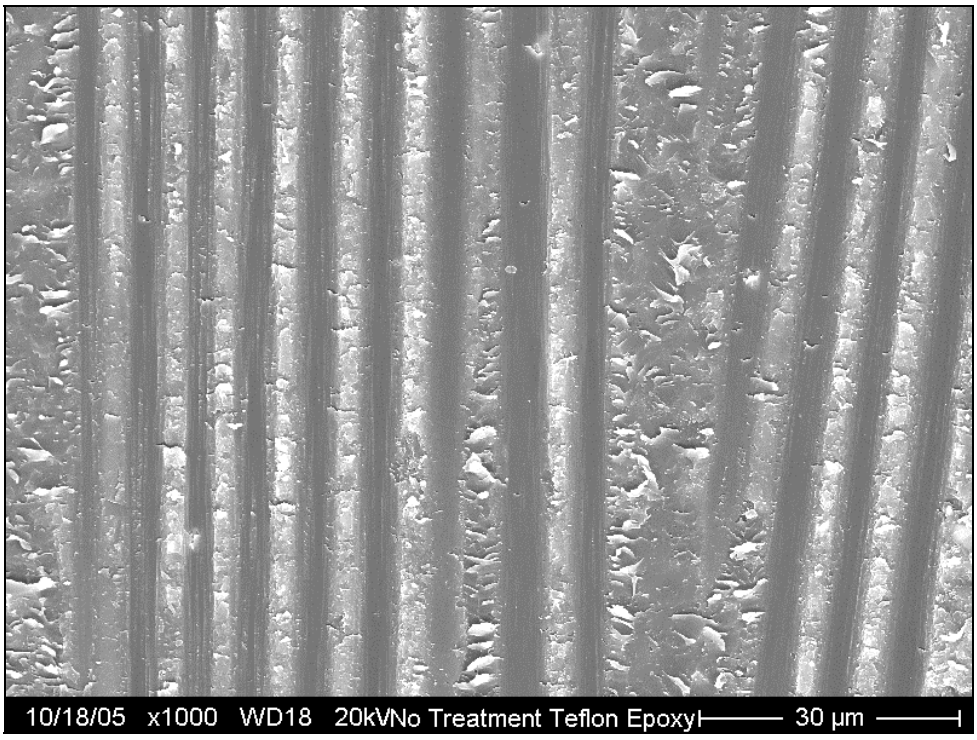

Figure 125: Post-tested secondary epoxy interface surface of untreated rod with Teflon spacing

Figures 126 through 128 are images of post-tested rod surface and epoxy interface from the (2, 1) erosion treatment. In the wide view in Figure 126, the rod surface appears to be sheared relatively smooth by the interface failure. Compared to the pre-tested surface in Figure 100, many of the surface fibers in Figure 127 still appear strongly bonded to the rod surface. This would suggest that the interface failed below the outer fiber layer on the rod surface. The images from Figure 128 seem to show some broken fibers stuck to the secondary epoxy. The large hole shown partially in Figure 128 is from a void at the interface from infusion.

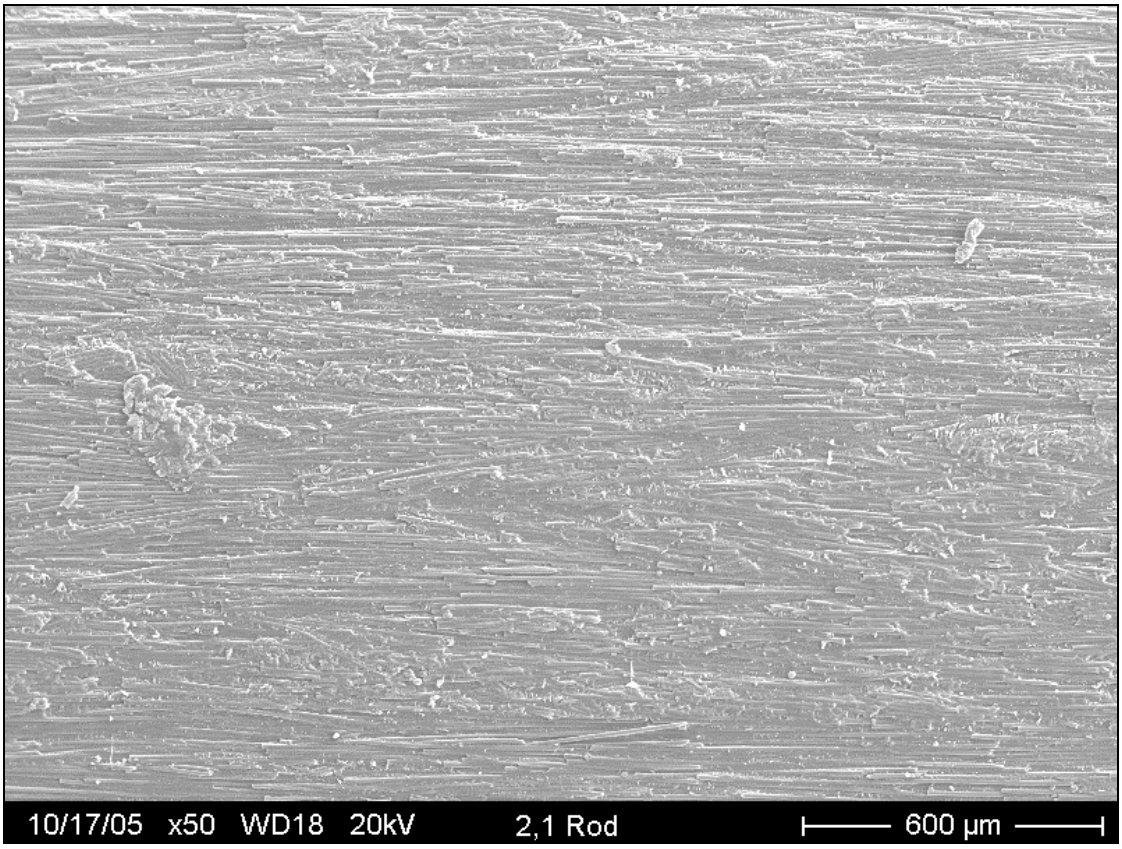

Figure 126: Post-tested (2, 1) erosion treated rod surface

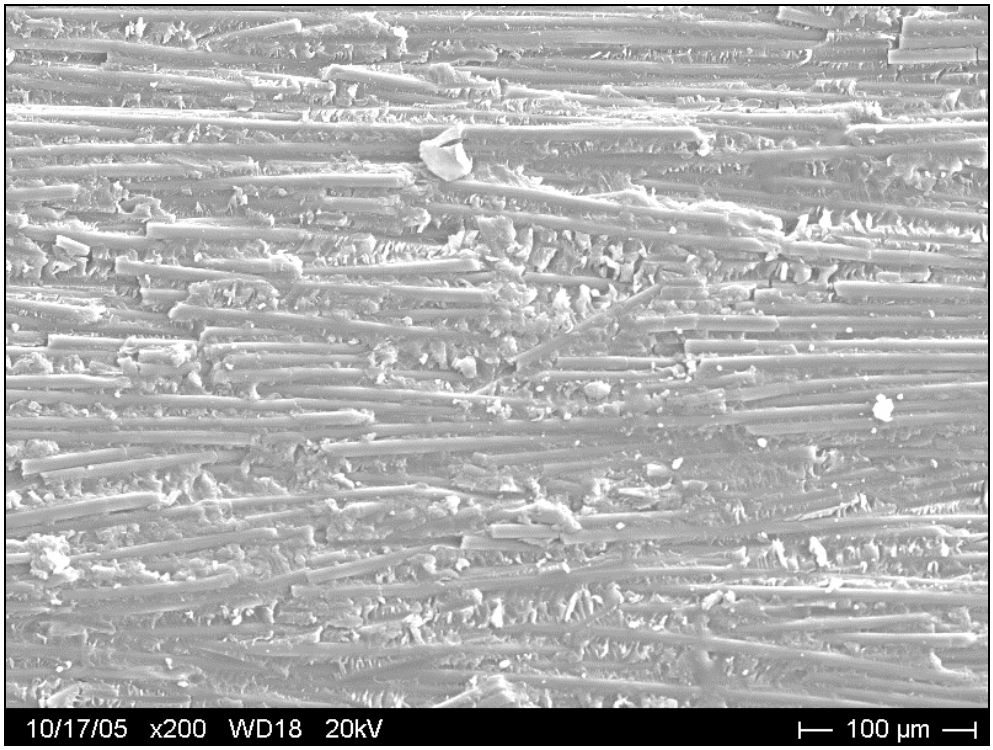

Figure 127: Magnified view of (2, 1) erosion treated rod surface

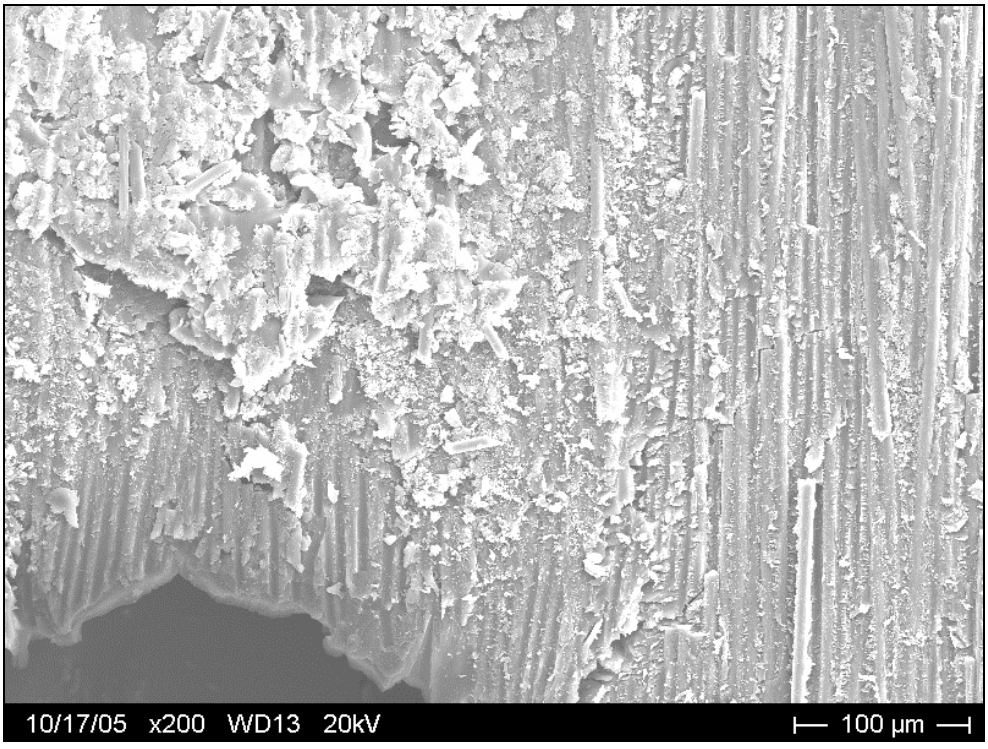

Figure 128: Post-tested secondary epoxy interface surface from (2, 1) erosion treated rod

Figures 129 through 131 are images of the rod and secondary epoxy interface of the (2, 4) erosion condition. While appearing similar to the (2, 2) erosion treatment in Appendix H, the surface in Figure 129 and 130 has had large portions of it sheared away. The secondary epoxy interface in Figure 131 shows that fibers have been taken off the pultrusion surface and some fiber indentations are left in the cured epoxy. This suggests that the interface failure delamination path was very tortuous along individual carbon fibers through a certain depth on the rod surface. This treatment ranked second for the largest shear strength criterion and this delamination path could be the reason why.

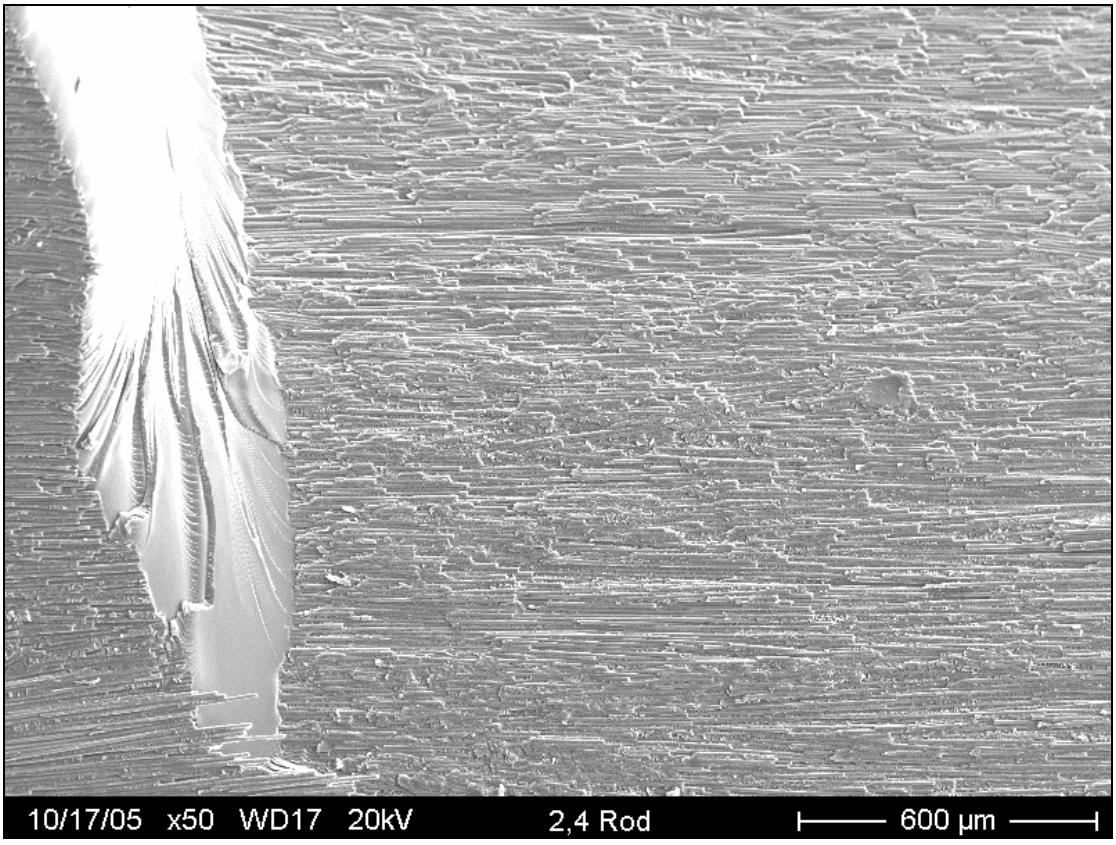

Figure 129: Post-tested (2, 4) erosion treated rod surface

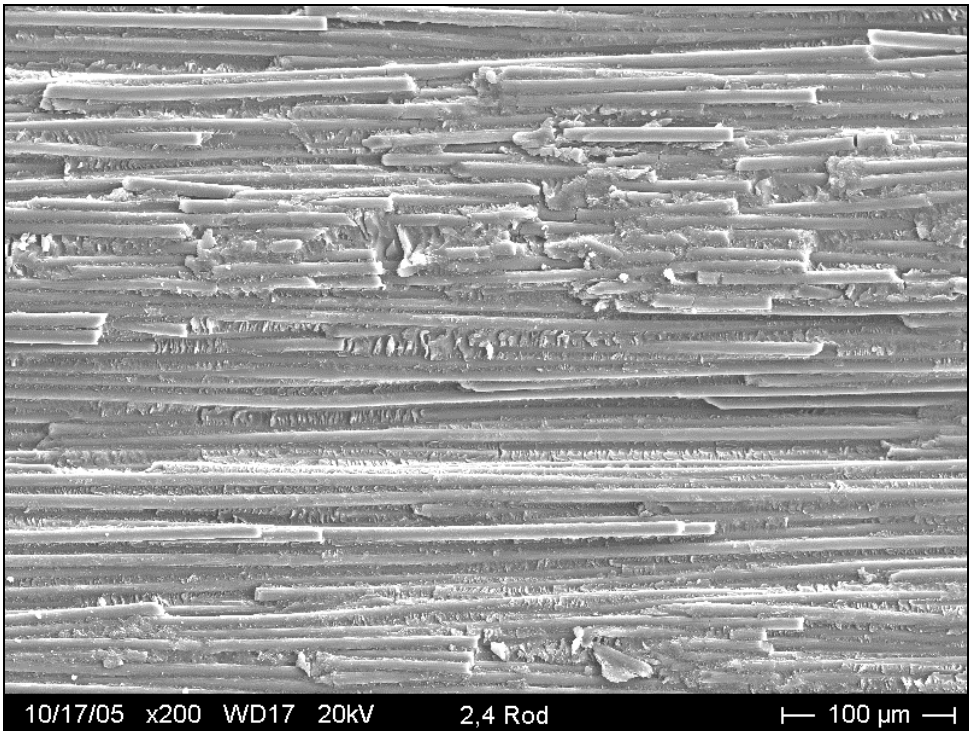

Figure 130: Magnified view of (2, 4) erosion treated rod surface

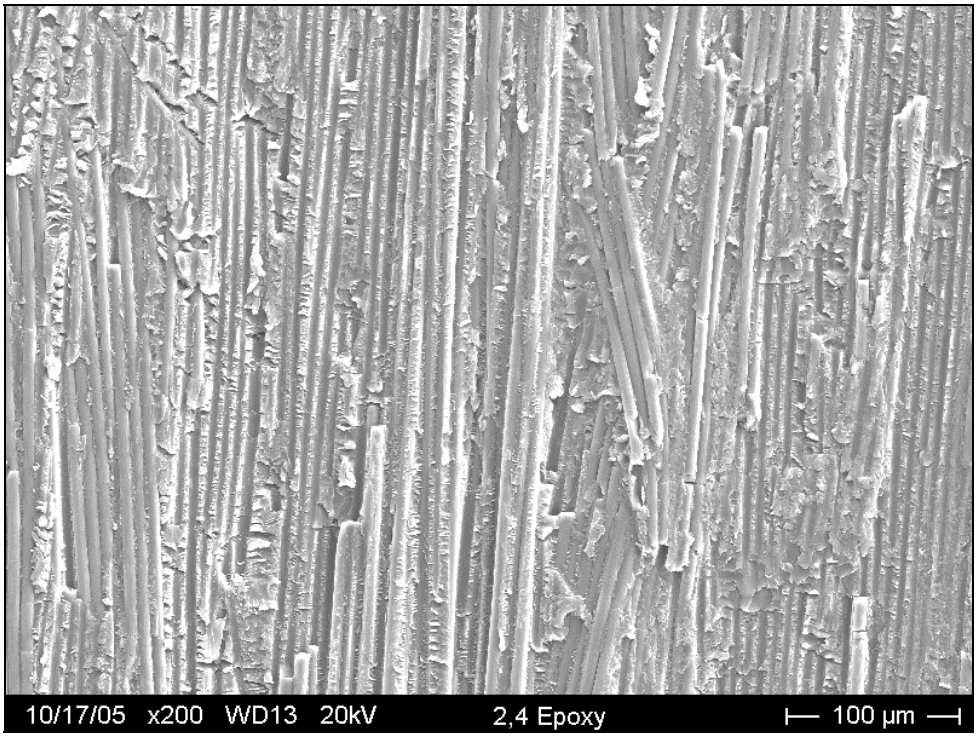

Figure 131: Post-tested secondary epoxy interface surface from (2, 4) erosion treated rod

Figures 132 through 134 are images of the post-tested surfaces of the rod and epoxy from the (3, 2) erosive treatments. Much of the same descriptions used previously in the erosion treatments can again be used here. All the 3 kg/cm^2 erosion air pressure treatments ranked in the top six spots for largest shear strength. This behavior is probably due to the large delamination surface the interface had to debond over. In the interface images on the secondary epoxy, there are fibers stuck to the interface as well as smoother fiber-like indentations from carbon fibers still on the surface of the rod. The (3, 2) rod is very smooth and a lot of the epoxy has been removed. The images of the other 3 kg/cm^2 treated rods seen in Appendix H still have a few jagged edges. These edges show where large chunks of the surface suddenly debonded. That is not really seen in the (3, 2) treated rod. This suggests that the delamination path had no easy route and had to intersect all possible carbon fiber / secondary epoxy interfaces.

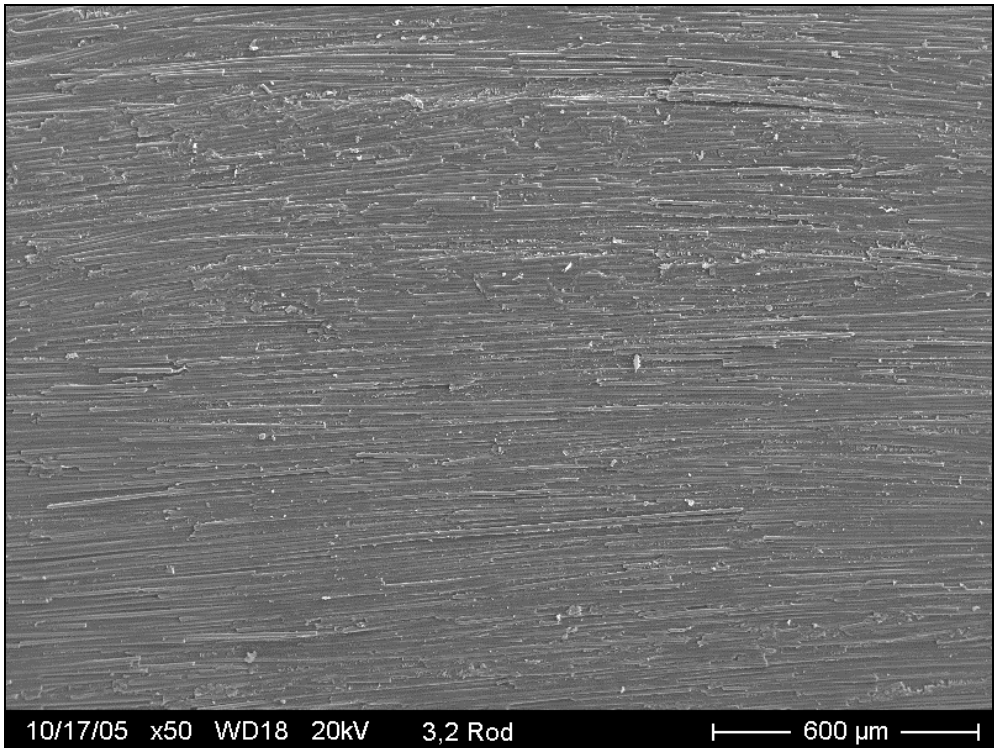

Figure 132: Post-tested rod surface with (3, 2) erosion treatment

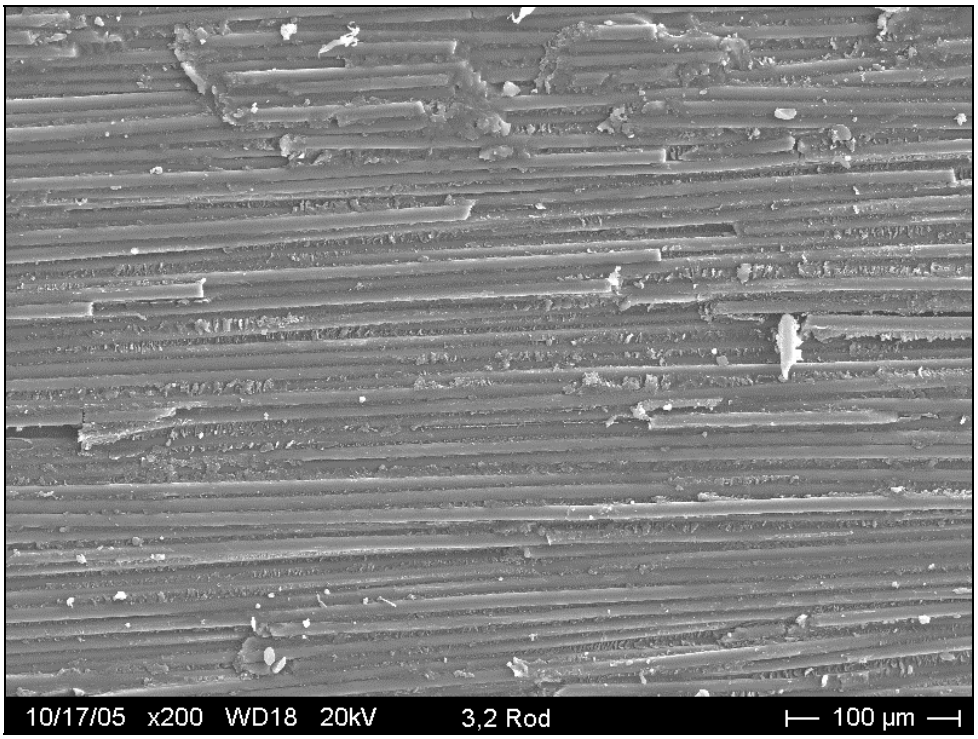

Figure 133: Magnified view of (3, 2) erosion treated rod surface

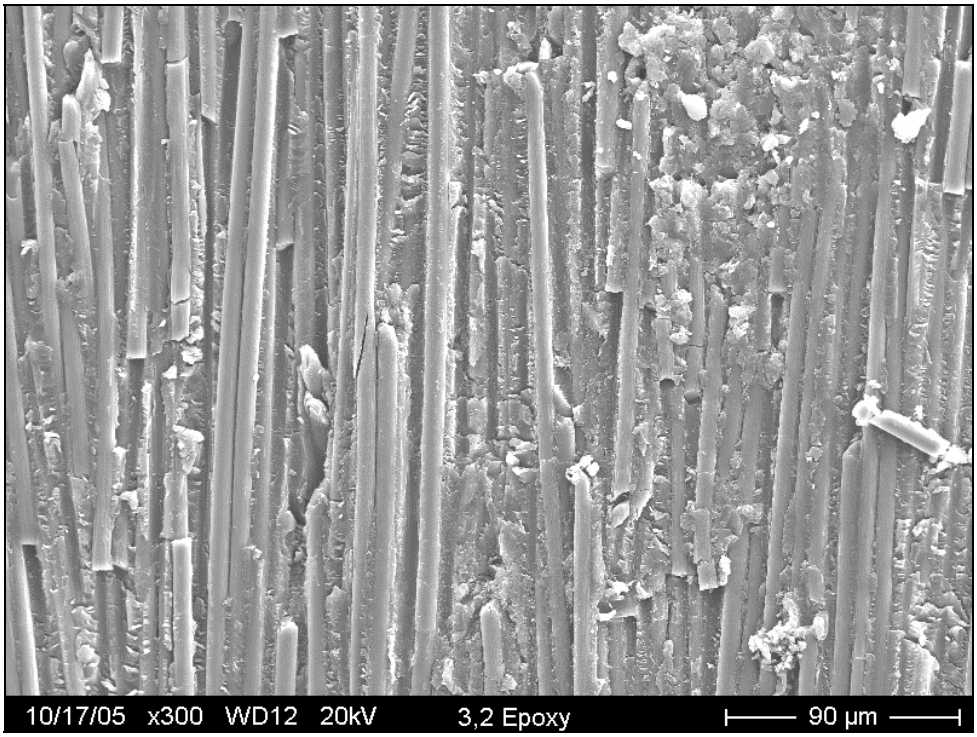

Figure 134: Post-tested secondary epoxy interface from (3, 2) erosion treatment

Figures 135 through 137 are images of post-tested rod and secondary epoxy surfaces from the 4 kg/cm^2 and 2 revolutions condition. The (4, 2) condition ranked fourth in the largest shear strength criterion in Table 7 where as the (4, 1) and the (4, 4) condition were seventh and eighth respectively.

The difference might lie in the delamination interface failure surfaces of the (4, 2) rod in Figures 136 and 137. There are again fibers and fiber indentations in the epoxy surface suggesting that the delamination path is complex and takes a lot of energy to separate the interface from the rod surface. It appears from Figure 137 that the crack growth had to travel underneath some fibers as well.

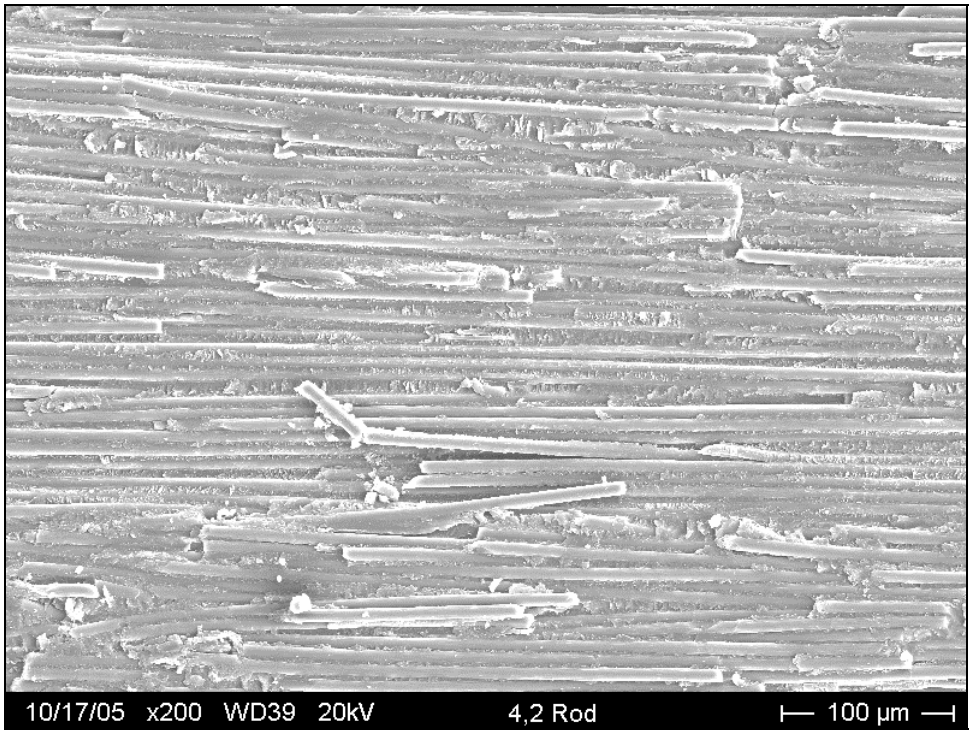

Figure 135: Post tested rod surface with (4, 2) erosion treatment

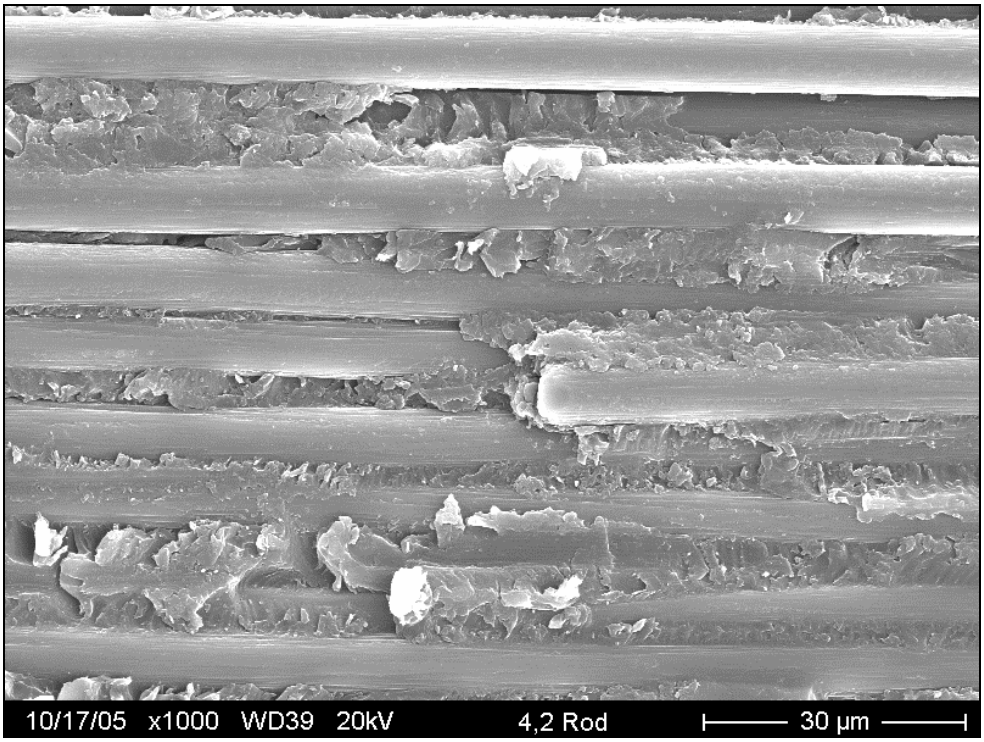

Figure 136: Magnified view of (4, 2) treated rod surface

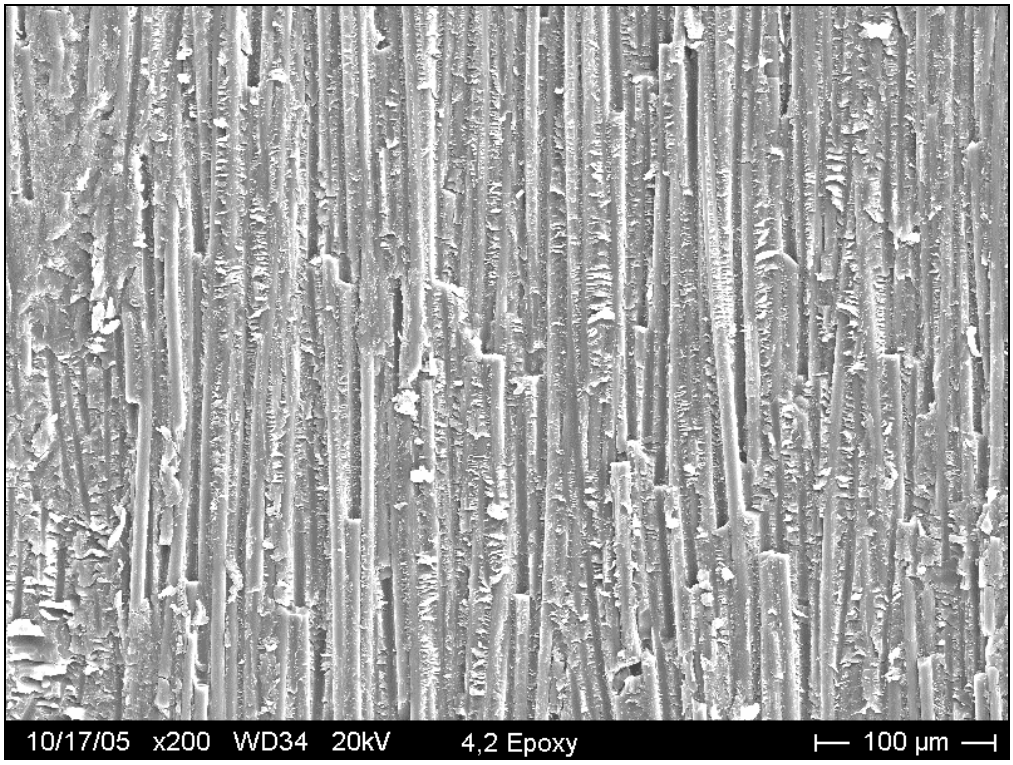

Figure 137: Post tested secondary (4, 2) epoxy interface

Figures 138 through 141 are images of a post-tested rod and secondary epoxy interface surfaces that have undergone a 15 min HNO_3 bath, soaked in distilled water for 5 days and dried in atmospheric conditions. As seen in Figure 138 and 139 the post tested rod surface consists of mostly loosely attached fibers. Much of the former rod surface has been separated from the rod by the interface failure. The weakened pultrusion epoxy from the oxidation could possibly have separated from the underlying fiber surfaces easier. Many corrosion pits are visible in Figure 140. The fact that the interface took with it so many fibers could suggest that the delamination path when the interface failed was fairly complex. Any possible chemical bonding of the oxidized fibers to the

secondary epoxy could force the delamination path to go under the surface of the pultrusion.

The post tested 30 min HNO_3 oxidation treated rod had similar surface appearances as the 15 min treated rods. The extent of the oxidation is only slightly more severe. These images can be seen in Appendix H.

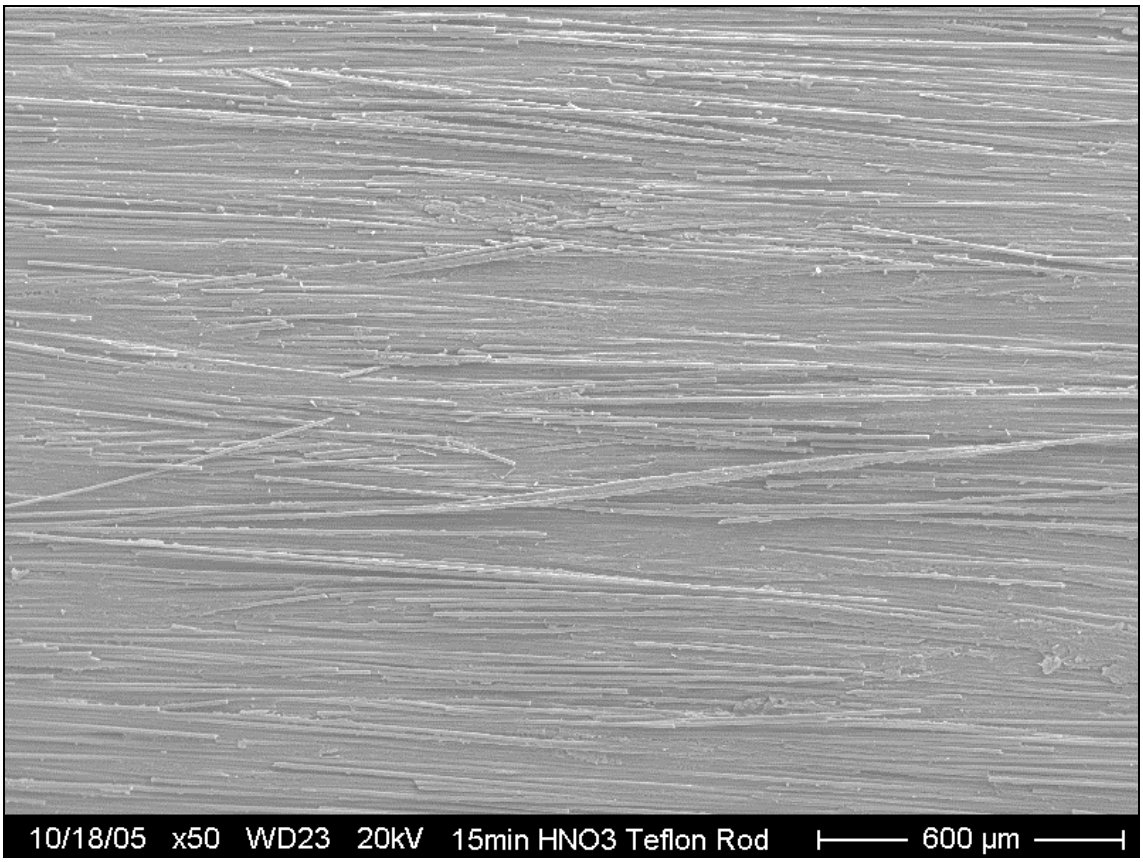

Figure 138: Post-tested 15 min HNO_3 rod surface

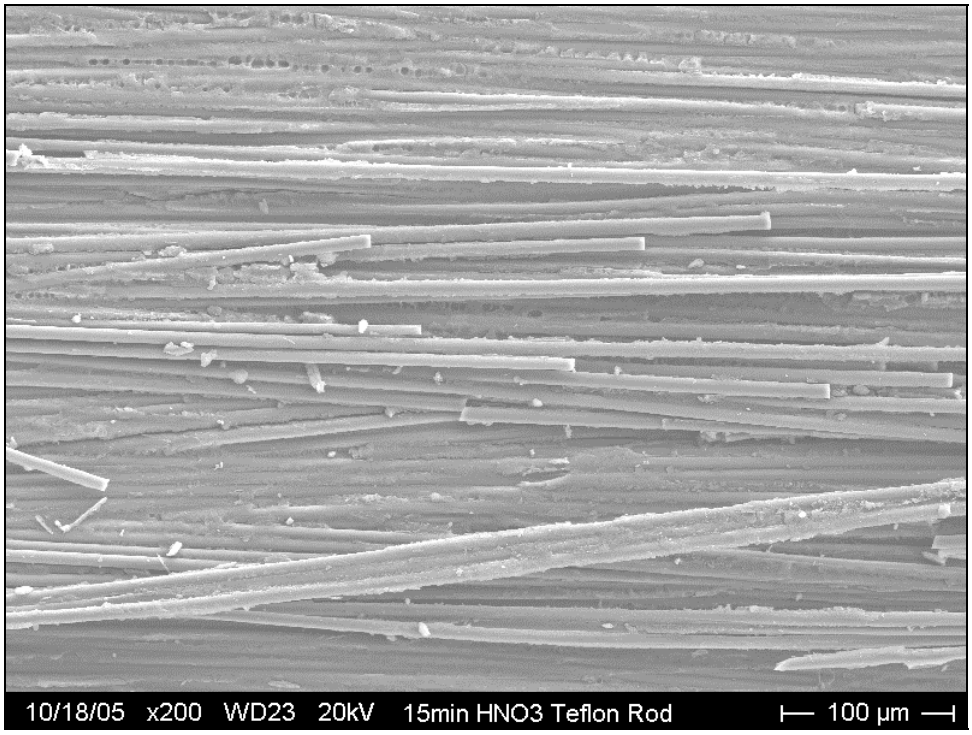

Figure 139: Magnified view of post-tested 15 min HNO_3 rod surface

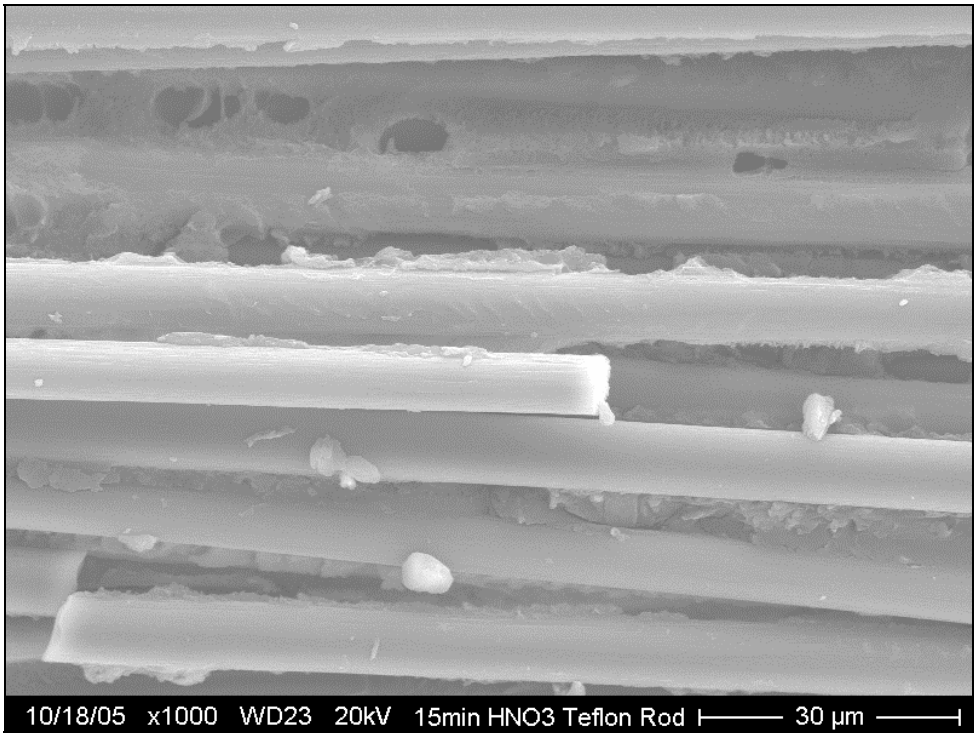

Figure 140: Close up view of 15 min HNO_3 post tested rod surface

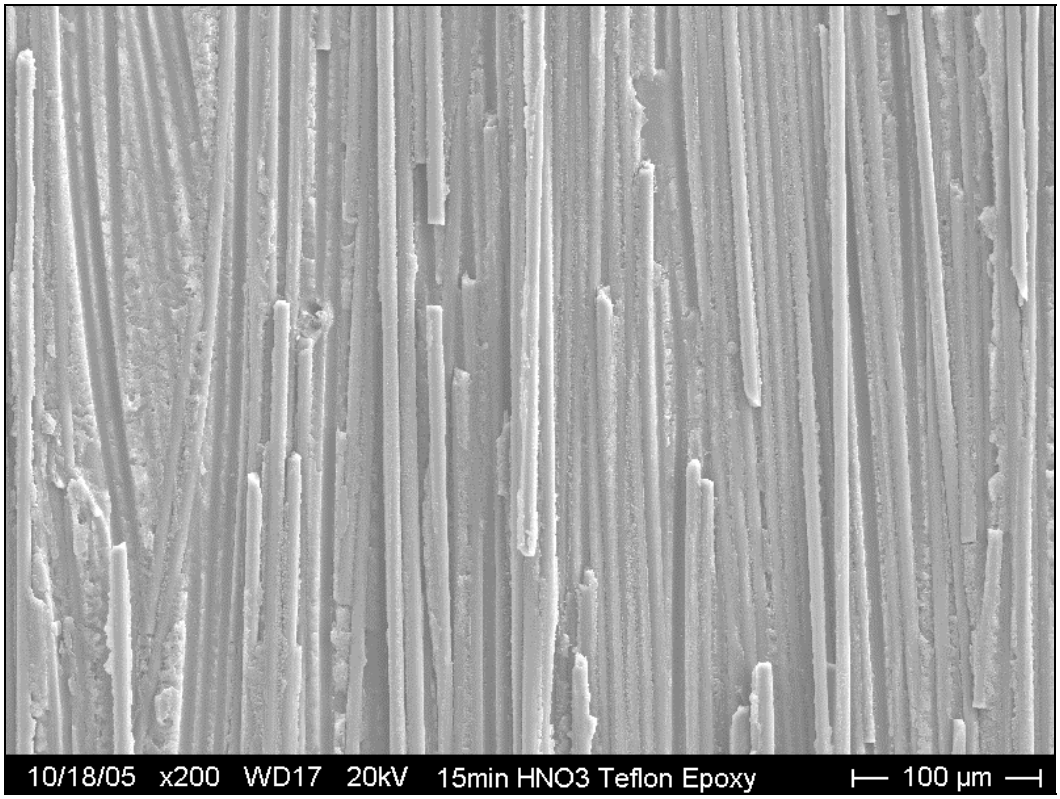

Figure 141: Post tested secondary 15 min HNO_3 epoxy

Figures 142 through 145 are images of the surfaces of the post tested rod and interface from the unwashed 60 min HNO_3 chemical treatment with both Teflon spacing. From the images in Figure 144, it appears there was a significant amount of porosity in this region of the rod. The interface connected with just the outer fibers in a few spots and was sheared off easily. As seen in Figure 144, the severe porosity limited the interface to a few points connecting a few fibers. The interface managed to pull off some fibers in Figures 144 and 145. By and large there was no significant interface in this coupon. The center rod was barely held in place before testing. The pitting and corrosion cracking are very severe.

The unwashed ortho spaced coupons in Appendix H suffered from the same lack of interface between the pultruded rod and the secondary epoxy. As listed in Table 7, these interfaces failed easily, sometimes during the cutting process. Treating composites with heated nitric acid for long times and having no acid removal procedures is not recommended.

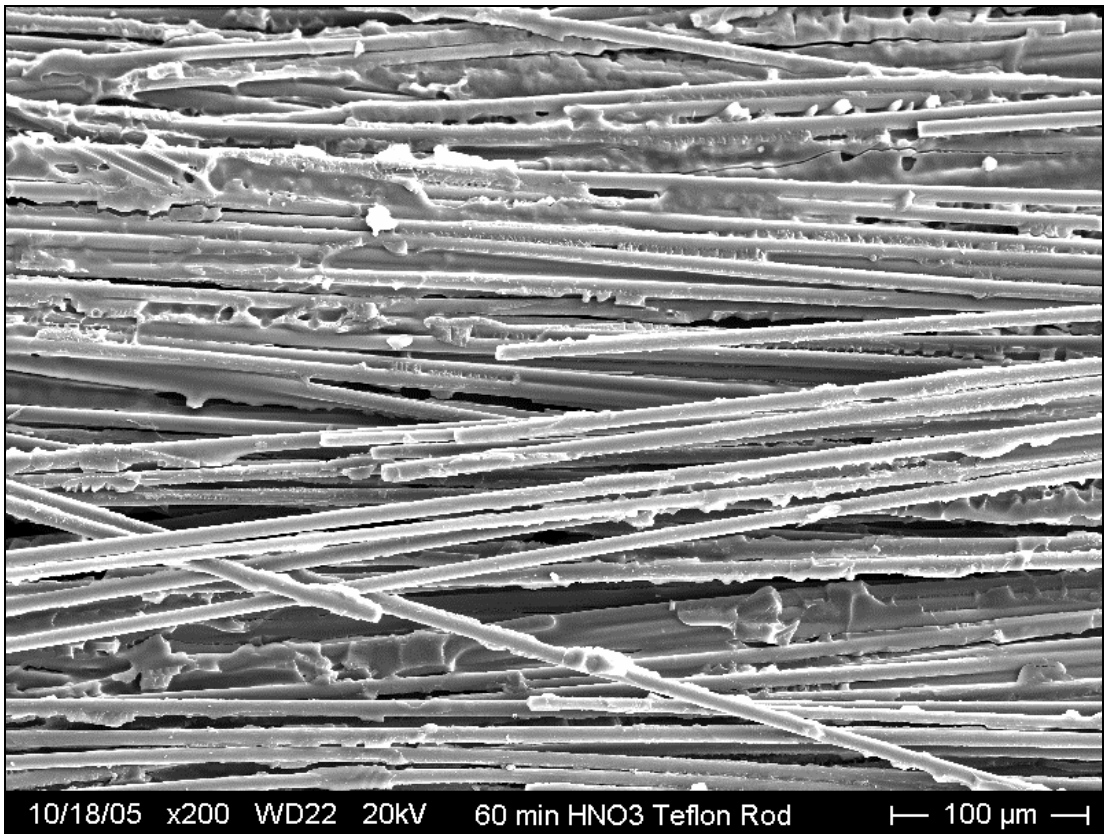

Figure 142: Post-tested unwashed 60 min HNO_3 treated rod with Teflon spacing

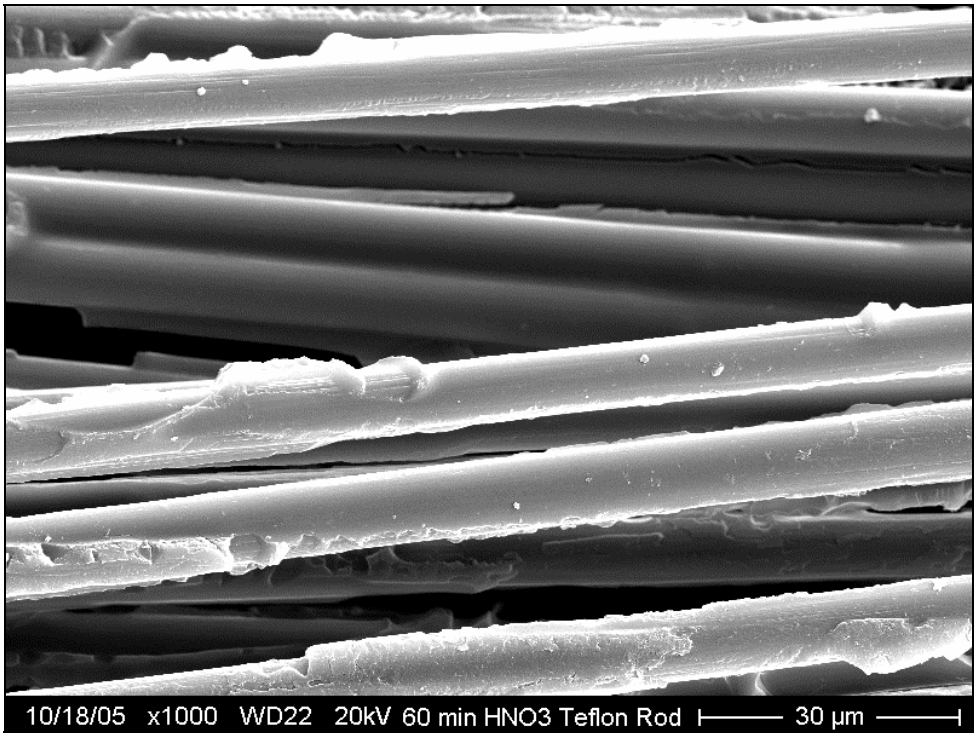

Figure 143: Magnified view of unwashed 60 min HNO_3 rod

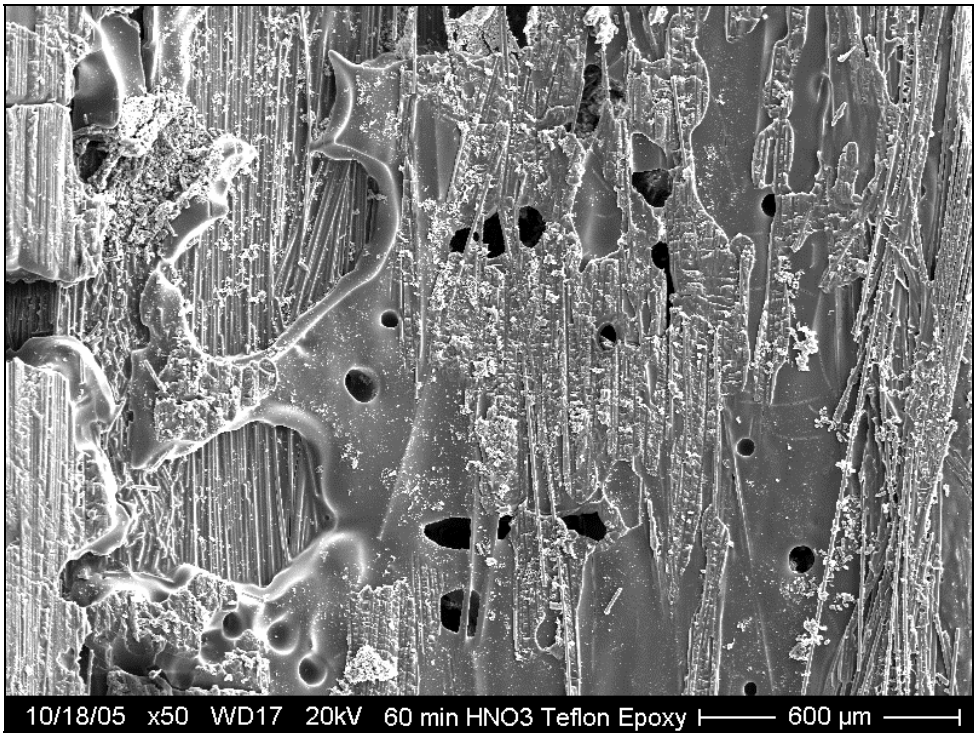

Figure 144: Post tested unwashed 60 min HNO_3 epoxy interface

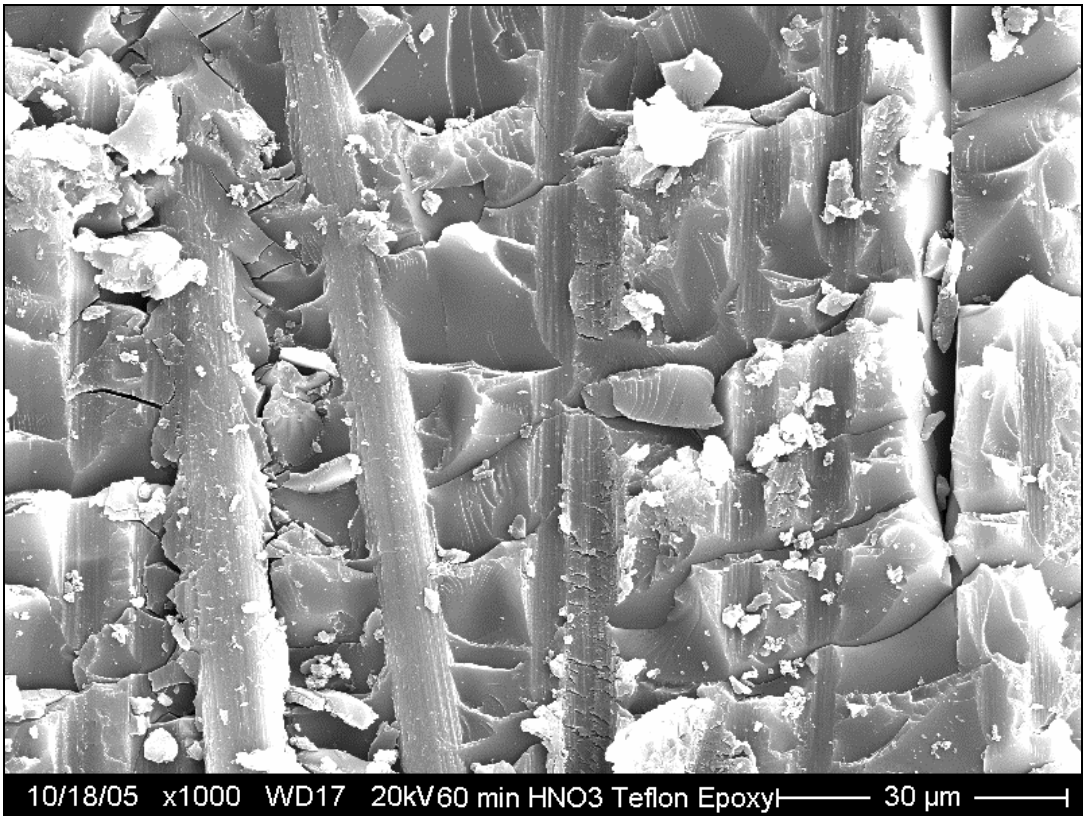

Figure 145: Magnified view of unwashed 60 min epoxy interface

Post tested images of washed 60 min HNO_3 exposed rods in the five day distilled water soak produced similar surface appearances to the 15 and 30 min HNO_3 treated rods. These images are in Appendix H.

Figures 146 through 149 are images of post-tested rod and interface surfaces with the 60 min HNO_3 / 1M NaOH chemical treatment. The loose fibers seen in Figure 146 were probably due to handling the specimen for SEM preparation. The interface between rod and secondary epoxy was primarily a mass of loose carbon fibers. Again the weak point for the interface seems to be the depth of the layer at which the corrosion stops and the secondary epoxy cannot fill in. However, this weak layer may vary in depth by quite a bit, making

the interface crack growth a random event until the cracks coalesce and delaminated from the interface.

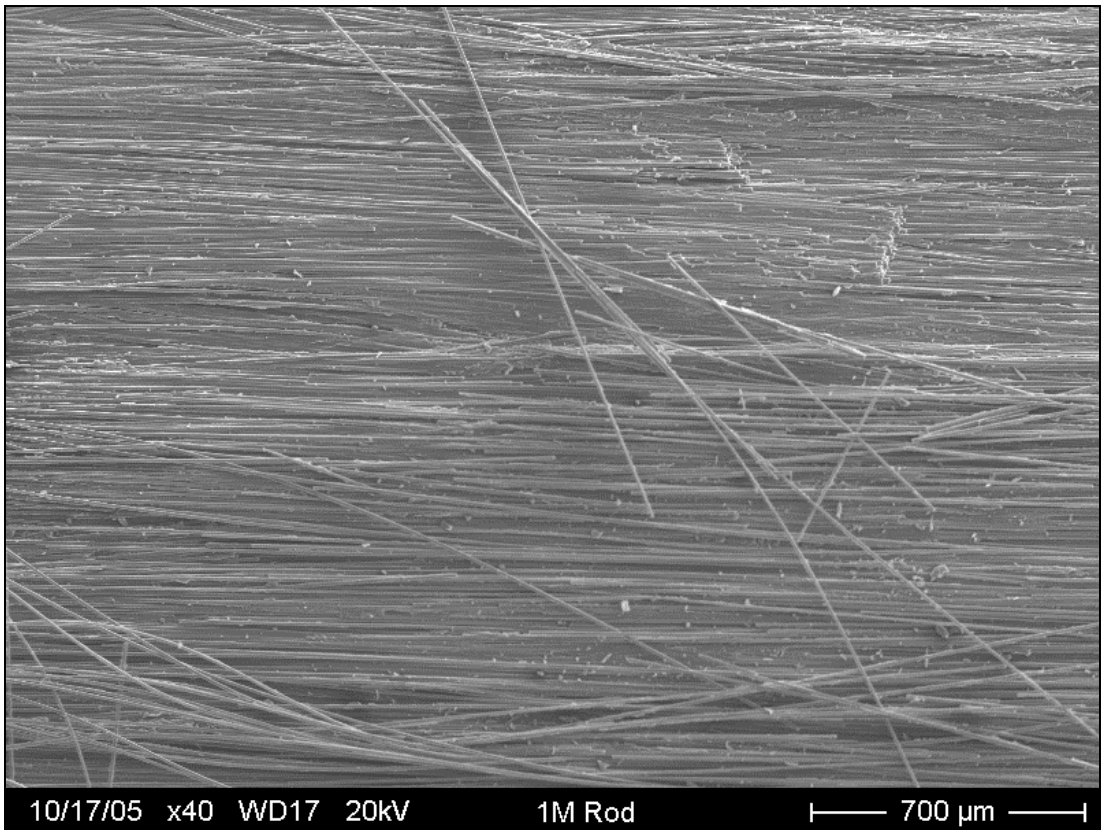

Figure 146: Post tested 1M NaOH surface appearance

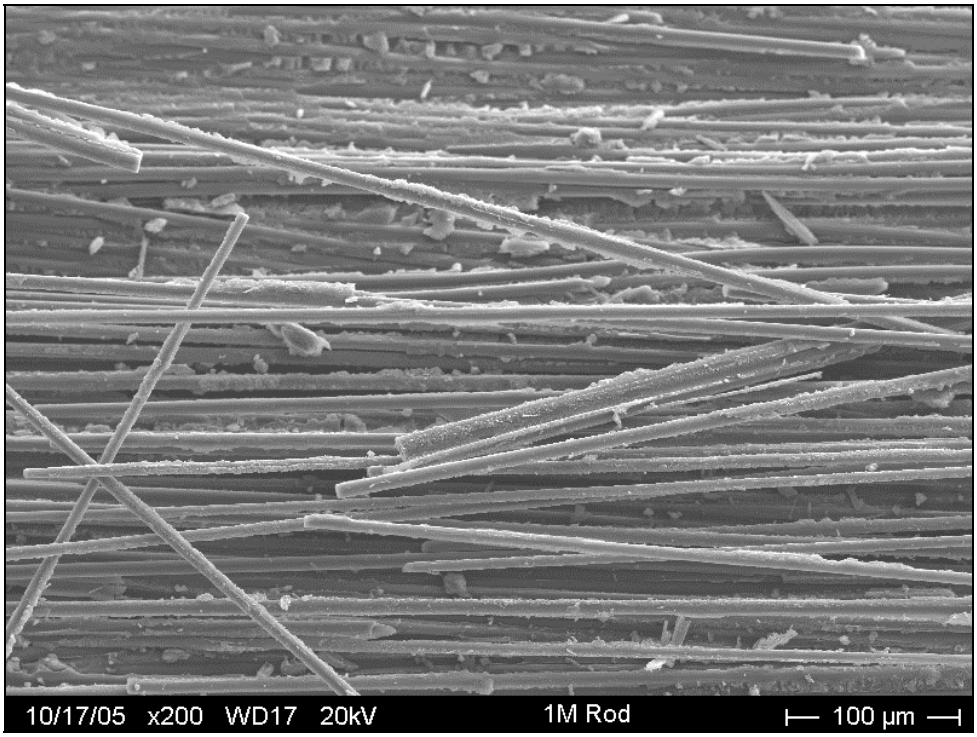

Figure 147: Magnified view of 1M NaOH post tested rod

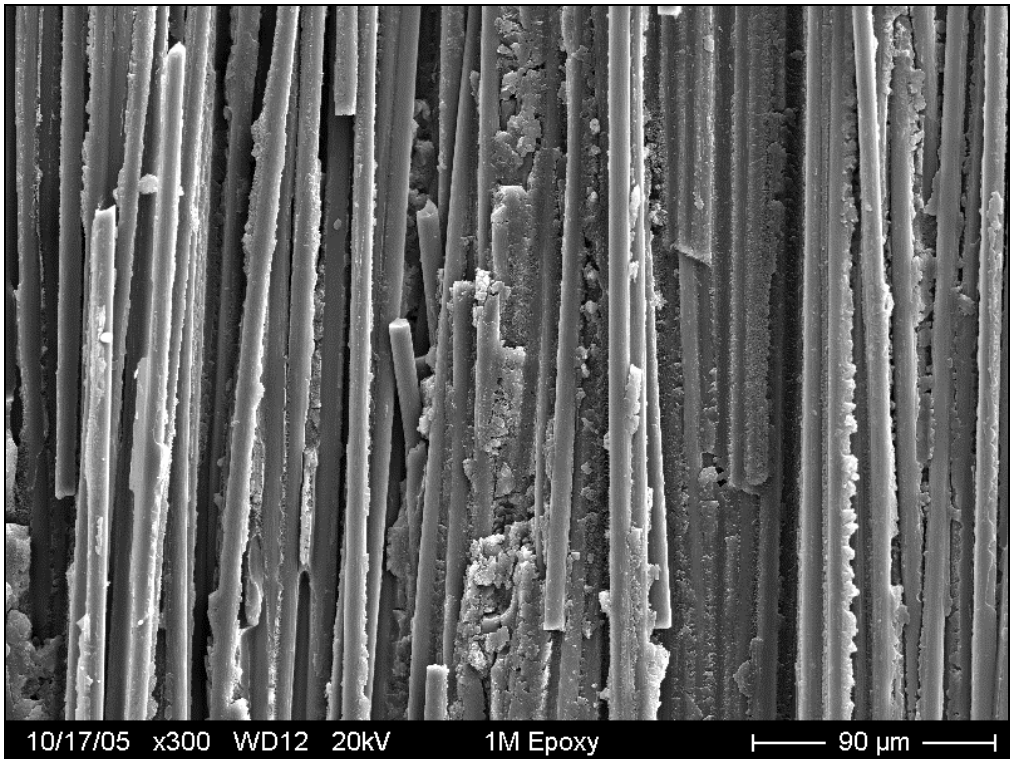

Figure 148: Secondary epoxy interface of the 1M NaOH rod

The 60 min HNO_3 / 5M NaOH in Figures 149 through 151 represents the most aggressive chemical treatment performed in this study. This condition performed the best in terms of having the lowest critical length of the chemical treatments. The interface appears to have debonded all available loose fiber from the rod surface. In Figure 150, there are many sites which can be seen where the epoxy had been sheared away. The weak plane on this condition was still bonded well to the surface of the rod. The interface cracking had harder path to debond the rod than the previous chemical treatments due to still strongly bonded fibers between the interface and the rod surface. The 60 min HNO_3 / 2M NaOH treatment rod appearances are a combination of the 1 and 5 molar NaOH treatments. These images are seen in Appendix H.

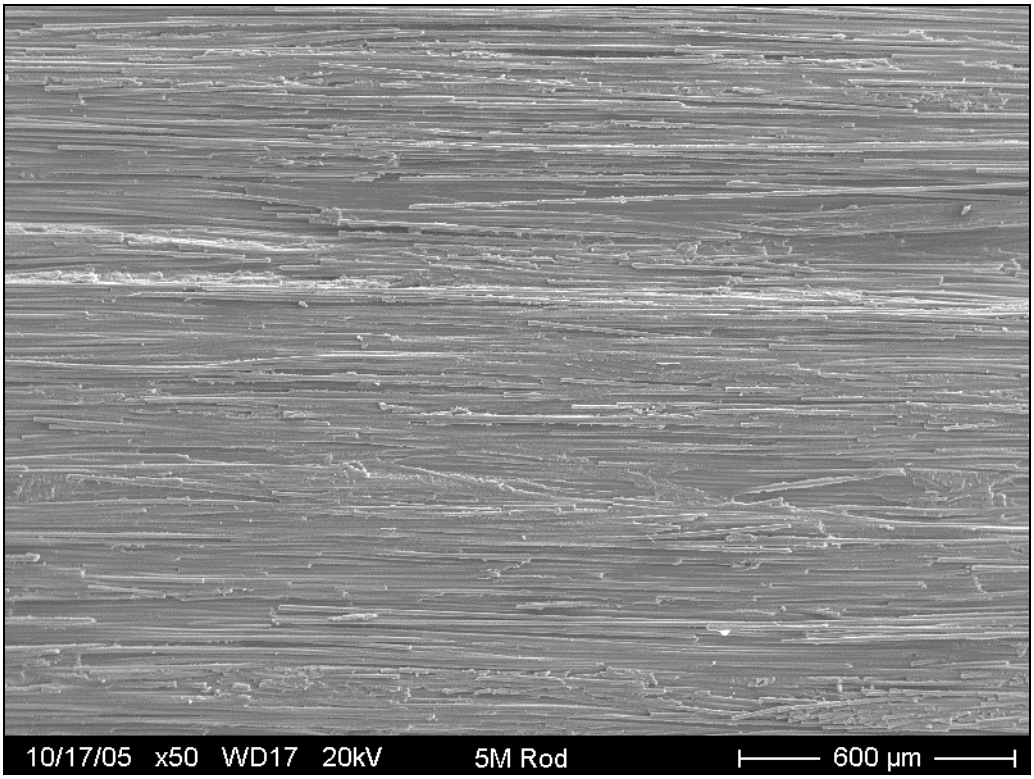

Figure 149: Post-tested 60 min HNO_3 / 5M NaOH rod surface

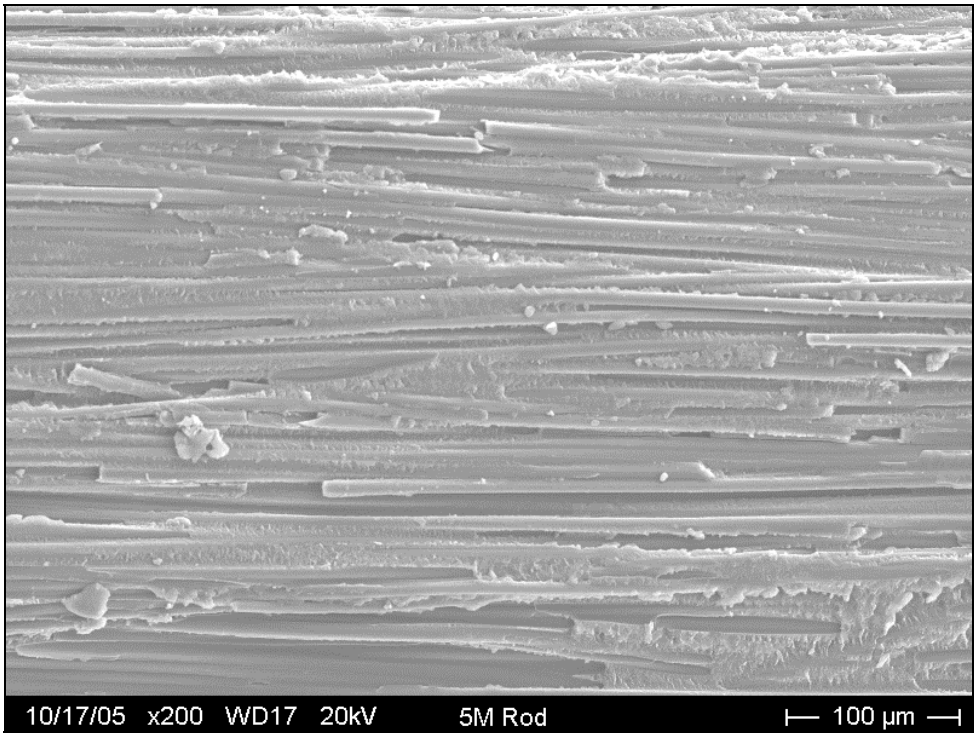

Figure 150: Magnified view of 5M NaOH treated rod surface

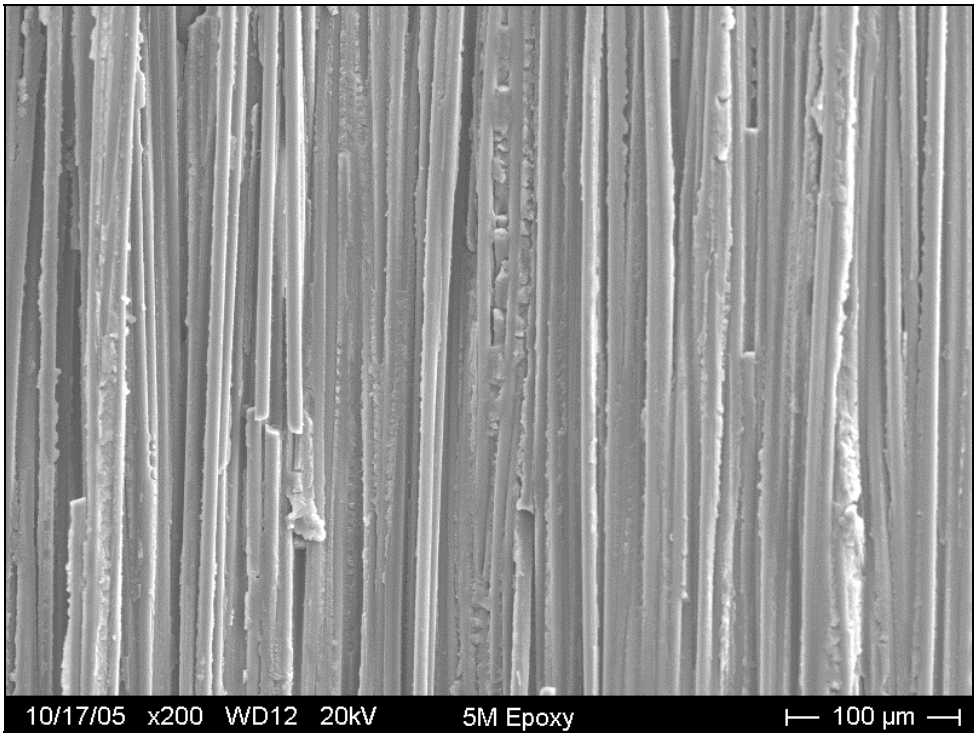

Figure 151: Post tested secondary 5M NaOH epoxy interface

Pultruded Rod Three-point Bending Test Results and Discussion

Carbon fiber performs very well in tension but it is its compression properties that constitute a relative weak point. The purpose of this test is to gage how well these pultruded rods perform in bending. Pultruded rod elements in a wind turbine blade component will likely see bending loads plus compression during operation when used as spar cap reinforcement. With this test the load a single rod can carry at its midpoint as well as elastic modulus in bending, maximum fiber stress on the tension side, and strain to failure can be numerically seen. ASTM standard D4476 was adapted to test the rods. Three point bending was performed instead of four-point bending for testing just to get an initial rough idea of the bending performance of an individual high fiber volume fraction unidirectional pultruded rod.

Results from the rod three-point bending tests listed in Table 8 show that the average elastic modulus of five rod coupons in three point bending was 139.4 GPa with a standard deviation of 5.99 GPa. The maximum outer fiber stress on the tension side before the rod failed in compression side fiber kinking was an average of 1.36 GPa with a standard deviation of 67 MPa. The strain on the outer fibers for this condition was an average of 0.97 % strain. The flexural rigidity of these rods averaged 8.32 $N*m^2$. Again, the rods failed in compression under the loading nose during testing. The break stress for the rods in tension as reported by Zoltek in their own tests was around 2 GPa with a modulus of 175 GPa. The maximum fiber stress is well below what a rod will typically break at for

one percent strain. An example of the fiber kinking and shearing failure mode of a three point bending coupon is shown below in Figure 152.

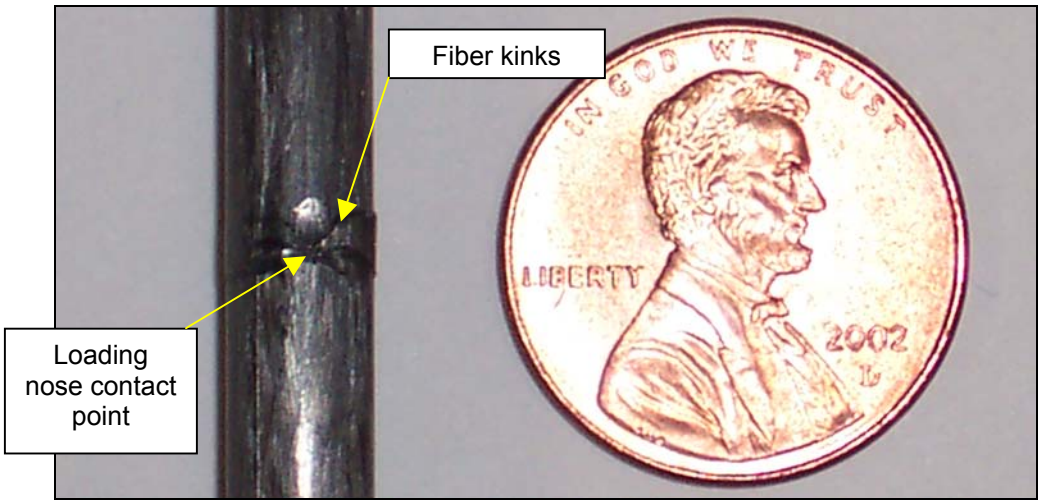

Figure 152: Fiber kinking failure in 3-pt. bending coupon

Table 8: Pultruded Rod Three-point Bending Test Summery

Coupon #	Maximum Carried load (N)	Flexural Rigidity (N*m^2)	Elastic Modulus in Bending (GPa)	Maximum Fiber Stress (MPa)	Percent strain (e*100)
6	856.5	8.6	144.7	1345.0	0.93
7	923.4	8.5	142.7	1450.0	1.02
8	854.7	8.4	141.0	1342.1	0.95
9	908.7	8.5	142.0	1427.0	1.01
10	877.3	8.2	138.0	1324.7	0.94
Test 3	843.6	7.6	128.0	1269.2	0.96
	Average (N)	Average (N*m^2):	Average (GPa):	Average (MPa):	Average:
	877.4	8.3	139.4	1359.7	0.97
	St. Dev.	St. Dev.	St. Dev.	St. Dev.	St. Dev.
	32.2	0.4	6.0	67.2	0.04

A typical force vs. displacement curve for a rod in three point bending is shown below in Figure 153.

Figure 153: Typical force vs. displacement curve for a pultruded rod in three-point bending

With most carbon fiber based composites under static loading, the failure of such composites are generally abrupt and catastrophic. If wind turbine blade structural composites are built using rod constituents, the blades could resist wind gusts and operational loads up to one percent strain without failure on the compression side over short periods of time. Strains above this value could lead to failure in some if not all of the rod constituent members. A theoretical spar cap, a roughly rectangular beam 5 meters by 50 mm, tightly packed with these 5.91 mm rods, would consist of 9,127 rods and would have a linear flexural rigidity of 7.594e4 $N*m^2$.

Rod and Flat Short Beam Shear (SBS) Strength Tests

Short beam shear strength is difficult to apply to any one material property. However, as the failure mode is dominated by the resin and interlaminar properties and repeatable, SBS tests can be used to determine comparative data regarding the quality of the composite in shear. Knowledge of the shear performance of a composite is very important whenever the interfacial bonding or matrix failure is critical, such as when a composite is subjected to compression loading. During loading, the fibers will try to slide past one another. This SBS test on the flats and rods will indicate how well the pultrusion will hold together and resist movement in severe loading. As the thickness of these flat coupons is 1.2 mm and have a typical span between 38.1 and 46.4 mm. With an L/t ratio over 30, the behavior of the coupon is mostly linear. It was not known at the time of the tests if the rods would behave linearly. The SBS test used in this study was adapted from ASTM standard D2344.

The results are listed in Tables 9 and 10. Typical force vs. displacement curves for both coupon types are shown in Figures 155 and 156. The Panex 19 tow coupon had average short beam shear (SBS) strength about 4 MPa higher than the 20 tow counterpart at 65.91 MPa. The Toray fiber flats had an average SBS strength around 67.86 MPa. The failure mode of the flats was by delamination of the pultrusion at the mid-depth of the coupon under the loading nose as seen in Figure 157. The average SBS strength of the pultrusion was 78.94 MPa. Failure of the rods was initiated by kinking of the fibers under the

loading nose and then cracks propagation throughout the composite as seen in Figure 154. If the short beam shear of the pultrusions is indicative of the interface strength of the carbon fibers and pultrusion matrix, then these intra-pultrusion interface strengths are stronger than the interface between the pultrusion and the embedding matrix recorded in Table 7. Thus a loaded composite laminate made of pultruded rods will likely experience debonding between the pultrusions and the *epoxy* embedding matrix *used in this study* before the pultrusions begin to fail.

Table 9: Pultruded Rod SBS Test Summery

Rod Coupon #	First Damage Load (N)	Apparent Shear Strength (MPa)
1	3283.8	79.9
2	3263.9	79.5
3	3264.0	79.5
4	3158.5	76.9
	Avg (N)	Average (MPa)
	3242.5	78.9
	St. Dev	St. Dev
	56.8	1.4

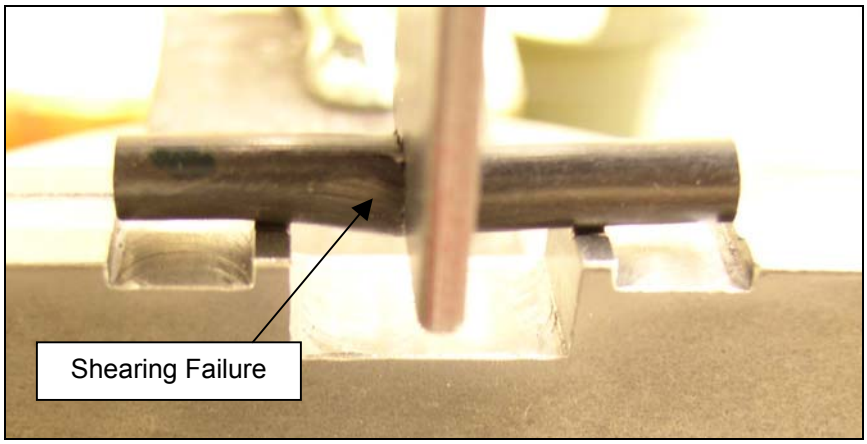

Figure 154: Failed SBS coupon with pure shear failure mode

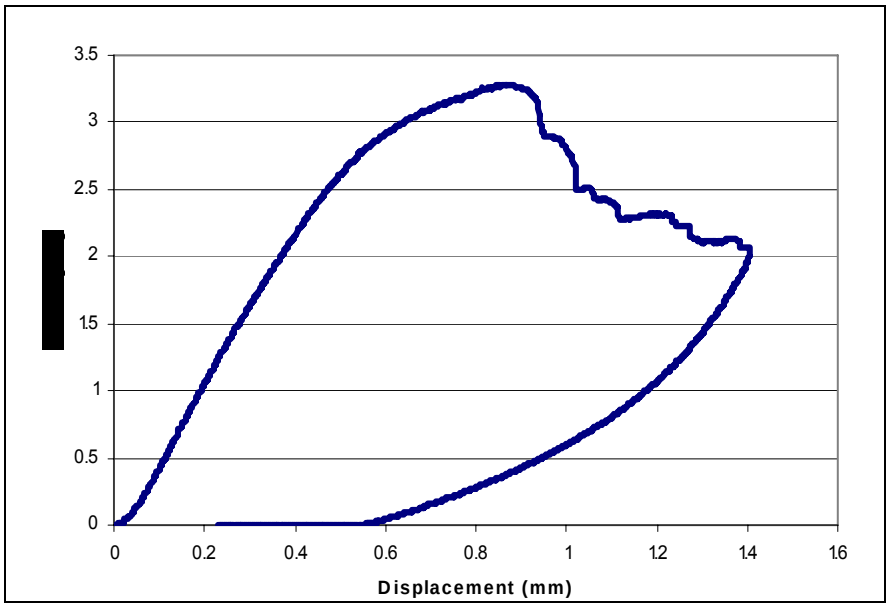

Figure 155: Typical force vs. displacement curve for a pultruded rod in short beam shear

Table 10: Pultruded Flat SBS Test Results Summery

Coupon	First Damage load (N)	Apparent Shear Strength (MPa)
Panex 19-1	1391.7	68.3
Panex 19-2	1369.8	68.0
Panex 19-3	1455.7	69.8
	SBS avg (MPa):	St. Dev
	68.7	0.97
Panex 20-1	1394.9	65.8
Panex 20-2	1471.4	66.5
Panex 20-3	1243.0	62.7
Panex 20-4	1344.6	68.5
Panex 20-5	1258.1	62.9
Panex 20-6	1381.2	69.2
	SBS avg (MPa):	St. Dev
	65.9	2.72
Toray 1	1366.7	69.0
Toray 2	1405.3	68.8
Toray 3	1537.8	68.2
Toray 4	1539.5	68.9
Toray 5	1325.0	65.0
Toray 6	1356.0	67.3
	SBS avg (MPa):	St. Dev
	67.9	1.52

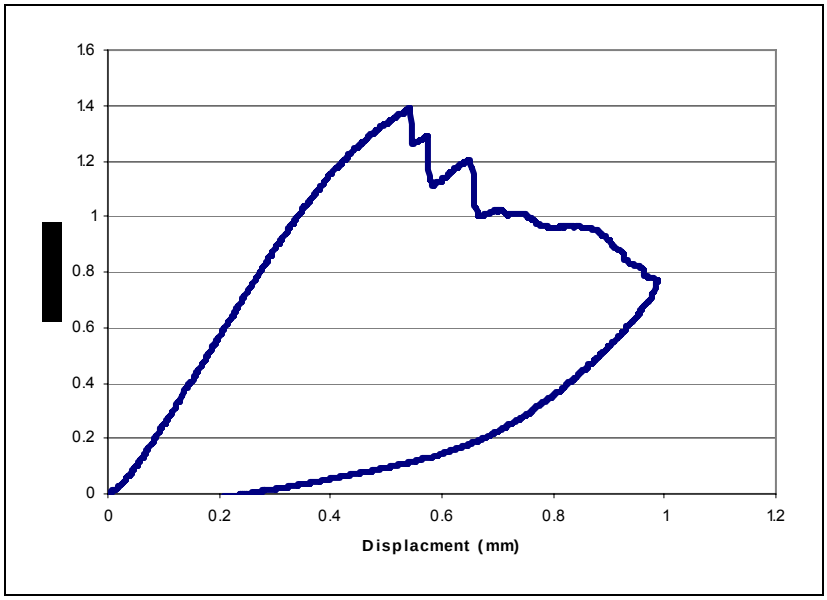

Figure 156: Typical force vs. displacement curve for a pultruded flat in short beam shear

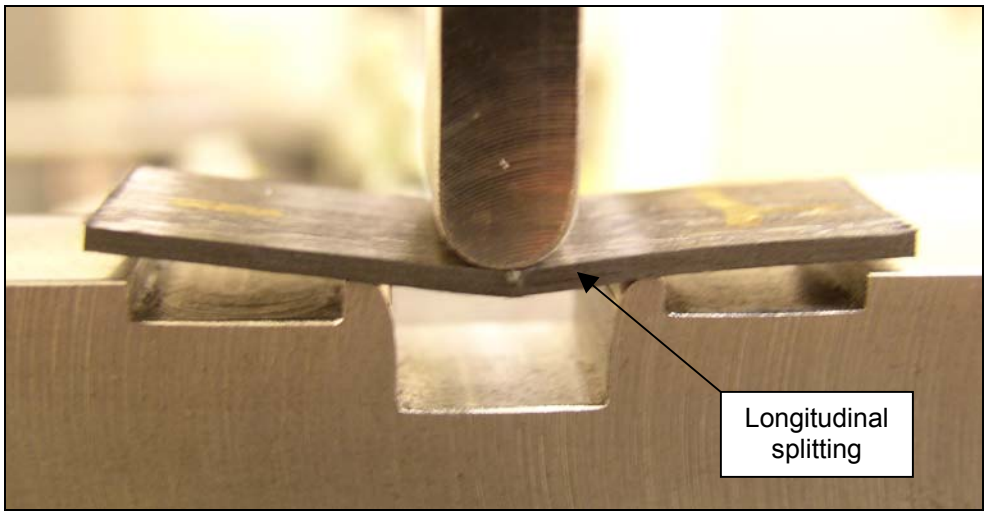

Figure 157: Failure mode of flat coupon in SBS testing apparatus

Pultrusion Tension Test Results on Panex 19 tow and Toray Flats

This test determines the upper limit of pultruded carbon fiber geometry performance. The tension properties and tension fatigue properties of carbon fiber are typically better than glass and this would demonstrate the theoretical

benefits of carbon fiber performance over the glass based wind turbine blades [16].

Tension tests done on the flat coupons between the 19 tow Panex fiber and the Toray fibers demonstrated that the Toray fiber flats broke at a higher stress level than the Panex fiber flats for equal cross-sectional areas. The Toray fiber flat also had a strain to failure higher than that of the Panex flats. However, the Panex flats have slightly more fibers contained within than the Toray flats. Both types of coupons had such enormous strain energy released upon breakage that the cross heads of the Instron testing screw machine shot up abruptly and the grips relaxed enough that the coupon was able to strike the cross head and ignite the grease on the crosshead. Comparing the two types of flats by fiber volume fraction, the Toray fiber based flats had a higher break stress averaging about 3.07 GPa for a typical fiber fraction of 0.695 percent. The Panex fiber based flats had a break stress around 2.23 GPa for a typical fiber fraction of 0.715 percent. Normalizing the break stresses by respective fiber volumes in Table 5, the Toray break stress is calculated at 4.42 GPa and the Panex 19 tow break stress is calculated at 3.12 GPa. A typical stress vs. strain plot is shown in Figure 158.

The single Toray flat fitted with a strain gage had a strain to failure of 1.83 percent while the two Panex flats had strains to failure of 1.28 and 1.49 percents. The modulus of the Panex flats was calculated at 155 GPa compared to the Toray flat modulus of 151 GPa. These values are summarized in Table 11 below.

Table 11: Panex 19-tow and Toray Carbon Fiber Pultruded Flat Tension Test Results Summery

Zoltek 19-tow Coupon #	Area (mm^2)	Load (kN)	Break Stress (GPa)	Break Stress Normalized by Vf (GPa)
1	26.91	61.61	2.29	3.20
2	27.75	54.98	1.98	2.77
3	26.51	61.96	2.34	3.27
4	27.495	63.57	2.31	3.23
		Average:	2.23	3.12
		St. dev.	0.167	
Toray Coupon #	Area (mm^2)	Load (kN)	Break Stress (GPa)	
1	28.08	84.20	3.00	4.31
2	27.96	83.76	3.00	4.31
3	27.49	89.54	3.26	4.69
4	27.73	84.12	3.03	4.37
		Average:	3.07	4.42
		St. dev.	0.125	

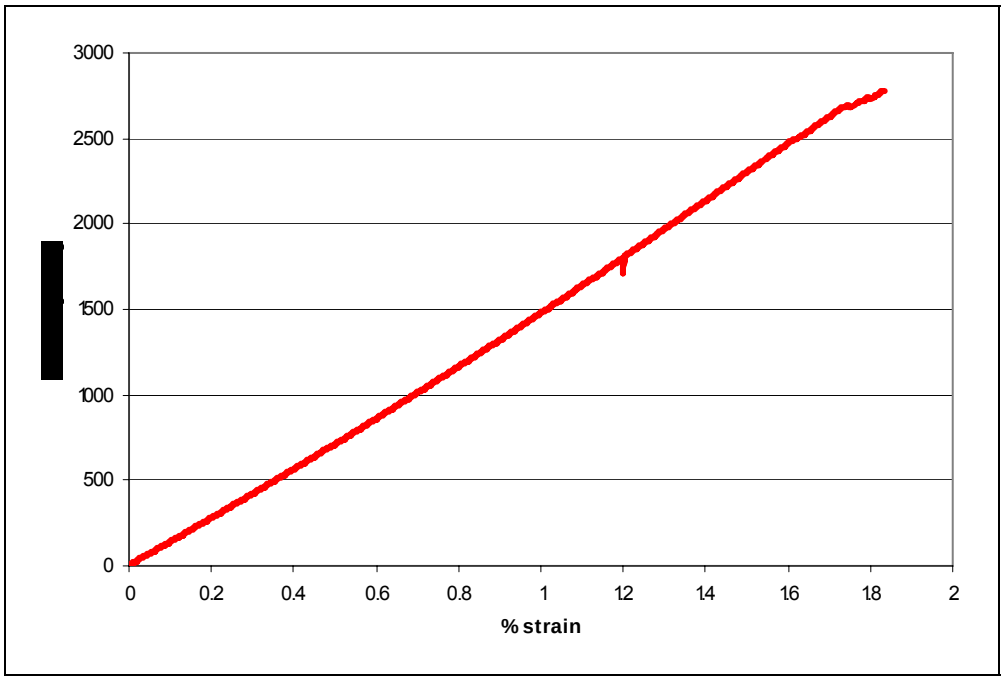

Figure 158: Typical stress vs. strain curve for a pultruded flat in tension

All flat tension failures were catastrophic and appear to start near the flat-tab boundary or just below it. The failure crack appears to propagate horizontally along this boundary through the fibers then vertically though the matrix of the coupon until the crack reaches the other horizontal side of the coupon. When the coupon failed, it also pulled out of the tabs. A typical failure is shown below in Figure 159.

Recalling the SEM micrographs of the carbon fiber ends in Figures 83-85, the Panex fibers appeared more misshapen and the diameters of the fibers themselves also varied noticeably compare to the much more uniformly shaped Toray fibers. The variability in the Panex fibers may be the cause of the lower break stresses in the Panex pultrusions compared to the Toray based pultrusions even though the Panex based pultrusions had many more fibers.

Another way to evaluate the performances of the pultrusions is to compare these break stress results with prepreg composites of similar fiber volume fractions. Table 12 below lists the above results from Table 11 along with selected carbon fiber prepreg composites tested in the MSU database [16].

Table 12: Comparison of Pultrusions and Unidirectional Prepreg Composites

	Pultrusions		Prepregs	
	Panex 32	Toray T-700	Hexcel M9.1 $[0]_3$	SP Systems $[0_3]$
Thickness (mm)	1.2	1.2	1.63	1.35
Fiber Volume Fraction	0.72	0.7	0.5	0.54
Break Stress (GPa)	3.1	4.4	3.7	4
Modulus (GPa)	155	151	105	124
Strain-to-Failure (%)	1.3	1.5	1.5	1.8

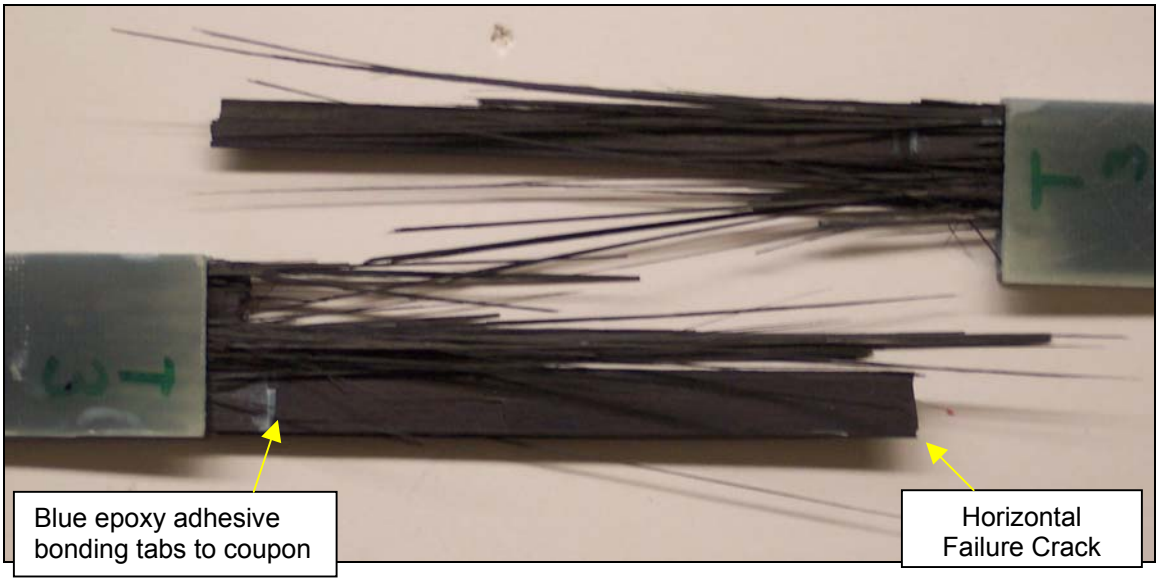

Figure 159: Failed Toray flat in tension

Compared to the prepregs, the pultrusions pack many more fibers into a smaller thickness with comparable tension break stresses. The moduli of the pultrusions are slightly higher than their prepreg counterparts with about equal strains-to-failure in tension. Judging from this chart, pultrusions have the edge on prepreg composites in tension.

With these interface and individual pultrusion testing results, some conclusions about their suitability in wind turbine blade structures can be made.

CONCLUSIONS AND FUTURE WORK

Recommendations on Pultruded Insert Preparations

Theoretical calculations can be made concerning the overall fiber volume fraction of laminate made with pultruded elements. In this case, the laminate is four rod diameters wide and one rod diameter tall. Both Teflon and orthodontic rubber band spacings will be included in the calculations. For Teflon spacing (0.127 mm), the laminate width would be 24 mm. The area fraction of the rods compared to the entire laminate area is 77.3%. Using a rod fiber volume fraction of 70%, this gives an overall fiber volume fraction of 54.1%. This is comparable to typical wind turbine blade laminates found the MSU Database. For ortho spacing (0.762 mm), the laminate width is 25.9 mm and the rod area cross section fraction drops a little to 71.6%. Multiplying this area fraction by a rod fiber volume fraction of 70% the overall fiber volume results in 50.1%. This fiber volume fraction is still good compared to other wind turbine blade laminates. The results imply that having smaller cross-sectional pultrusions of the same pultrusion fiber volume spaced as close as possible is desirable.

The good adhesion between the fibers and epoxy within the pultrusion imply that when used in a structure the structural epoxy / pultrusion interface is more likely to fail before the pultrusion does. The intact pultrusion would still have some load carrying capacity. This ‘macro-fiber’ behavior may be easier to analyze strengths and stiffnesses as a large structure.

The ease of infusion due the already cured pultrusions could decrease structure processing times with many race tracking avenues. Applying a vacuum should remove almost all voids. High infusion pressures may not be as necessary. If high infusion pressures are required, the pultruded elements are less likely to be misaligned because of their stiffness. Although the resin rich areas may be of concern if spacing between pultruded elements gets too large.

Pultrusions offer enough to include them in a wind turbine blade laminate, how can they be fully utilized? One way is to enhance their load transfer efficiency. Various surface treatments both mechanical and chemical have been applied to the pultruded rods used in this study to see their effect on the interfacial shear stress of a directly loaded rod. These surface treatments were compared to rods having no surface treatment loaded in the same conditions.

The surface treatments used in this study were physically applied Silicon Carbide (SiC) particle abrasion, Glass bead impingement erosion, and heated nitric acid exposure surface oxidation. The primary evaluation parameter was the shear strength of the interface calculated by the maximum force used to completely delaminate a pultruded rod of known length from its embedding epoxy.

Initial tests into interface and surface treatment evaluation were in pulling a single treated rod out of cured Epon 826 epoxy. The treatments used in this test were SiC particles of various sizes compared with no treatment. These tests indicated that having some sort of surface modification was beneficial compared

to no treatment. The tests singled out SiC 320 grit particles (average 46 micron in diameter) as the most beneficial to increasing the shear strength for load transfer compared to rods having no treatment. The calculated shear strength for the SiC 320 grit treated rod was 36.8 MPa compared to the untreated rod having a interface shear strength at 13.9 MPa. All other SiC treatments had critical lengths that fell in between these two values.

Further tests into surface treatments switched to rod pushout testing as more coupons could be made from the pultruded elements due the smaller size necessary for testing and the ability to incorporate the in-situ effects of similarly treated rods in close proximity to the tested rod.

The surface treatments conducted in this part of the study included no treatment, SiC 320 grit particles applied for 20 seconds, glass bead erosion at pressures of 2, 3, and 4 kg/cm^2 with respective particle speeds of about 78, 115, and 213 m/s for about 1, 2, and 4 seconds, 60 min nitric acid exposure with no attempted acid removal, 15, 30, and 60 min nitric acid exposure with 5 days distilled water soak and 15 days atmospheric drying, and 60 min nitric acid exposure with 10-20 sec exposure to 1, 2, and 5 molar sodium hydroxide solutions then with same distilled water soak and dry schedule as others.

These center rod pushout tests showed that the erosion surface treatment resulted in largest shear strengths of all the treatments tested. The highest interface shear strength was from the 3 kg/cm^2 air pressure and 2 revolution treatment with a value of 57.6 MPa. The lowest shear strength out of the erosion

treatments was the 2 kg/cm^2 air pressure and one revolution treatment with a value of 51.0 MPa. The SiC 320 abrasion and untreated rod pushout coupons had similar interface shear stresses. The cause of this phenomenon is the fact that both interface tests inadvertently use a stress concentration at the surfaces of the coupons to induce delamination in the interface. The delaminations in all coupons roughly start at the same force. The difference in shear strengths result from the delamination crack growth characteristics determined in part by the surface treatment.

The smaller Teflon spacing had larger interface shear strengths than the larger orthodontic rubber band spacing. The shear stresses increased around 60 percent as the spacing between the rods went from 0.127 mm to 0.762 mm.

Observations of these surface treatments and test results show several advantageous and disadvantageous aspects and applications.

- Mechanical surface treatments shorten the length needed for the rod to achieve equal shear stress and pultruded element stress carrying capability compared to having no treatment on the rods. Erosive treatments performed very well in this study.
- The treatment applications depend on some extent on the skill of the user, especially the mechanical treatments. These treatments might work best as an additional automated process during pultrusion manufacturing. As the decrease in critical length might be due in large part to the increase in

surface area, perhaps positive or negative grooves could be made in the pultrusion by the pultrusion die.

- The removal of mass during the treatments is beneficial to weight-concerned structures like wind turbine blades, but the removal might compromise the load carrying ability of the pultruded element depending on the treatment variables.
- The increase in surface area and friction component in resisting the shear stress created, as well as the exposed carbon fibers for bonding created by the erosion and abrasion treatments might be excellent in the short term, but the cracked surface created on the pultrusion could be a problem in long term. Conversely, the chemical treatments, although longer critical lengths, might be better in the long term due to possible direct bonding by the secondary epoxy to the energized fibers. The length of time needed to process the chemical treatments for the rods in this study might make them impractical for industrial scale applications.
- The free fibers created on the pultrusion surface by the 60 min and 60 min / NaOH chemical treatments enable a tougher interphase between rods because these free fibers are aligned in all directions. Crack growth through these areas will potentially require a lot of energy and the resin rich areas are essentially filled with carbon fiber. The disadvantage is the lost load carrying capacity in the applied load direction and trapped volatiles during infusion.

- The results indicated the rods need to be as close together as possible for maximum effect in terms of increasing the overall fiber volume and interfacial stress resistance. The effect of having no spacing was not investigated and the potential and problems of contacting pultruded elements is unknown.

The use of pultruded composite elements as reinforcement in large composite structures should be investigated. The results of this study show promise in increasing the performance in wind turbine blades as at least an augmentation to traditional materials and manufacturing processes. More research needs to be done on the performance in both long and short term of pultrusions in demanding environments such as wind turbine blade operations. A directly applicable use is in blade spar cap reinforcement. The thick spar cap can be made easily with unidirectional pultruded elements in some capacity with off-axis fabric inbetween. This method might reduce processing times and keep a majority of the fibers aligned in the load carrying direction.

Much more research is needed in this area of pultruded composite interface to resin as this study is believed to be one of the first to apply wholesale surface treatments to an entire finished composite. Surface treatments that disrupt the surface and leave jagged and uneven crevasses and exposed fibers for new resin impregmentation display better load transfer capability than having no treatment, but the long term durability of this treatment was not addressed. Chemical oxidation treatments did not perform as well as the mechanical surface

treatments but have potential for more durable bonding and load transfer but the oxidation mechanism has not been determined in this study and requires further research for optimization.

Surface treatments may play a key role in the long-term durability and performance of wind turbine blades expected to last thirty or more years. Further work is needed to find the right combination for the maximum load transfer efficiency. More suggestions on possible research directions are described in the next section.

Future Work Recommendations

This thesis is an initial foray into the possible issue of enhancing the load transfer capability of pultruded carbon fiber / epoxy composites. Since these pultrusions are finished composites by the time they are used as reinforcement, the secondary infusion process typically will not bond fiber to new resin. This is a potential delamination problem if an inadequate load transfer interface between pultrusion and structural resin is established.

The following list is recommendations for continuing the work started in this study.

- Further optimization of surface treatment variables is needed for selected surface treatment techniques. For mechanical techniques, the more important variables include particle type and size, time of exposure, pultruded surface temperature under treatment, speed of particle

application, wet or dry particles, and removal of loose and free particles during and after treatment.

- Surface treatments resulting in the addition of rough, friction inducing surfaces should also be investigated as an alternative to mass subtraction techniques used in this study. Also the possibility of adding sizing to the entire pultrusion similar to adding sizing to fibers might be worth investigating as a simple and easily introduced alternative to other surface treatments.
- Interfacial shear stress study of pultruded elements in interfacial contact. As seen from the fiber volume fraction calculations, the pultruded elements need to be as close together as possible. This would increase the overall fiber volume fraction as well as minimize the resin rich areas between pultrusions. The pultrusion spacings in this study did not include a ‘no-spacing’ option.
- Strength, stiffness, and mass loss tests on individual pultruded elements after surface treatments. The surface treatments may increase the load transfer efficiency, but at the cost of compromising the load carrying capability of the pultruded element.
- Tests incorporating pultruded elements in simple geometries such as thin and thick plates in compression and bending should be conducted. Cylindrical elements such as the rod packs used in this study could be subjected to pure compression. This is to examine the performance of a

laminate with multiple loaded pultruded elements. Optimal pultruded element arrangements and associated surface treatments could be highlighted.

- Impact tolerant pultruded elements using a tensioned overwind as proposed by Wisnom described in chapter 2 could be investigated for potential use in wind turbine blade laminates. The compression and impact strength increases could lead to decreased employment of the pultruded elements and still maintain excellent performance in compression, bending, and impact areas. Tensioned glass fiber tows could provide impact and environmental resistance.

REFERENCES

[1] Mason, Karen Fisher. (2004). Wind Energy: Change in the Wind. Composites Technology. April 2004.

[2] http://www.blog.loxon7.com/vestas-v66.jpg

[3] Dan Ancona and Jim McVeigh. (2001). Wind Turbine-Materials and Manufacturing Fact Sheet. For Office of Industrial Technologies, USDOE by Princeton Energy Resources International, LLC. August 29, 2001.

[4] Cairns D.S., McKittrick L., Combs D., Mandell J.F., Rabern D., and VanLuchene R. "Design/Manufacturing Synthesis of a Composite Blade for the AOC 15/50 Wind Turbine Blade" 1999 ASME Wind Energy Symposium, pp. 58-65.

[5] www.afm.dtu.dk/ wind/smep/vestas.html

[6] Mandell, J.F., Samborsky, D.D., Li. M., Orozco, R., and Cairns, D.S., "Selection of Fiberglass Matrix Resins for Increased Toughness and Environmental Resistance in Wind Turbine Blades," 2000 ASME Wind Energy Symposium, ASME/AIAA, AIAA-2000-0057, pp. 354- 366. (2000)

[7] Jon D. Skramstad. (1999). Evaluation of hand Lay-up and Resin Transfer Molding in composite Wind Turbine Blade Manufacturing. Master's Thesis, Mechanical Engineering, Montana State University, Bozeman, Montana, U.S.A.

[8] W.D. Brouwer, E.C.F.C. van Herpt, M. Labordus. (2003). Vacuum injection moulding for large structural applications. Composites Part A: applied science and manufacturing. 34, 551-558.

[9] D. A. Griffin, T.D. Ashwill. (2003). Alternative Composite Materials for Megawatt-Scale Wind Turbine Blades: Design Considerations and Recommended Testing. AIAA-2003-0696

[10] Barbero, E. J. Introduction to composite Materials. 1999 Taylor and Francis, Philadelphia, PA, USA. Pg 46-47.

[11] www.bath.ac.uk/event/

[12] http://www.ndsu.nodak.edu/ndsu/klemen/05_10_99.htm

[13] Bahl, O.P., Zengmin Shen, J. Gerard Lavin, Roger A. Ross. (1998). Manufacture of Carbon Fiber. In Jean-Baptiste Donnet, Tong Kuan Wang, Jimmy C.M. Peng, Serge Rebouillat (Eds.), Carbon Fibers, 3rd Edition (pp . 1-83). New York: Marcel Dekker, Inc.

[14] www.epa.gov/ttn/chief/ap42/ch11/final/c11s13.pdf

[15] Tullo, Alexander H., (2004, August 30). Nothing But Blue Skies. Chemical and Engineering News, 82, 35, 40-41.

[16] Mandell, J.F., and Samborsky, D.D., "DOE/MSU Composite Material Fatigue Database: Test Methods, Materials, and Analysis," Contractor Report, SAND97-3002, December 1997

[17] R.J. Diefendorf and E. Torkarsky. (1975). High-Performance Carbon Fibers. Polymer Engineering and Science. Vol. 15, No. 3, p 150-159

[18] Avery, D.P., D.D. Samborsky, J.M. Mandell, and D.S. Cairns. (2004). Compression Strength Of Carbon Fiber Laminates Containing Flaws With Fiber Waviness. 2004 ASME Wind Energy Symposium. Reno, NV Jan 5-8. 54-63.

[19] Mandell, J.F., Samborsky, D.D., Cairns, D.S. (2002) Fatigue of Composite Marerials and Substructures for Wind Turbine Blades. Sandia National Laboratory, SAND REPORT: SAND2002-0771. pg 179.

[20] Lei Wang. (2001). Effects of In-plane Fiber Waviness on the Static and Fatigue Strength of Fiberglass. Masters Thesis, Chemical Engineering, Montana State University, Bozeman, Montana, U.S.A.

[21] Cronkhite, J.D., T.C. Anderson, R.V. Dompka, K. Nunn. (1999). Low-cost bonded IML-tooled tiltrotor wing program. 55th Annual Forum proceedings of the American Helicopter Society. May 25-27, 1999. Washington, D.C. 767-776.

[22] Sumerak, J.E. and J.D. Martin. Pultrusion. ASM Handbook Vol. 21 Composites. Materials Park, OH, USA. Dec 2001.

[23] Jang, Bor Z., Advanced Polymer Composites: Principles and Applications. ASM International, Materials Park, OH, USA. 1994.

[24] Sumerak, J.E., and Hartman, P.H. (2000). Selective Interval Pulshaping™ – Introducing Variable Cross-Section Geometry Features to Thermoset Pultruded Products. 45th International SAMPE Symposium and Exhibition. Long Beach, California, USA. May 21-25, 2000. 1466-1480.

[25] Sumerak, J.E. and Bradshaw, L. (2000). A Study of the Integrity of the Transition Region of Variable Cross-Section Thermoset Pultrusions Produced via Selective Interval Pulshaping™. Composites 2000. Las Vegas, Nevada, USA. Oct 3-6, 2000. 1-11

[26] www.fibrotec.es/

[27] Brosius, D. (2003). Advanced pultrusion takes off in commercial aircraft structures. High-Performance Composites. Vol 11, No. 5. September 2003. 36-39.

[28] http://www.continuo.com/marske/ARTICLES/Carbon%20rods/carbon.htm or http://marskeflyingwings.com/carbonrod.html

[29] Pilakoutas, K. (2000). Composites in Concrete Construction. In E.E. Gdoutos, K. Pilakoutas, and C.A. Radapoulos (Eds.), Failure Analysis of Industrial Composite Materials (pp 449-497). New York, McGraw-Hill.

[30] Meier, U, Spencer, N, and Erath, M. (1995). Strengthening with pultruded CFRP laminates. 40th International SAMPE Symposium and Exhibition. Anaheim, California, USA. 552-561.

[31] El-Hacha, R, Wight, R.G., and Green, M.F. (2001). Prestressed fibre-reinforced polymer laminates fore strengthening structures. Prog. Struct. Engng Mater. Vol 3. 111-121.

[32] Bakis, C.E., Bank, L.C., Brown, V.L., Cosenza, E., Davalos, J.F., Lesko, J.J., Machida, A., Rizkalla, S.H., and Triantafillou, T.C. (2002) Fiber-Reinforced Polymer Composites for Construction – State-of-the-Art Review. Journal of Composites for Construction. Vol 6, No. 2. 73-87.

[33] http://www.edgest.com/edgeprojintro.html
Figure 20: http://www.edgest.com/edgeprojbuildcol.html
Figure 21: http://www.edgest.com/edgeprojnavy.html

[34] Bakis, C.E., Uppuluri, V.S., Nanni, A. and Boothby, T.E. (1998). Analysis of Bonding Mechanisms of Smooth and Lugged FRP Rods Embedded in Concrete. Composites Science and Technology, 58, 1307-1319.

[35] Sumitani, A., Kikuchi, M., Sotooka, M., Akimoto, H., and Ozawa, N. (1998). Pultruded CFRP rods for ground anchor application. Advanced Composite Materials, 7, 4, 395-401.

[36] Nordin, H. (2005). Strengthening structures with externally prestressed tendons: Literature Review (Technical Report). Lulea University of Technology: Lulea, Sweden.
[37] Smith, S.J., Bank, L.C., Gentry, T.R., Nuss, K.H., Hurd, S.H., Duich, S.J., and Oh, B. (2000). Analysis and testing of a prototype pultruded composite causeway structure. Composite Structures, 49, 141-150.

[38] Keller, T. (2001). Recent all-composite and hybrid fibre-reinforced polymer bridges and buildings. Prog. Struct. Engng Mater, 3, 132-140.

[39] Bank, L.C., Gentry, T.R., Nuss, K.H., Hurd, S.H., Lamanna, A.J., Duich, S.J. and Oh, B. (2000). Construction of a Pultruded Composite Structure: Case Study. Journal of Composites for Construction, Vol 4, No 3, 112-119.

[40] Wisnom, M.R., Potter, K.D. (1999). Unidirectional Carbon fiber Rods for High Performance Structures. Designing High Performance Stiffened Structures, published by IMechE seminar series. 2000. pg 59-70.

[41] K.D. Potter, M.R. Wisnom. (2002). Composites of Extreme Anisotropy: Initial Experiments. Sixth International Conference on Deformation and Fracture of Composites. Manchester, UK. April 4-5, 2001.

[42] K.D. Potter, F. Schweickhardt, M.R. Wisnom. (2000). Impact Response of Unidirectional Carbon Fibre Rod with and without an Impact Protection Layer. Journal of Composite Materials, Vol. 34. No. 17. 1437-1455.

[43] M.R. Wisnom. (1999). Supression of Splitting and Impact Sensitivity of Unidirectional Carbon fibre composite Rods using tensioned overwind. Composites Part A. 30. 661-665.

[44] A. Clark, M.R. Wisnom, and K. Potter. (1998). Develpoment of High Strength Unidirectional Carbon Tubular Elements from Small Diameter Precured Rod. 7th ICFRC pgs 45-52.

[45] Dr. Douglas Cairns. Personal Conversation. 8/2005

[46] Wen-Shyong Kuo. (1997). Topology of Three-Dimensionally Braided Fabrics Using Pultruded Rods as Axial Reinforcements. Textile Research Journal. Issue 67, Vol 9. 623-634.

[47] Wen-Shoyong Kuo and Horn-I Chen. (1997). Fabrication and MicroGeometry of Two-Step Braided Composites Incorporating Pulturded Rods. Composites Science and Technology, 57, 1457-1467.

[48] Wen-Shyong Kuo, Tse-Hao Ko, and Horn-I Chen. (1998). Elastic moduli and damage mechanisms in 3D braided composites incorporating pultruded rods. Composites Part A, 29A, 681-692.
[49] Wen-Shyong Kuo, and Lin-Chyuan Lee. (1998). Impact Response of 3-D Woven Composites Reinforced by Consolidated Rods. Polymer Composites, 19, 2, 156-165.

[50] Wen-Shyong Kuo, Kuo-Bing Cheng. (1999). Processing and microstructures of 3D woven-fabric composites incorporating solid rods. Composites Science and Technology. 59, 1833-1846.

[51] Wen-Shyong Kuo and Tse-Hao Ko. (2000). Compressive damage in 3-axis orthogonal fabric composites. Composites Part A, 31, 1091-1105.

[52] Zoltek Companies, Inc.
3101 McKelvey Rd.
St. Louis, Missouri 63044
800-325-4409
(314) 291-5110
(314) 291-8536 Fax
www.zoltek.com

[53] http://www.entec.com/

[54] www.zoltek.com/panex_products/ or
http://www.zoltek.com/panex_products/PANEXBRO.PDF

[55] http://www.resins.com/resins/am/pdf/SC3032.pdf

[56] http://www.shellchemicals.com/home/

[57] Private Communication, Mike Moran, Zoltek, 8/2004

[58] EPON 862 http://www.resins.com/resins/am/pdf/RP4048.pdf

[59] http://www.ehjournal.net/content/2/1/3/figure/F1

[60] EPICURE 3234: http://www.resins.com/resins/am/pdf/sc1674.pdf

[61] http://msds.pcd.go.th/searchName.asp?vID=214

[62] Wingfield, J.R.J. (1993). Treatment of composite surfaces for adhesive bonding. International Journal of Adhesion and Adhesives. Vol 13, No. 3, 151-156

[63] U.S. Department of Transportation: FAA Office of Aviation Research. (2004). Effects of Surface Preparation on the Long-Term Durability of Adhesively Bonded Composite Joints. (Report No. DOT/FAA/AR-03/53). Washington, D.C.: Bardis, J. and Kedward, K.

[64] Pool, K.V., Dharan, C.K.H., and Finnie, I. (1986). Erosive Wear of Composite Materials. Wear, 107, 1-12.

[65] Finnie, I. (1995). Some reflections on the past and future of erosion. Wear, 186-187, 1-10.

[66] Gardner, S.D., Singamsetty, C.S.K., Zhihong Wu, and Pittman, C.U. (1996). XPS/ISS Investigation of Carbon Fibers Sequentially Exposed to Nitric Acid and Sodium Hydroxide. Surface and Interface Analysis, 24, 311-320.

[67] Parker, B.M. and Waghorne, R.M. (1982). Surface Pretreatment of Carbon Fiber Reinforced Composites for Adhesive Bonding. Composites, Vol 13, Issue 3, 280-288.

[68] Matz, C.W. (1987). Adhesion on Carbon fibre-reinforced Plastics. Journal of Adhesion. Vol 22. 61-65.

[69] Dillard, J.G. Surface Preparation of Composites. ASM Engineered Materials Handbook Vol 3: Adhesives and Sealants. ASM International, Materials Park, OH, USA. 1990. pg 281-297

[70] Barkoula, N.M., Papanicolaou, G.C., and Karger-Kocsis, J. (2002). Prediction of the residual tensile strengths of carbon-fiber/epoxy laminates with and without interleaves after solid particle erosion. Composites Science and Technology, 62, 121-130.

[71] Donnet, J.B., Papierer, E., Dauksch, H. (1974). Nitric Acid Surface treatments on carbon fibers. Proceedings of the International Conference by The Plastics Institute, London, UK, pgs 58-64.

[72] Narkis, M., Chen, E.J.H., and Pipes, R.B. (1988). Review of Methods for Characterization of Interfacial Fiber-Matrix Interactions. Polymer Composites, 9, 4, 245-251.

[73] Mandell, J.F., Grande, D.H., Tsiang, T.H., and McGarry, F.J. (1986). Modified Microdebonding Test for Direct In-Situ Fiber / Matrix Bond Strength Determination in Fiber Composites. Composite Materials: Testing and Design

(Seventh Conference), ASTM STP 893, J.M. Whitney, ED., American Society for Testing and Materials, Philadelphia, 87-108.

[74] www.struers-us.com/pages/12html_consumable/StCat02.pdf pg. 30-31

[75] http://www.coe.montana.edu/composites/facilities.htm

[76] Ruff, A.W. and Ives, L.K. (1975). Measurement of solid particle velocity in erosive wear. Wear, 35, 195-199.

[77] http://www.physics.montana.edu/ical/ical.html

[78] www.adobe.com

[79] http://www.systat.com/products/SigmaScan/

[80] Lam, W.P.W, C. Kerr, A.J. Chaudhary, S.M. Grimes. (2004). The use of Physical Grinding with SiC Abrasive Papers as Preparation Techniques for increasing the Surface Area of a Substrate Material. Struers eJournal of Materialography. 1/2004.

APPENDICES

APPENDIX A

Test Result Tables

Table A1: Individual pullout coupon test results

Coupon #	Particle Size (μm)	Ult Load (kN)	Total Debonded Surface Area (mm^2)	Shear Stress (MPa)	Avg. Stress (MPa)
C-1	0	18.50	1404.03	13.2	13.9
C-2	0	21.16	1405.32	15.1	
C-3	0	18.98	1415.53	13.4	
120-1	115	27.49	658.30	41.8	26.7
120-2	115	26.31	1417.01	18.6	
120-3	115	28.00	1419.05	19.7	
220-1	58	25.75	1408.66	18.3	17.8
220-2	58	25.75	1417.94	18.2	
220-3	58	23.99	1421.09	16.9	
320-1	46	25.87	671.49	38.5	36.8
320-2	46	26.04	668.20	39.0	
320-3	46	21.82	663.48	32.9	
800-1	22	20.39	1435.75	14.2	22.5
800-2	22	21.30	820.40	26.0	
800-3	22	22.20	808.15	27.5	
1200-1	15	15.92	774.69	20.6	28.2
1200-2	15	22.45	766.68	29.3	
1200-3	15	22.82	796.37	28.7	
MC 1000-1*	15	22.50	658.30	34.2	

*: Abraided with 1200 grit size

MC: Matrix cracked before test

Table A2: Individual pushout coupon test results (No surface treatment – Teflon spacing)

Coupon	Height (mm)	Side Down	Load (N)	Max Shear Stress (MPa)
2A	13.0048	1	10253.15	42.50
2B	11.7348	1	5911.687	27.15
3A	12.192	2	13727.21	60.69
3B	11.2522	2	5106.559	24.46
5A	13.1826	2	9132.2	37.34
5B	13.2842	1	12374.95	50.21
9A	9.3726	1	9407.99	54.10
11A	10.0584	2	3585.267	19.21
11B	10.4648	2	11027.14	56.80
		Average:	8947.35	41.38
		St. Dev:	3420.37	15.20

Table A3: Individual pushout coupon test results (No surface treatment – ortho spacing)

Coupon	Height (mm)	Side Down	Load (N)	Max Shear Stress (MPa)
1	20.955	1	12165.89	31.29
2	24.638	1	12050.23	26.36
3	24.511	1	12428.33	27.33
4	26.035	2	12005.75	24.86
5	23.368	1	8834.169	20.38
6	14.097	2	4434.877	16.96
8	21.9456	2	13211.22	32.45
9	24.384	1	13544.84	29.94
10	23.7998	1	7975.662	18.06
11	21.59	2	7014.846	17.51
		Average:	10366.58	24.51
		St. Dev:	3085.58	5.91

Table A4: Individual pushout coupon test results
(SiC 320 surface treatment – Teflon spacing)

Coupon	Height (mm)	Side Down	Load (N)	Max Shear Stress (MPa)
2A	11.4554	2	10448.87	49.16
3A	11.3792	1	5542.48	26.25
3B	12.3698	1	6369.85	27.76
4A	12.3952	2	8215.87	35.73
5B	9.5758	1	5066.52	28.52
6B	10.9982	2	11271.79	55.24
8A	12.192	2	9003.20	39.80
9A	10.7442	1	7063.78	35.44
12A	10.668	2	6814.68	34.43
		Average:	7755.23	36.93
		St. Dev:	2144.73	9.82

Table A5: Individual pushout coupon test results
(SiC 320 surface treatment – ortho spacing)

Coupon	Height (mm)	Side Down	Load (N)	Max Shear Stress (MPa)
3A	10.795	2	3278.34	16.37
3B	11.684	1	5297.83	24.44
4A	11.0744	2	4483.81	21.82
6B	10.668	1	4790.74	24.21
7A	11.303	1	6263.10	29.87
8A	10.2362	1	2984.76	15.72
10B	10.2616	2	4394.84	23.08
11A	10.795	1	3149.34	15.73
12A	12.4206	2	9265.65	40.21
		Average:	4878.71	23.49
		St.Dev:	1964.50	7.87

Table A6: Individual pushout coupon test results
(Unwashed 60 min HNO_3 surface treatment – Teflon spacing)

Coupon	Height (mm)	Side Down	Load (N)	Max Shear Stress (MPa)
1	13.51	2	471.51	1.88
2	11.89	2	662.79	3.00
3	10.77	1	542.68	2.72
4	12.11	1	920.78	4.10
5	10.26	2	653.89	3.44
6	11.28	1	814.02	3.89
8	11.24	1	707.27	3.39
9	10.8	2	920.78	4.60
10	10.78	1	435.93	2.18
		Average:	681.07	3.24
		St. Dev:	179.42	0.89

Table A7: Individual pushout coupon test results
(Unwashed 60 min HNO_3 surface treatment – ortho spacing)

Coupon	Height (mm)	Side Down	Load (N)	Max Shear Stress (MPa)
1	10.4	1	515.99	2.67
2	12.14	1	685.03	3.04
3	11.48	2	689.47	3.24
4	11.26	1	409.24	1.96
5	11.99	1	524.89	2.36
6	10.64	2	262.45	1.33
7	10.85	2	360.31	1.79
8	10.78	2	364.75	1.82
9	11.98	1	600.51	2.70
10	12.03	1	569.37	2.55
		Average:	498.20	2.35
		St. Dev	144.67	0.61

Table A8: Individual pushout coupon test results
(Washed 15 min HNO_3 surface treatment – Teflon spacing)

Coupon	Height (mm)	Side Down	Load (N)	Max Shear Stress (MPa)
1	12.06	2	6178.58	27.61
2	11.80	2	5288.94	24.16
3	11.20	2	4590.57	22.09
4	9.49	1	3816.13	21.67
5	9.27	1	4316.11	25.10
6	10.06	1	5079.87	27.22
7	10.86	2	5155.49	25.59
8	12.16	2	5199.97	23.05
9	10.90	1	7259.50	35.90
10	12.24	2	5360.11	23.60
		Average:	4998.42	24.46
		St. Dev:	680.96	2.10

Table A9: Individual pushout coupon test results
(Washed 30 min HNO_3 surface treatment – Teflon spacing)

Coupon	Height (mm)	Side Down	Load (N)	Max Shear Stress (MPa)
1	10.82	2	4136.85	20.61
2	11.12	1	4087.03	19.81
3	10.69	1	3740.95	18.86
4	10.84	2	3870.4	19.25
5	10.96	2	4732.91	23.28
6	10.40	1	2978.53	15.44
7	11.09	1	4266.29	20.74
8	10.60	2	3478.51	17.69
9	11.06	1	4523.84	22.05
		Average:	3979.48	19.75
		St. Dev:	536.68	2.33

Table A10: Individual pushout coupon test results
(Washed 60 min HNO_3 surface treatment – Teflon spacing)

Coupon	Height (mm)	Side Down	Load (N)	Max Shear Stress (MPa)
1	10.60	2	3832.59	19.49
2	9.15	1	2807.27	16.54
3	11.47	2	5364.56	25.21
4	12.34	1	5013.15	21.90
5	10.67	1	5858.31	29.59
6	11.54	2	4643.94	21.69
7	10.64	2	4786.29	24.25
8	9.54	1	3053.70	17.25
9	10.53	1	4977.56	25.48
10	12.34	2	4599.46	20.09
		Average:	4493.68	22.15
		St. Dev:	977.44	4.05

Table A11: Individual pushout coupon test results
(Washed 60 min HNO_3 / 30 sec 1M NaOH surface treatment – Teflon spacing)

Coupon	Height (mm)	Side Down	Load (N)	Max Shear Stress (MPa)
1	10.94	1	3878.85	19.11
2	11.12	2	5284.49	25.61
3	11.27	1	3682.68	17.61
4	11.32	1	5124.35	24.40
5	10.61	1	4853.01	24.65
6	9.44	2	4132.84	23.60
7	10.69	2	4541.63	22.90
8	10.30	1	4257.84	22.28
9	10.26	2	3303.69	17.36
10	10.88	2	4772.94	23.65
		Average:	4383.23	22.12
		St. Dev:	645.34	3.00

Table A12: Individual pushout coupon test results
(Washed 60 min HNO_3 / 30 sec 2M NaOH surface treatment – Teflon spacing)

Coupon	Height (mm)	Side Down	Load (N)	Max Shear Stress (MPa)
1	11.11	2	7237.26	35.11
2	11.52	1	7197.22	33.67
3	11.22	1	5965.07	28.66
4	9.94	1	4426.43	24.00
5	10.58	2	7628.70	38.87
6	10.6	2	6610.06	33.61
7	10.66	2	6227.51	31.49
8	11	1	6120.75	29.99
9	11.46	2	5920.58	27.85
10	10.13	1	6102.96	32.47
		Average:	6356.56	31.58
		St. Dev:	958.75	4.43

Table A13: Individual pushout coupon test results
(Washed 60 min HNO_3 / 30 sec 5M NaOH surface treatment – Teflon spacing)

Coupon	Height (mm)	Side Down	Load (N)	Max Shear Stress (MPa)
1	11.54	2	5515.80	25.76
2	10.66	2	5097.66	25.78
3	11.05	2	5039.84	24.58
4	11.2	1	7619.80	36.67
5	10.04	1	6850.26	36.78
6	10.64	2	6819.12	34.54
7	11.72	1	6854.71	31.53
8	10.54	2	7513.05	38.42
9	10.12	2	6067.37	32.32
10	11.38	1	8393.79	39.76
		Average:	6577.14	32.61
		St. Dev:	1126.05	5.59

Table A14: Individual pushout coupon test results
(2 kg/cm^2, 1 revolution erosion surface treatment – Teflon spacing)

Coupon	Height (mm)	Side Down	Load (N)	Max Shear Stress (MPa)
1	13.15	2	7508.60	30.78
2	10.21	1	10822.52	57.13
3	10.89	2	12588.47	62.31
4	11.04	1	11369.66	55.51
5	12.26	2	9341.27	41.07
6	10.86	1	6885.85	34.18
7	11.6	2	11534.24	53.60
8	9.69	1	10644.60	59.21
9	11.63	2	12632.95	58.55
10	11.02	1	11743.31	57.44
		Average:	10507.15	50.98
		St. Dev:	1993.34	11.30

Table A15: Individual pushout coupon test results
(2 kg/cm^2, 2 revolutions erosion surface treatment – Teflon spacing)

Coupon	Height (mm)	Side Down	Load (N)	Max Shear Stress (MPa)
1	11.07	1	12094.72	58.89
2	11.39	2	5729.31	27.11
3	11.85	2	12810.88	58.27
4	9.61	2	9514.75	53.37
5	11.47	2	13455.87	63.23
6	9.45	1	9230.06	52.65
7	10.66	2	11449.72	57.89
8	11.37	1	9888.40	46.88
9	11.08	2	10649.04	51.80
10	11.76	2	13229.01	60.63
		Average:	10805.18	53.07
		St. Dev:	2351.78	10.32

Table A16: Individual pushout coupon test results
(2 kg/cm^2, 4 revolutions erosion surface treatment – Teflon spacing)

Coupon	Height (mm)	Side Down	Load (N)	Max Shear Stress (MPa)
1	11.3	1	8340.42	39.78
2	10.45	2	11836.72	61.05
3	11.05	2	7891.15	38.49
4	10.73	2	12023.54	60.40
5	10.19	1	11516.45	60.92
6	10.5	1	12463.92	63.98
7	12.76	1	14946.03	63.13
8	10.45	2	11512.00	59.38
9	11.65	2	13793.94	63.82
10	11.82	1	13024.39	59.39
		Average:	11734.85	57.04
		St. Dev:	2191.73	9.58

Table A17: Individual pushout coupon test results
(3 kg/cm^2, 1 revolution erosion surface treatment – Teflon spacing)

Coupon	Height (mm)	Side Down	Load (N)	Max Shear Stress (MPa)
1	10.29	2	10568.98	55.36
2	10.13	1	11592.07	61.68
3	10.57	1	11592.07	59.11
4	10.05	2	8536.14	45.78
5	10.63	2	10671.28	54.11
6	11.05	2	12383.85	60.41
7	11.98	2	10106.36	45.47
8	11.02	2	9167.79	44.84
9	11.65	1	7788.84	36.04
10	11.42	1	12250.40	57.82
		Average:	10465.78	52.06
		St. Dev:	1569.05	8.51

Table A18: Individual pushout coupon test results
(3 kg/cm^2, 2 revolutions erosion surface treatment – Teflon spacing)

Coupon	Height (mm)	Side Down	Load (N)	Max Shear Stress (MPa)
1	9.67	2	8460.52	47.16
2	11.37	1	13237.91	62.76
3	10.48	2	12588.47	64.74
4	11.56	2	10075.22	46.98
5	10.19	1	11351.86	60.05
6	11.14	1	9714.92	47.01
7	10.27	2	11658.79	61.19
8	11.47	1	12953.22	60.87
9	12.99	2	15622.16	64.82
10	11.42	1	12890.95	60.84
		Average:	11855.40	57.64
		St. Dev:	2067.82	7.48

Table A19: Individual pushout coupon test results
(3 kg/cm^2, 4 revolutions erosion surface treatment – Teflon spacing)

Coupon	Height (mm)	Side Down	Load (N)	Max Shear Stress (MPa)
1	11.1	2	11778.89	57.20
2	11.4	1	11996.85	56.72
3	9.72	2	11044.94	61.25
4	10.95	2	12188.13	60.00
5	9.75	1	12001.30	66.35
6	11.87	1	10791.39	49.00
7	12.118	2	15284.09	67.98
8	10.56	1	5462.42	27.88
9	11.69	2	10088.57	46.52
10	10.96	2	13509.25	66.44
		Average:	11414.58	55.93
		St. Dev:	2549.22	12.18

Table A20: Individual pushout coupon test results
(4 kg/cm^2, 1 revolution erosion surface treatment – Teflon spacing)

Coupon	Height (mm)	Side Down	Load (N)	Max Shear Stress (MPa)
1	10.53	2	7797.73	39.91
2	12.33	2	9256.75	40.47
3	9.53	1	10675.73	60.38
4	11.38	2	12779.74	60.53
5	10.5	2	11236.21	57.68
6	10.19	1	10444.43	55.25
7	10.87	1	12188.13	60.44
8	11.04	2	12214.82	59.64
9	10.65	2	4870.80	24.65
10	10.39	2	11649.89	60.44
		Average:	10311.42	51.94
		St. Dev:	2428.21	12.53

Table A21: Individual pushout coupon test results
(4 kg/cm^2, 2 revolutions erosion surface treatment – Teflon spacing)

Coupon	Height (mm)	Side Down	Load (N)	Max Shear Stress (MPa)
1	10.36	1	11609.86	60.40
2	11.06	1	13073.32	63.71
3	10.81	2	6819.12	34.00
4	12.06	1	14550.13	65.03
5	13.57	2	13722.76	54.51
6	9.08	2	10635.70	63.14
7	10.68	2	7134.95	36.01
8	11.45	1	12045.79	56.71
9	11.21	2	12797.53	61.53
10	11.56	1	12966.57	60.46
		Average:	11535.57	55.55
		St. Dev:	2636.55	11.28

Table A22: Individual pushout coupon test results
(4 kg/cm^2, 4 revolutions erosion surface treatment – Teflon spacing)

Coupon	Height (mm)	Side Down	Load (N)	Max Shear Stress (MPa)
1	9.9	1	9786.09	53.28
2	11.38	2	12281.54	58.17
3	10.52	1	10537.84	53.99
4	11.51	2	11721.06	54.89
5	12.64	2	9127.75	38.92
6	10.56	2	10818.08	55.22
7	11.32	2	11560.93	55.05
8	10.47	2	8763.00	45.11
9	11.51	1	8376.00	39.22
10	9.97	1	10751.35	58.12
		Average:	10372.36	51.20
		St. Dev:	1321.39	7.34

Table A23: Individual three-point pultruded rod bending test results

Coupon #	Maximum Carried load (N)	Flexural Rigidity (N*m^2)	Elastic Bending Modulus (GPa)	Maximum Fiber Stress (MPa)	Maximum Strain in outer fibers	Percent strain (e*100)
6	856.50	8.64	144.69	1344.97	0.0093	0.9295
7	923.35	8.52	142.66	1449.94	0.0102	1.0163
8	854.70	8.41	140.92	1342.14	0.0095	0.9524
9	908.74	8.47	141.92	1426.99	0.0101	1.0055
10	877.31	8.24	137.99	1324.71	0.0094	0.9438
Test 3	843.60	7.64	127.99	1269.23	0.0096	0.9600
	Average (N)	Average (N*m^2):	Average (GPa):	Average (MPa):	Average:	Average:
	877.37	8.32	139.36	1359.66	0.0097	0.9679
	St. Dev.	St. Dev.	St. Dev.	St. Dev.	St. Dev.	St. Dev.
	32.21	0.36	5.99	67.24	0.0003	0.0350

Table A24: Individual pultruded flat short beam shear (SBS) test results

Coupon	First Damage load (N)	Apparent Shear Strength (MPa)
Panex 19-1	1391.74	68.29
Panex 19-2	1369.78	68.01
Panex 19-3	1455.75	69.81
Average:	1405.76	68.70
St. Dev:	44.66	0.97
Panex 20-1	1394.86	65.76
Panex 20-2	1471.41	66.45
Panex 20-3	1242.97	62.71
Panex 20-4	1344.56	68.51
Panex 20-5	1258.14	62.87
Panex 20-6	1381.19	69.15
Average:	1348.85	65.91
St. Dev:	86.76	2.72
Toray 1	1366.69	68.94
Toray 2	1405.32	68.83
Toray 3	1537.78	68.18
Toray 4	1539.52	68.86
Toray 5	1325.04	65.02
Toray 6	1356.00	67.33
Average:	1421.73	67.86
St. Dev:	94.14	1.52

Table A25: Individual pultruded rod short beam shear (SBS) w/ narrow nose test results

Rod Coupon #	First Damage Load (N)	Apparent Shear Strength (MPa)
1	3283.81	79.94
2	3263.86	79.46
3	3263.94	79.46
4	3158.53	76.89
Average (MPa)	3242.54	78.94
St. Dev	56.79	1.38

Table A26: Individual pultruded flat tension test results

Zoltek 19-tow		Modulus (Pa):	1.55E+11			
#	Width (mm)	Height (mm)	Area mm^2	Load (kN)	Break Stress (GPa)	Break Stress Normalized by V_f (GPa)
1	23.0	1.17	26.91	61.61	2.29	3.20
2	23.5	1.18	27.75	54.98	1.98	2.77
3	22.9	1.17	26.51	61.96	2.34	3.27
4	23.5	1.17	27.50	63.57	2.31	3.23
				Average:	2.23	3.12
				St. dev.	0.17	0.23
Toray		Modulus (Pa):	1.51E+11			
#	Width (mm)	Thickness (mm)	Area mm^2	Load (kN)	Break Stress (GPa)	Break Stress Normalized by V_f (GPa)
1	23.4	1.2	28.08	84.20	3.00	4.31
2	23.3	1.2	27.96	83.76	3.00	4.31
3	23.3	1.18	27.494	89.54	3.26	4.69
4	23.3	1.19	27.727	84.12	3.03	4.37
				Average:	3.07	4.42
				St. dev.	0.12	0.18

Strain to Failure

Zoltek # 2	1.28%
Zoltek # 4	1.49%
Toray # 1	1.83%

APPENDIX B

Individual Pullout Test Coupon Force vs. Displacement Curves

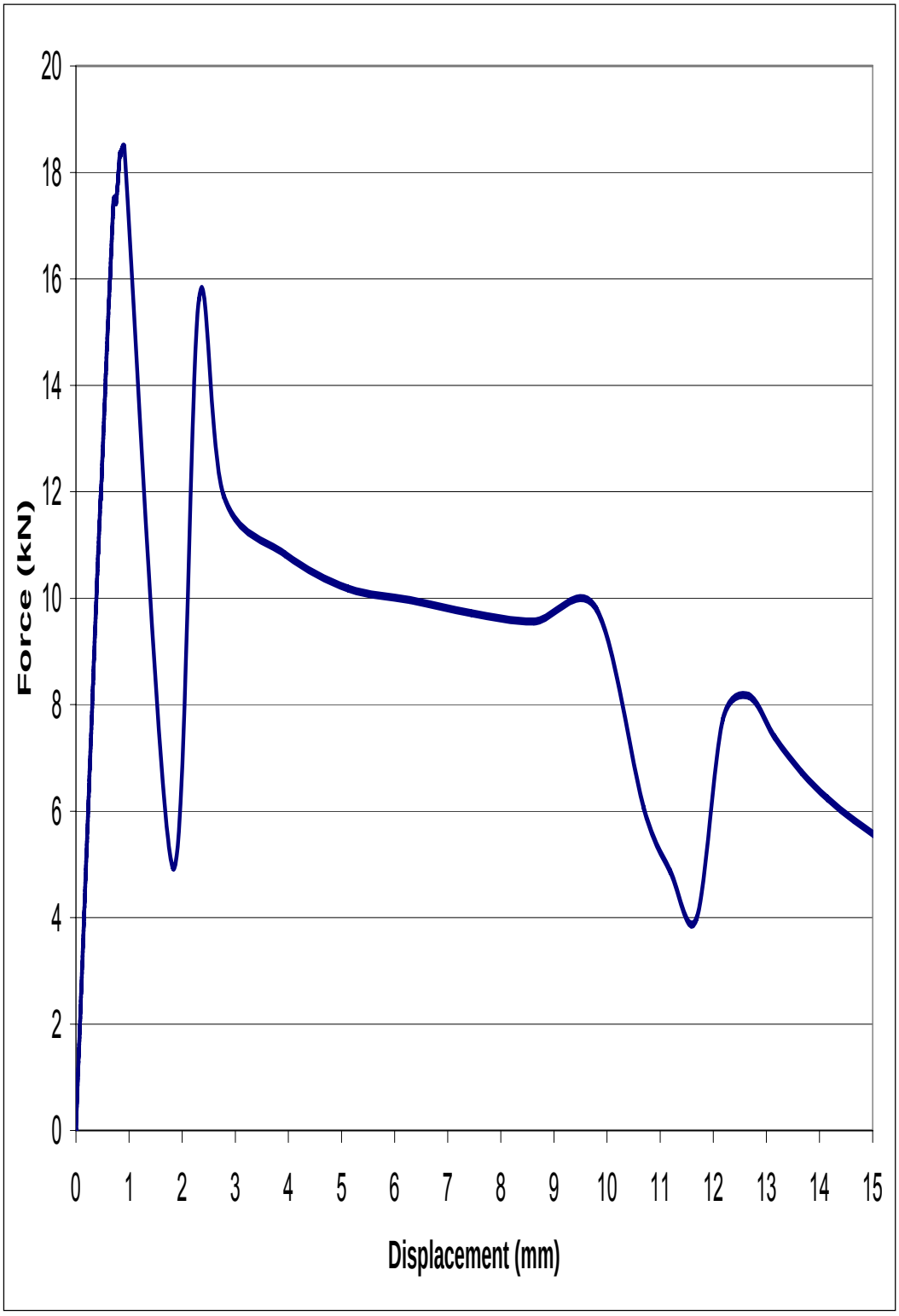

Figure B-1: Pullout coupon C-1 force vs. displacement curve

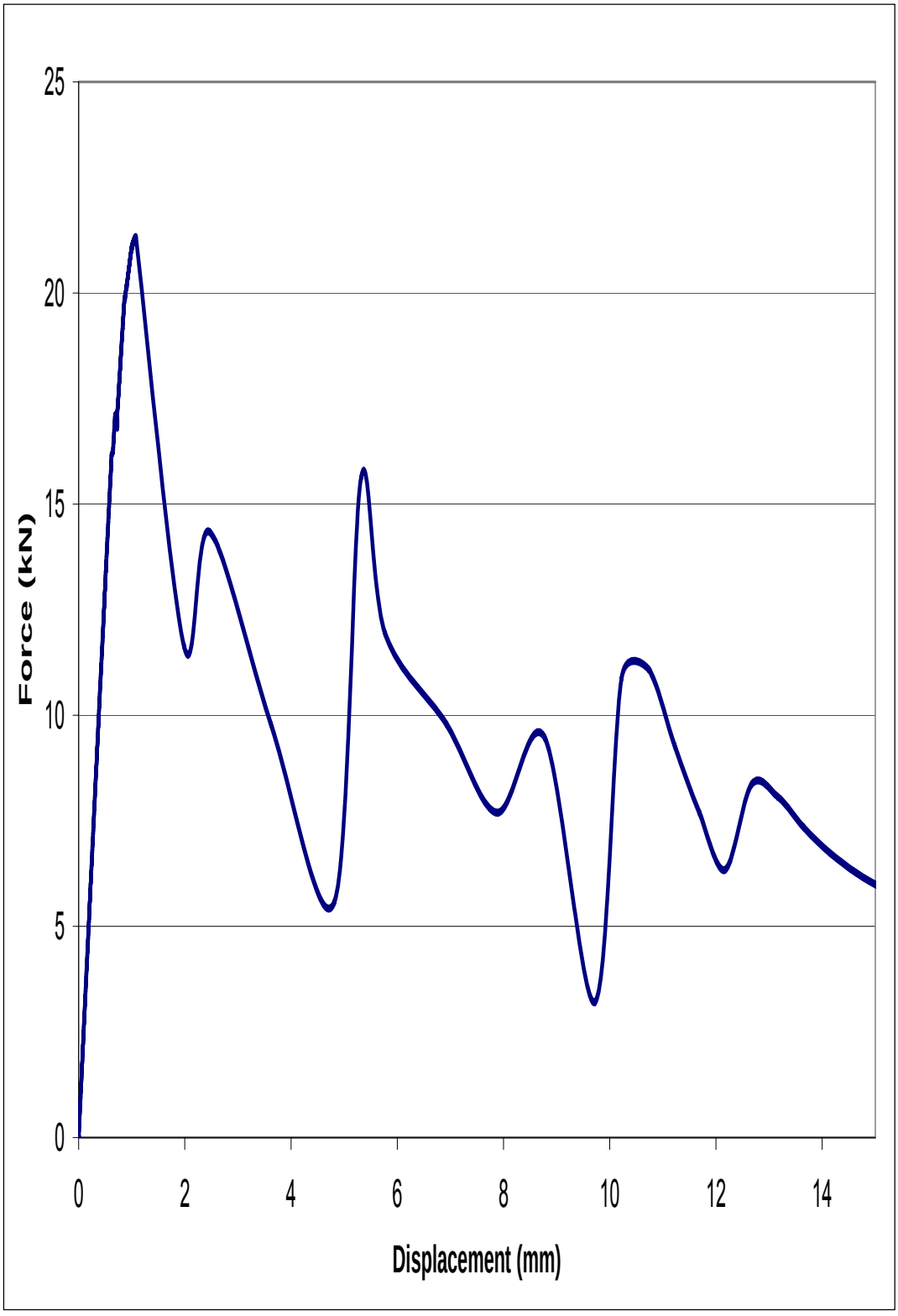

Figure B-2: Pullout coupon C-2 force vs. displacement curve

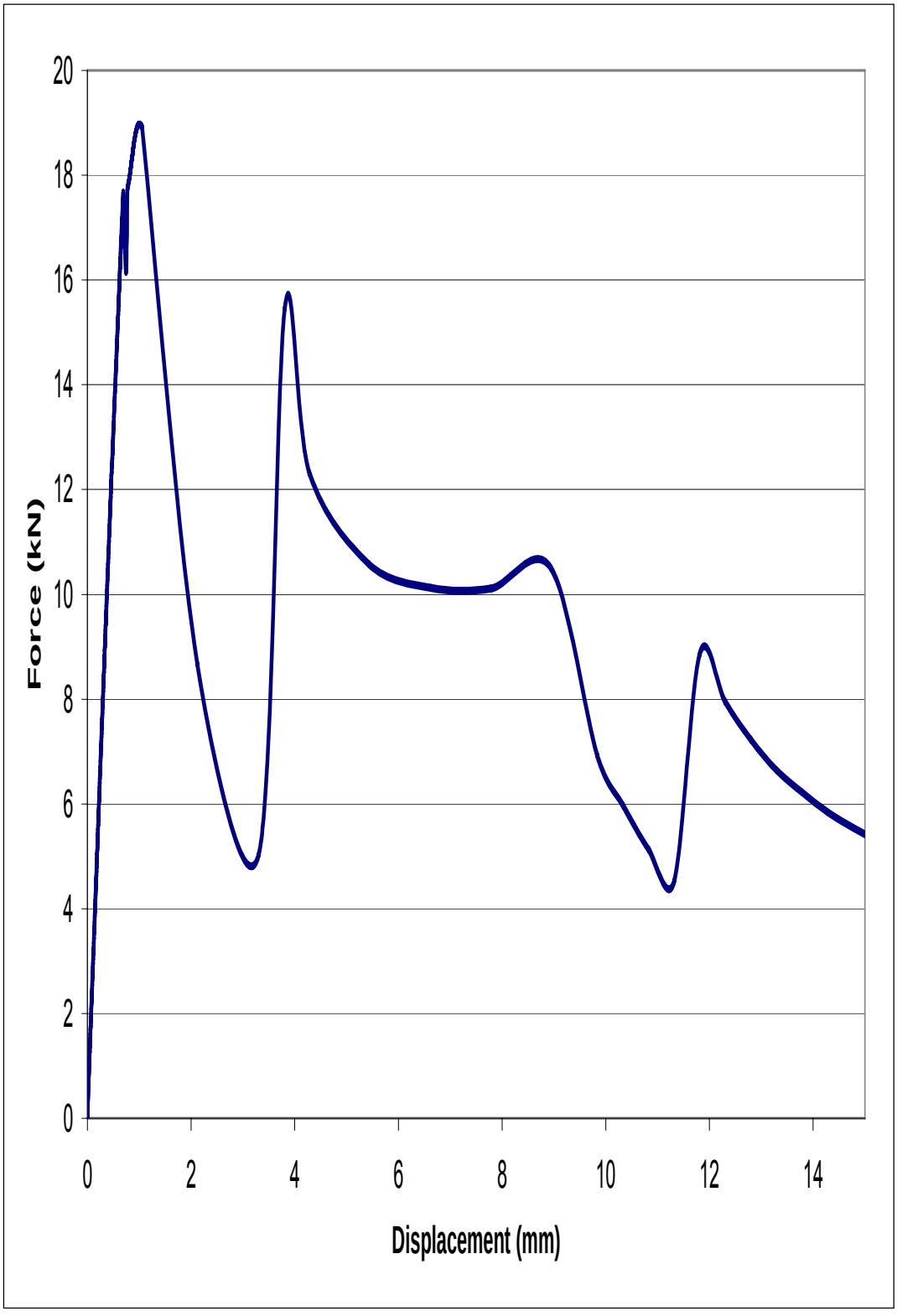

Figure B-3: Pullout coupon C-3 force vs. displacement curve

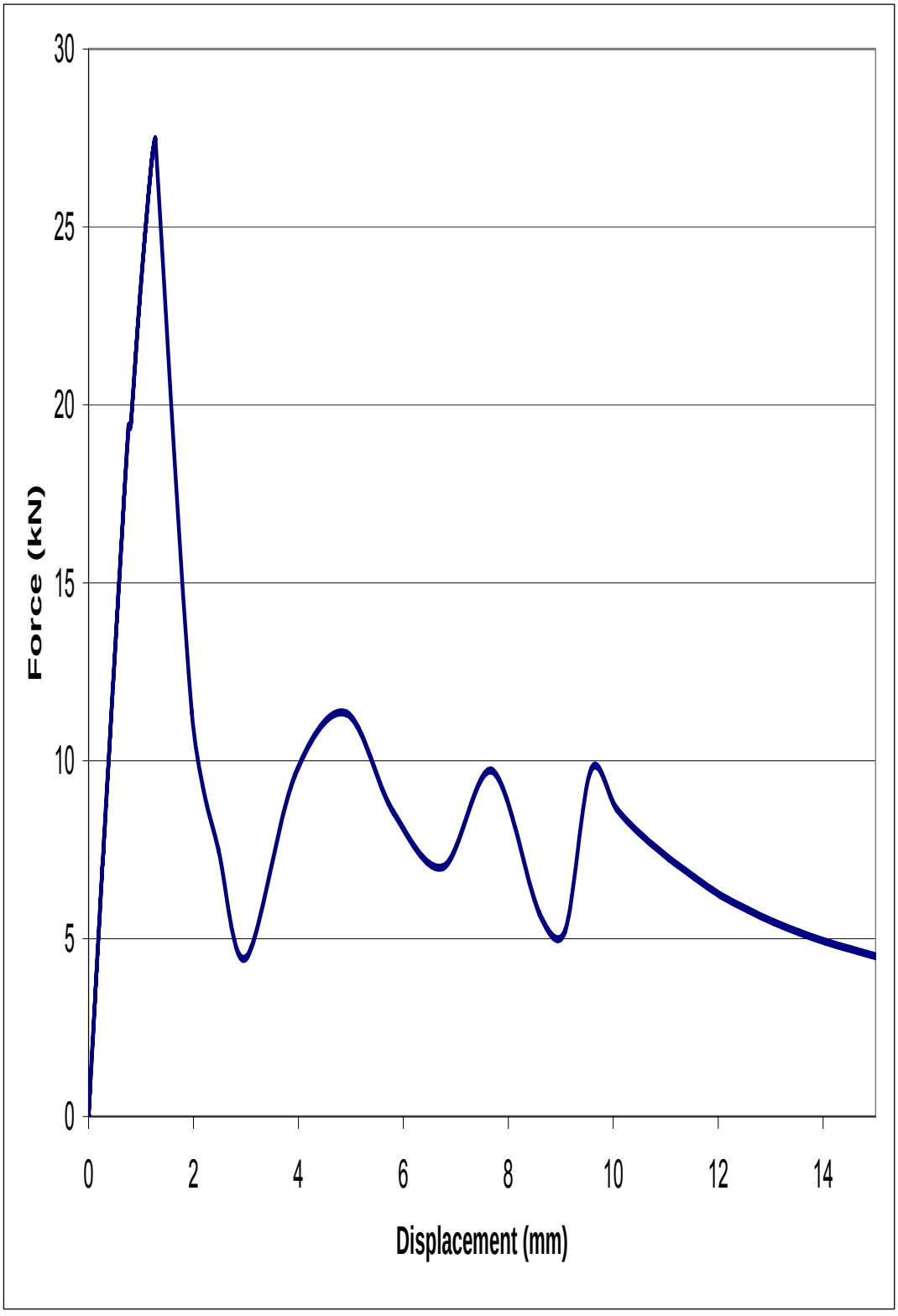

Figure B-4: Pullout coupon 120-1 force vs. displacement curve

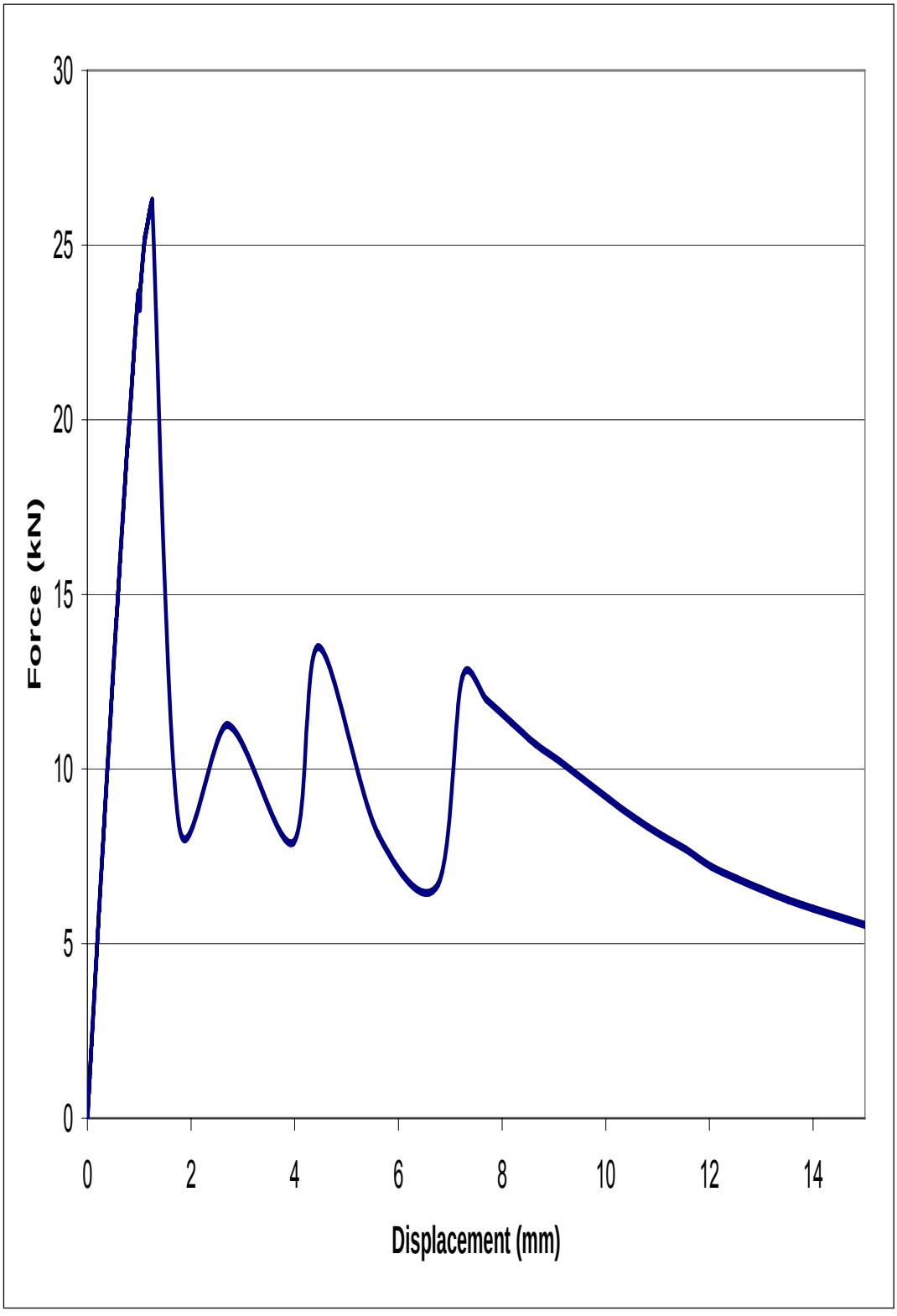

Figure B-5: Pullout coupon 120-2 force vs. displacement curve

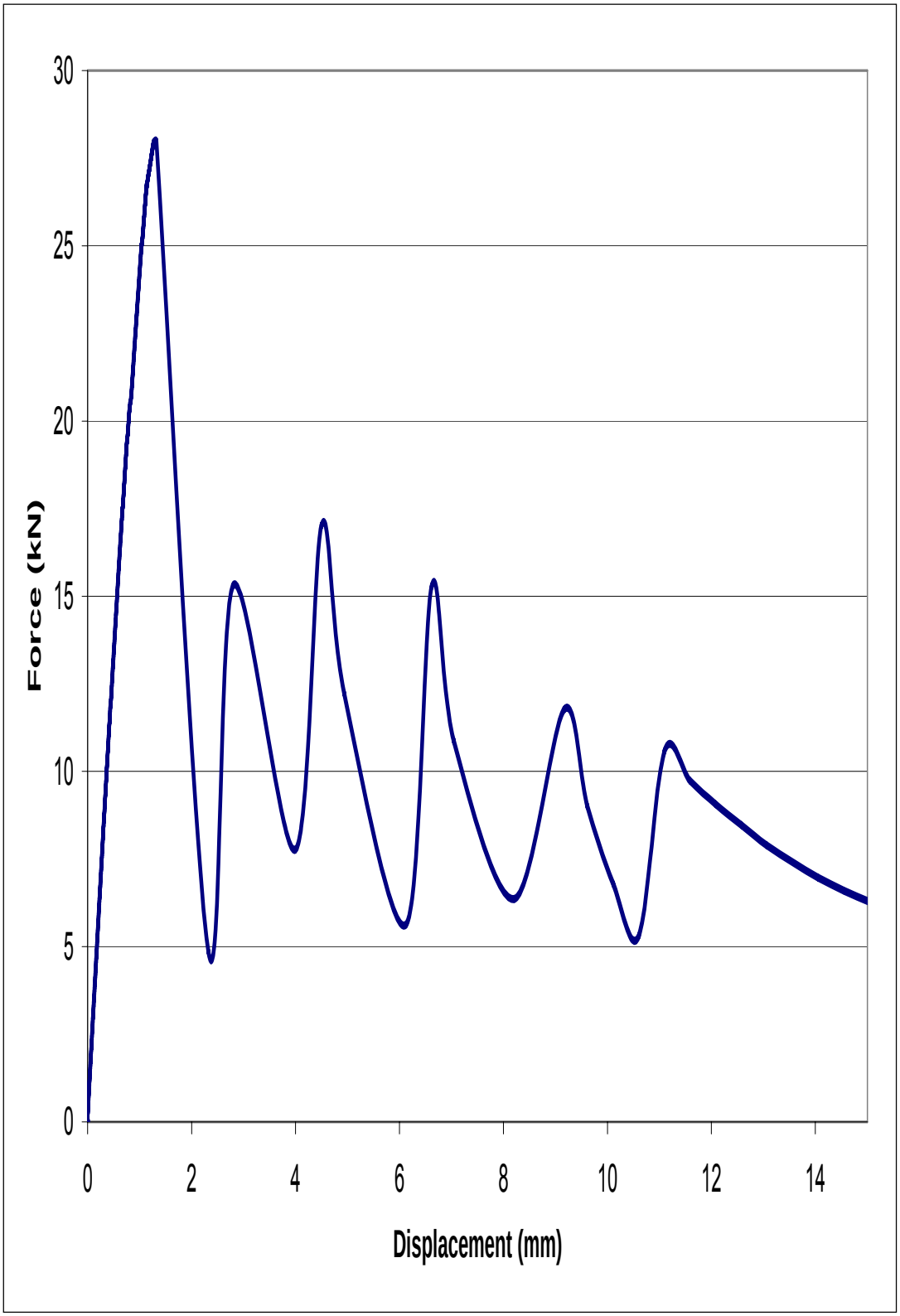

Figure B-6: Pullout coupon 120-3 force vs. displacement curve

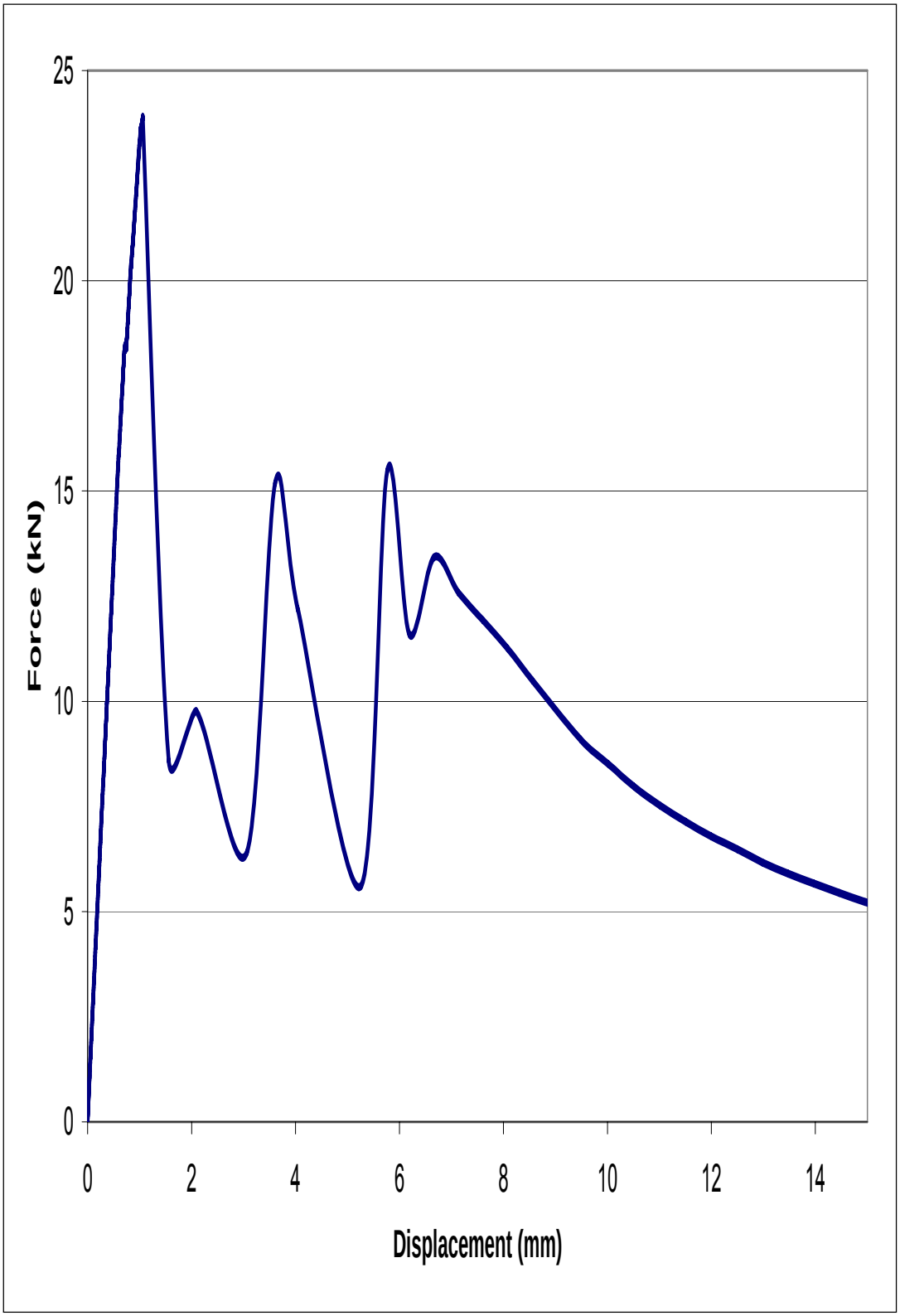

Figure B-7: Pullout coupon 240-1 force vs. displacement curve

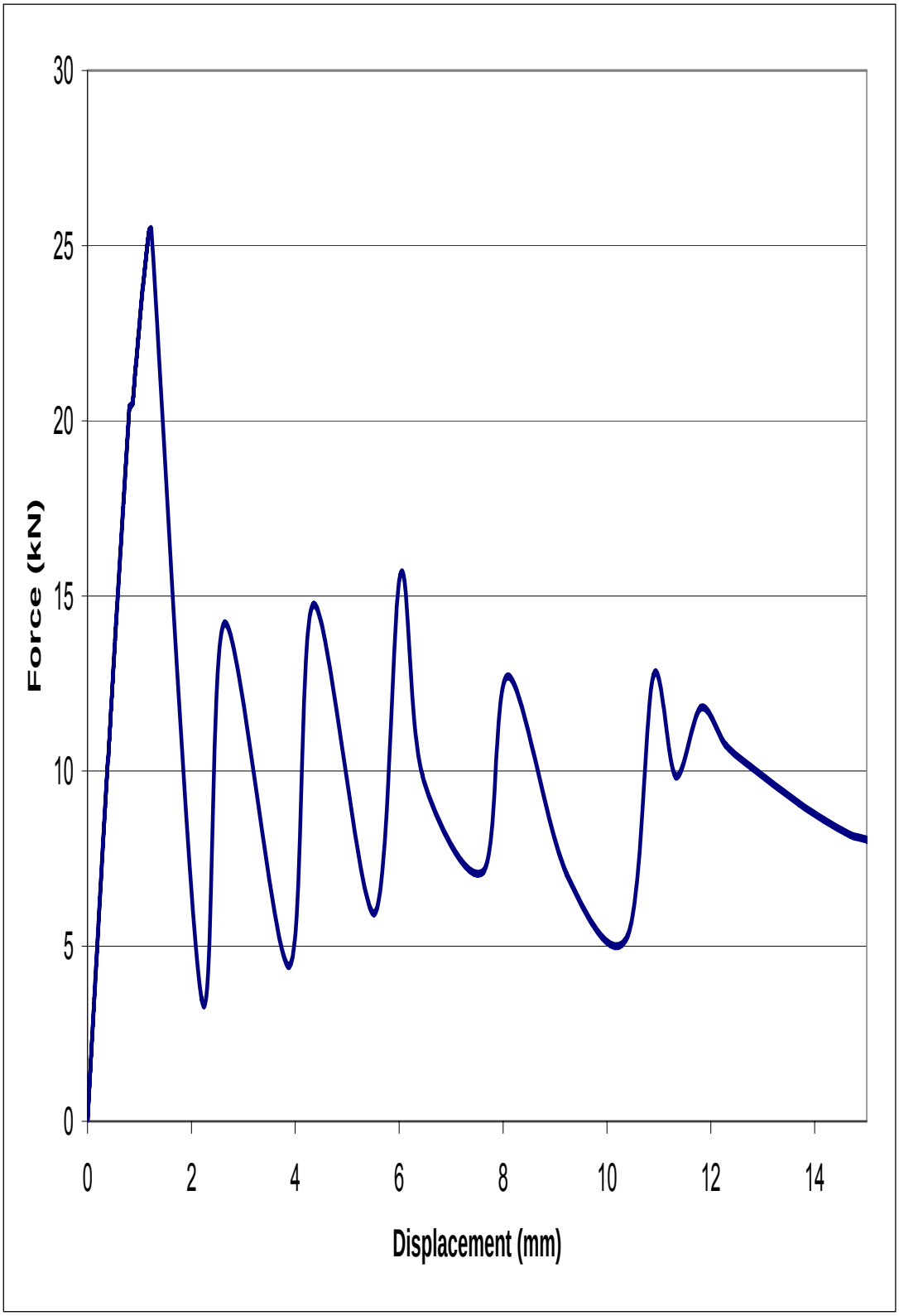

Figure B-8: Pullout coupon 240-2 force vs. displacement curve

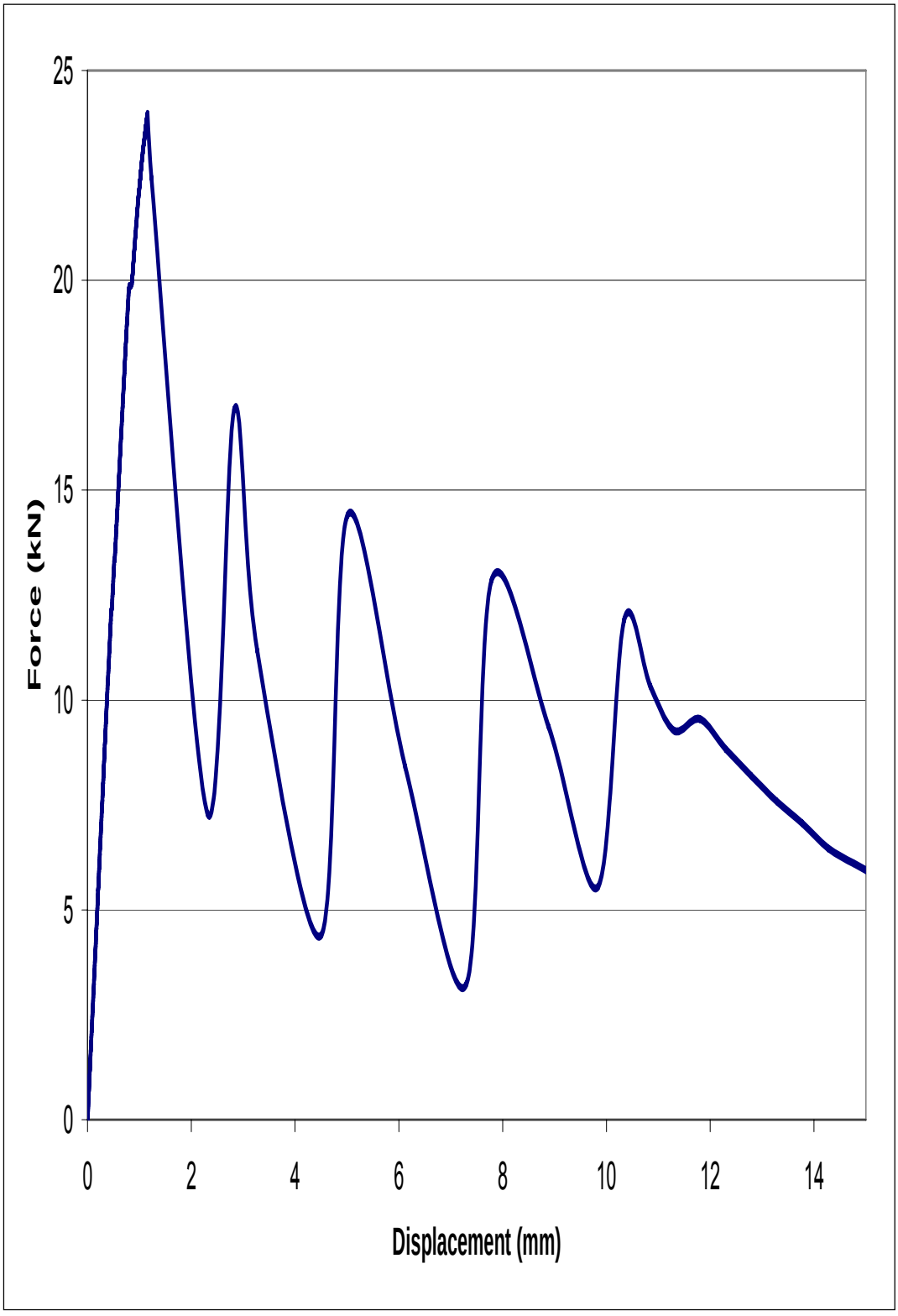

Figure B-9: Pullout coupon 240-3 force vs. displacement curve

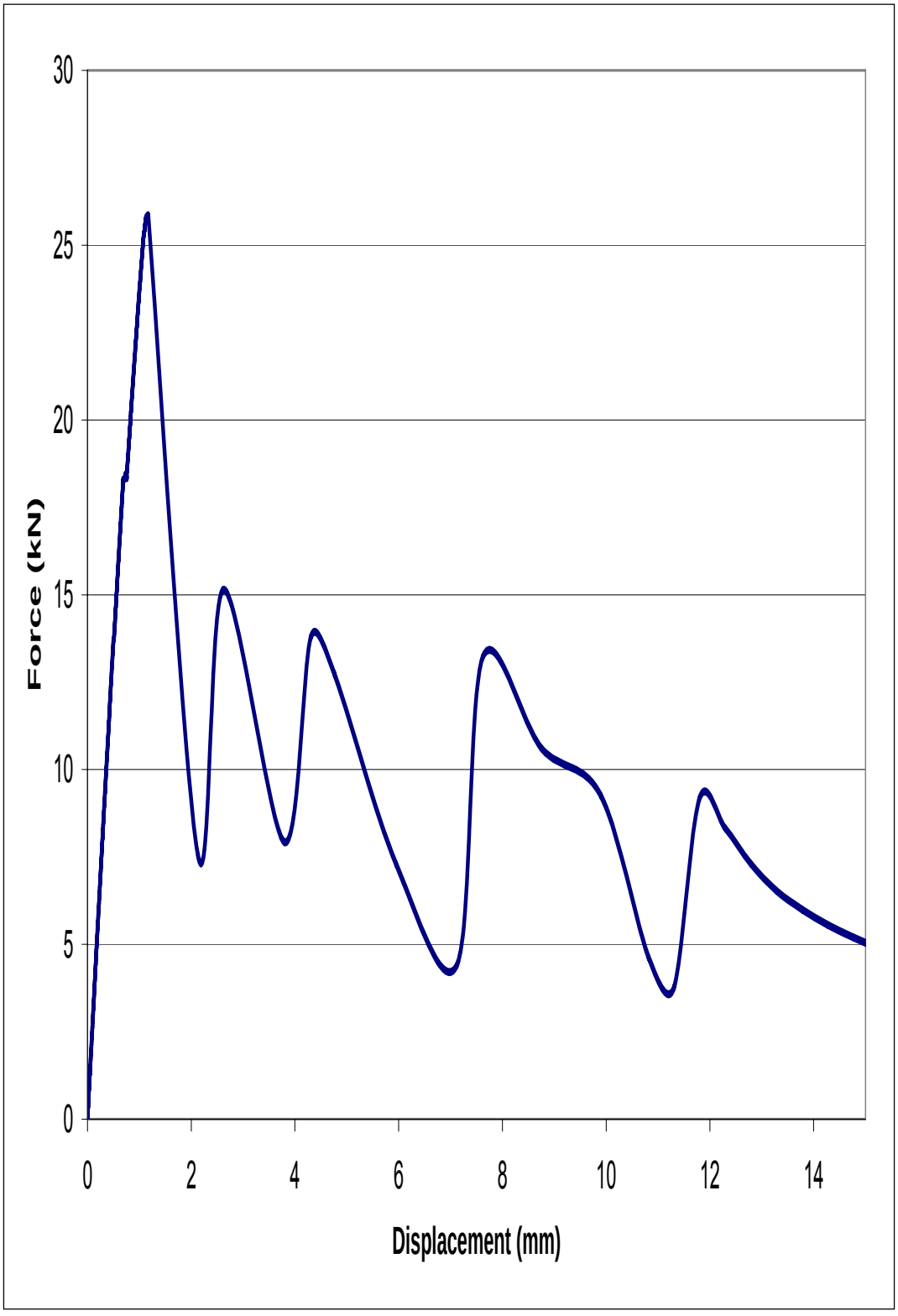

Figure B-10: Pullout coupon 320-1 force vs. displacement curve

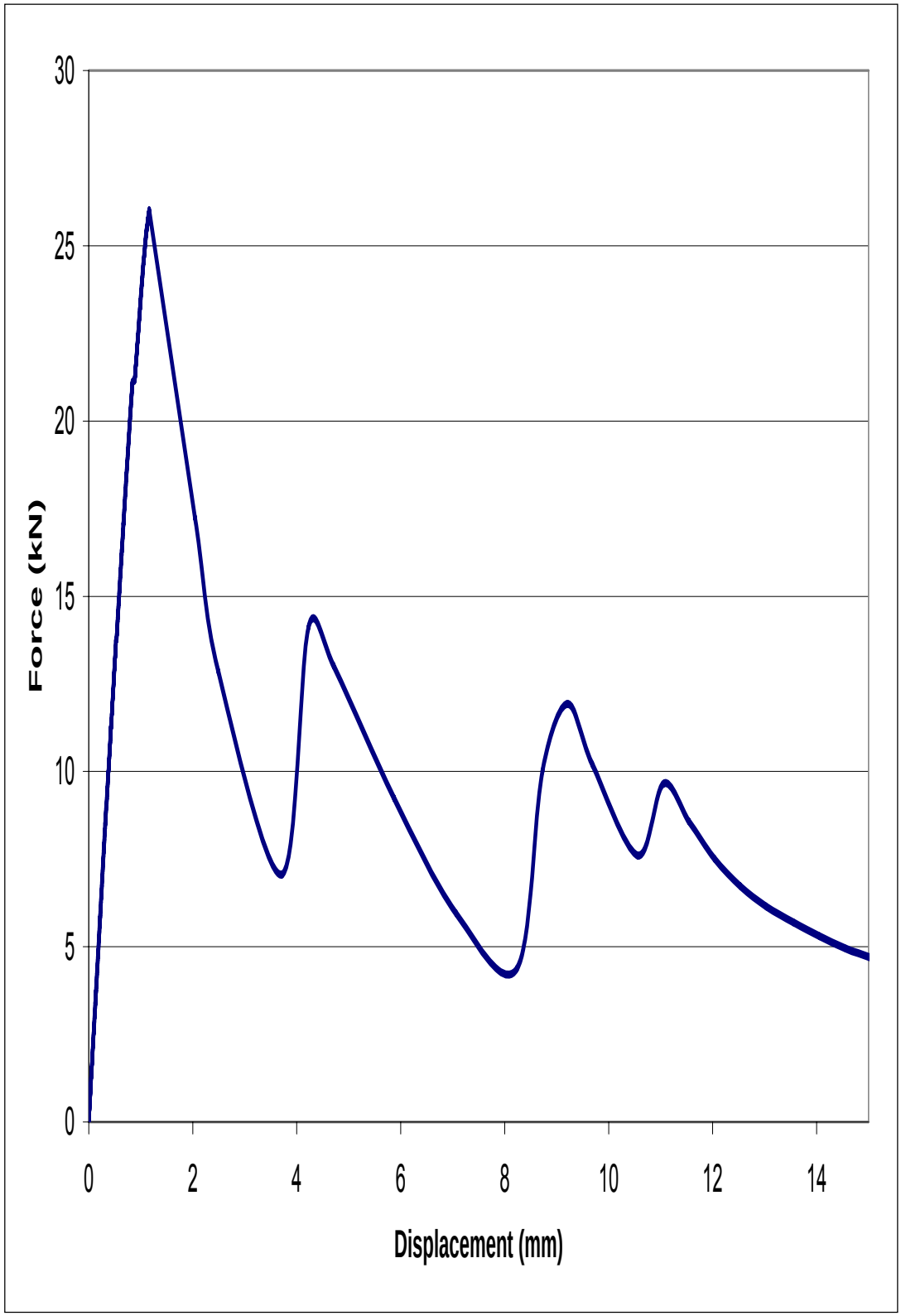

Figure B-11: Pullout coupon 320-2 force vs. displacement curve

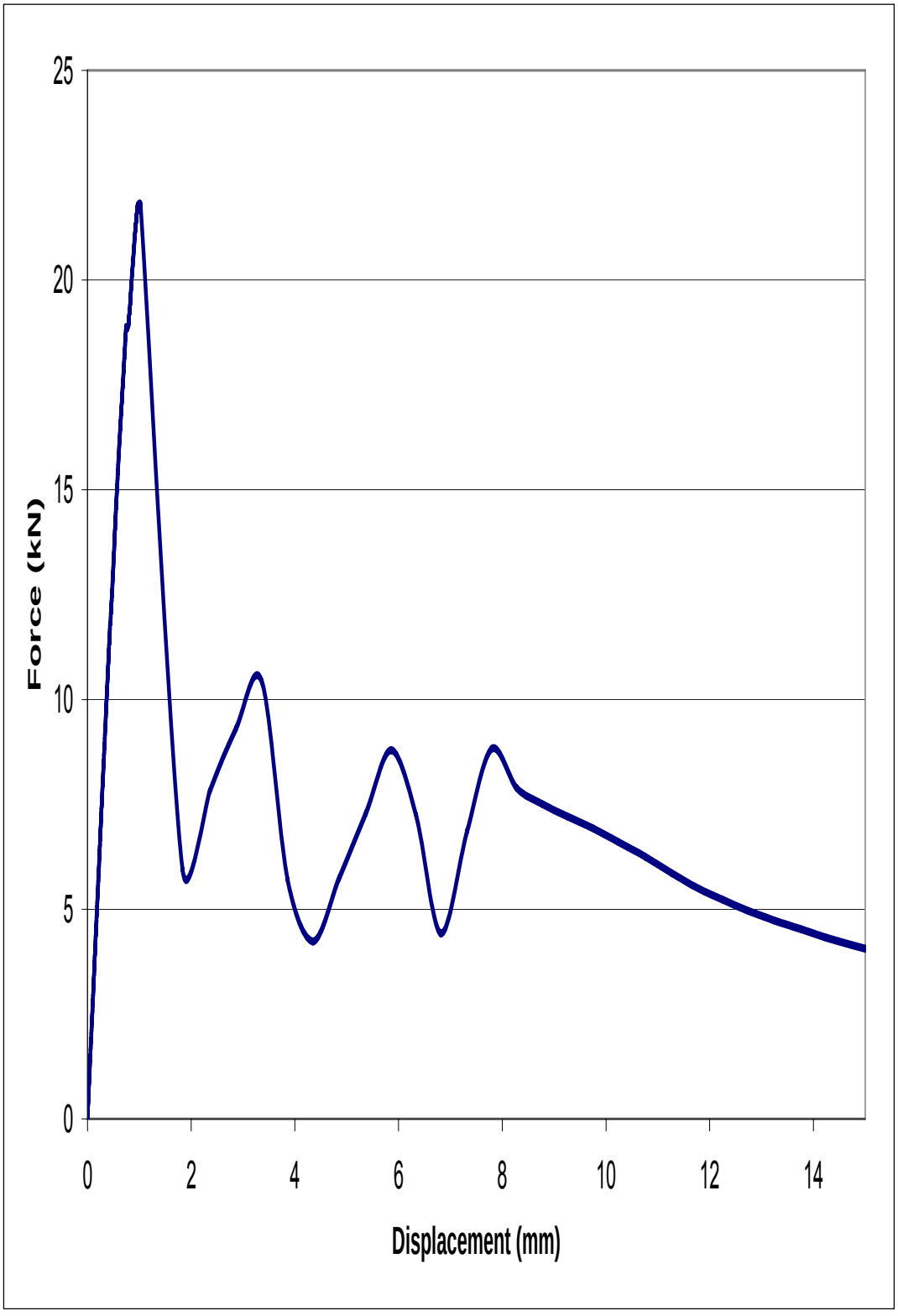

Figure B-12: Pullout coupon 320-3 force vs. displacement curve

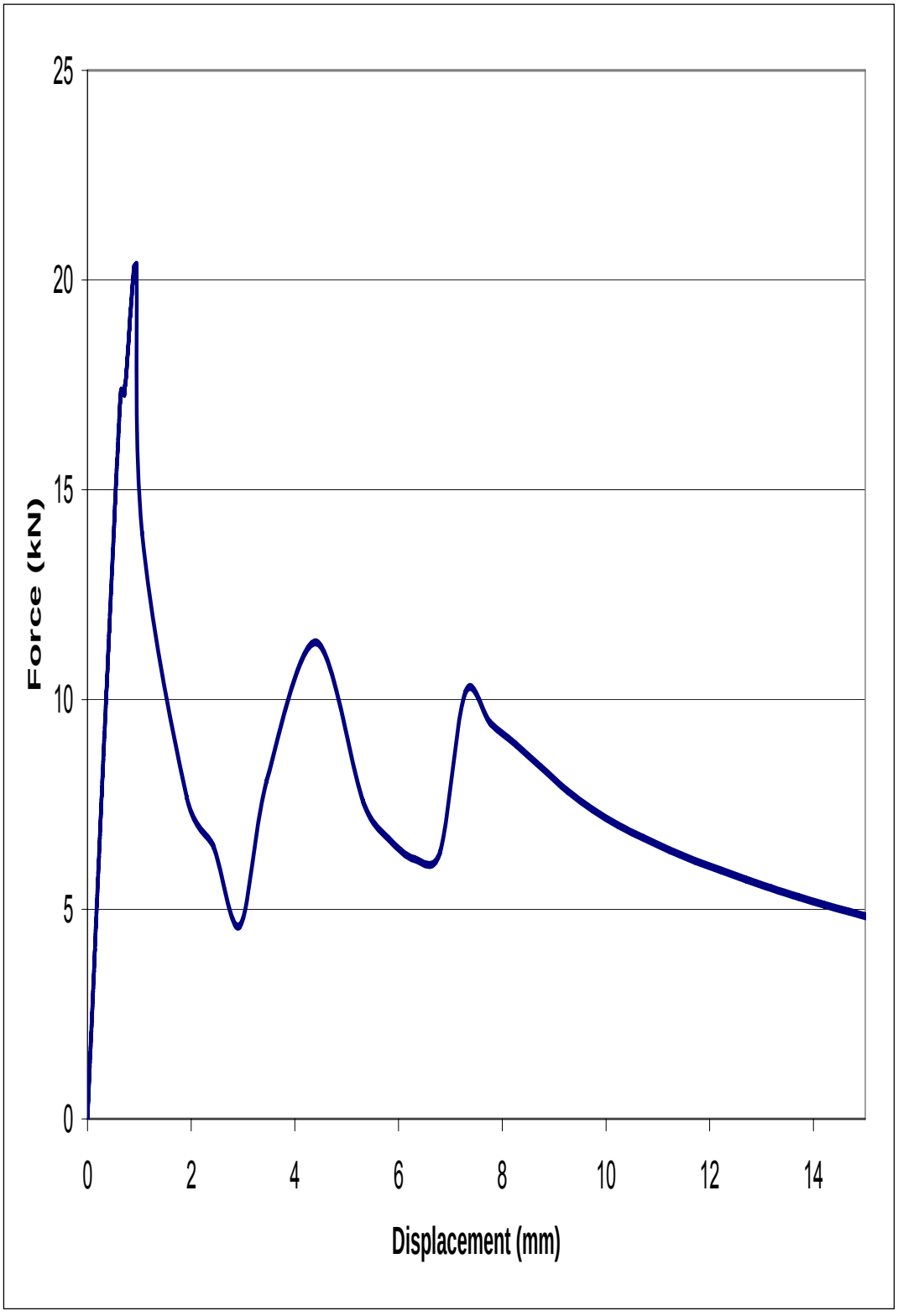

Figure B-13: Pullout coupon 800-1 force vs. displacement curve

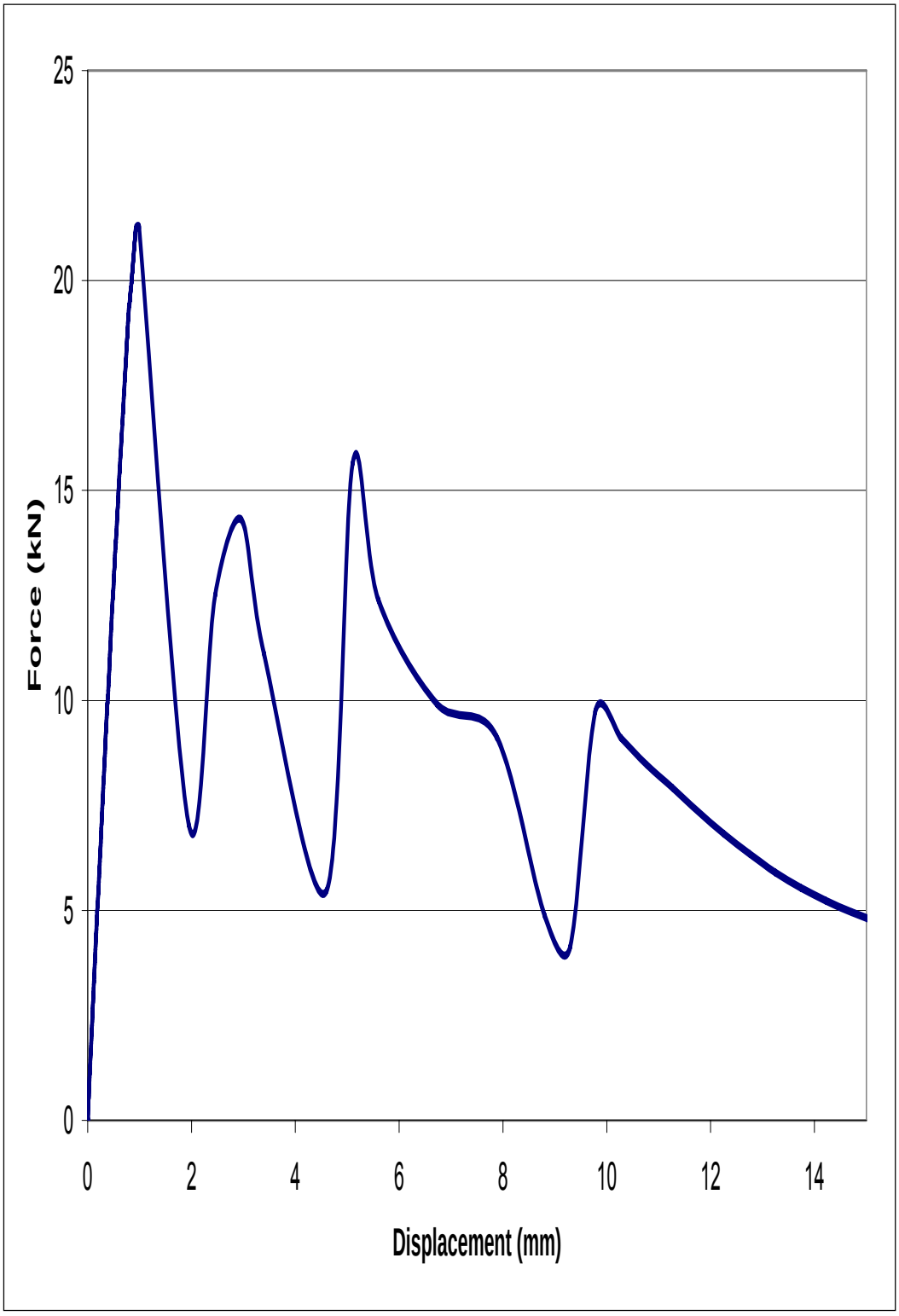

Figure B-14: Pullout coupon 800-2 force vs. displacement curve

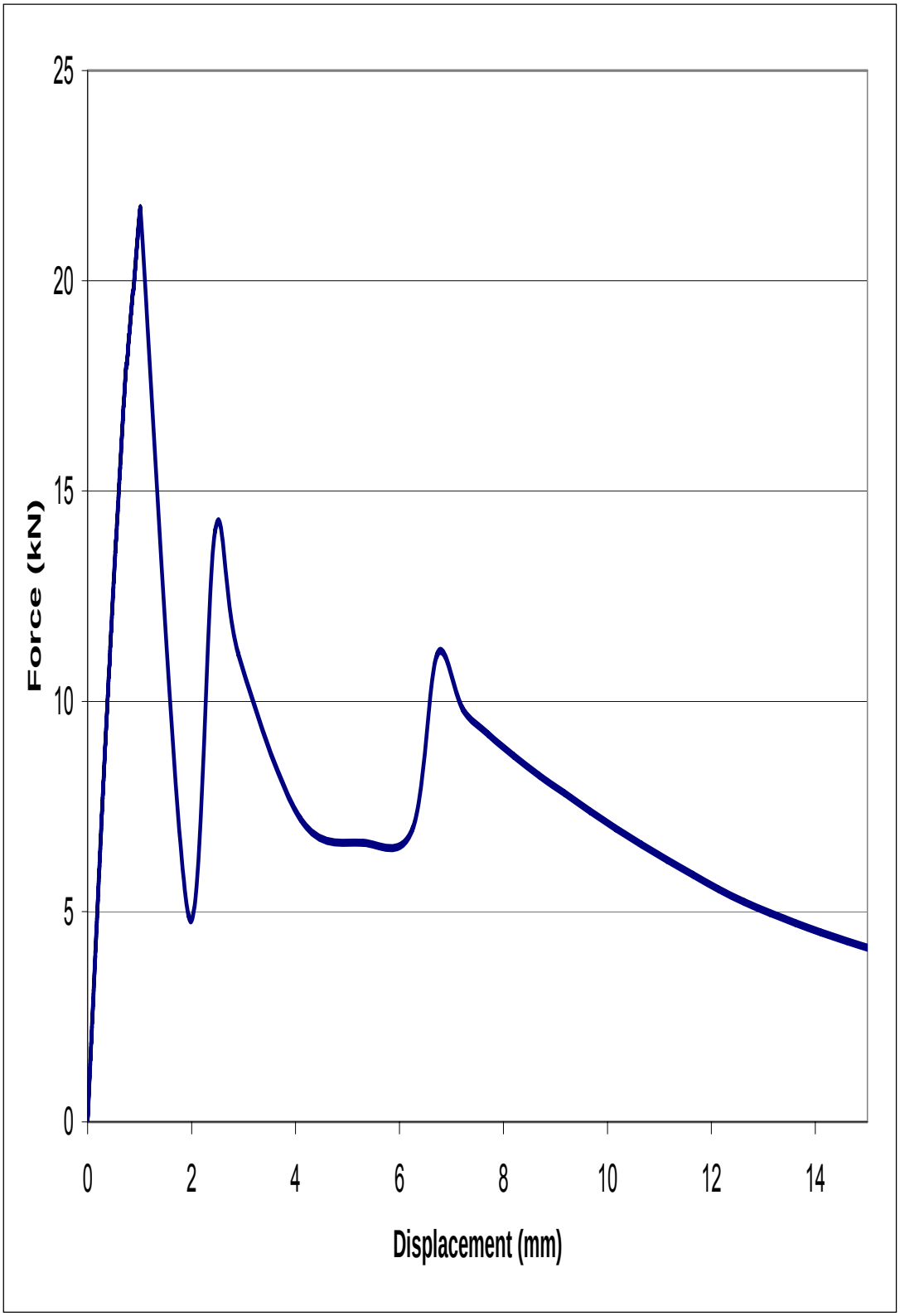

Figure B-15: Pullout curve 800-3 force vs. displacement curve

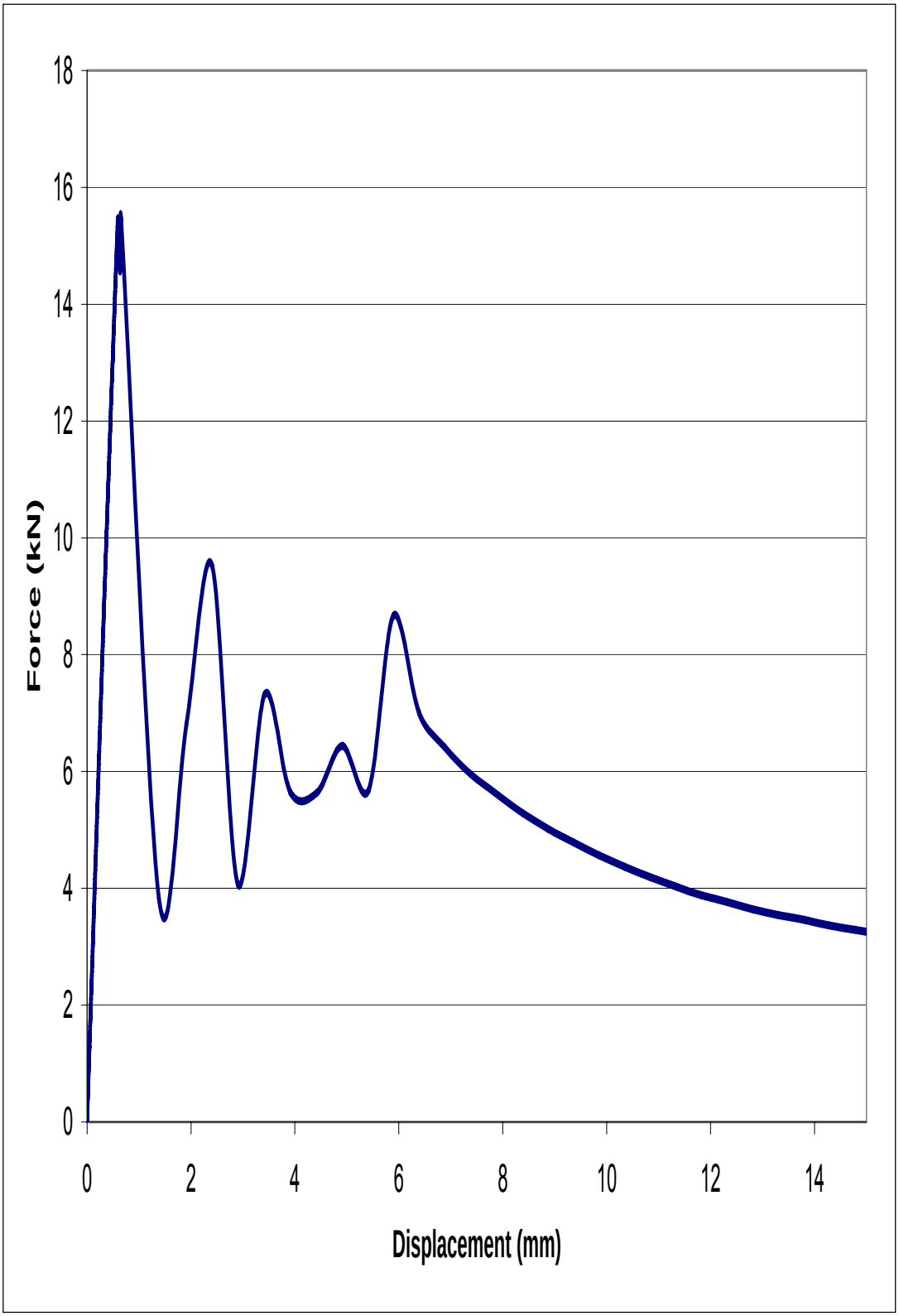

Figure B-16: Pullout coupon 1200-1 force vs. displacement curve

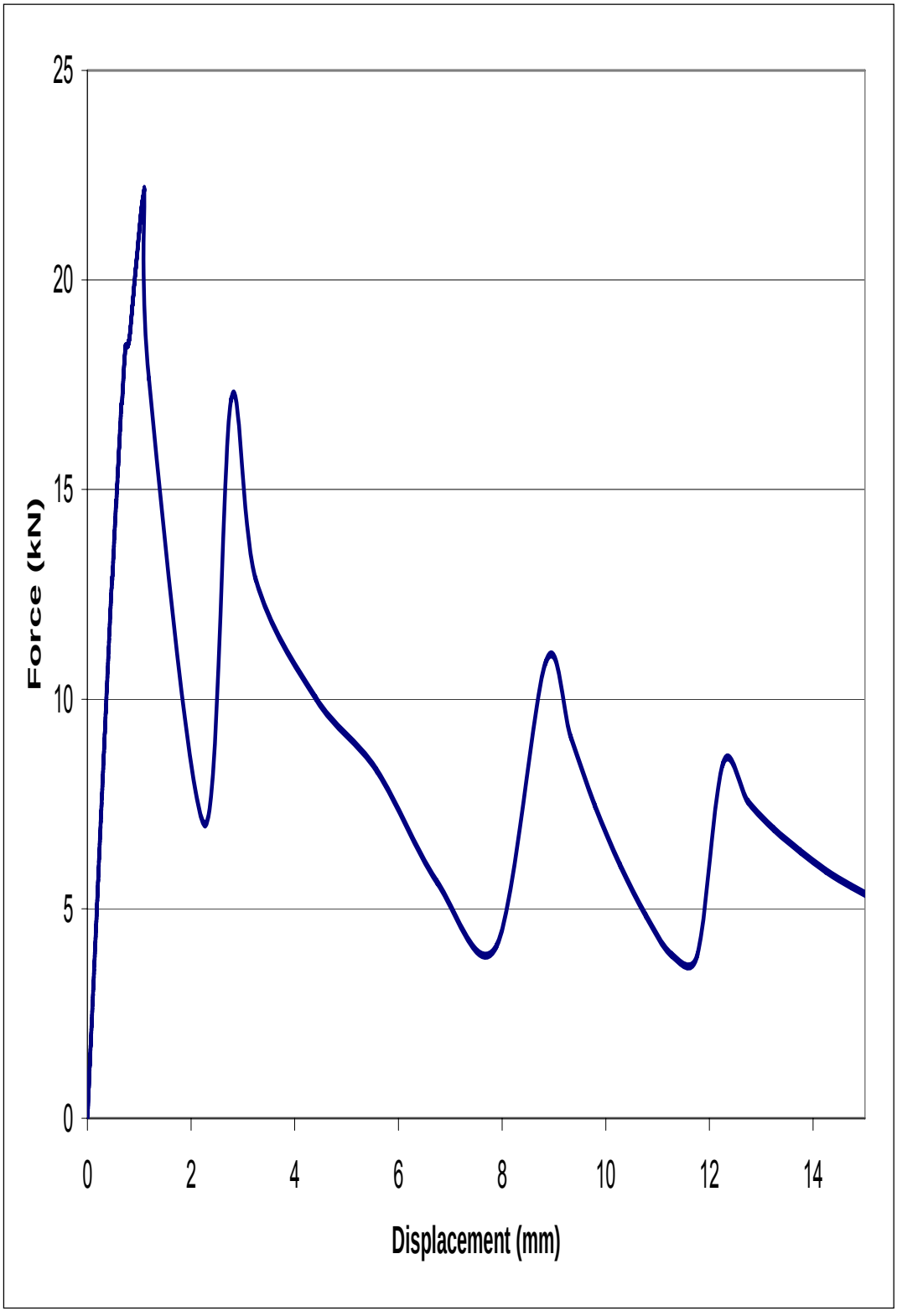

Figure B-17: Pullout coupon 1200-2 force vs. displacement curve

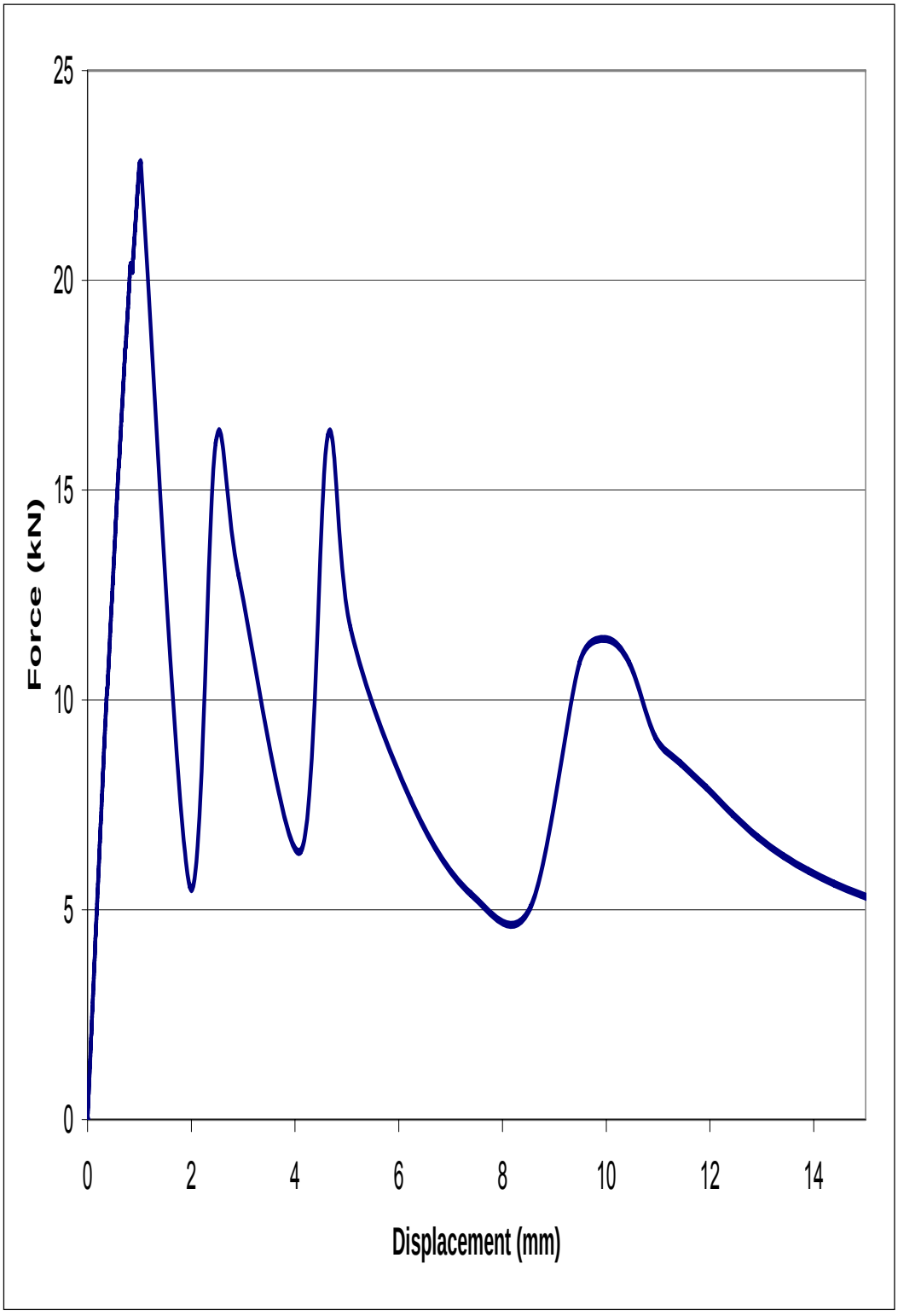

Figure B-18: Pullout coupon 1200-3 force vs. displacement curve

APPENDIX C

Selected Individual Pushout Coupon Force vs. Displacement Curves

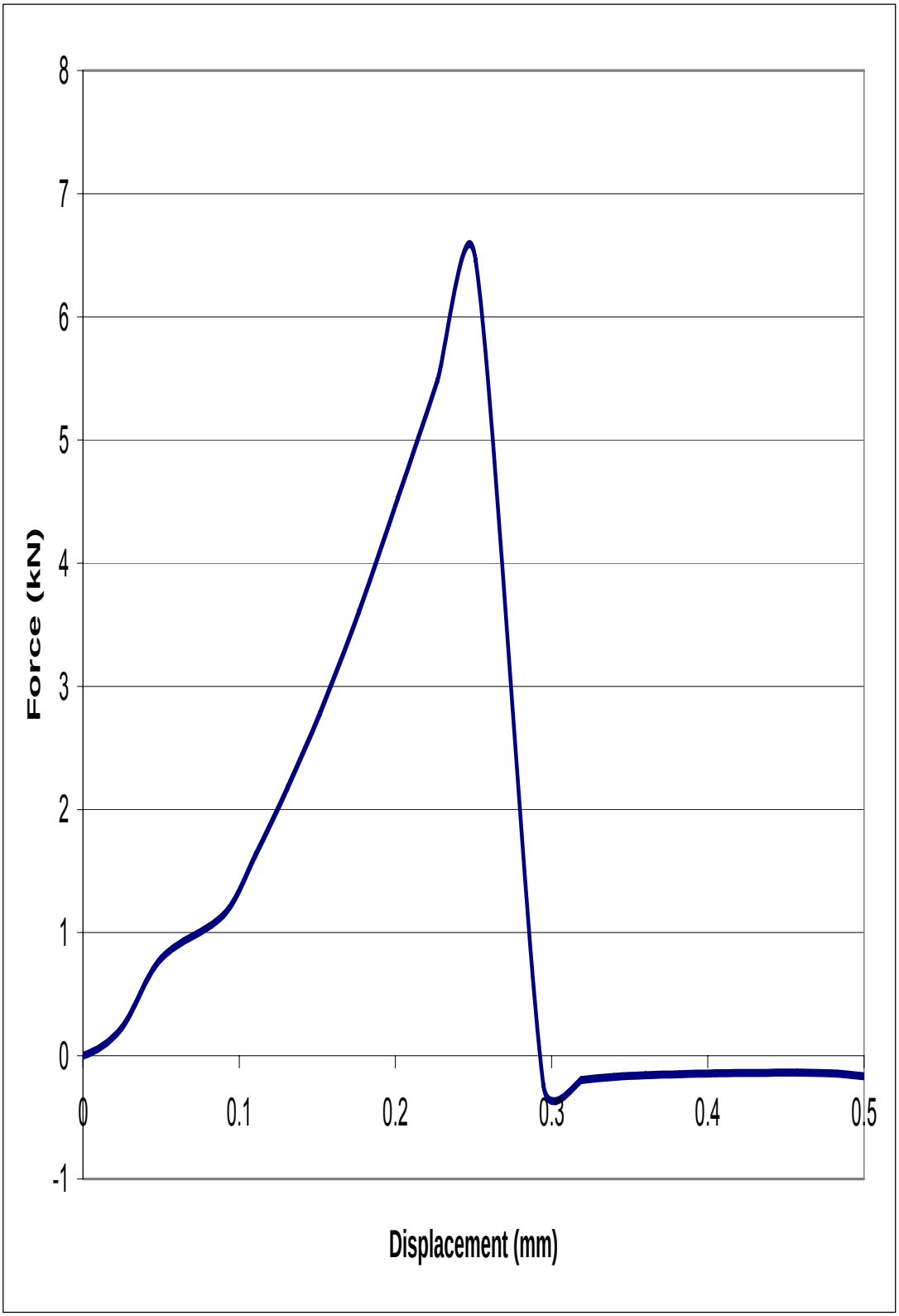

Figure C-1: Pushout coupon (2, 1) -1 force vs. displacement curve

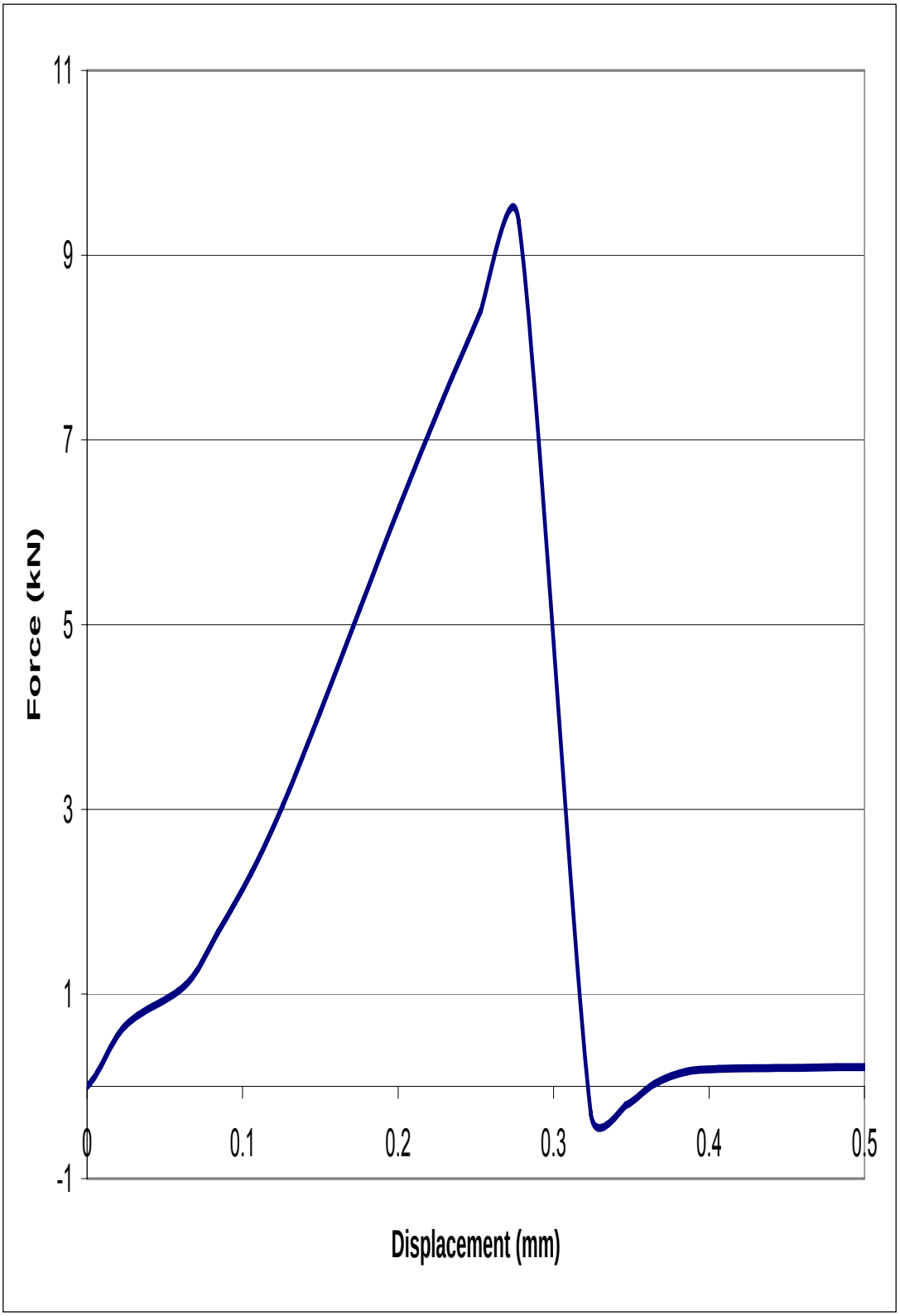

Figure C-2: Pushout coupon (2, 1) -2 force vs. displacement curve

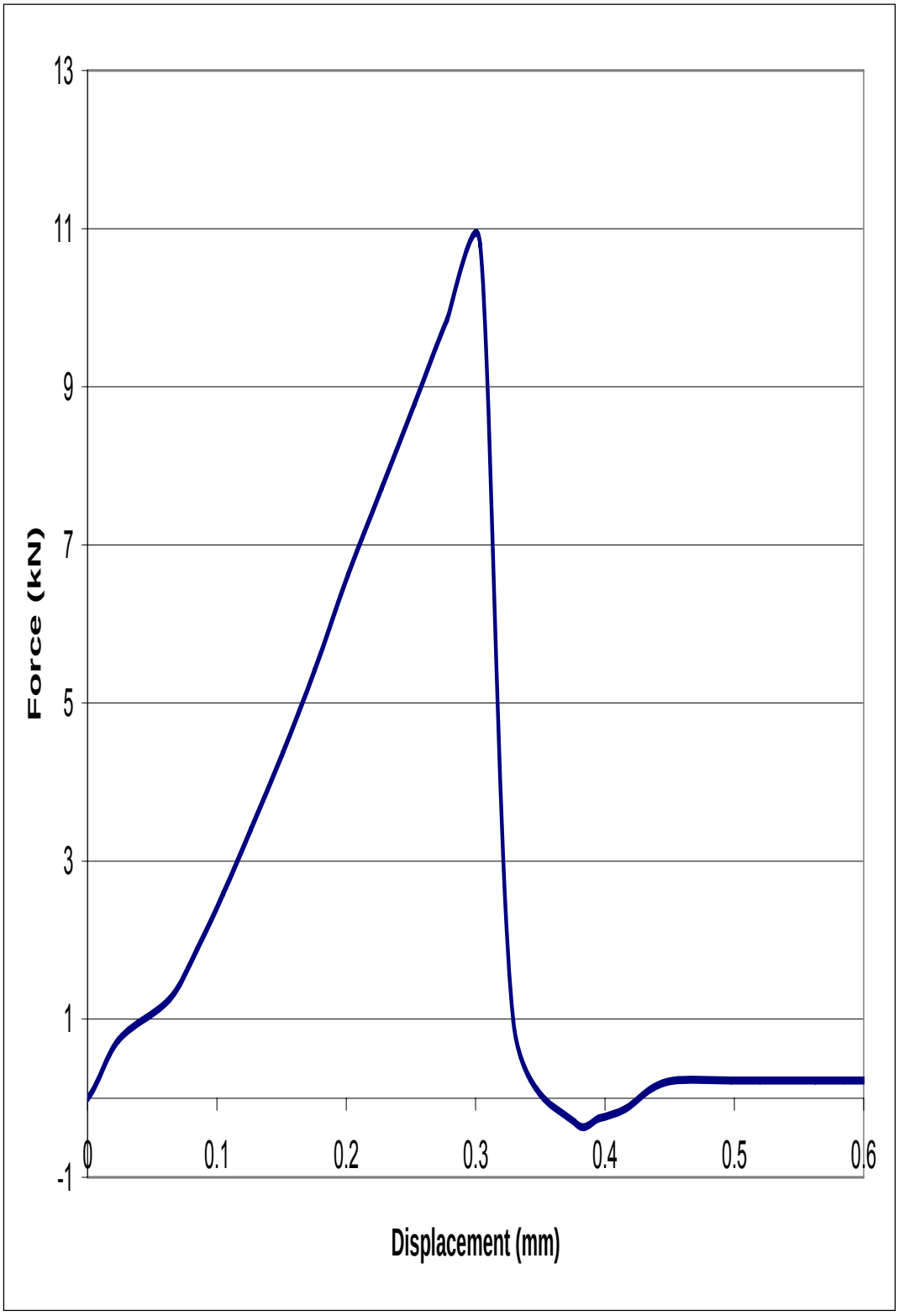

Figure C-3: Pushout coupon (2, 1) -3 force vs. displacement curve

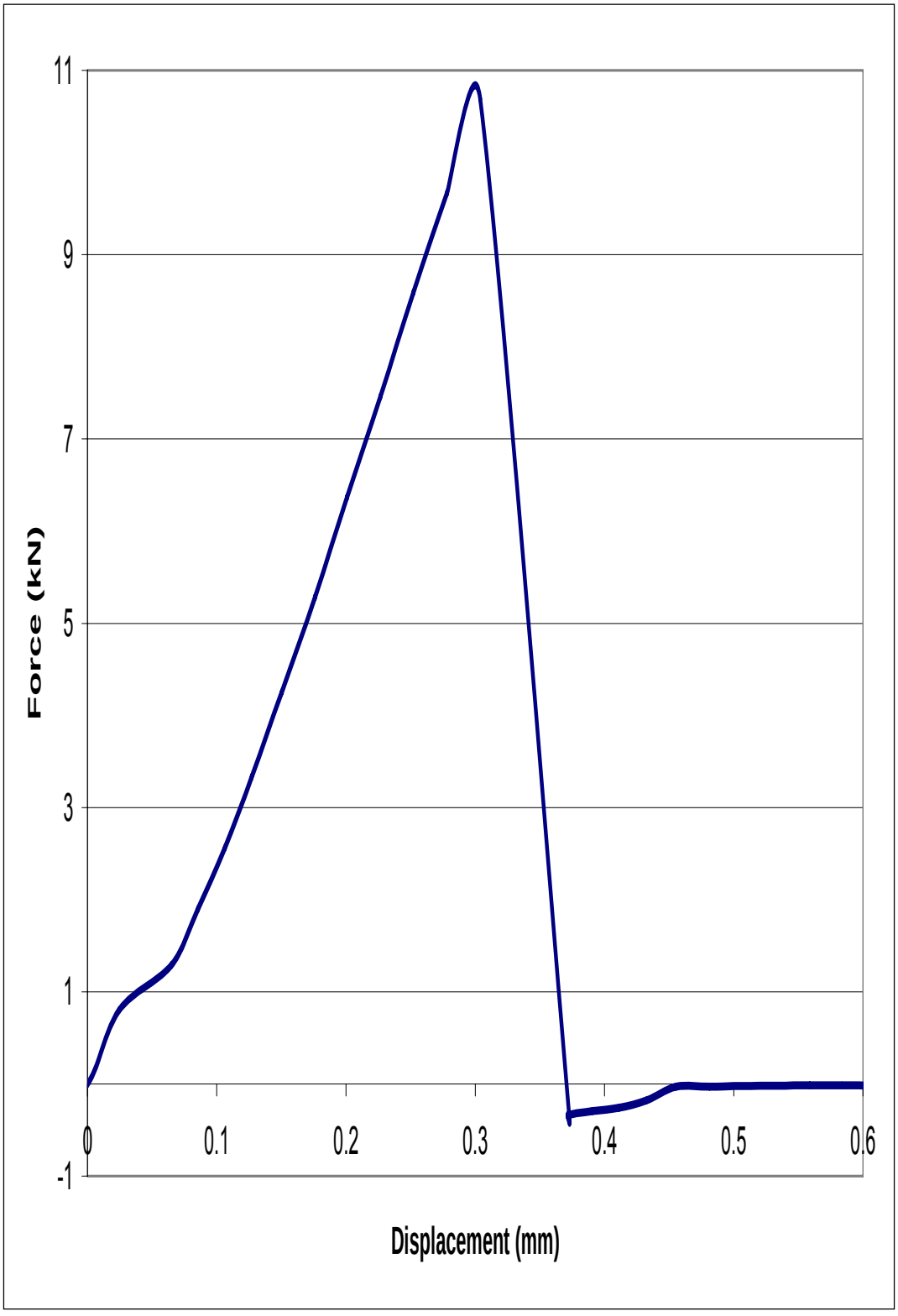

Figure C-4: Pushout coupon (2, 2) -1 force vs. displacement curve

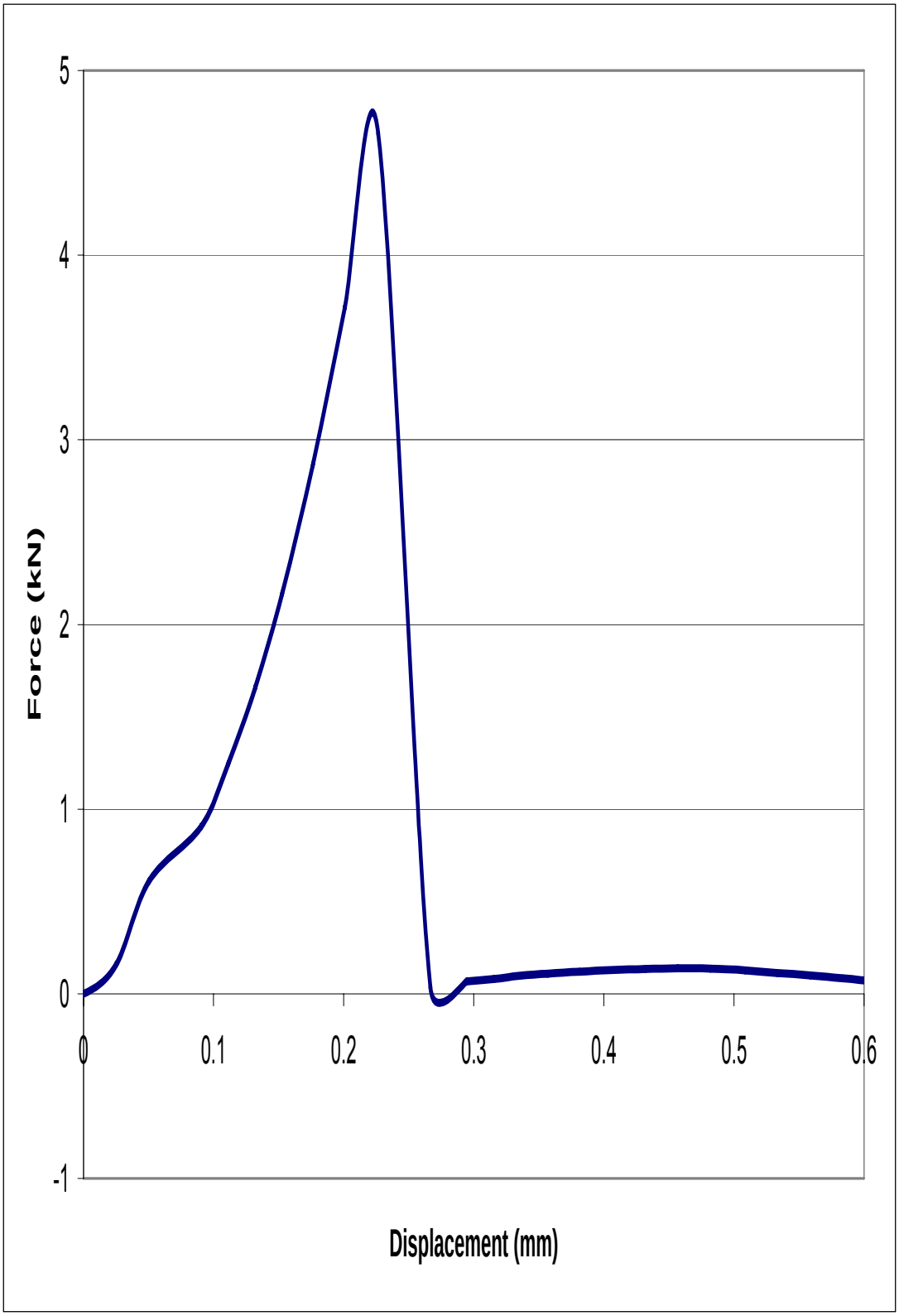

Figure C-5: Pushout coupon (2, 2) -2 force vs. displacement curve

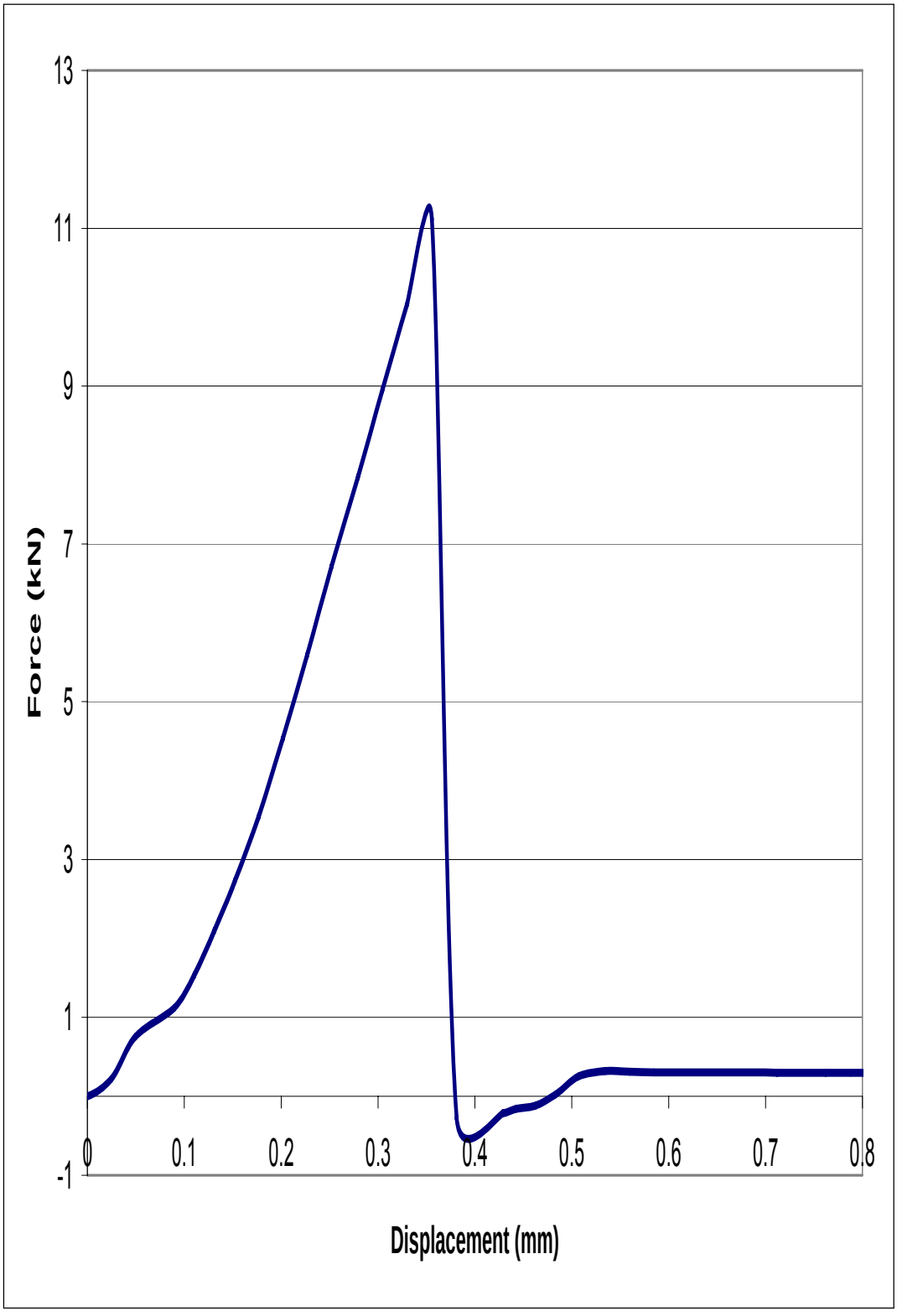

Figure C-6: Pushout coupon (2, 2) -3 force vs. displacement curve

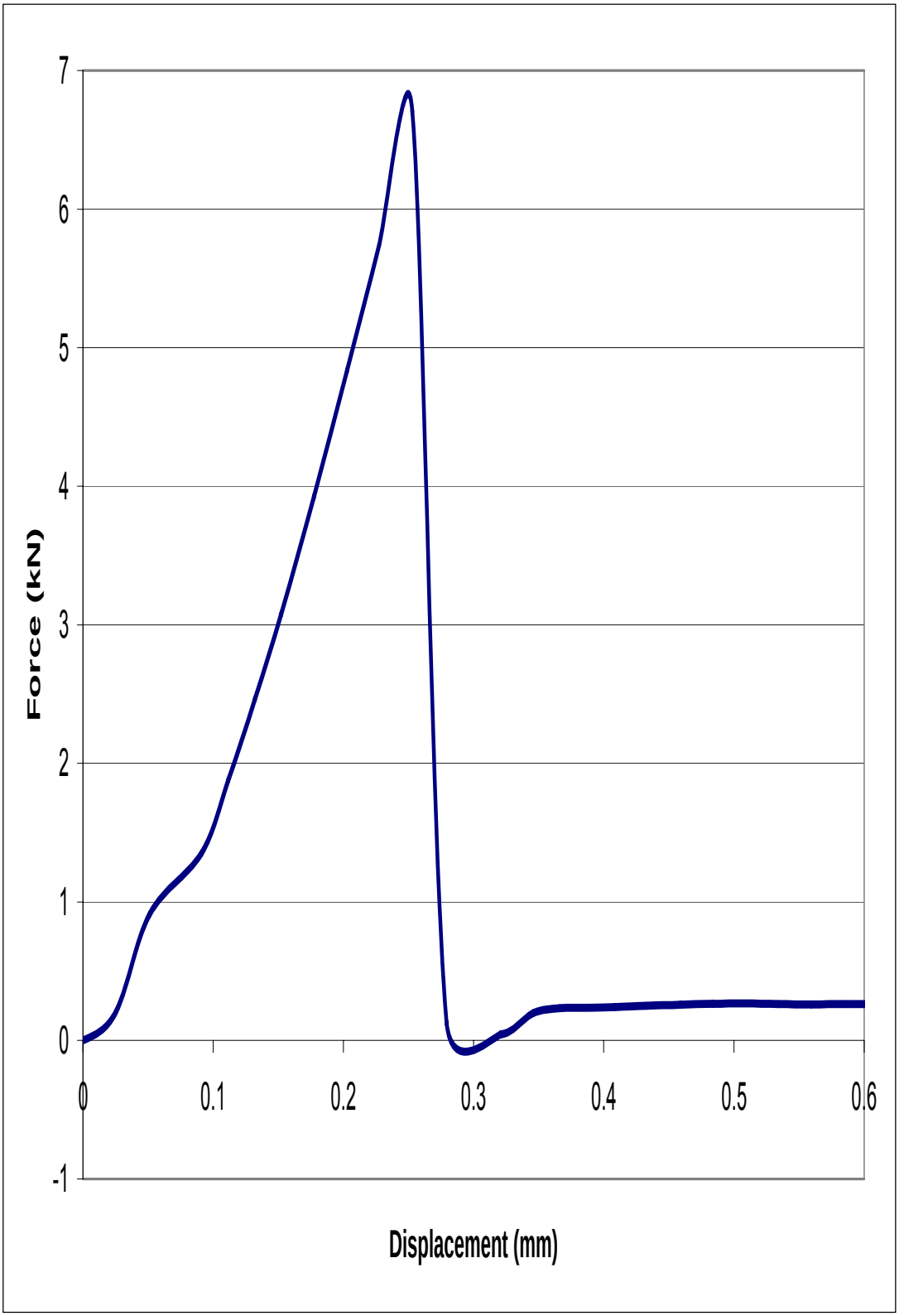

Figure C-7: Pushout coupon (2, 4) -1 force vs. displacement curve

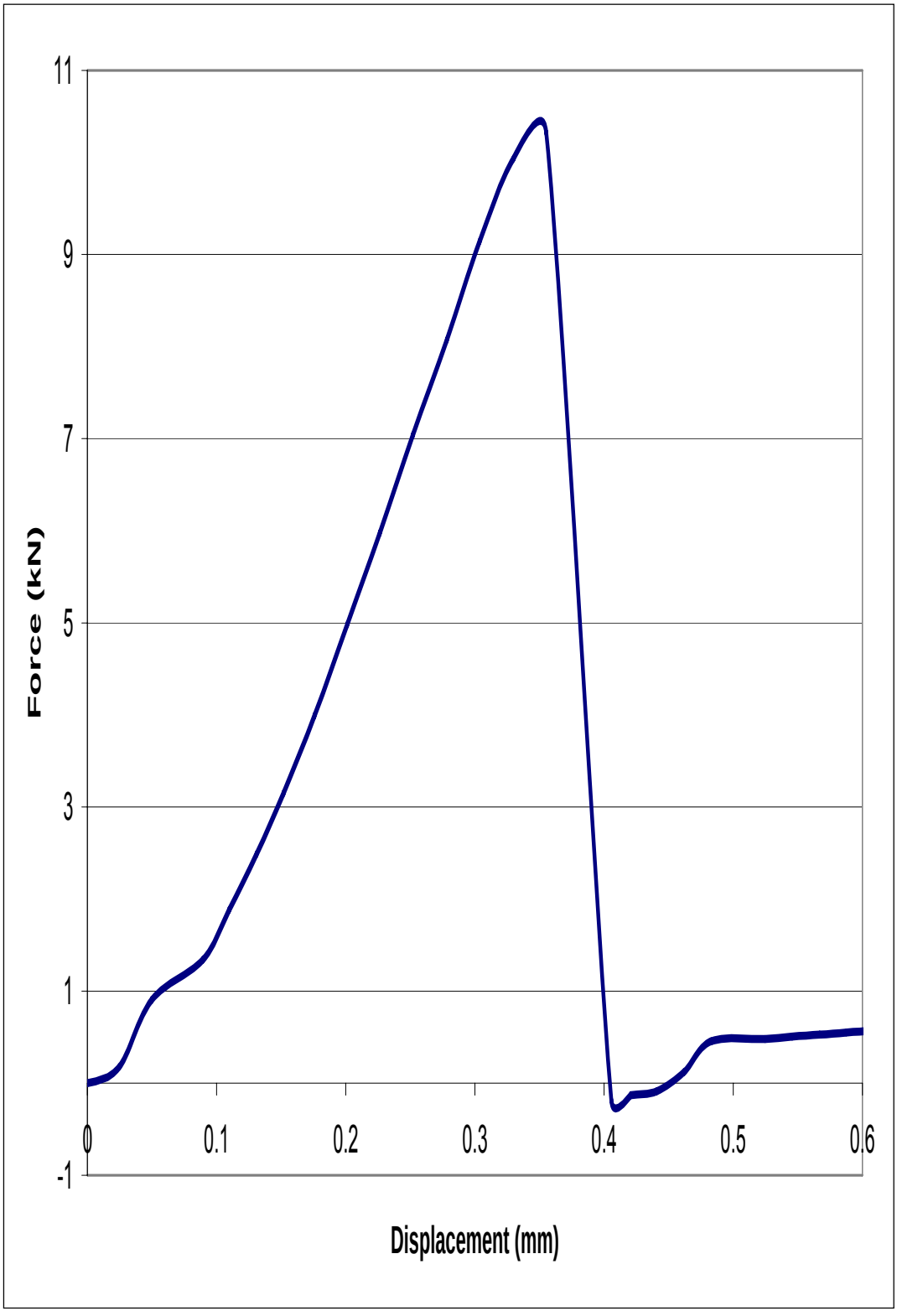

Figure C-8: Pushout coupon (2, 4) -2 force vs. displacement curve

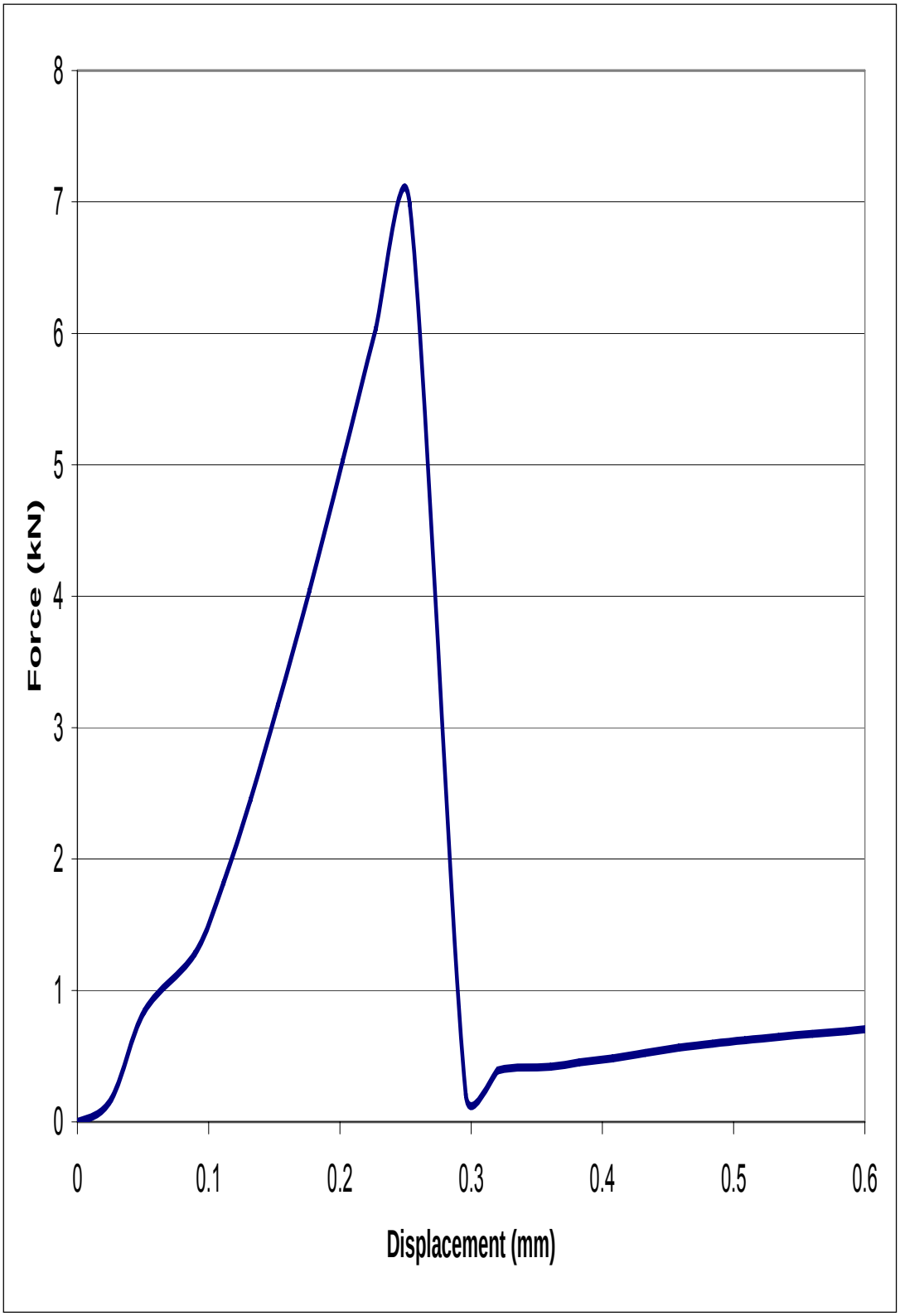

Figure C-9: Pushout coupon (2, 4) -3 force vs. displacement curve

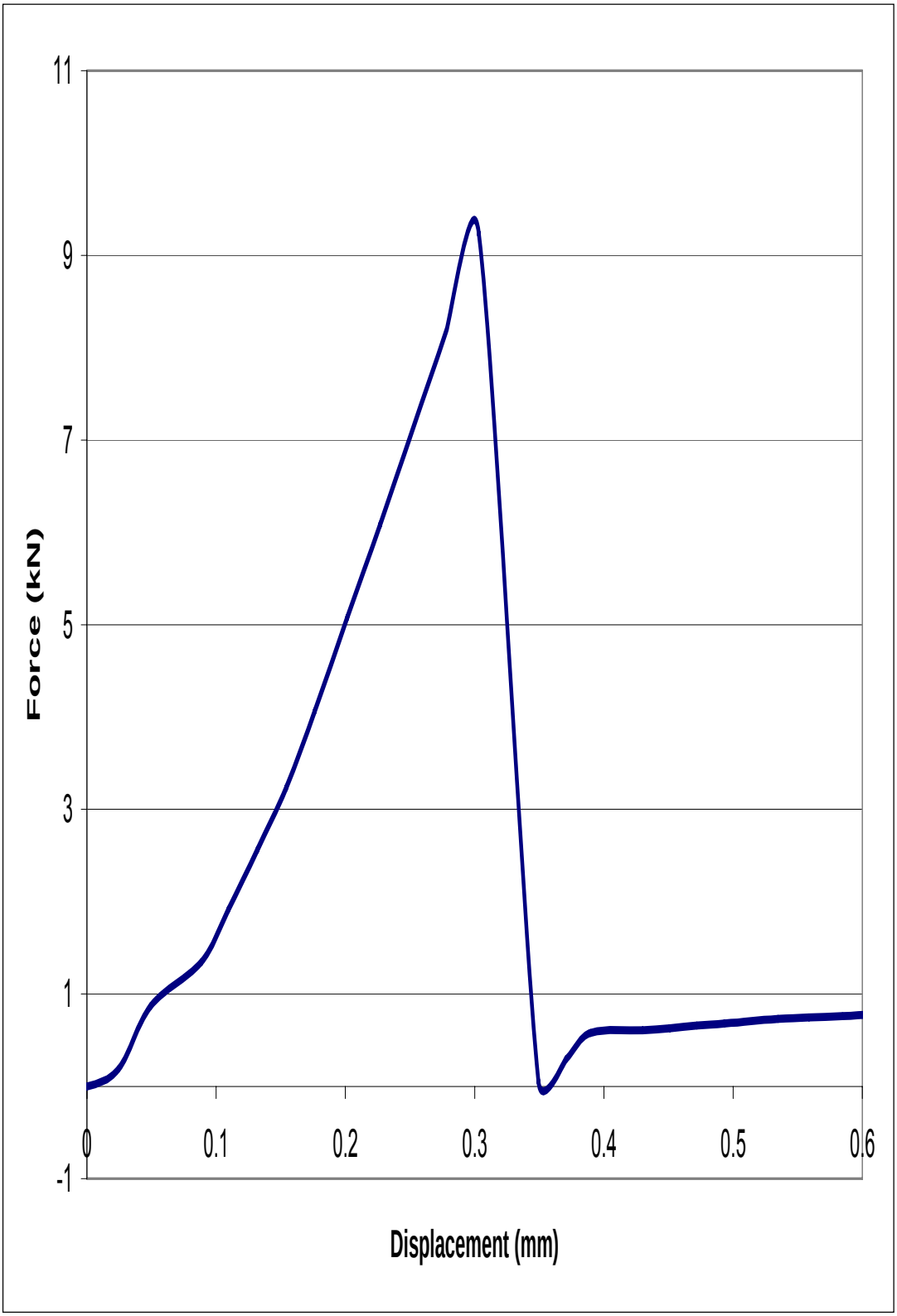

Figure C-10: Pushout coupon (3, 1) -1 force vs. displacement curve

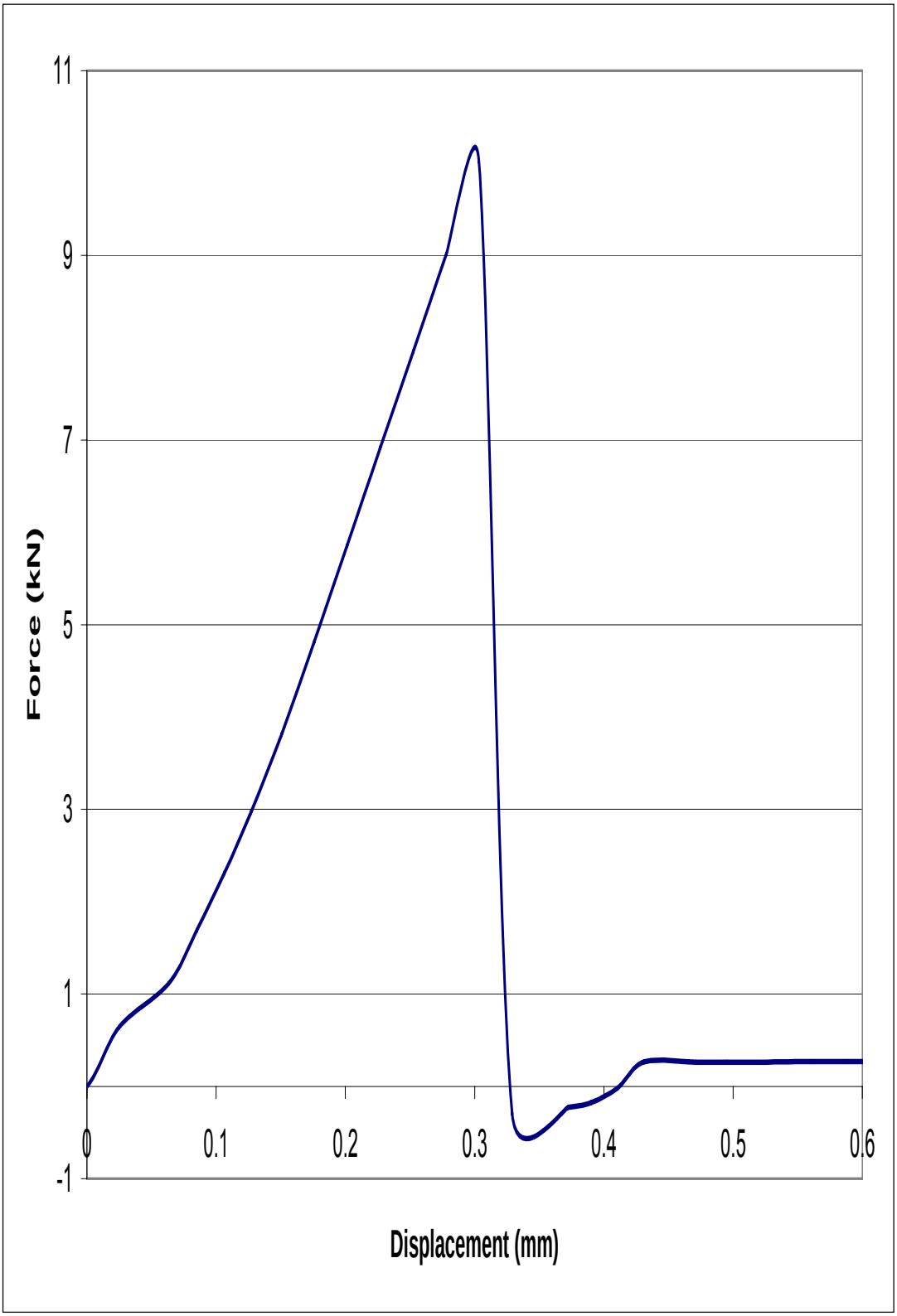

Figure C-11: Pushout coupon (3, 1) -2 force vs. displacement curve

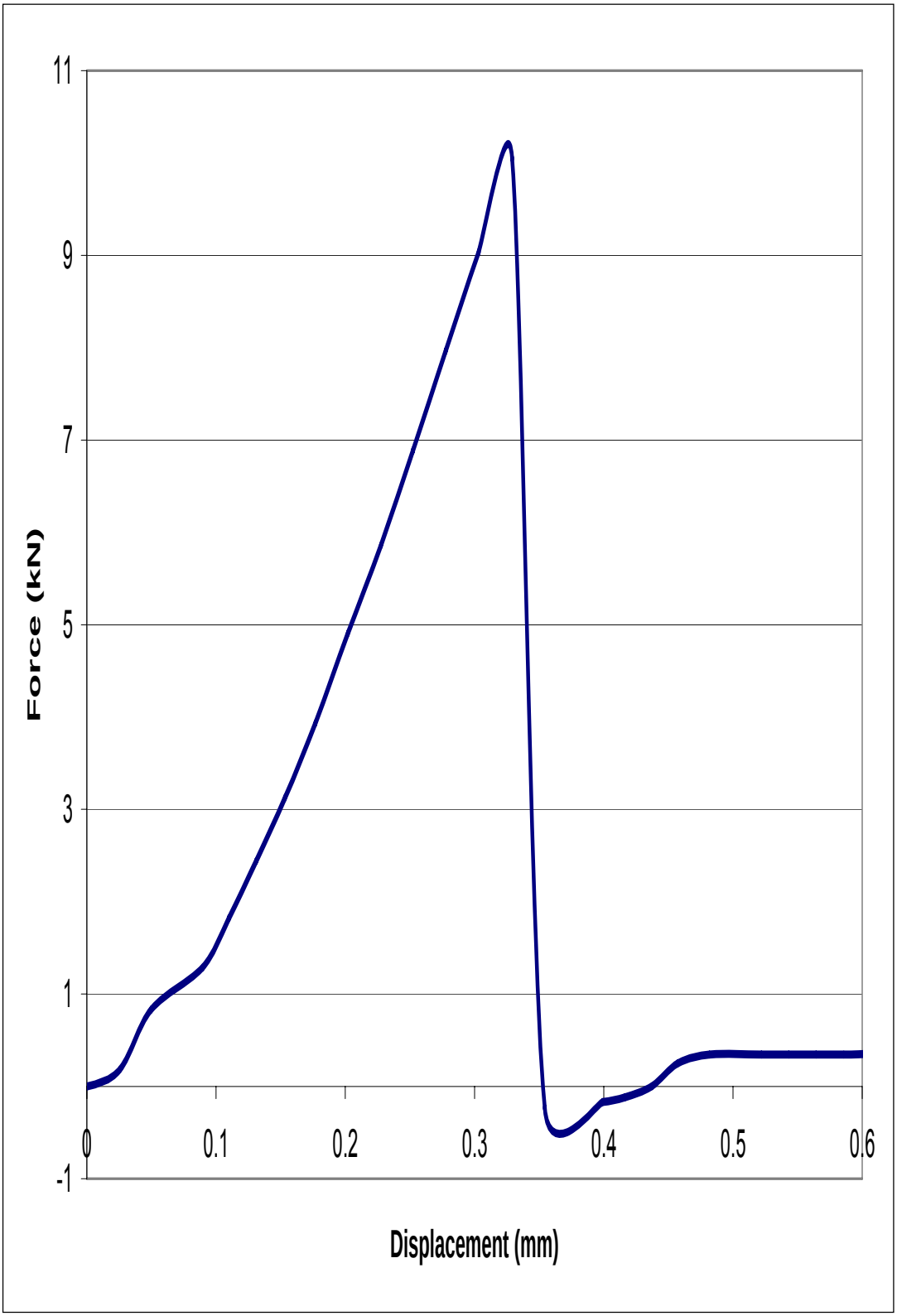

Figure C-12: Pushout coupon (3, 1) -3 force vs. displacement curve

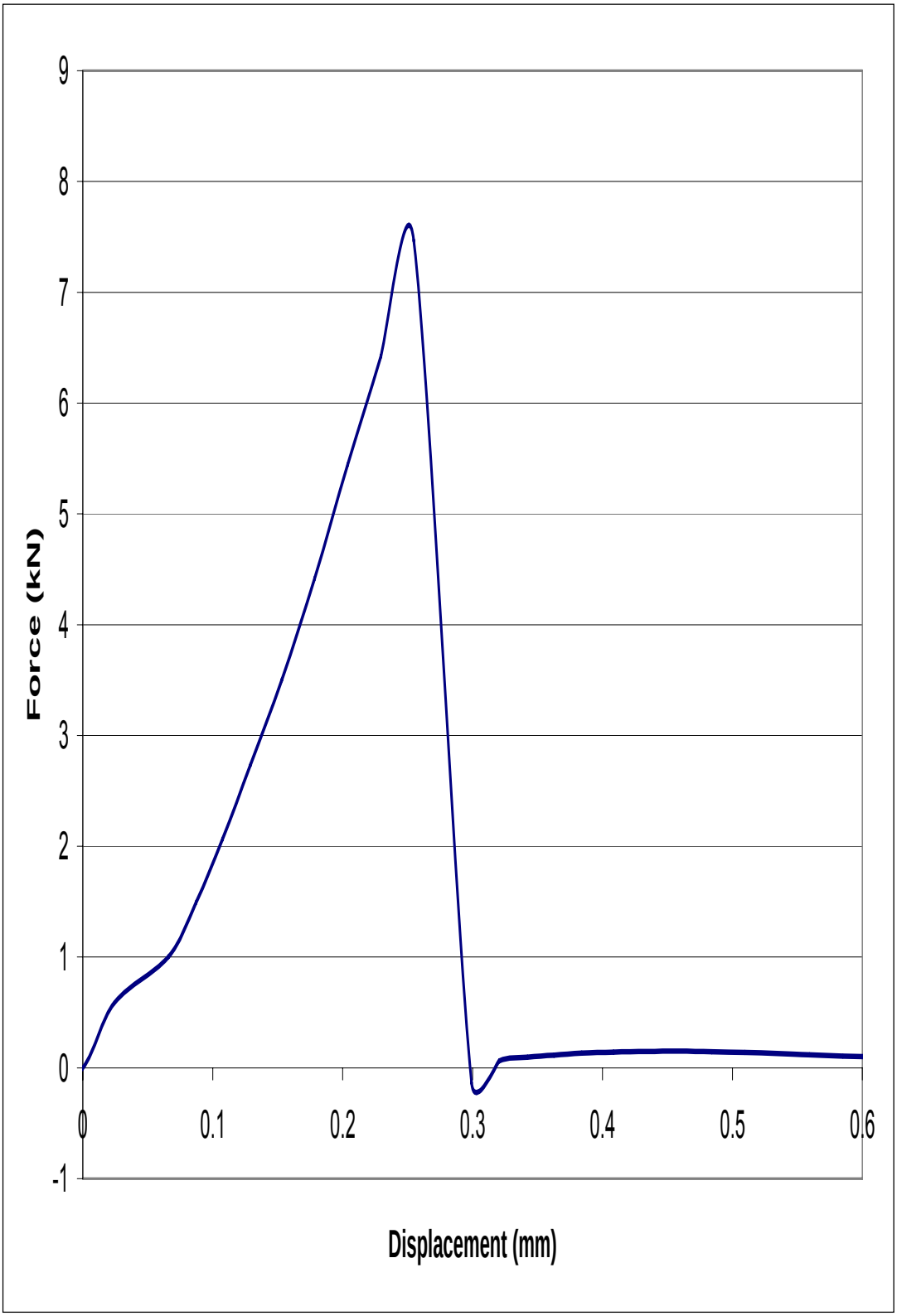

Figure C-13: Pushout coupon (3, 2) -1 force vs. displacement curve

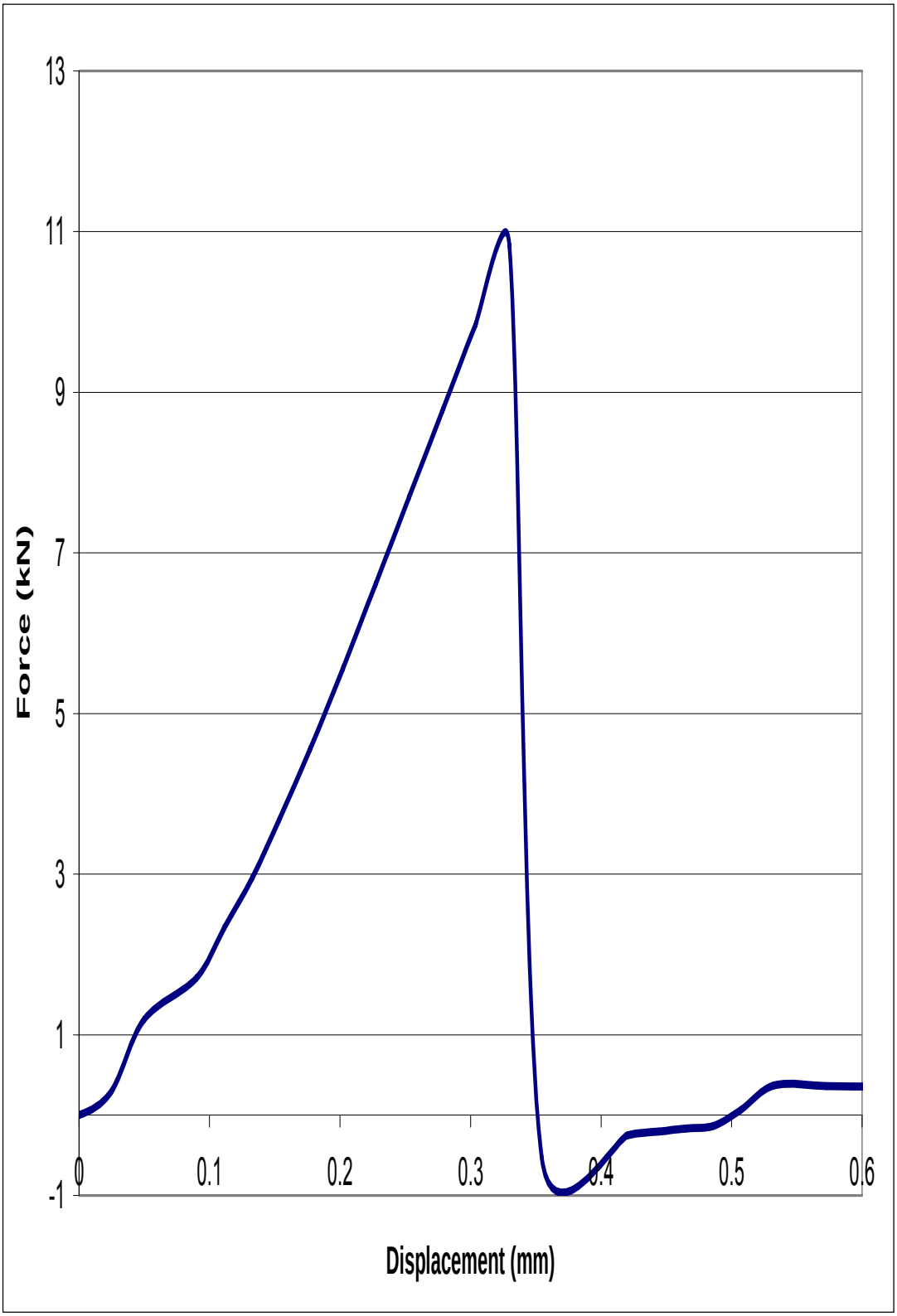

Figure C-14: Pushout coupon (3, 2) -2 force vs. displacement curve

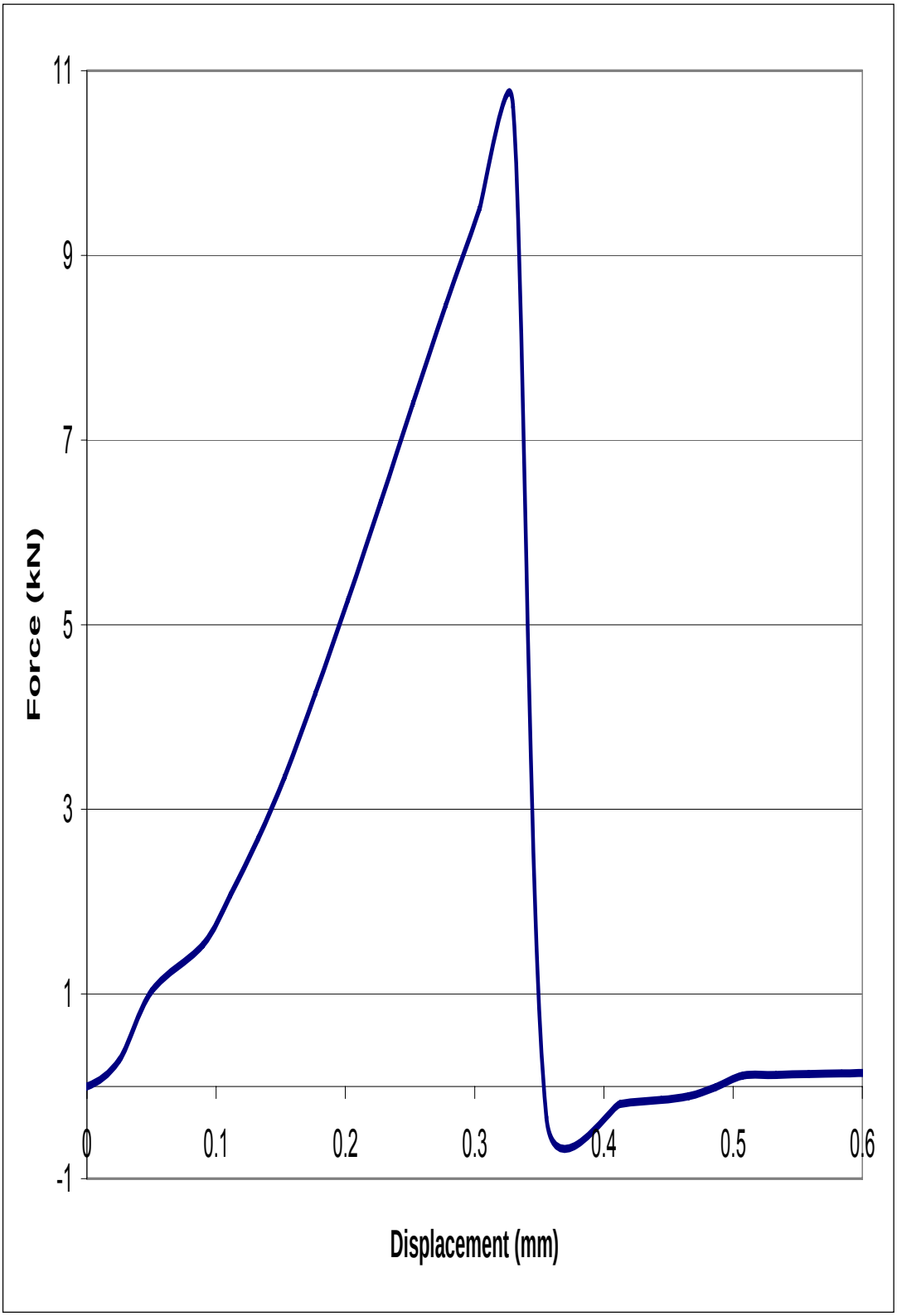

Figure C-15: Pushout coupon (3, 2) -3 force vs. displacement curve

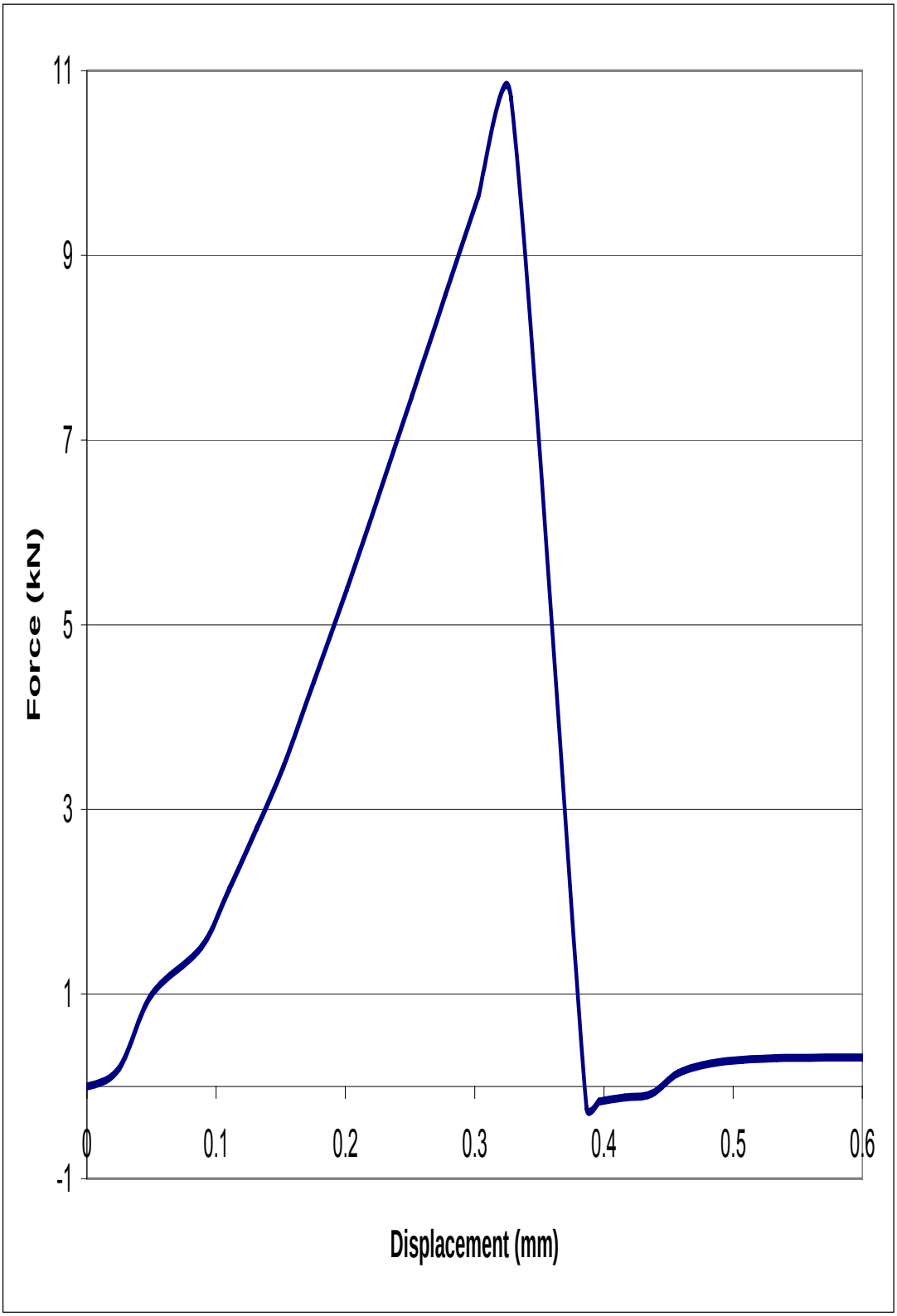

Figure C-16: Pushout coupon (3, 4) -1 force vs. displacement curve

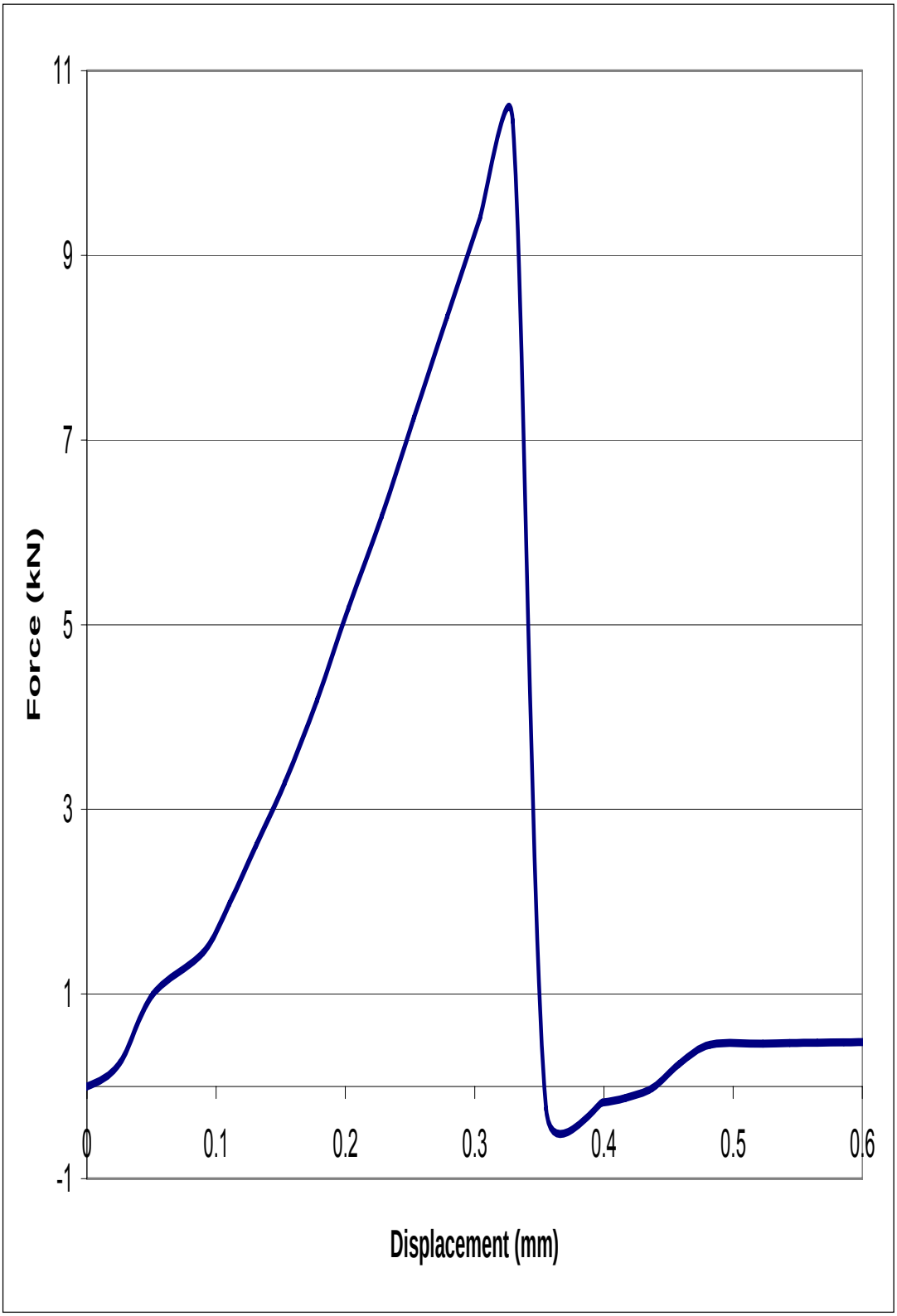

Figure C-17: Pushout coupon (3, 4) -2 force vs. displacement curve

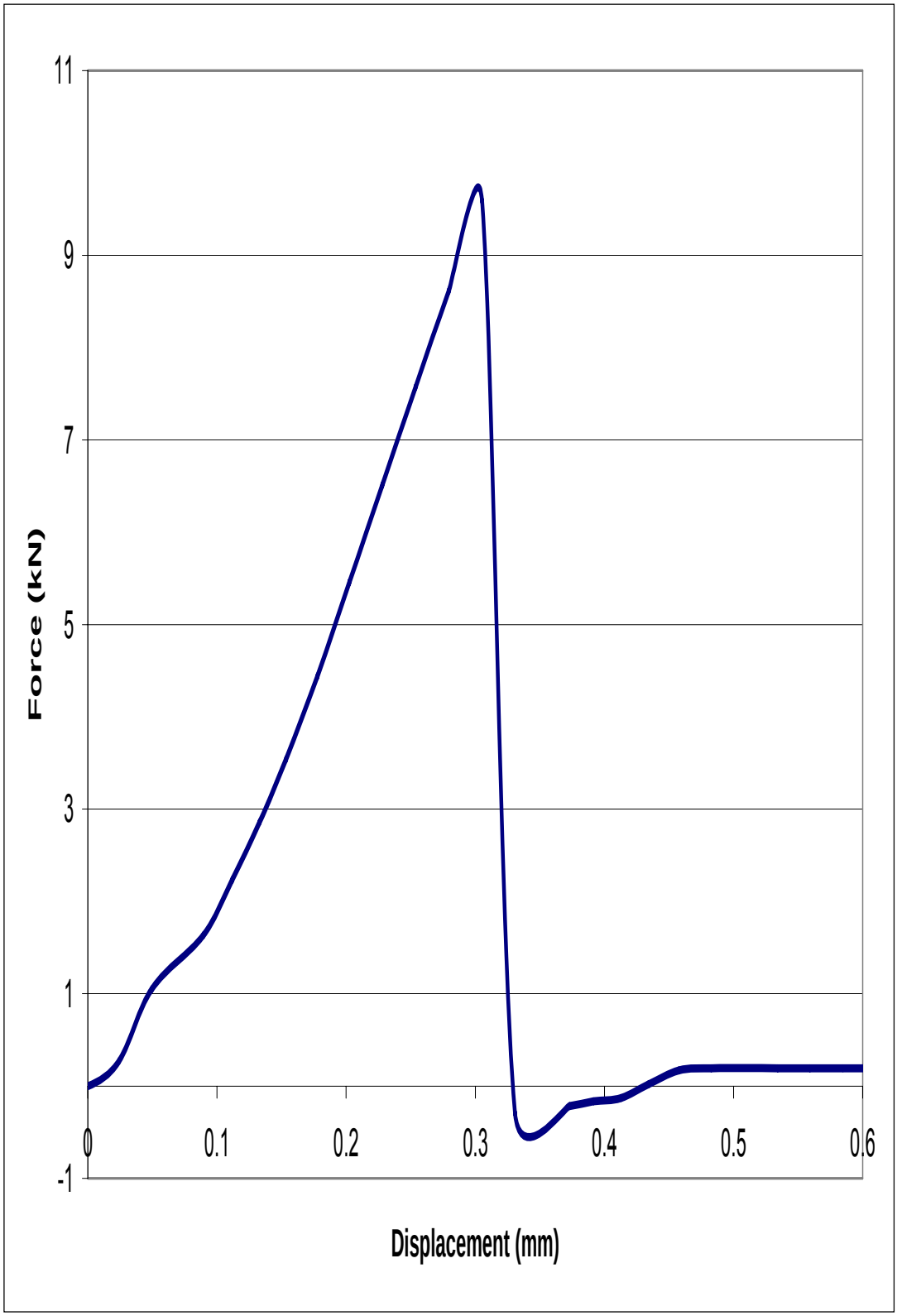

Figure C-18: Pushout coupon (3, 4) -3 force vs. displacement curve

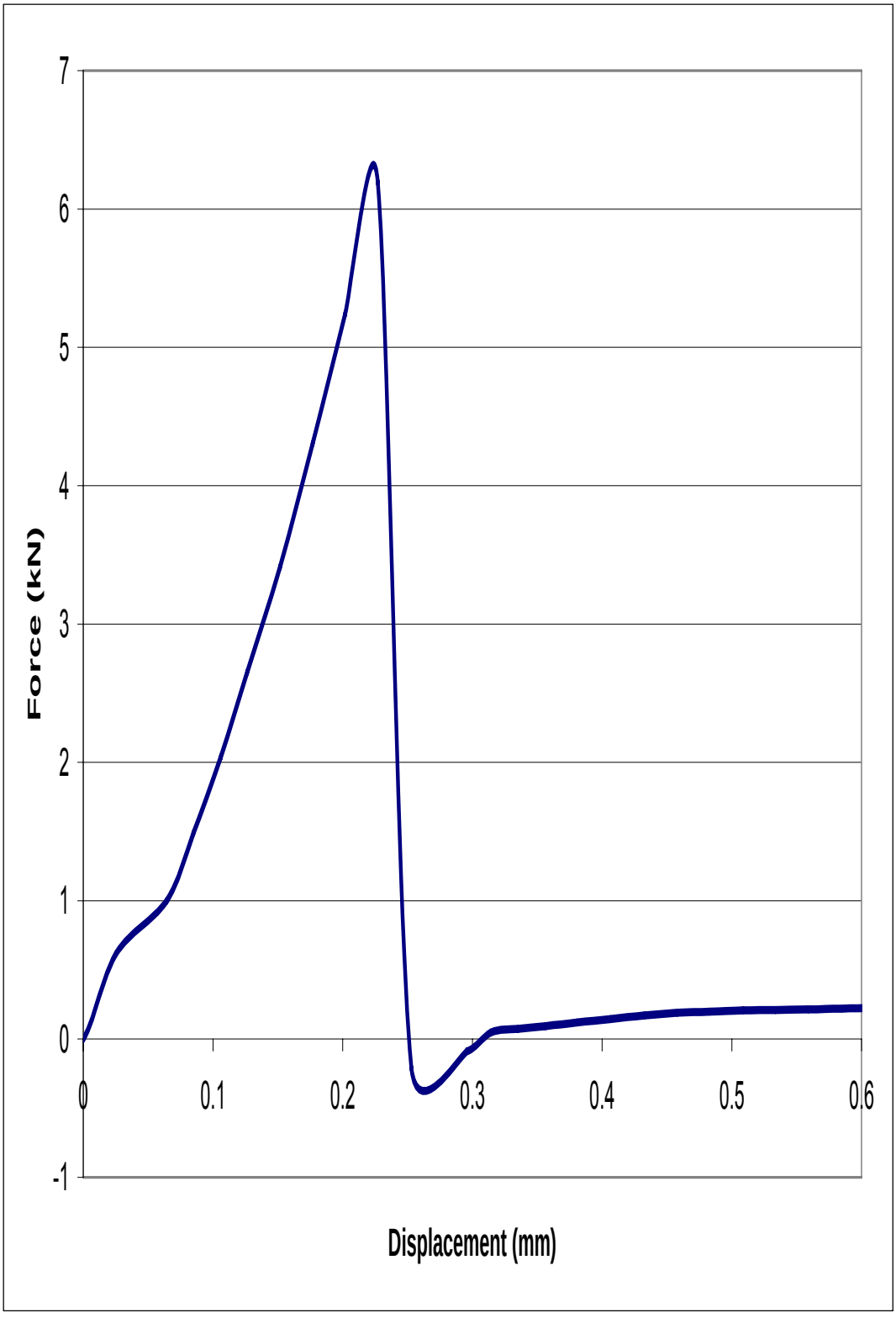

Figure C-19: Pushout coupon (4, 1) -1 force vs. displacement curve

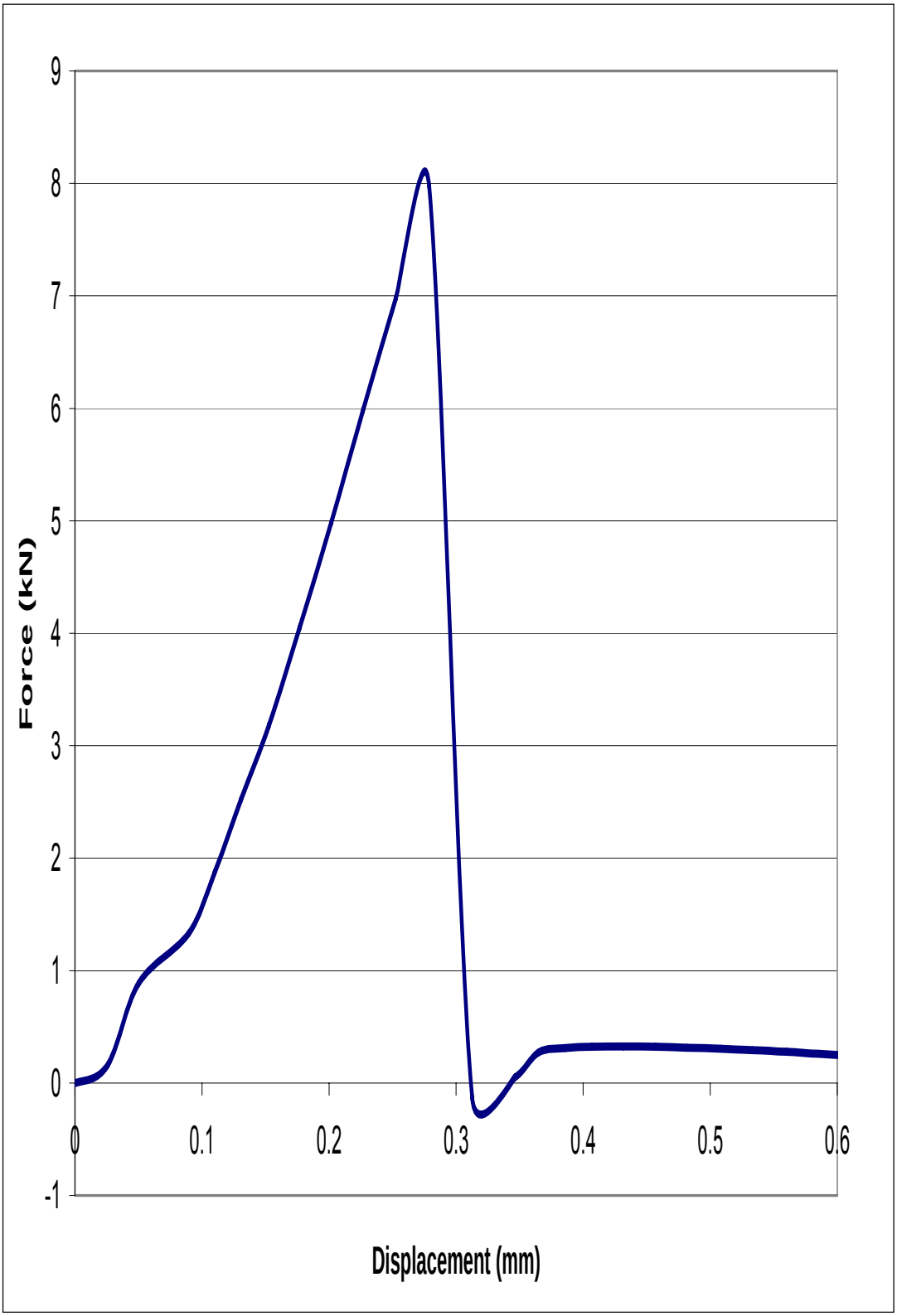

Figure C-20: Pushout coupon (4, 1) -2 force vs. displacement curve

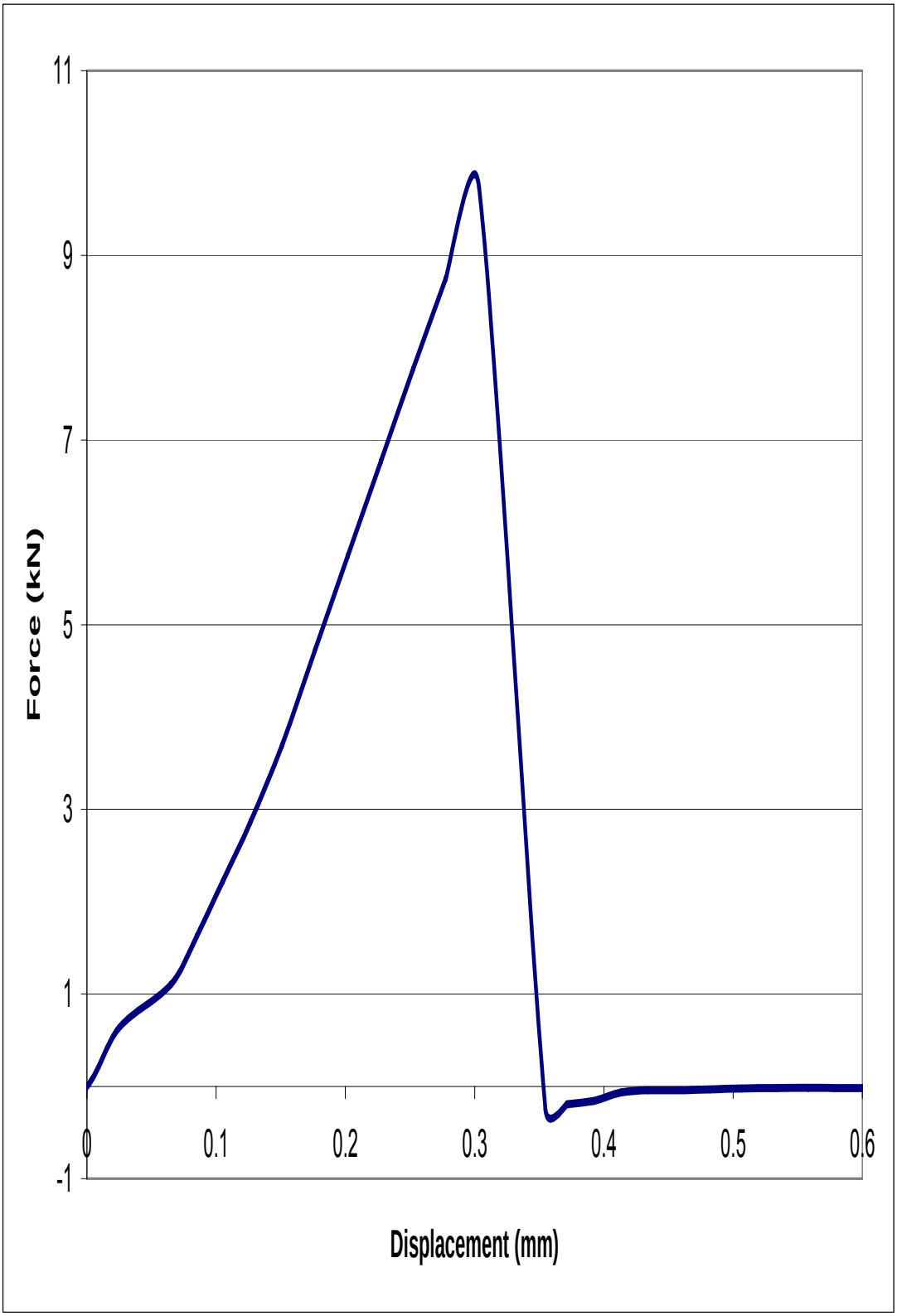

Figure C-21: Pushout coupon (4, 1) -3 force vs. displacement curve

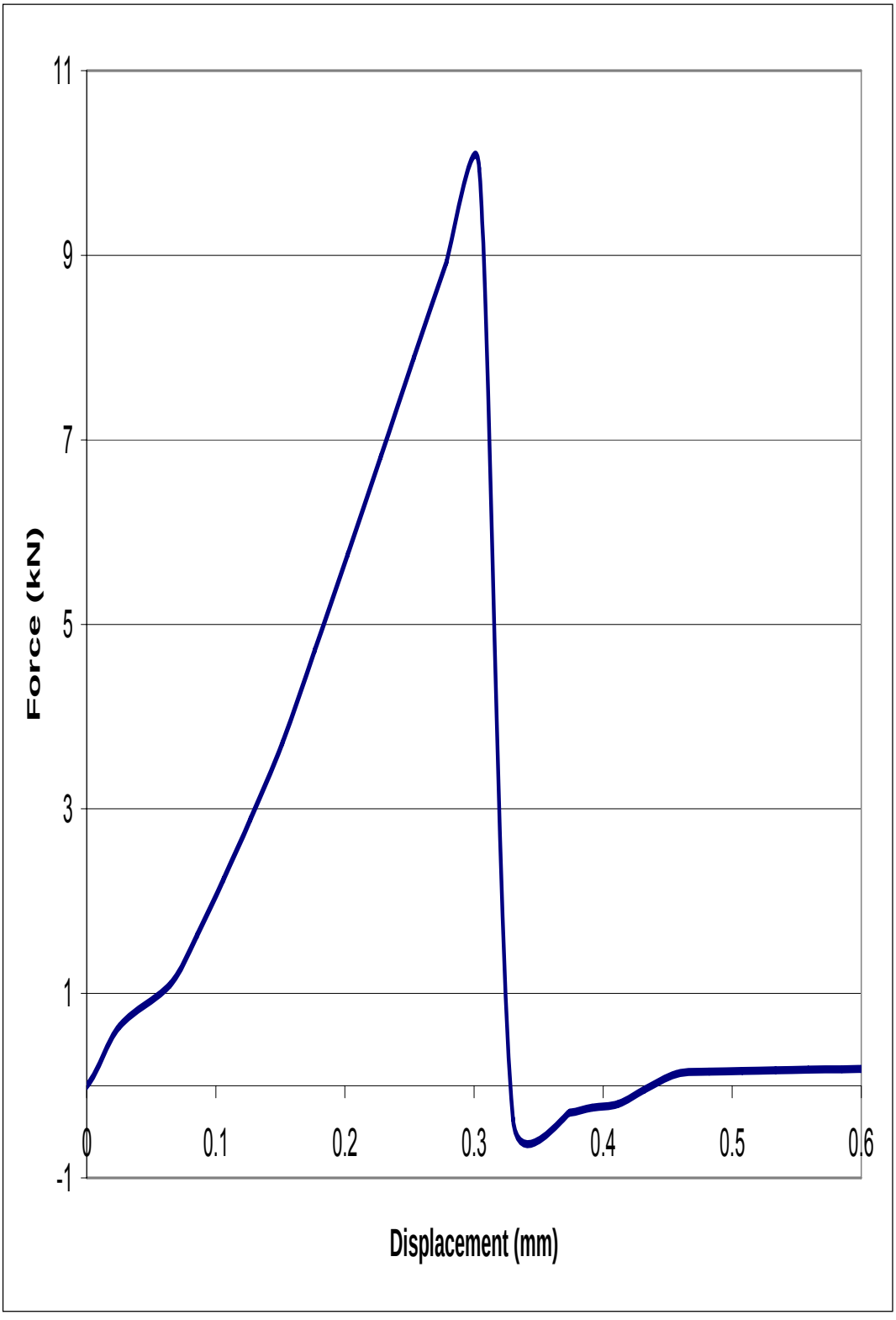

Figure C-22: Pushout coupon (4, 2) -1 force vs. displacement curve

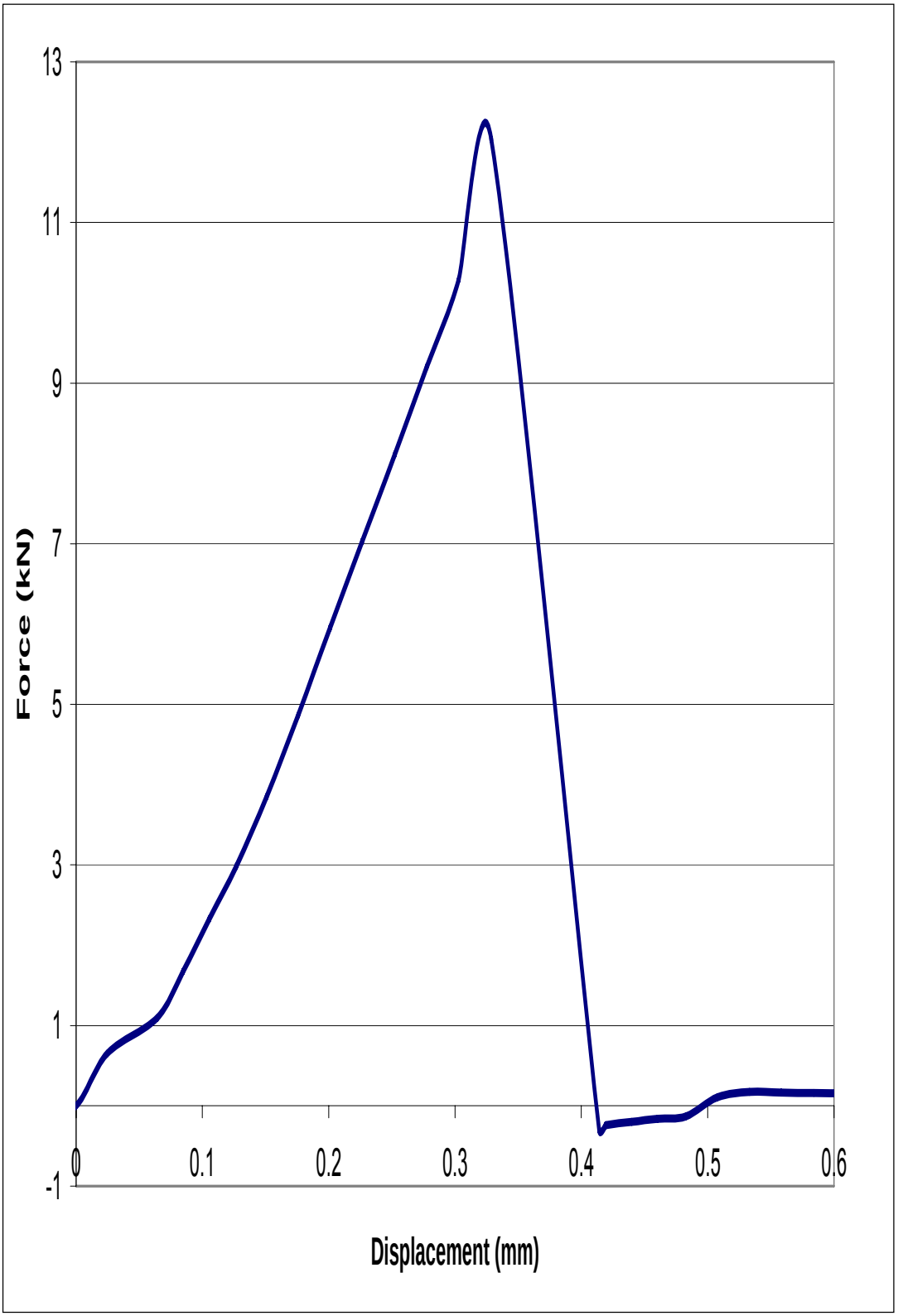

Figure C-23: Pushout coupon (4, 2) -2 force vs. displacement curve

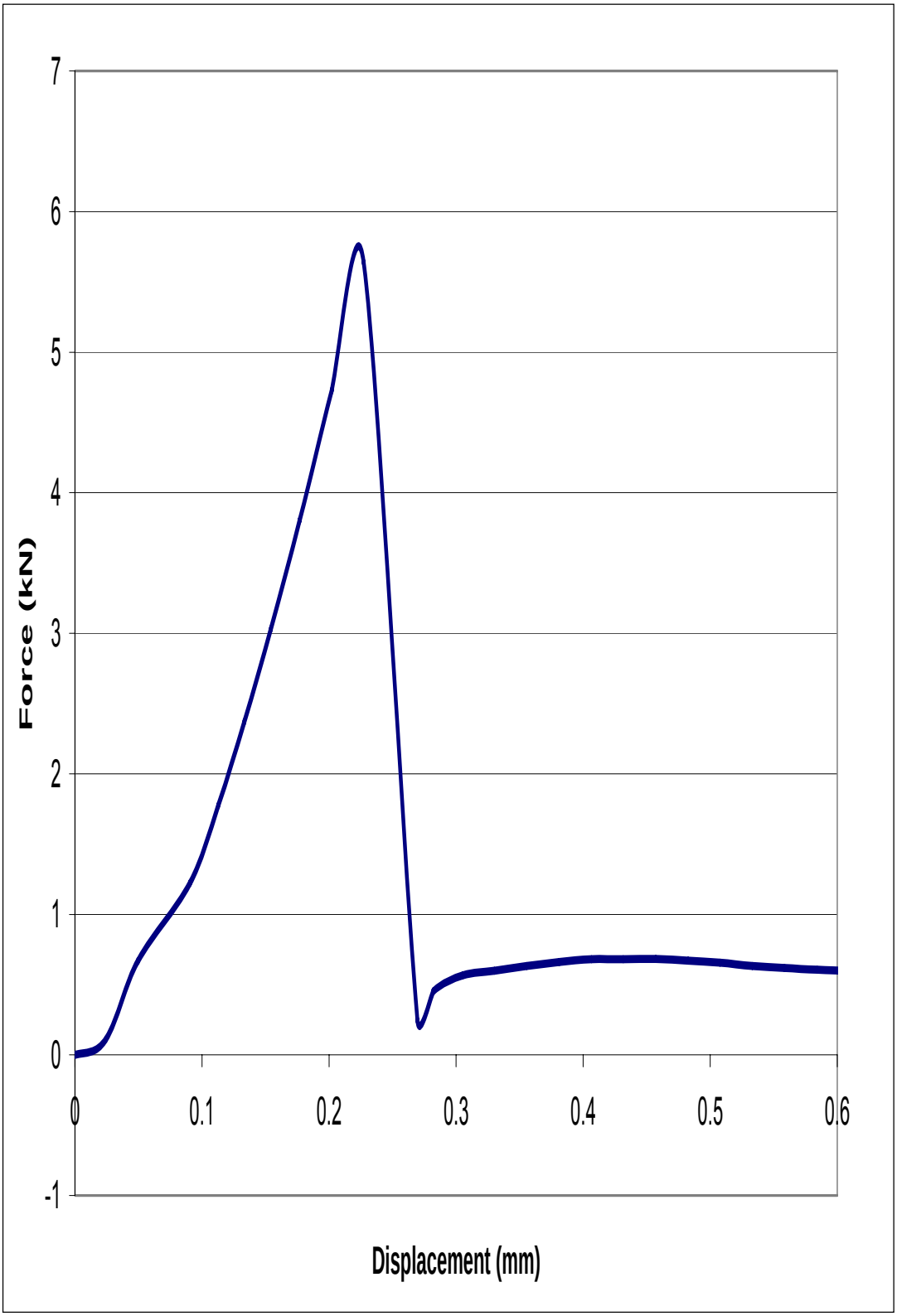

Figure C-24: Pushout coupon (4, 2) -3 force vs. displacement curve

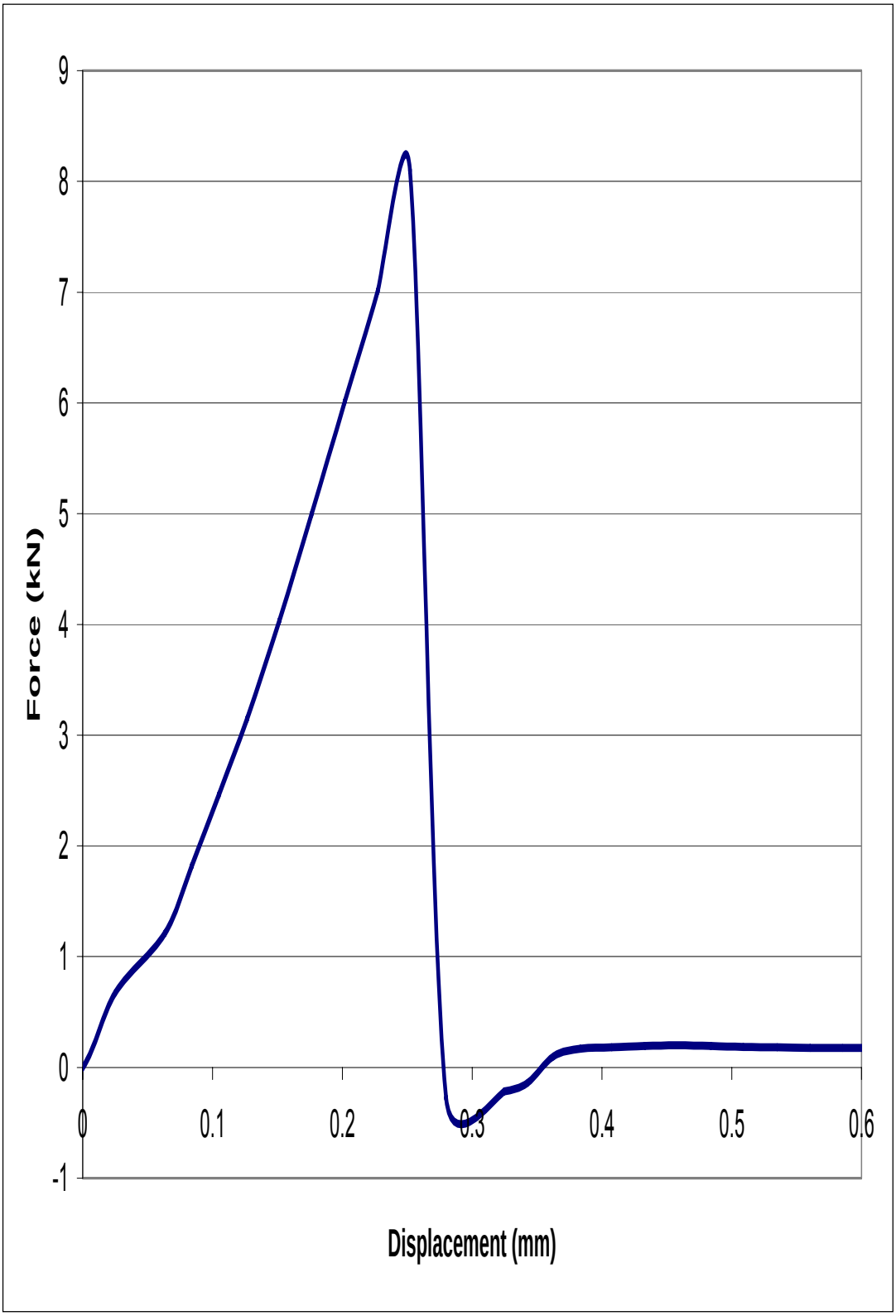

Figure C-25: Pushout coupon (4, 4) -1 force vs. displacement curve

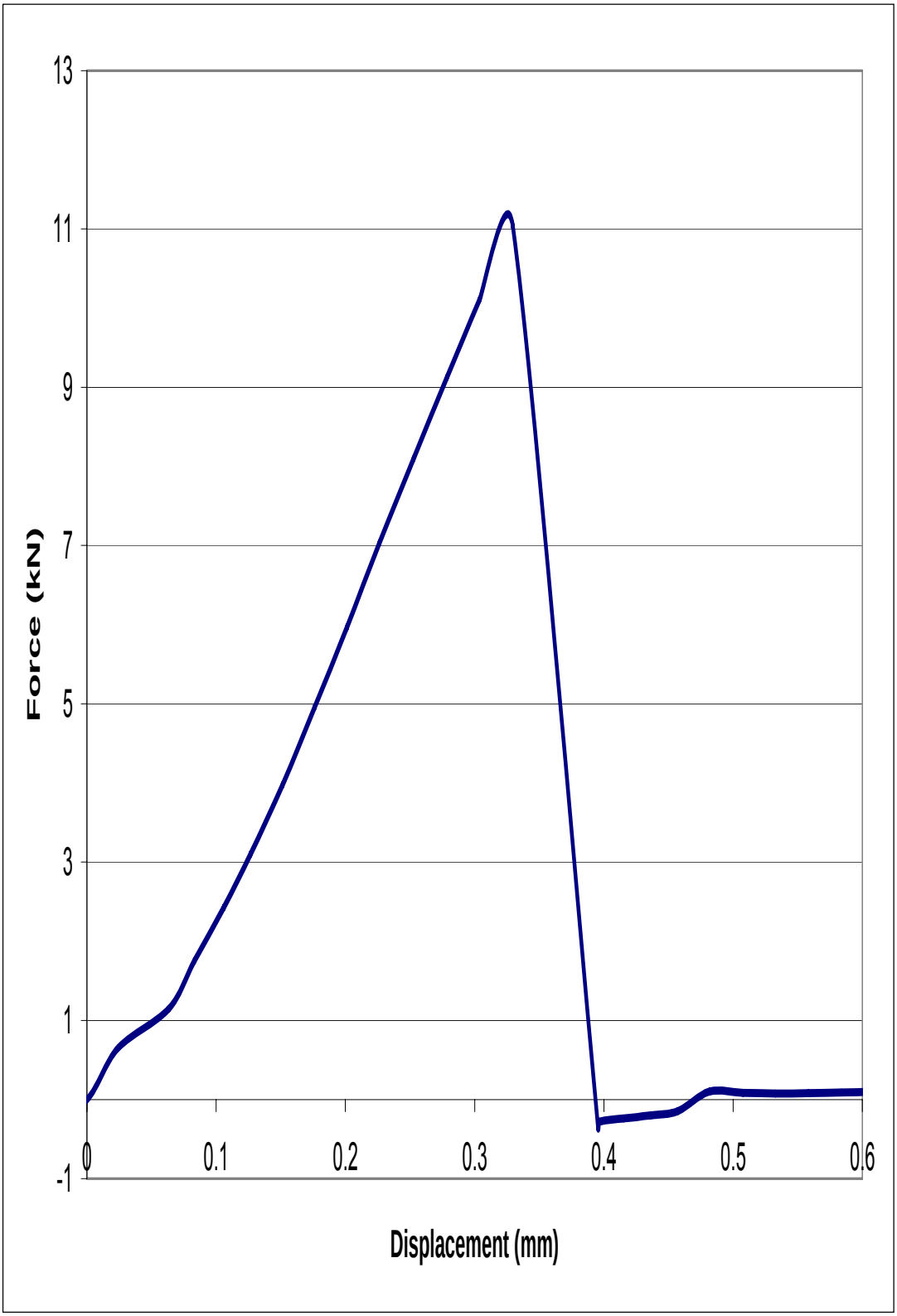

Figure C-26: Pushout coupon (4, 4) -2 force vs. displacement curve

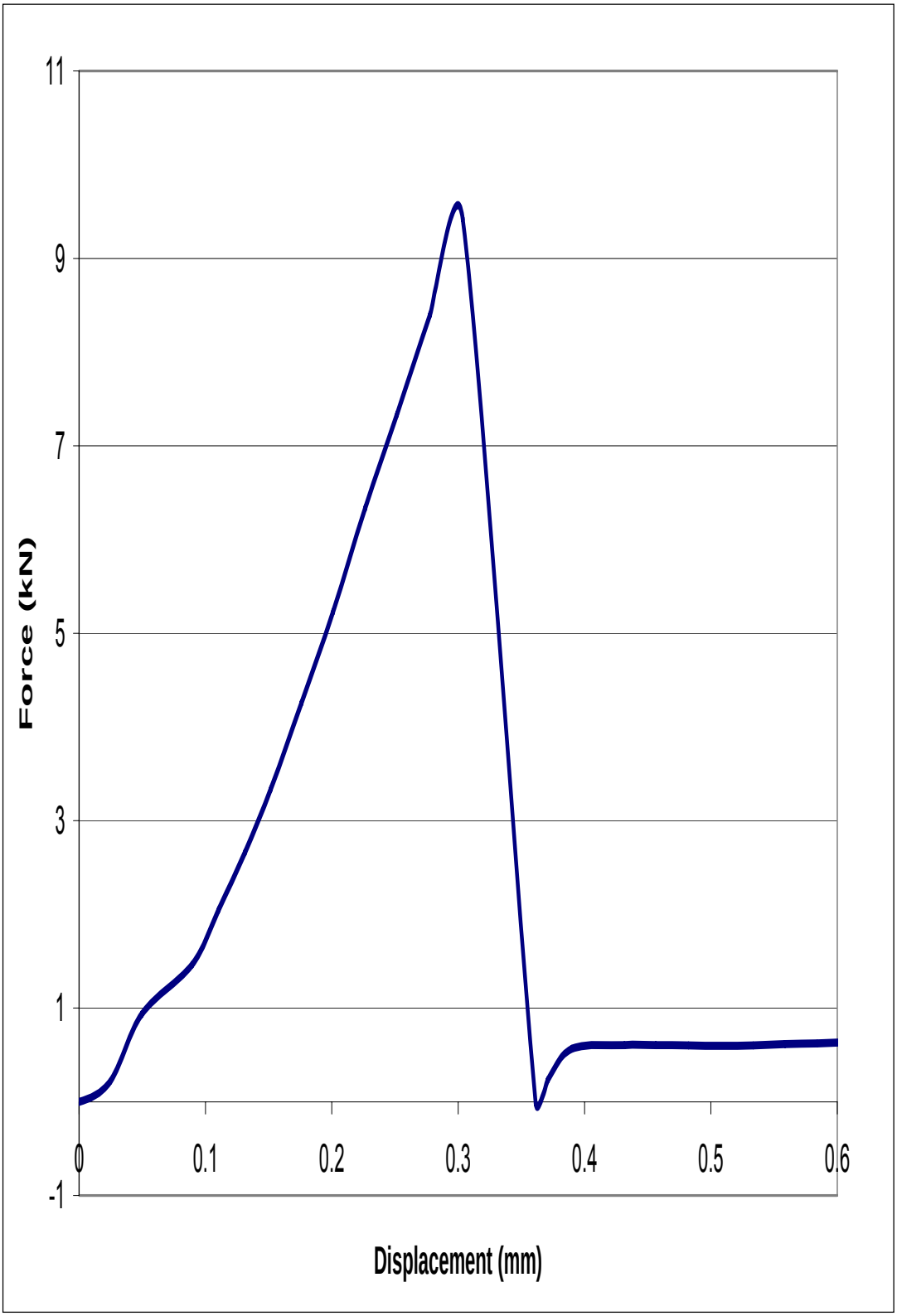

Figure C-27: Pushout coupon (4, 4) -3 force vs. displacement curve

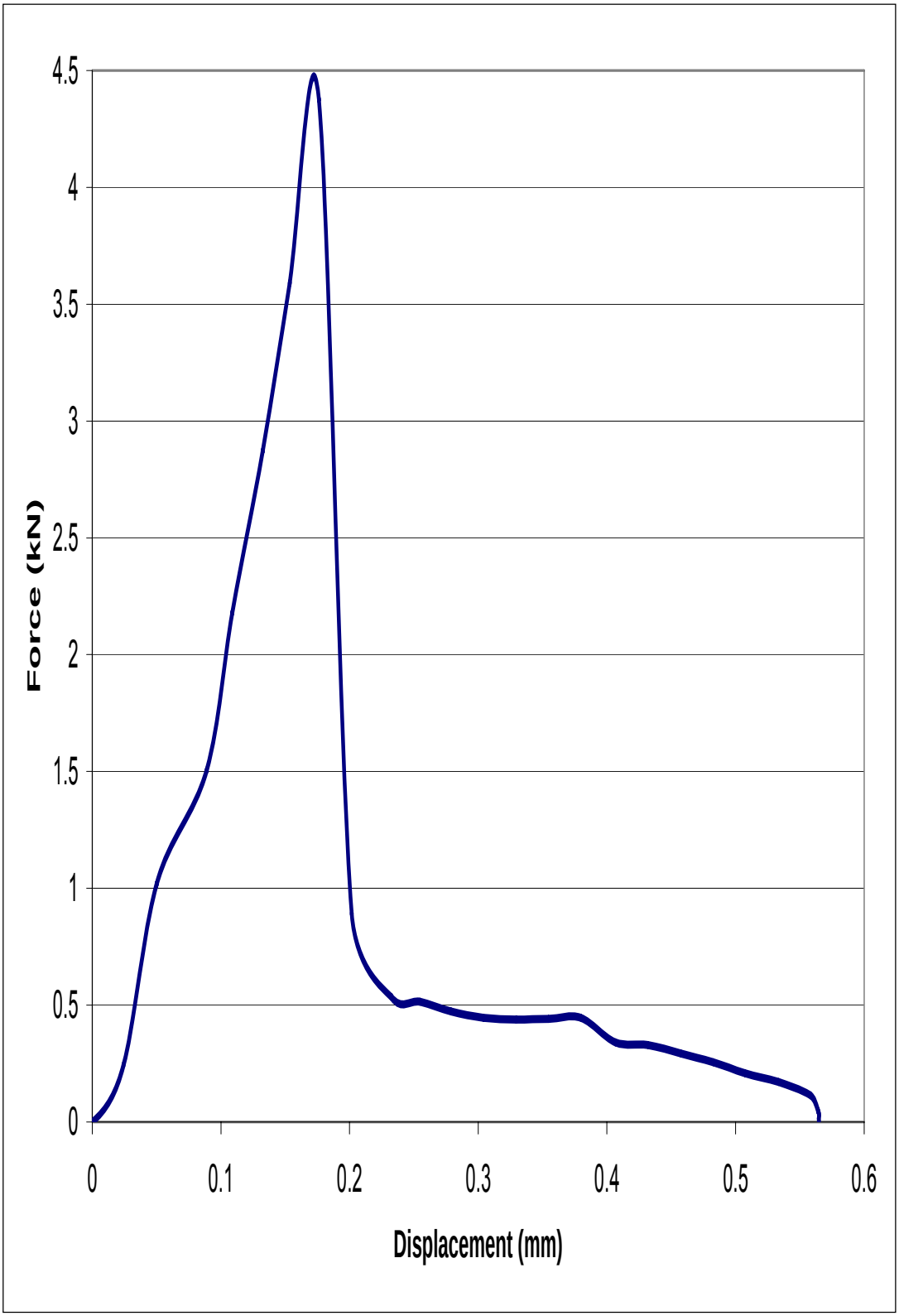

Figure C-28: Pushout coupon 60 min HNO_3 / 2M NaOH -9 force vs. displacement curve

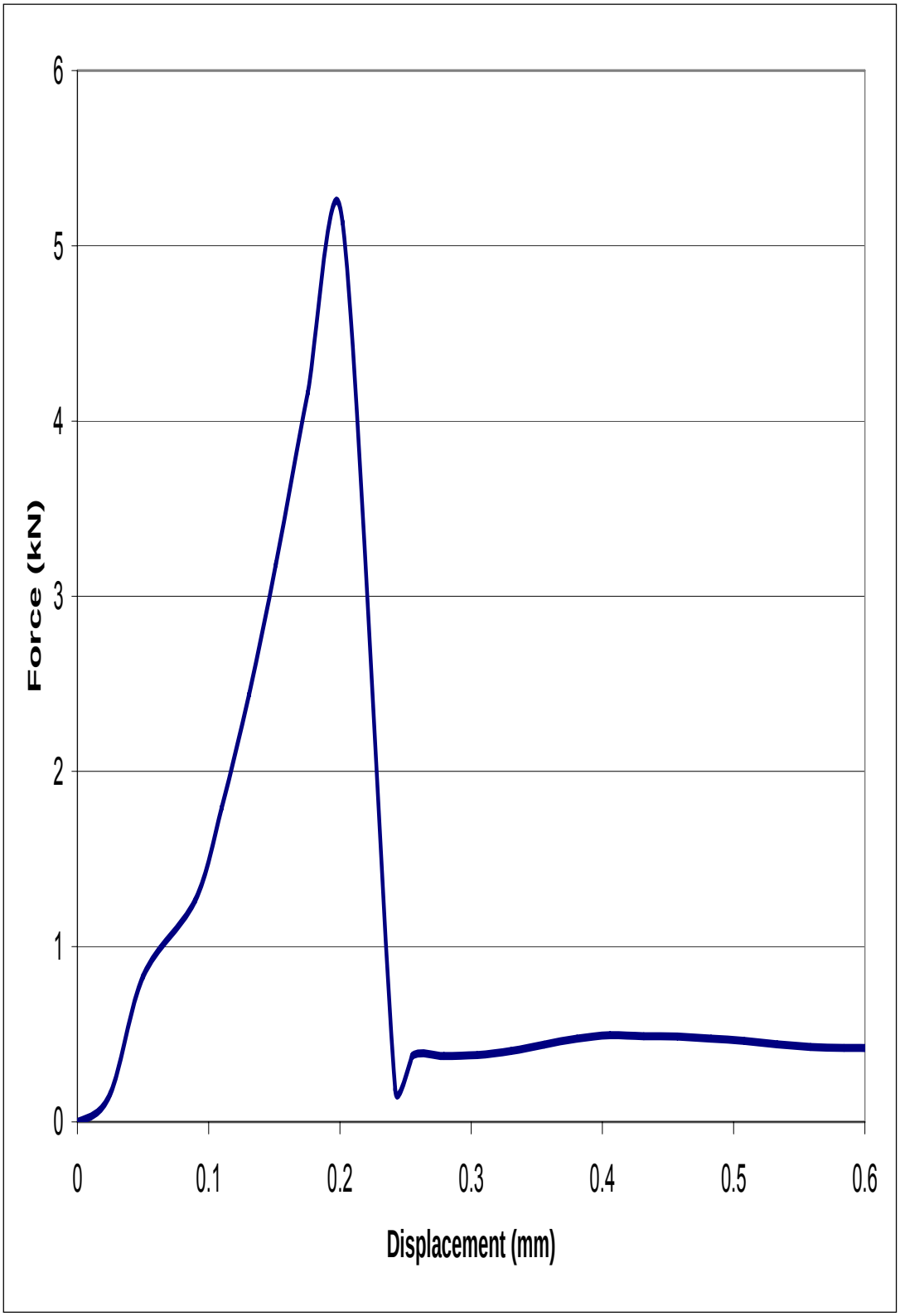

Figure C-29: Pushout coupon 60 min HNO_3 / 2M NaOH -10 force vs. displacement curve

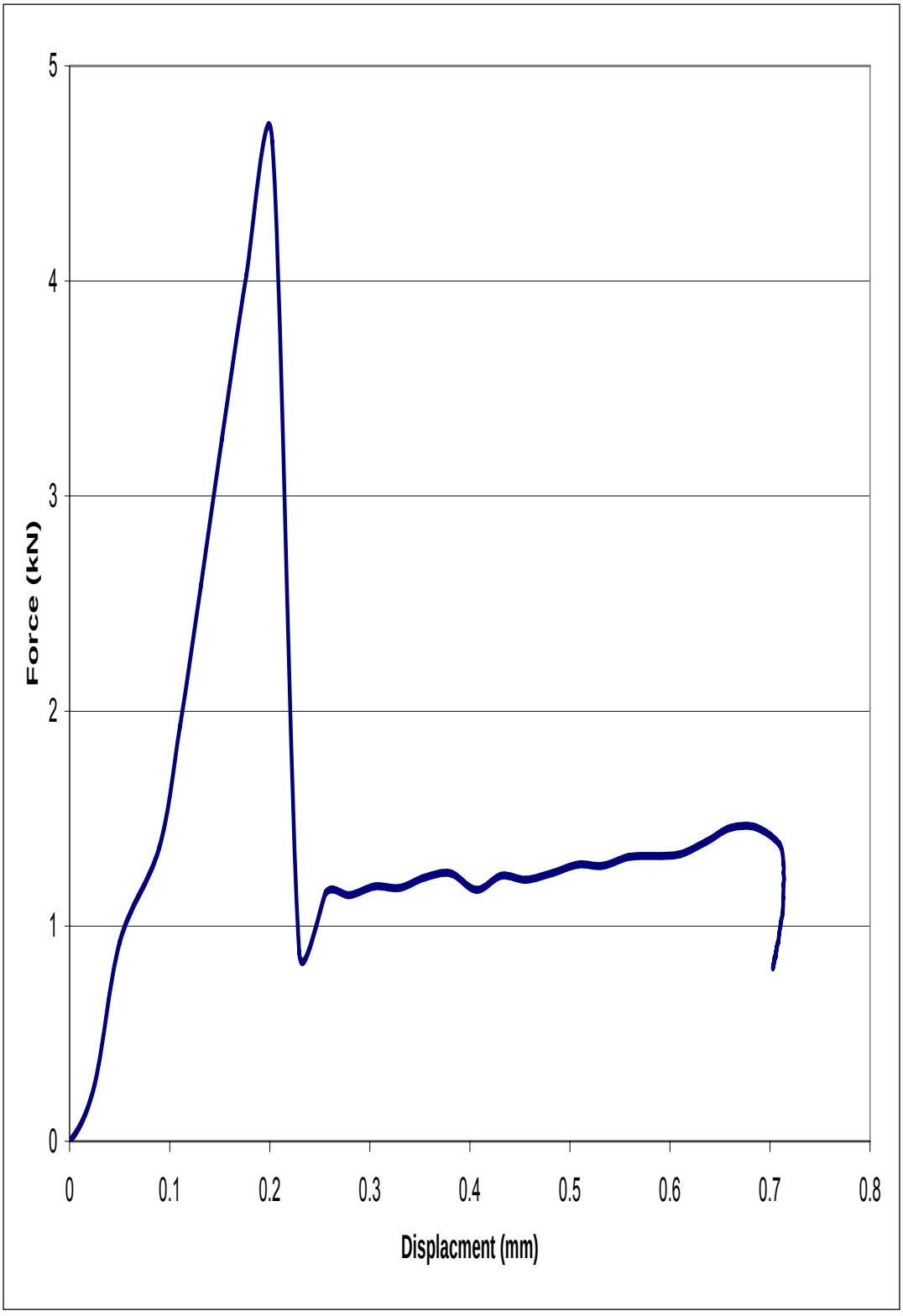

Figure C-30: Pushout coupon 60 min HNO_3 / 5M NaOH -1 force vs. displacement curve

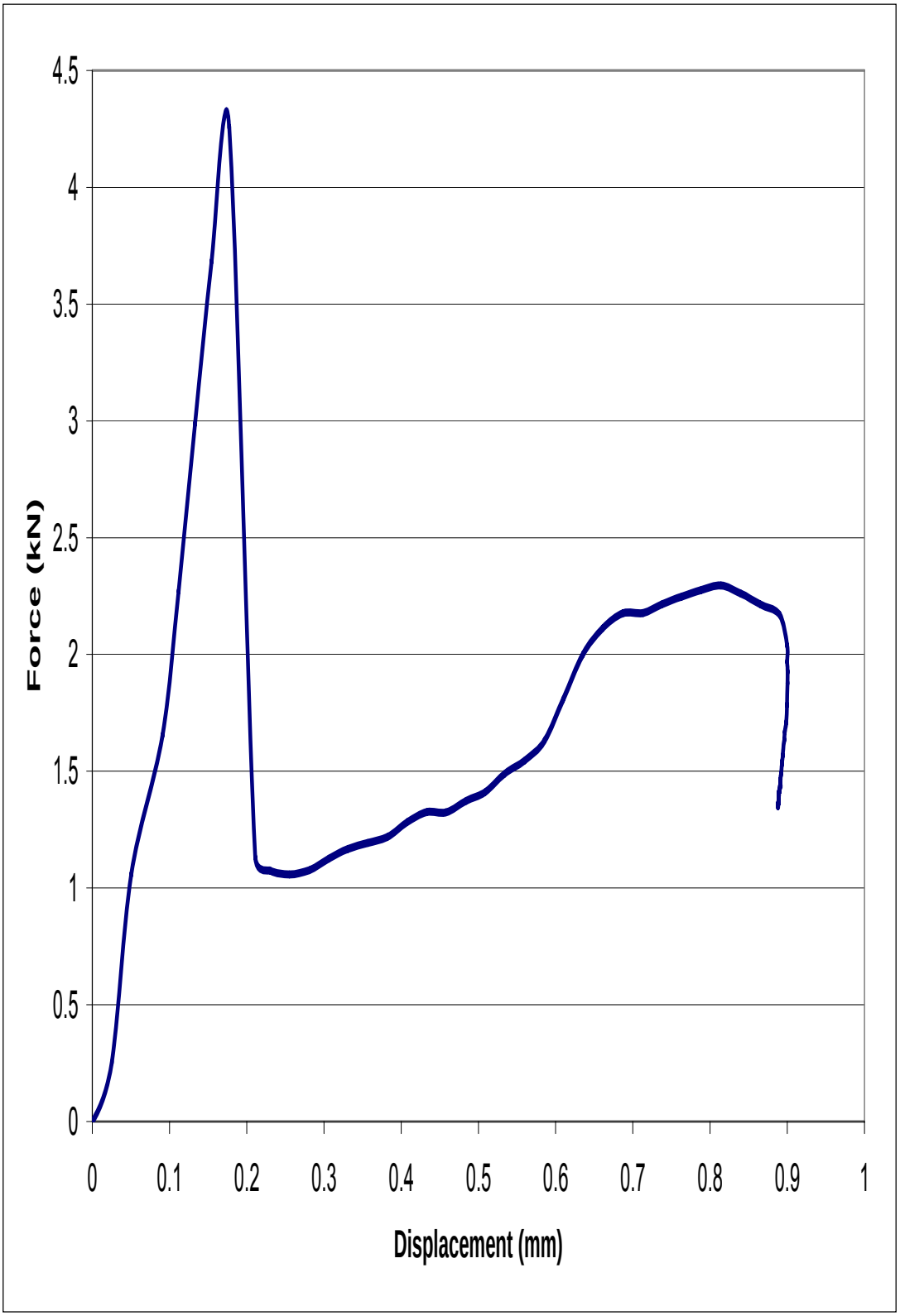

Figure C-31: Pushout coupon 60 min HNO_3 / 5M NaOH -2 force vs. displacement curve

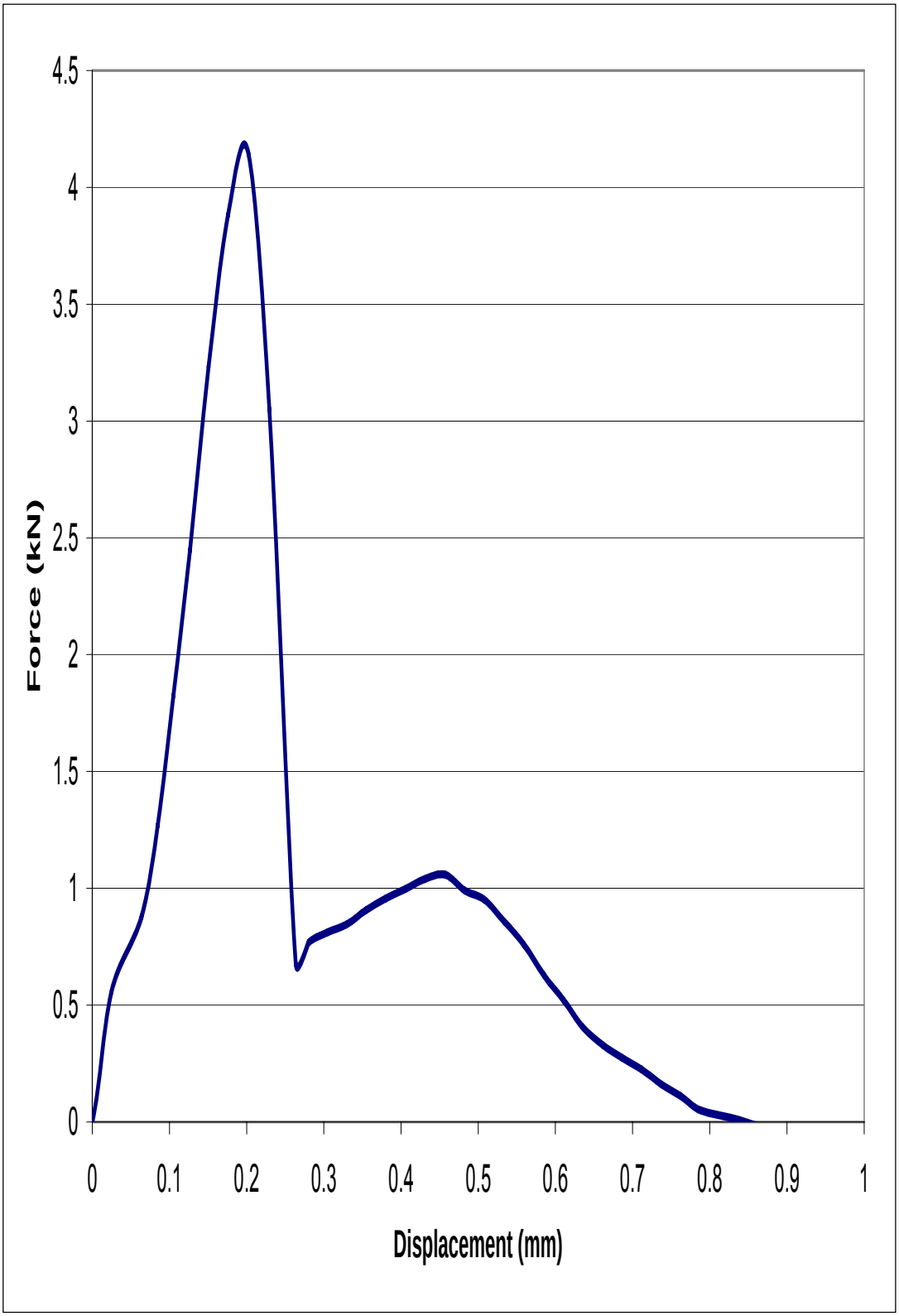

Figure C-32: Pushout coupon 60 min HNO_3 / 5M NaOH -3 force vs. displacement curve

APPENDIX D

Individual Pultruded Rod Three-point Bending Force vs. Displacement Curves

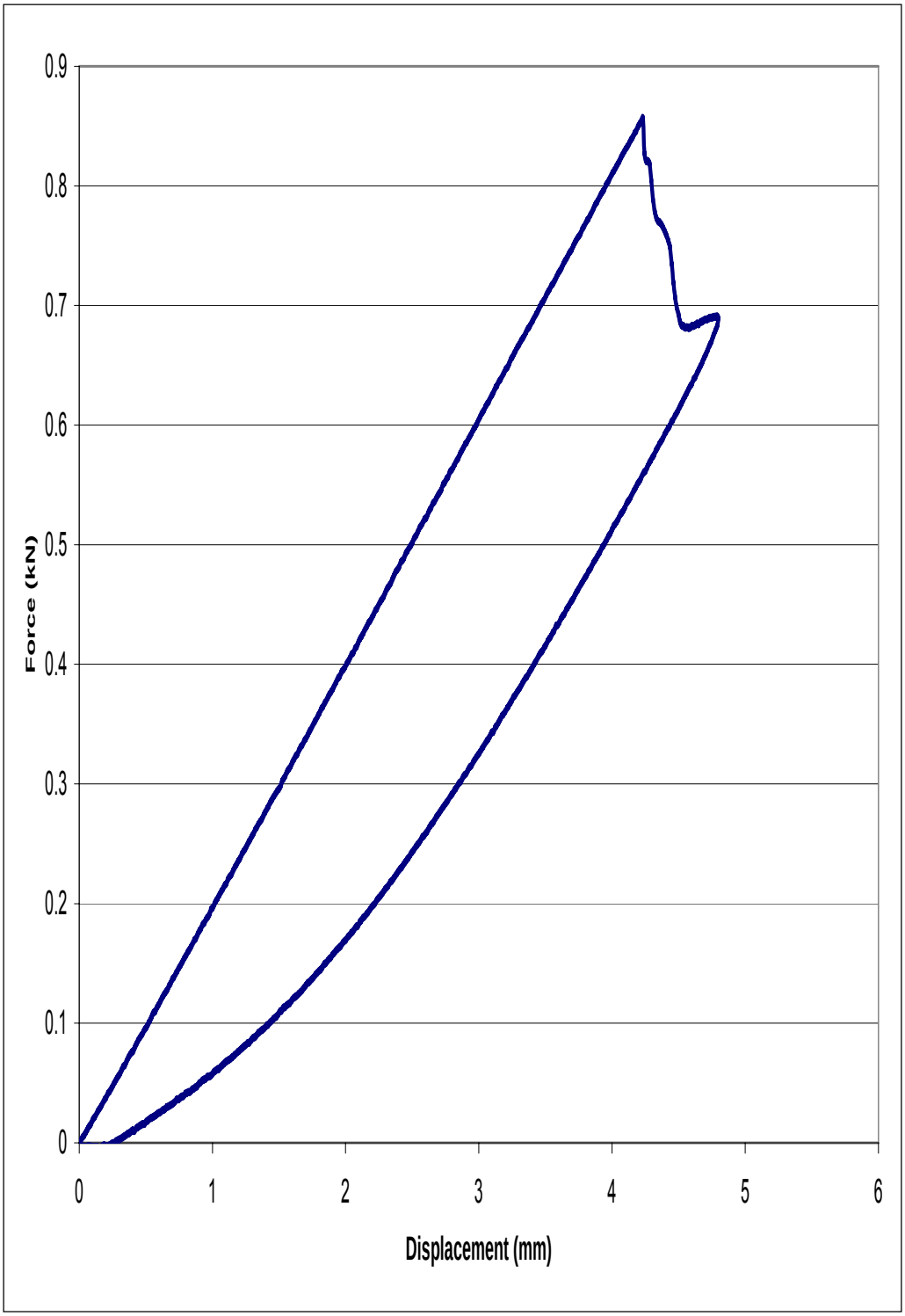

Figure D-1: Three-point bending force vs. displacement curve for coupon 6

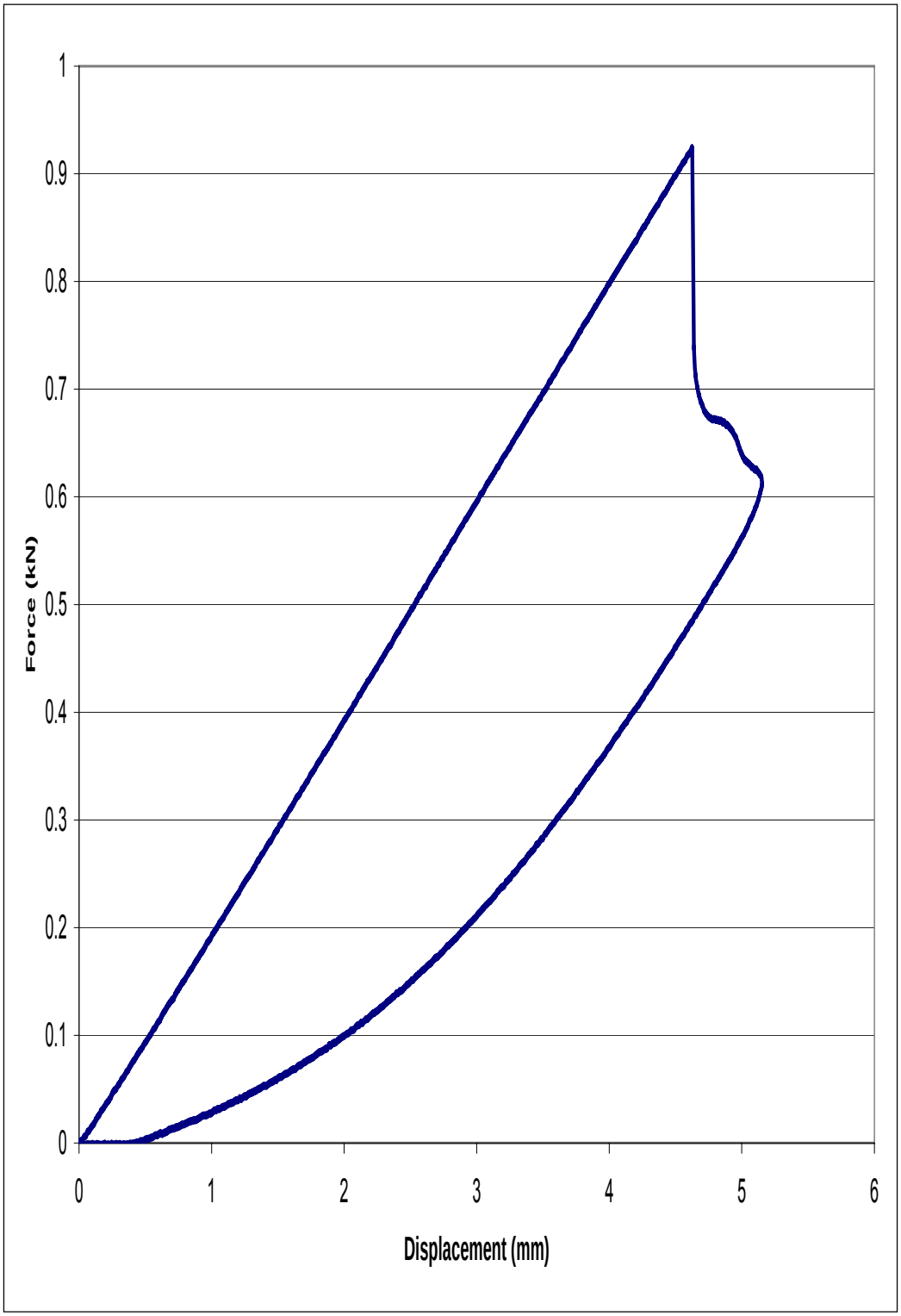

Figure D-2: Three-point bending force vs. displacement curve for coupon 7

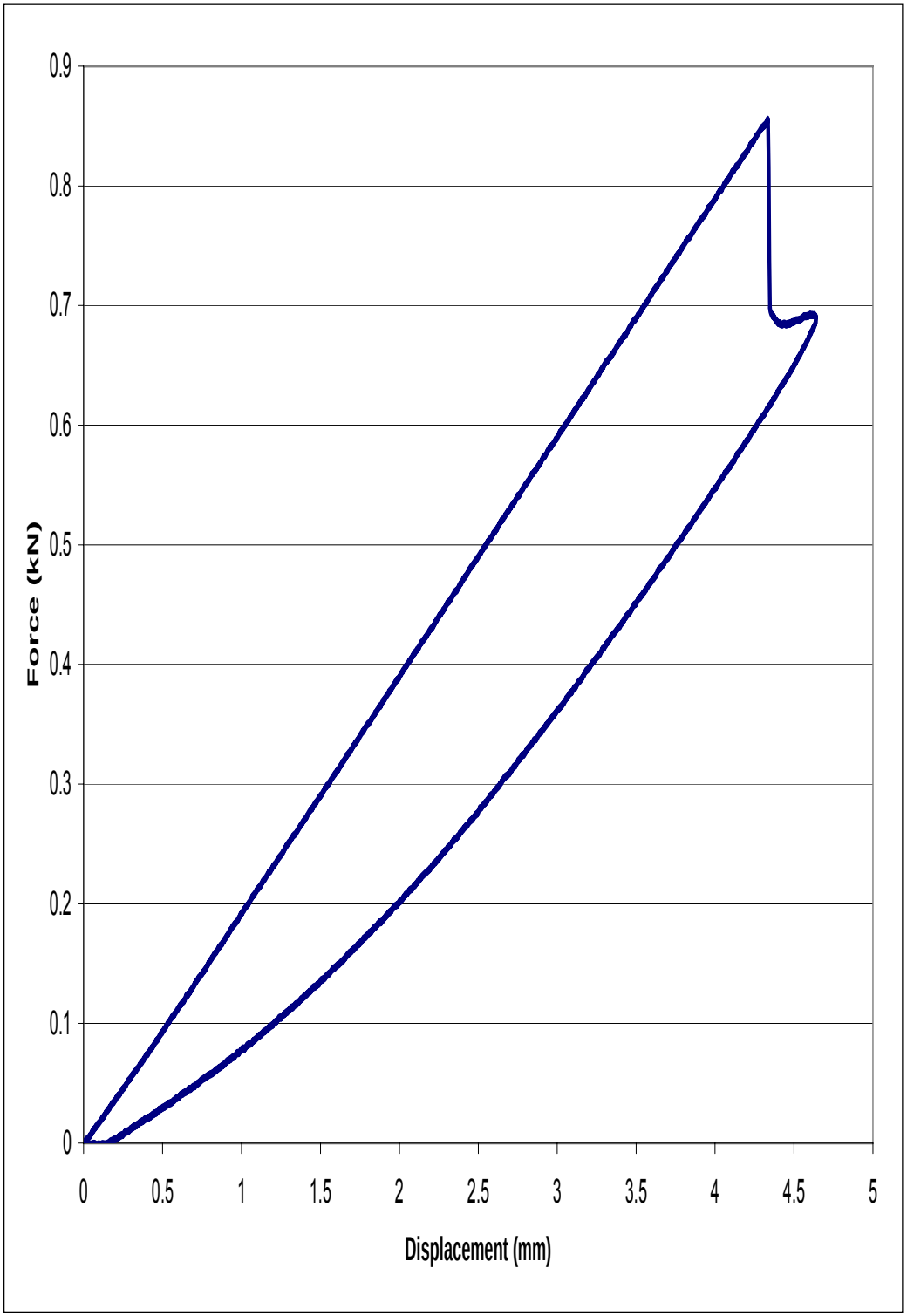

Figure D-3: Three-point bending force vs. displacement curve for coupon 8

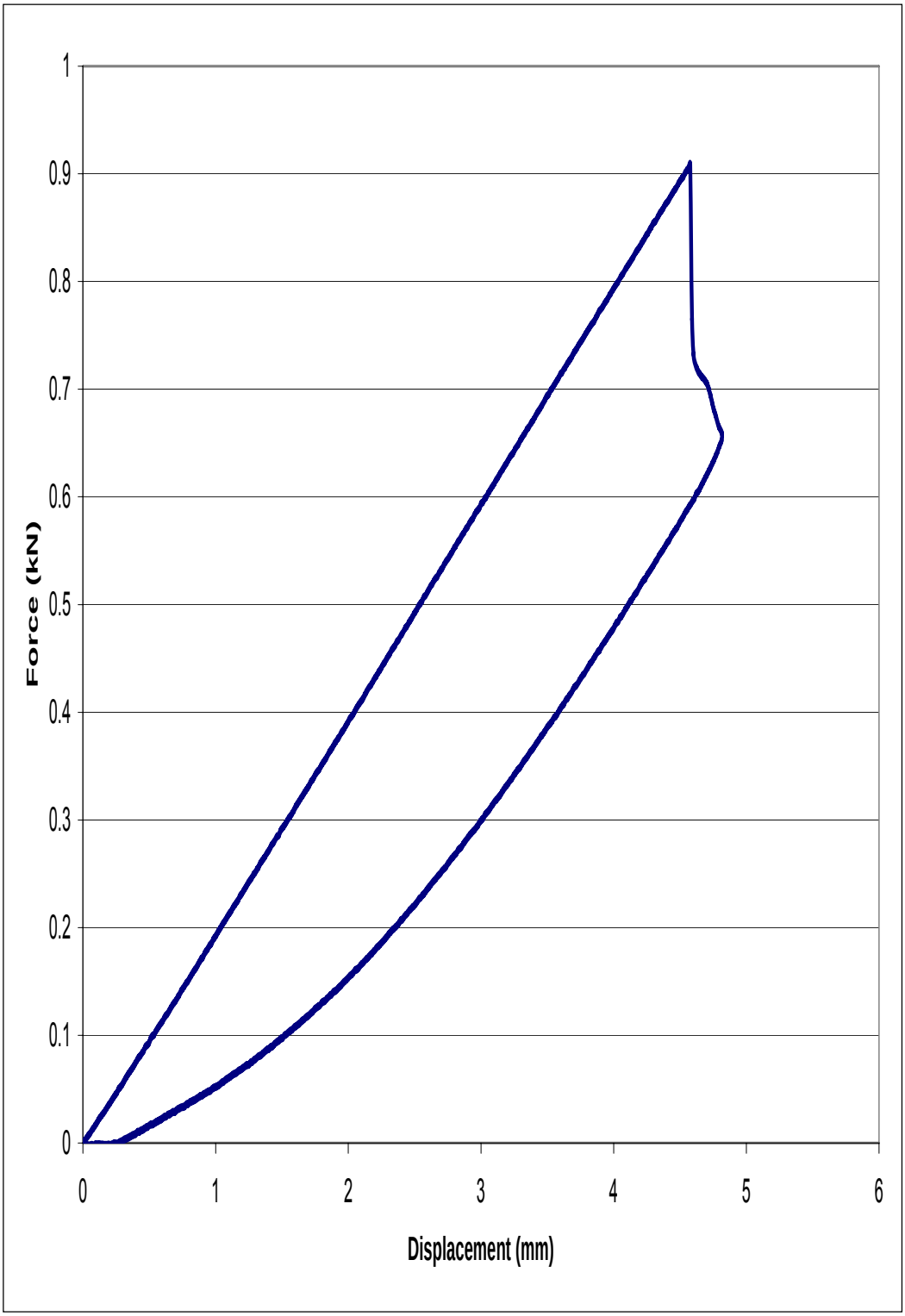

Figure D-4: Three-point bending force vs. displacement curve for coupon 9

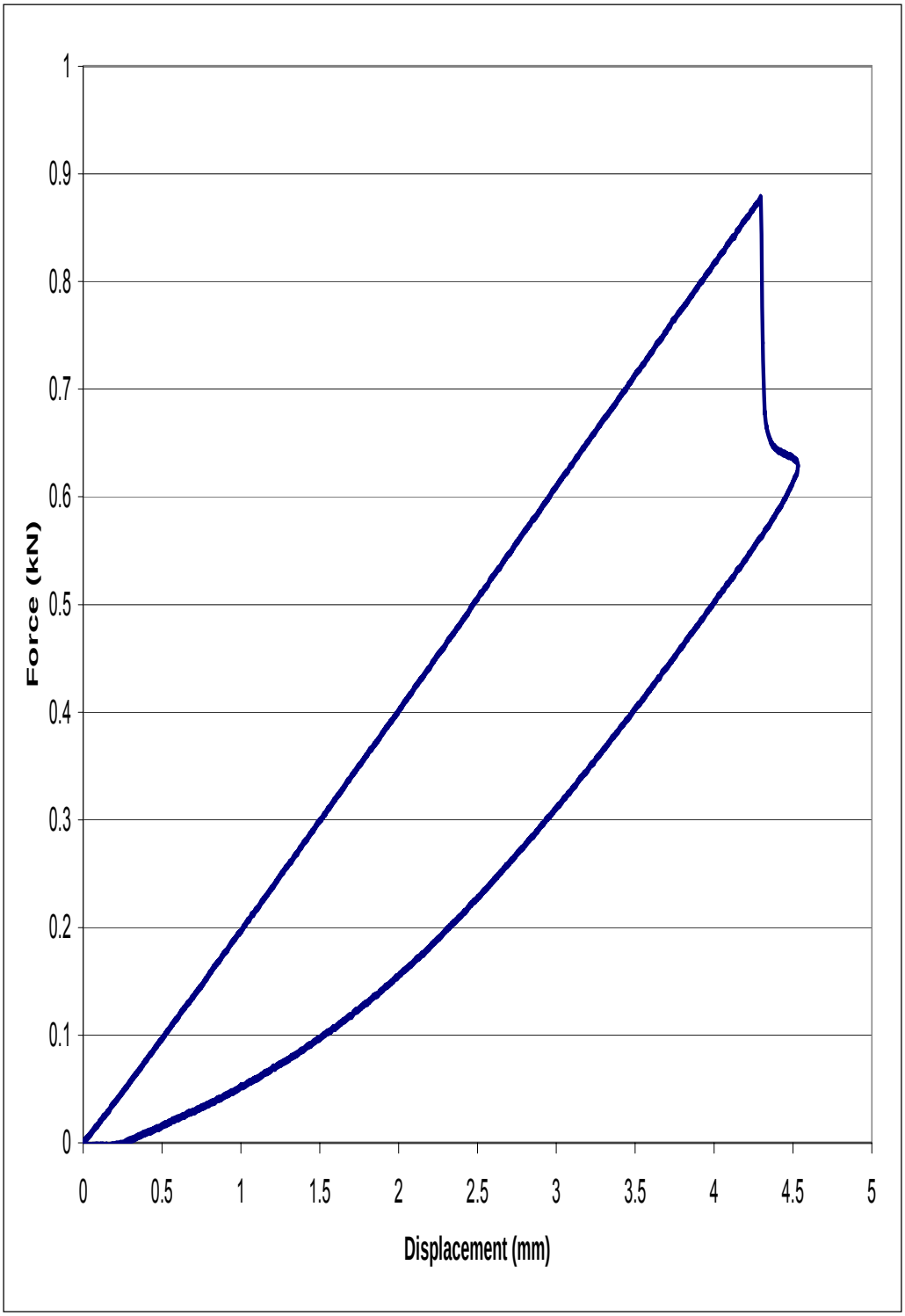

Figure D-5: Three-point bending force vs. displacement curve for coupon 10

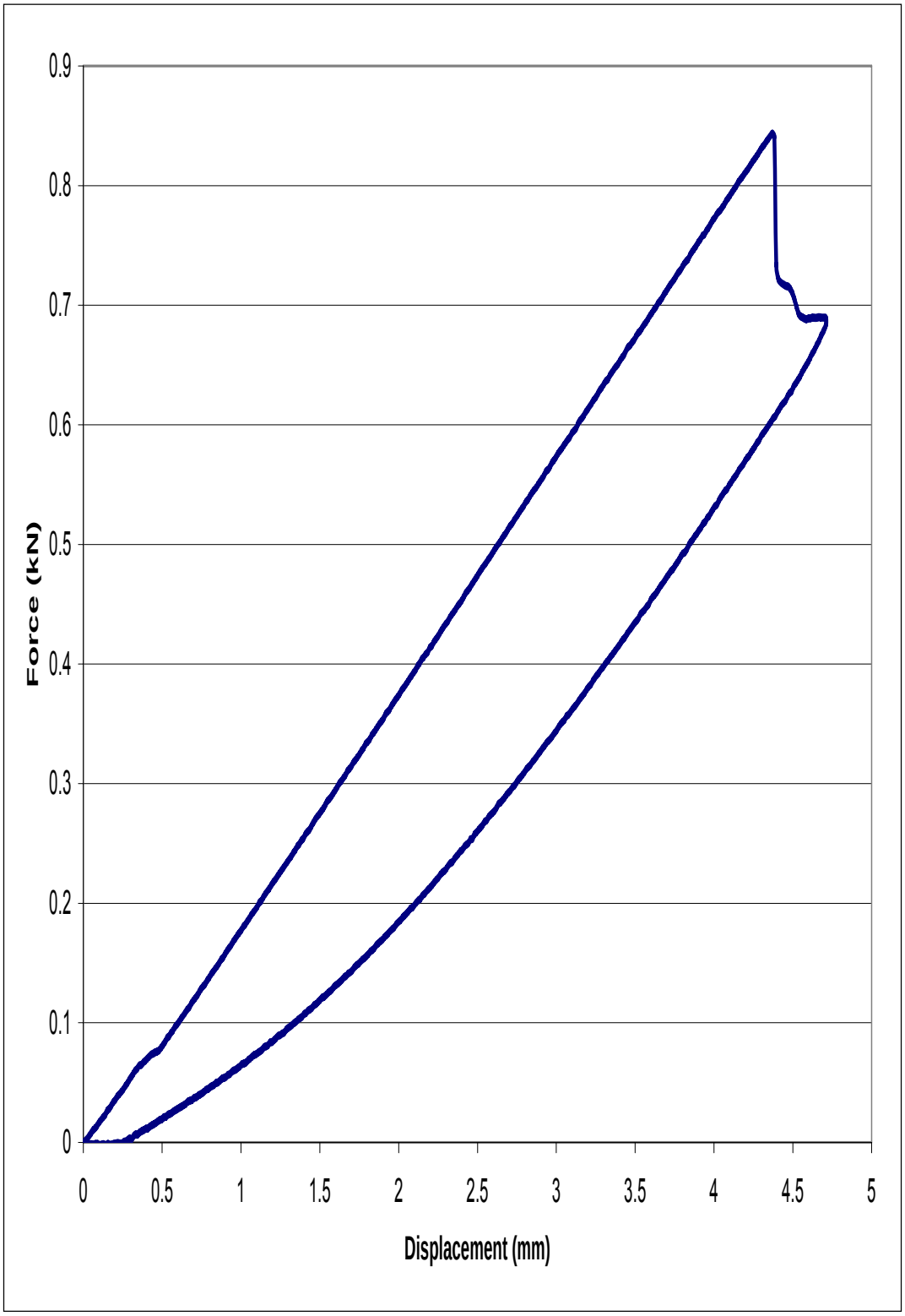

Figure D-6: Three-point bending force vs. displacement curve for coupon test 3

APPENDIX E

Individual Rod and Flat Coupon Short Beam Shear Force vs. Displacement Curves

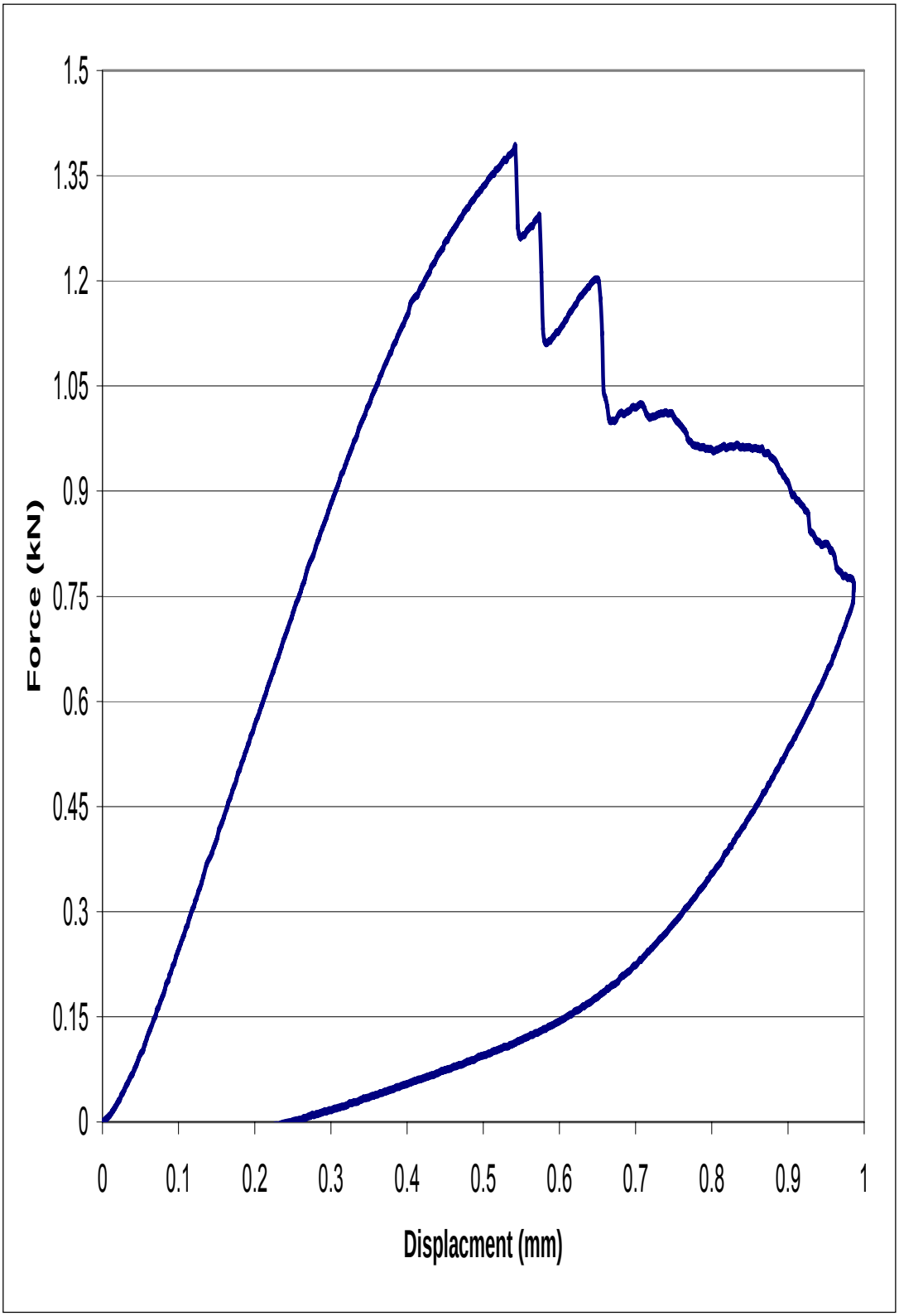

Figure E-1: SBS pultruded flat coupon Panex 19-1 force vs. displacement curve

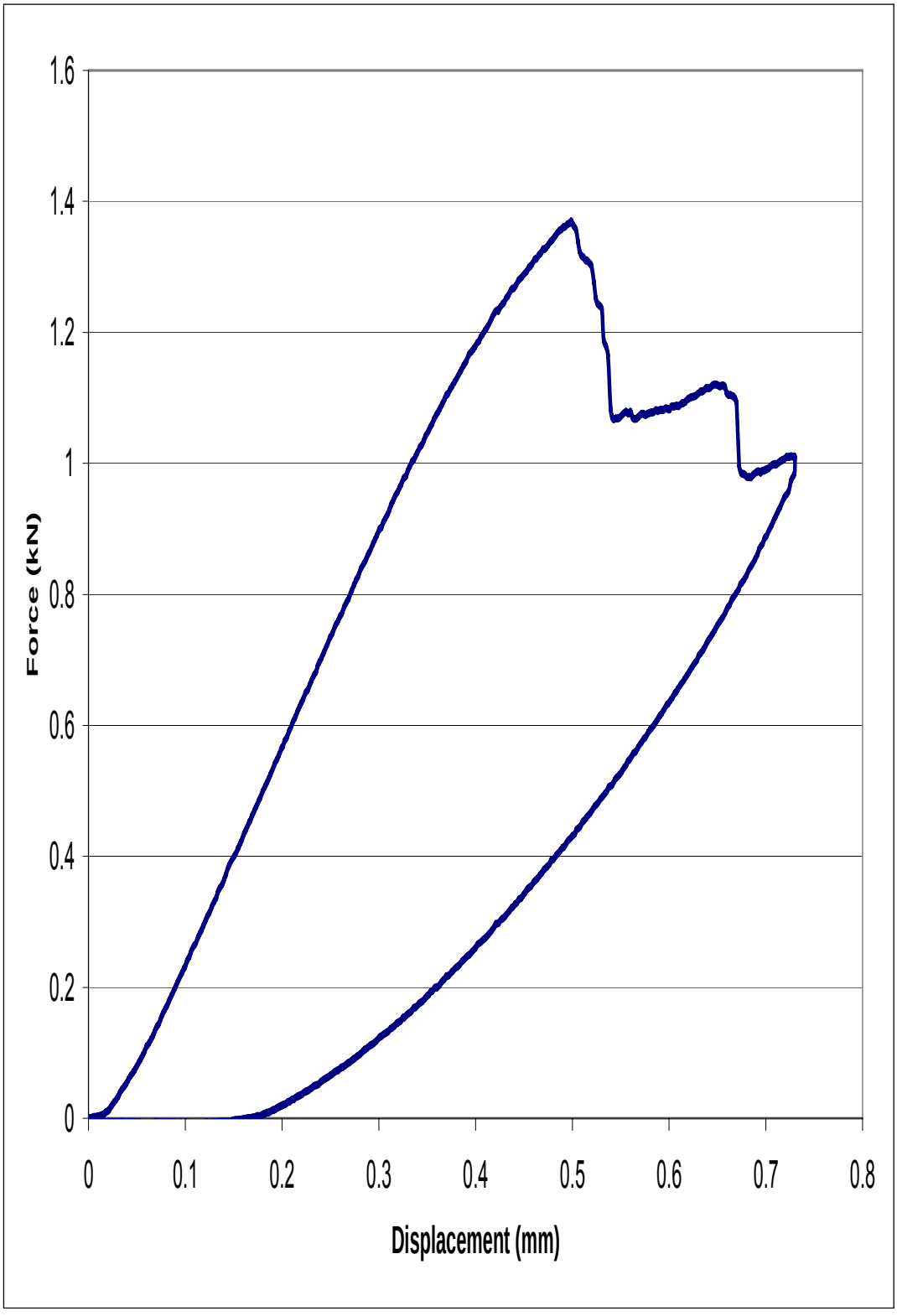

Figure E-2: SBS pultruded flat coupon Panex 19-2 force vs. displacement curve

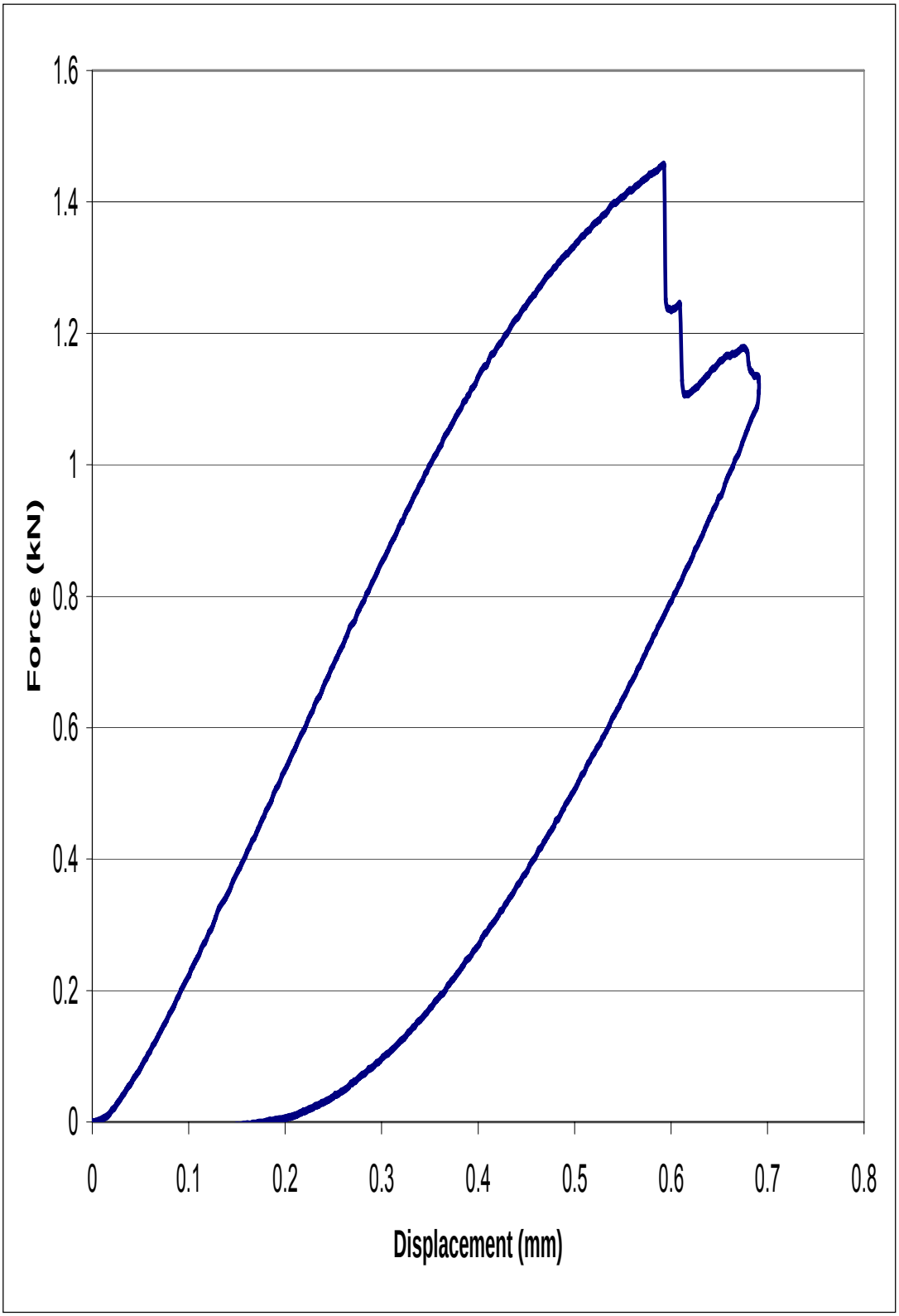

Figure E-3: SBS pultruded flat coupon Panex 19-3 force vs. displacement curve

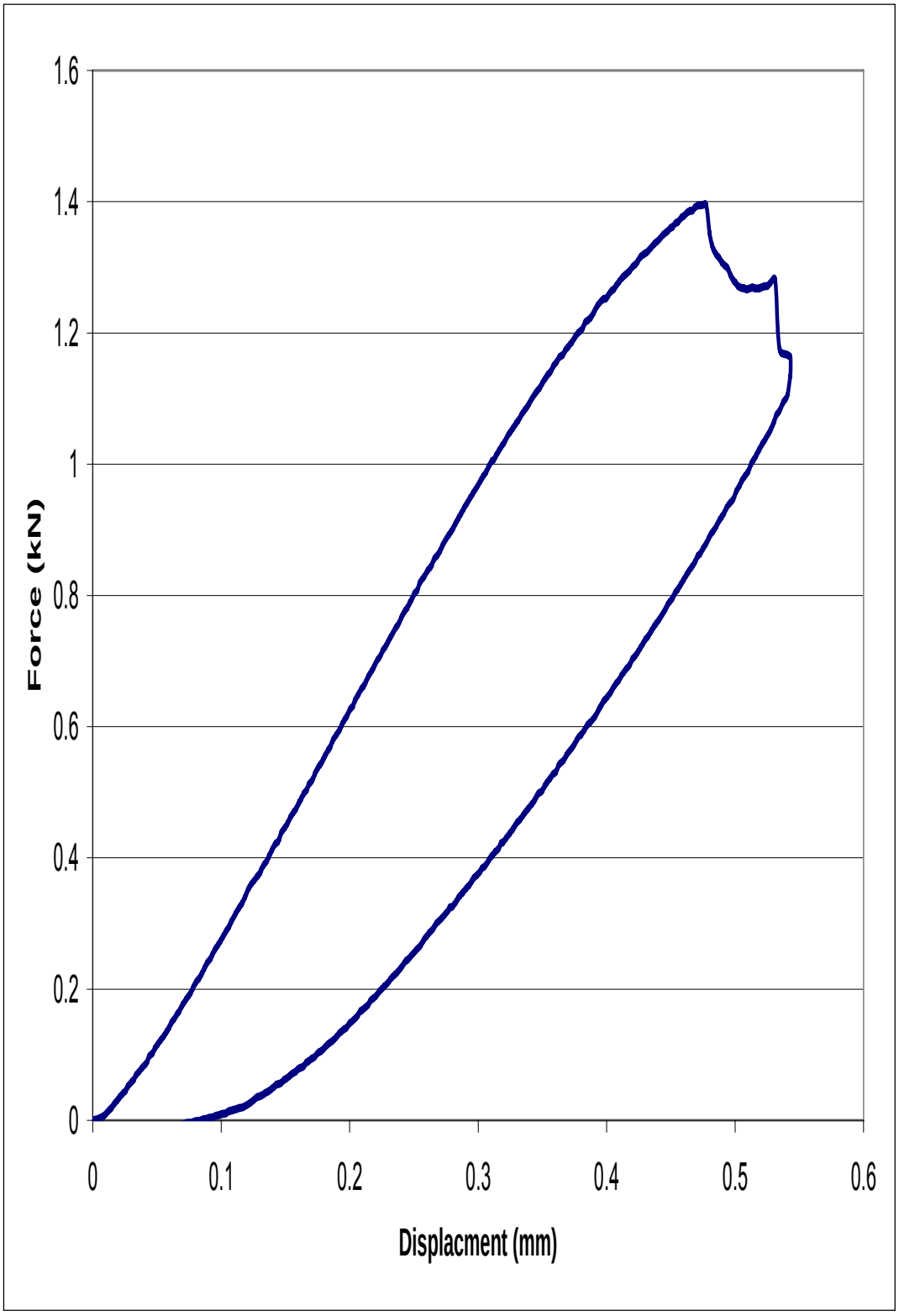

Figure E-4: SBS pultruded flat coupon Panex 20-1 force vs. displacement curve

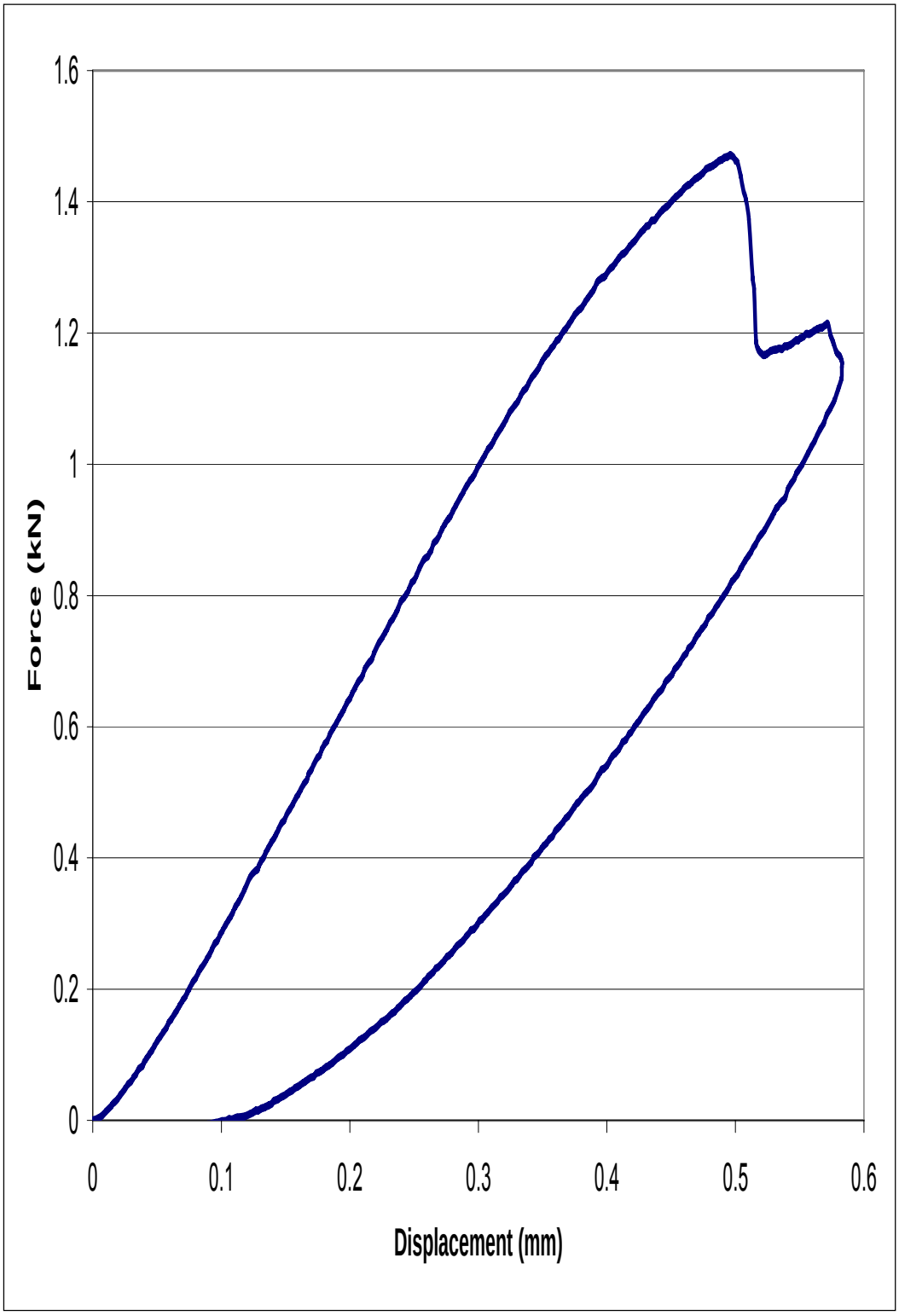

Figure E-5: SBS pultruded flat coupon Panex 20-2 force vs. displacement curve

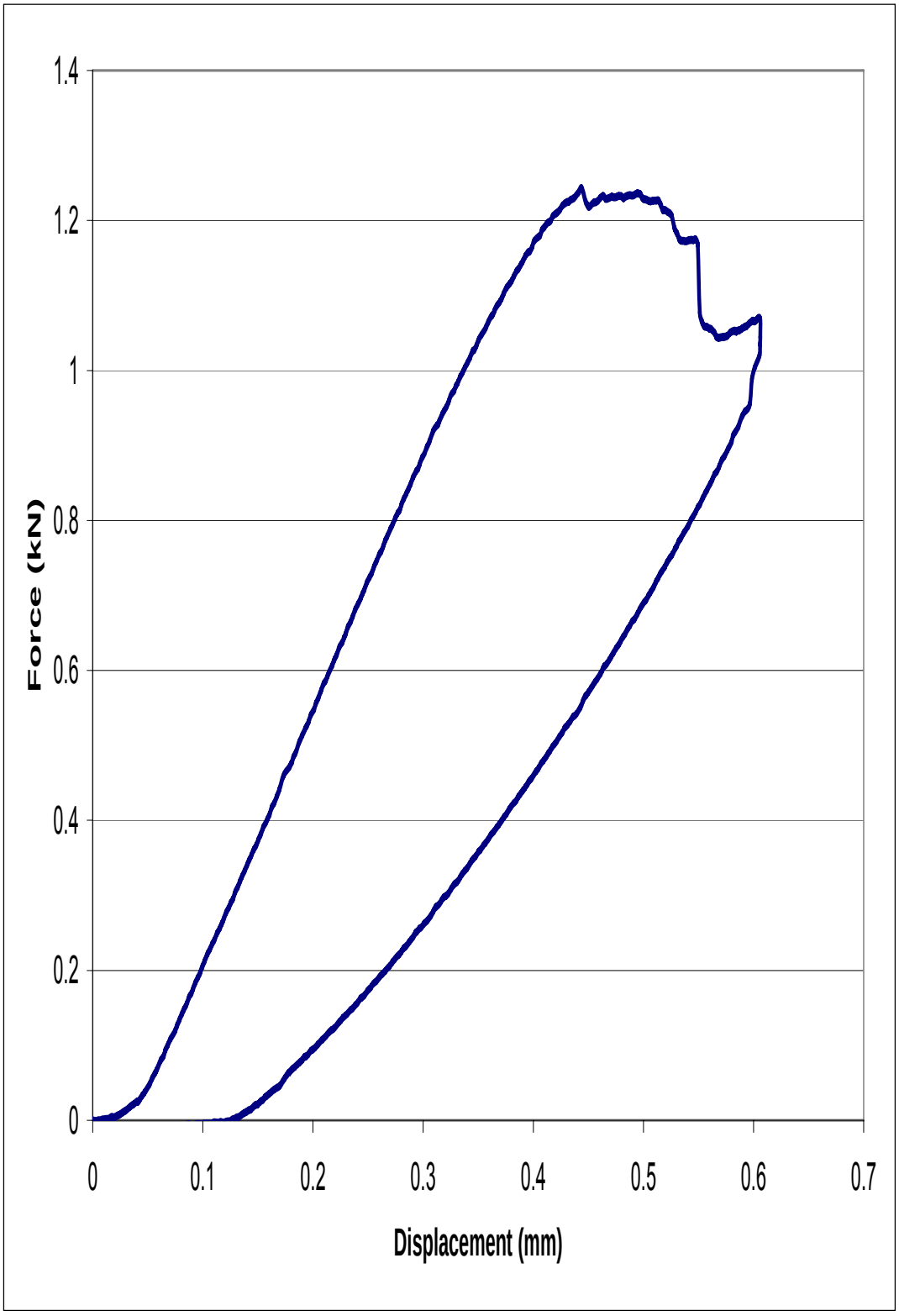

Figure E-6: SBS pultruded flat coupon Panex 20-3 force vs. displacement curve

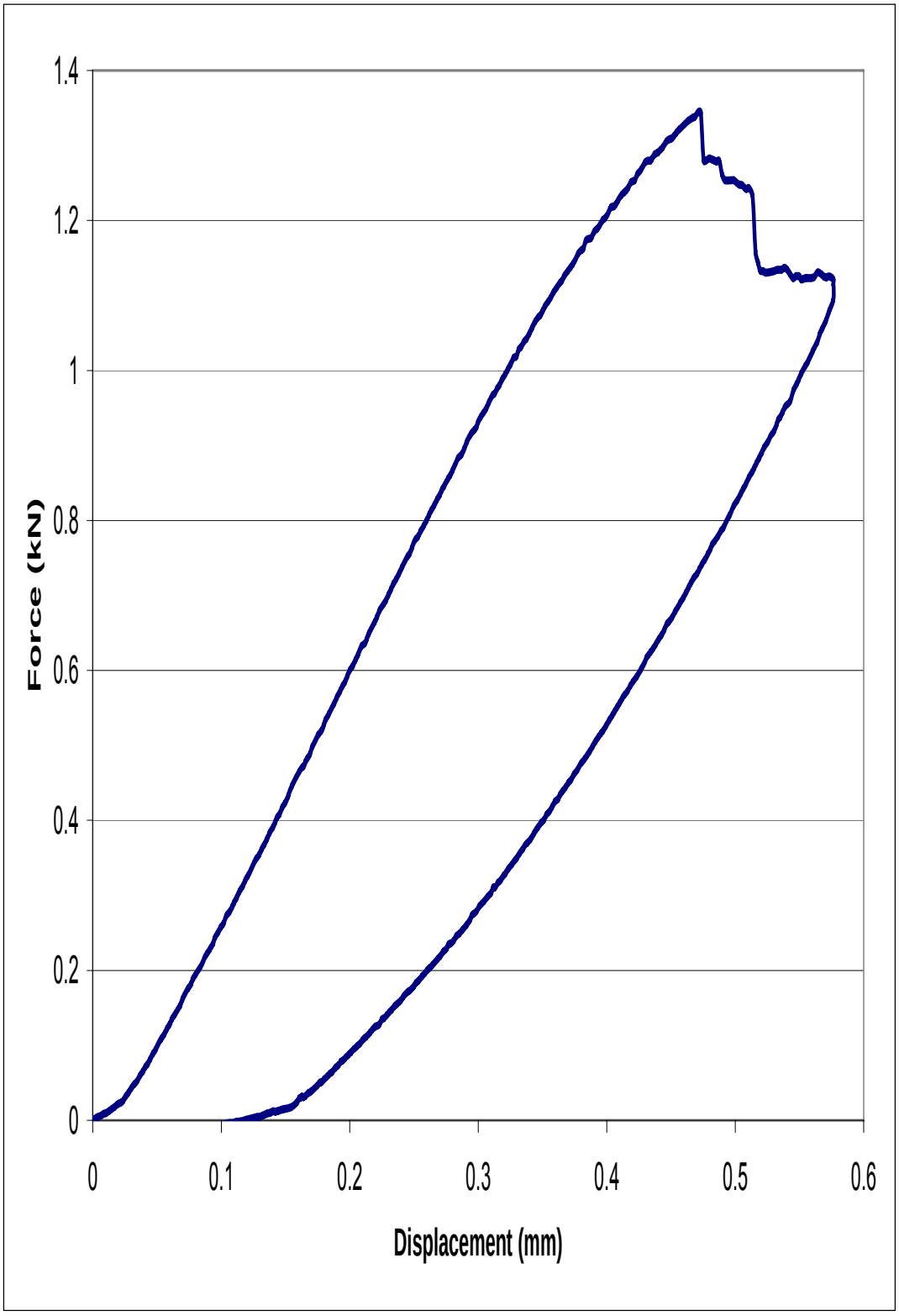

Figure E-7: SBS pultruded flat coupon Panex 20-4 force vs. displacement curve

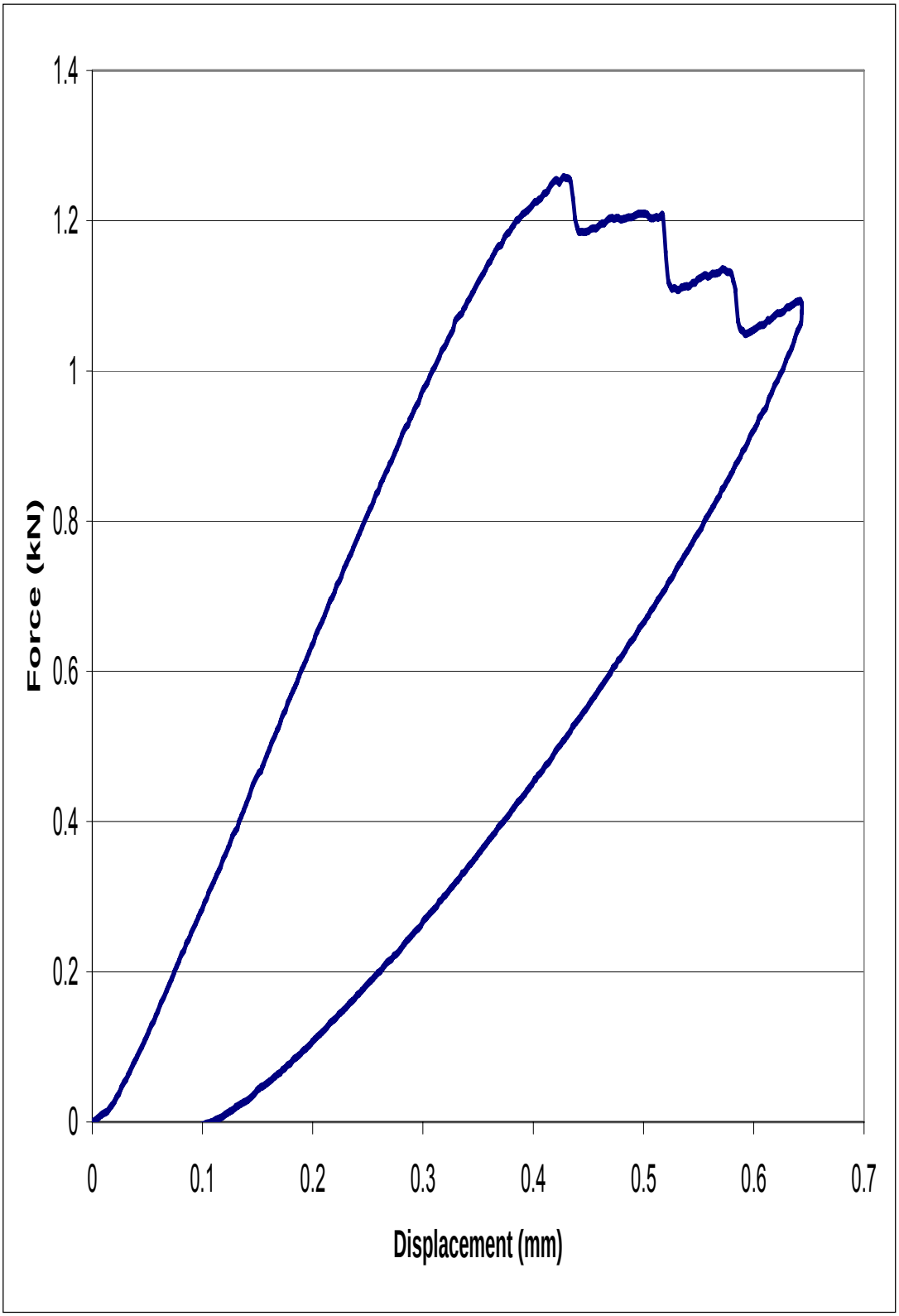

Figure E-8: SBS pultruded flat coupon Panex 20-5 force vs. displacement curve

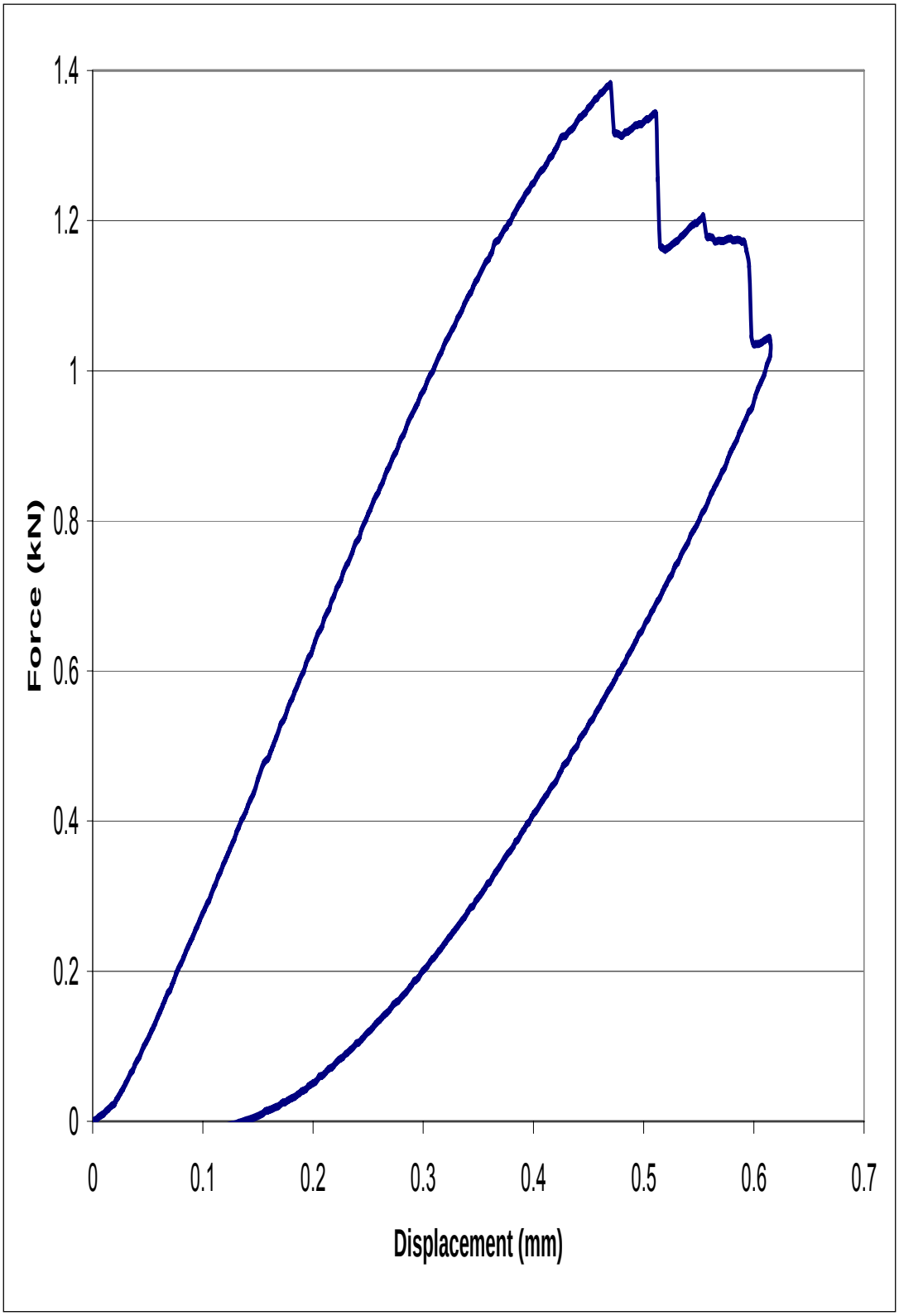

Figure E-9: SBS pultruded flat Panex 20-6 force vs. displacement curve

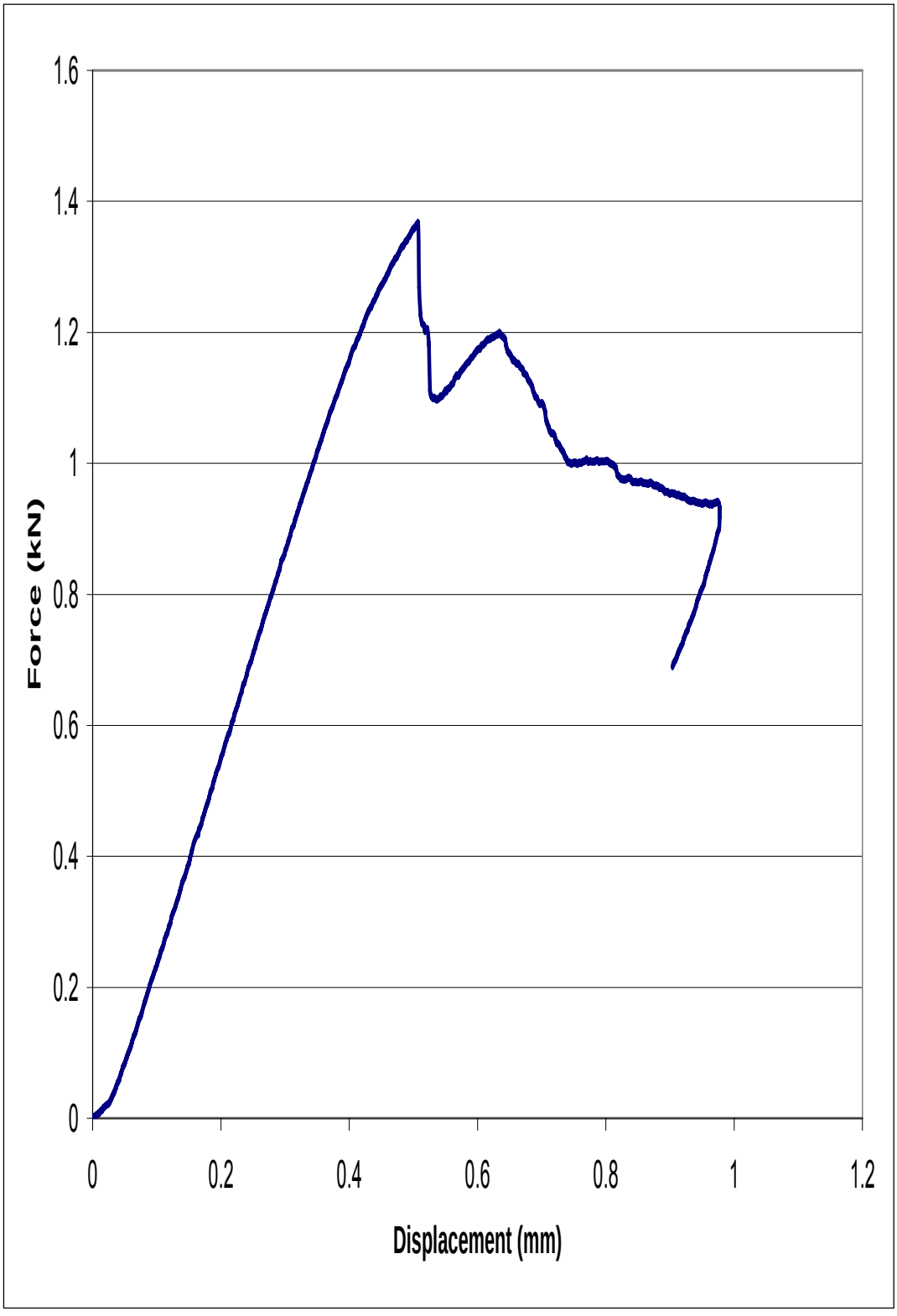

Figure E-10: SBS pultruded flat coupon Toray-1 force vs. displacement curve

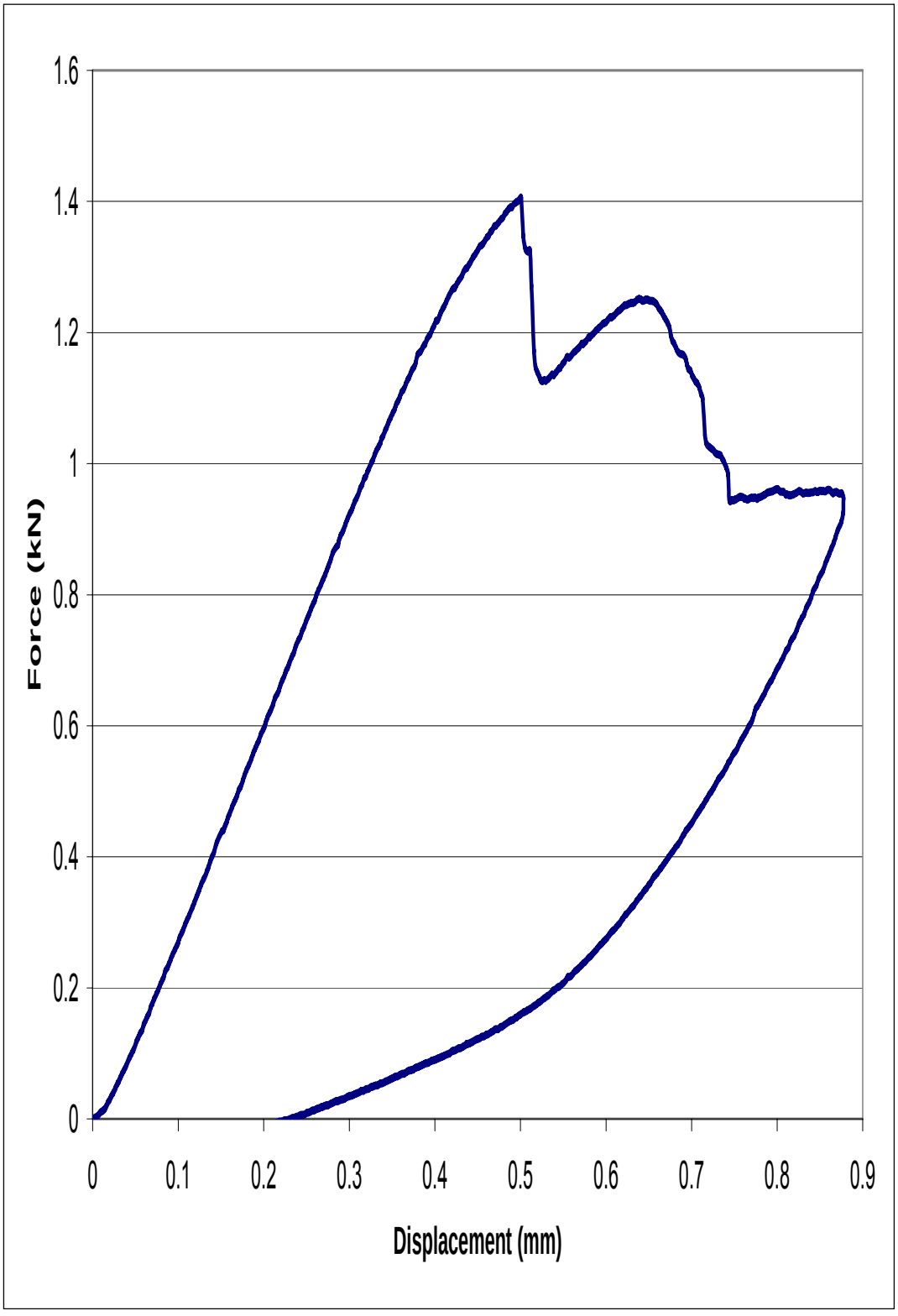

Figure E-11: SBS pultruded flat coupon Toray-2 force vs. displacement curve

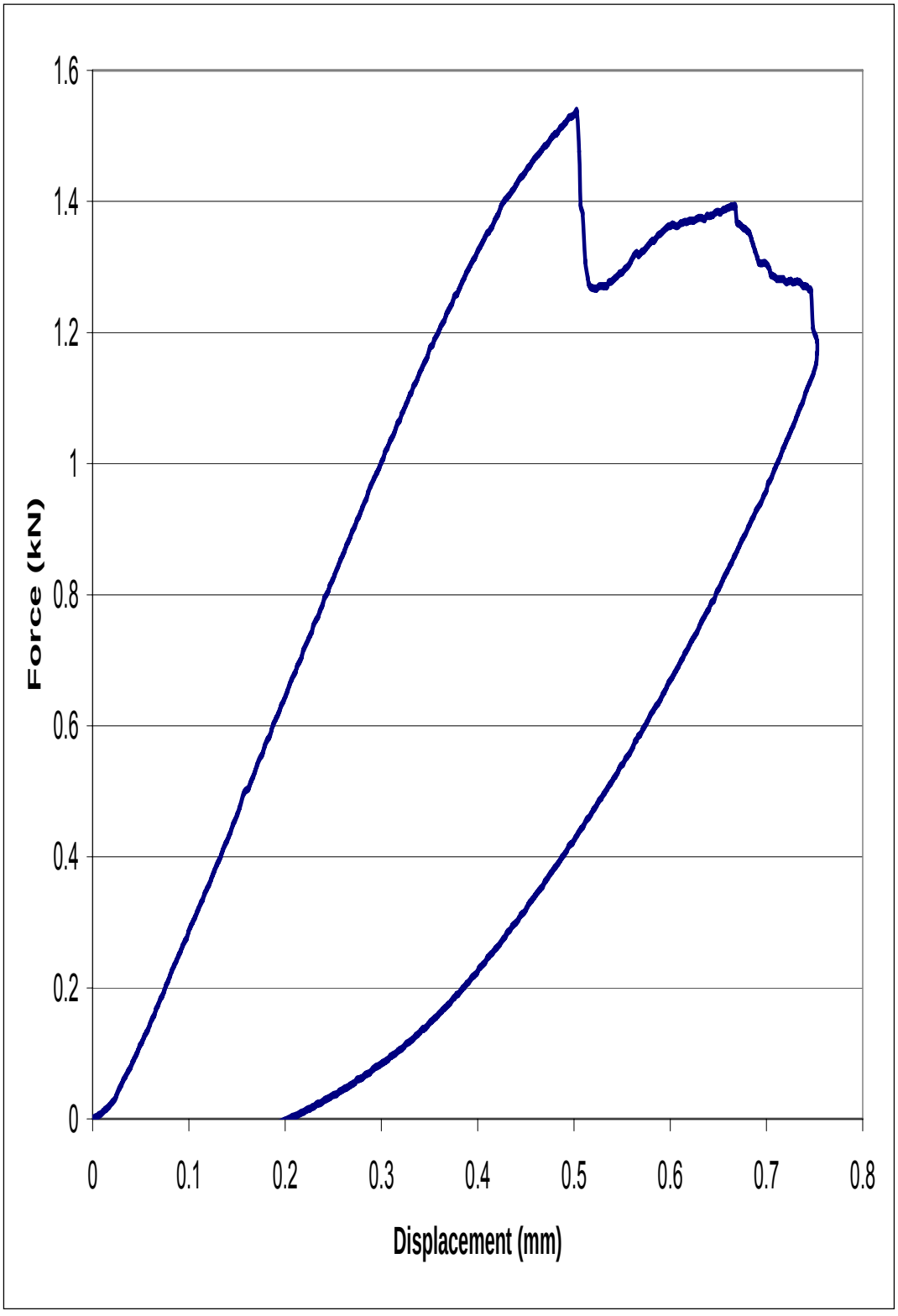

Figure E-12: SBS pultruded flat coupon Toray-3 force vs. displacement curve

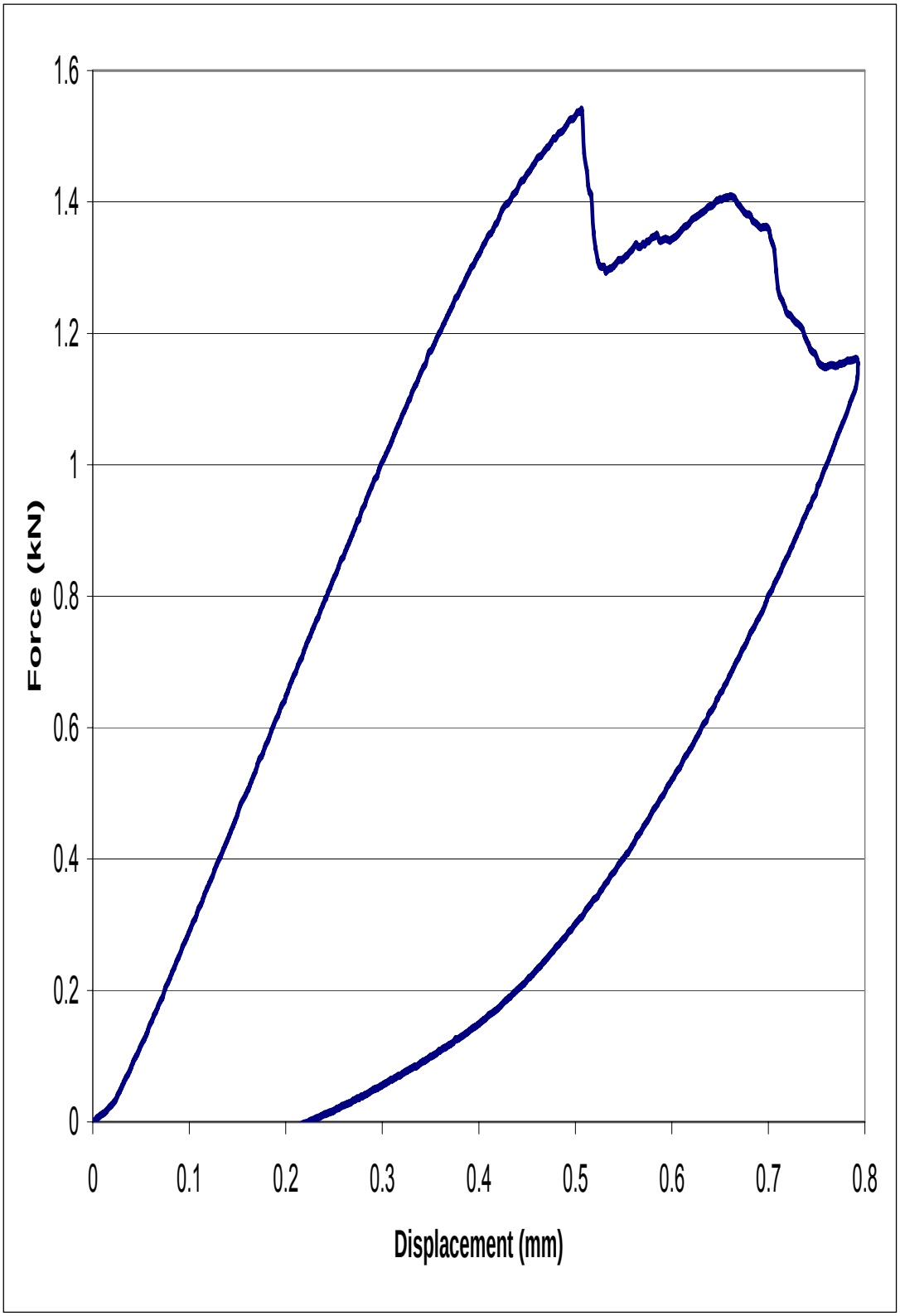

Figure E-13: SBS pultruded flat coupon Toray-4 force vs. displacement curve

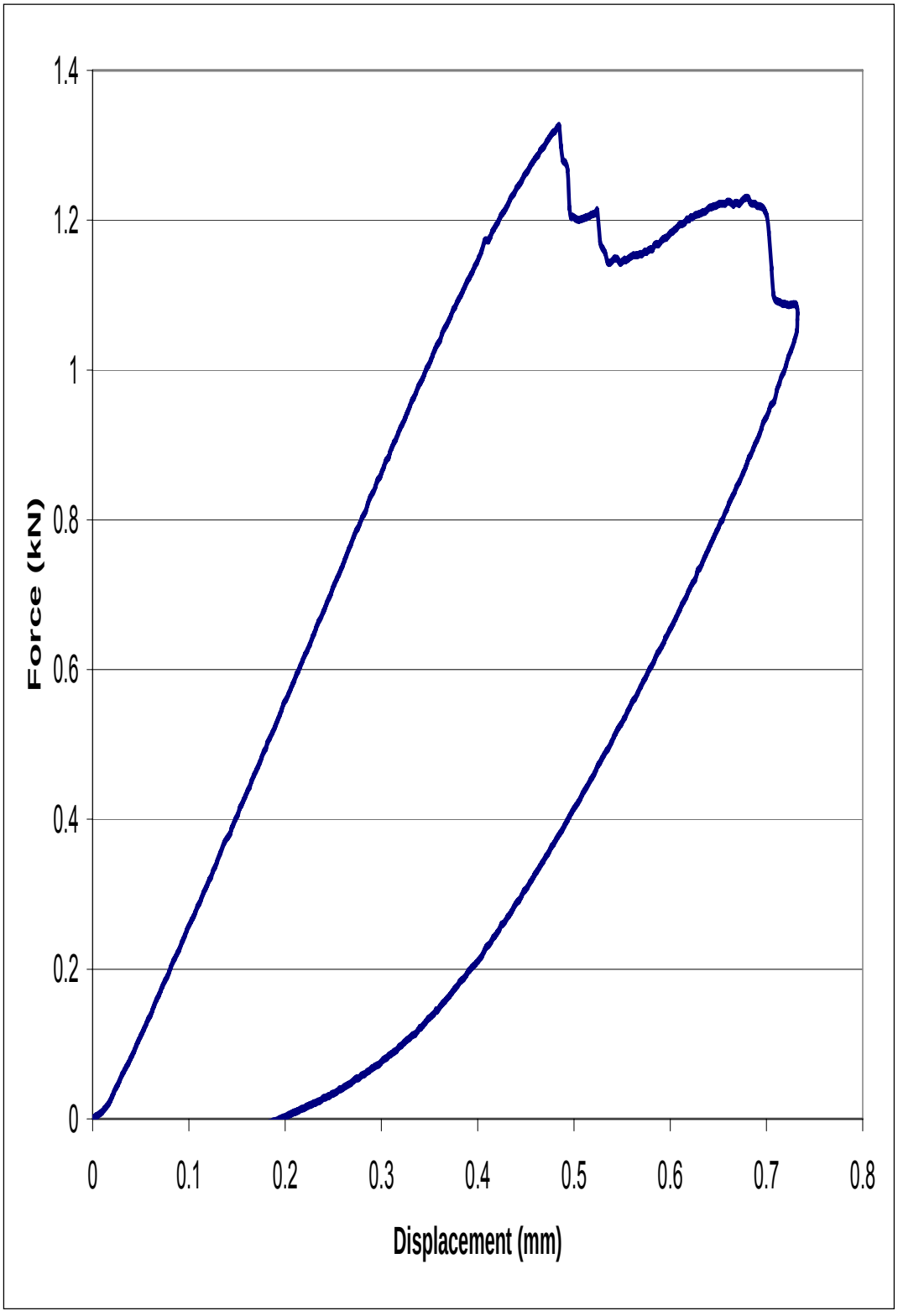

Figure E-14: SBS pultruded flat coupon Toray-5 force vs. displacement curve

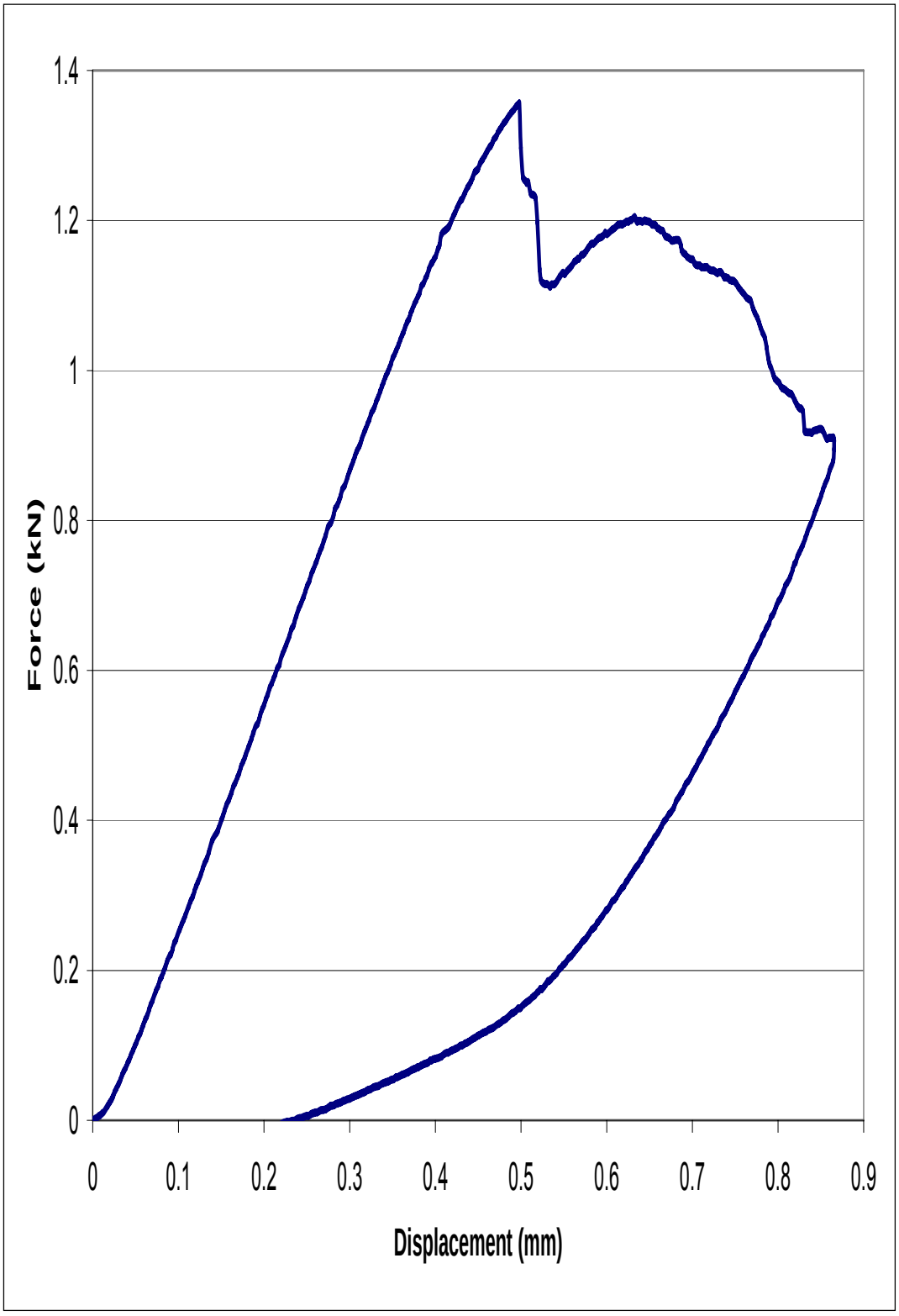

Figure E-15: SBS pultruded flat coupon Toray-6 force vs. displacement curve

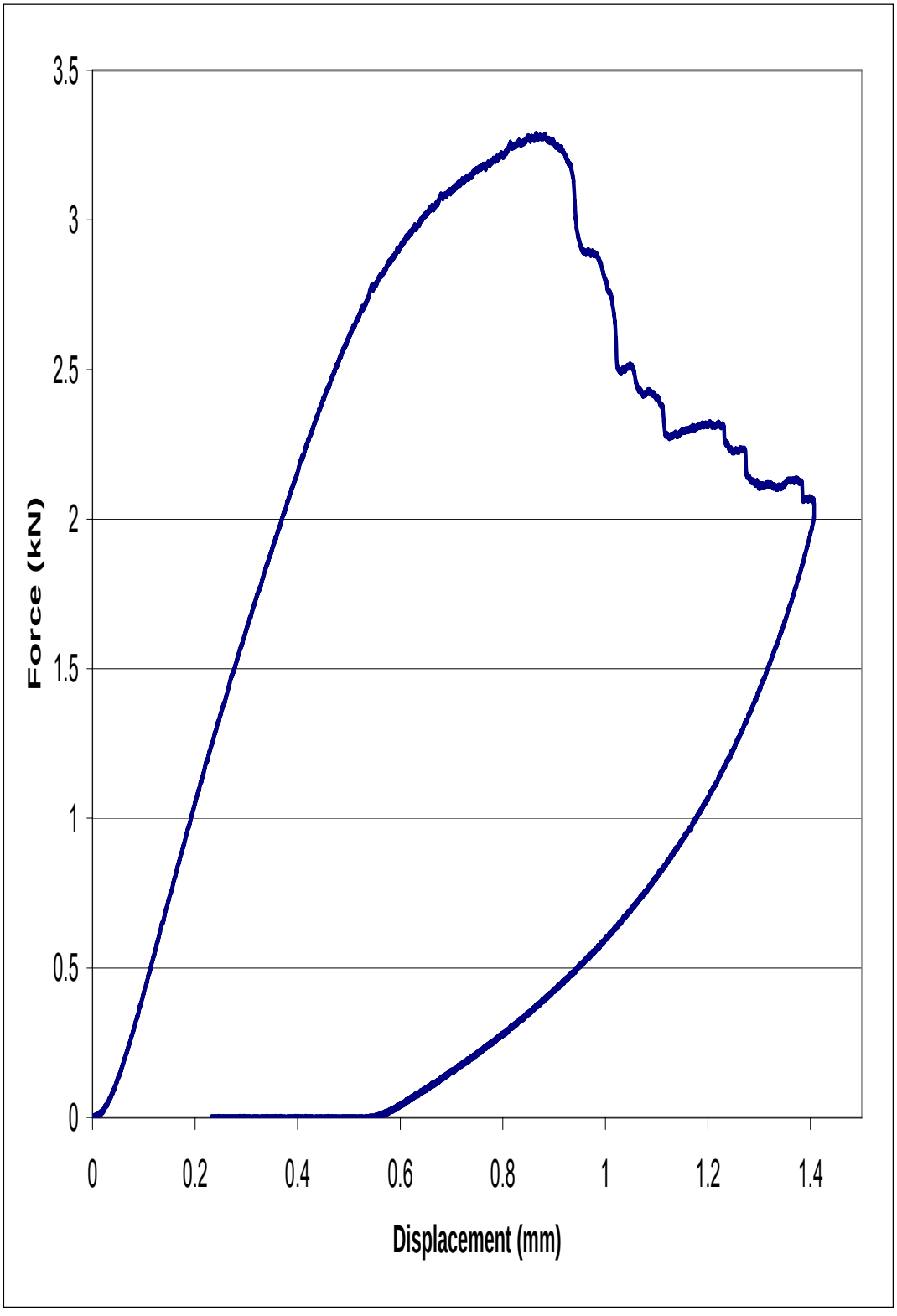

Figure E-16: SBS pultruded rod coupon 1 force vs. displacement curve

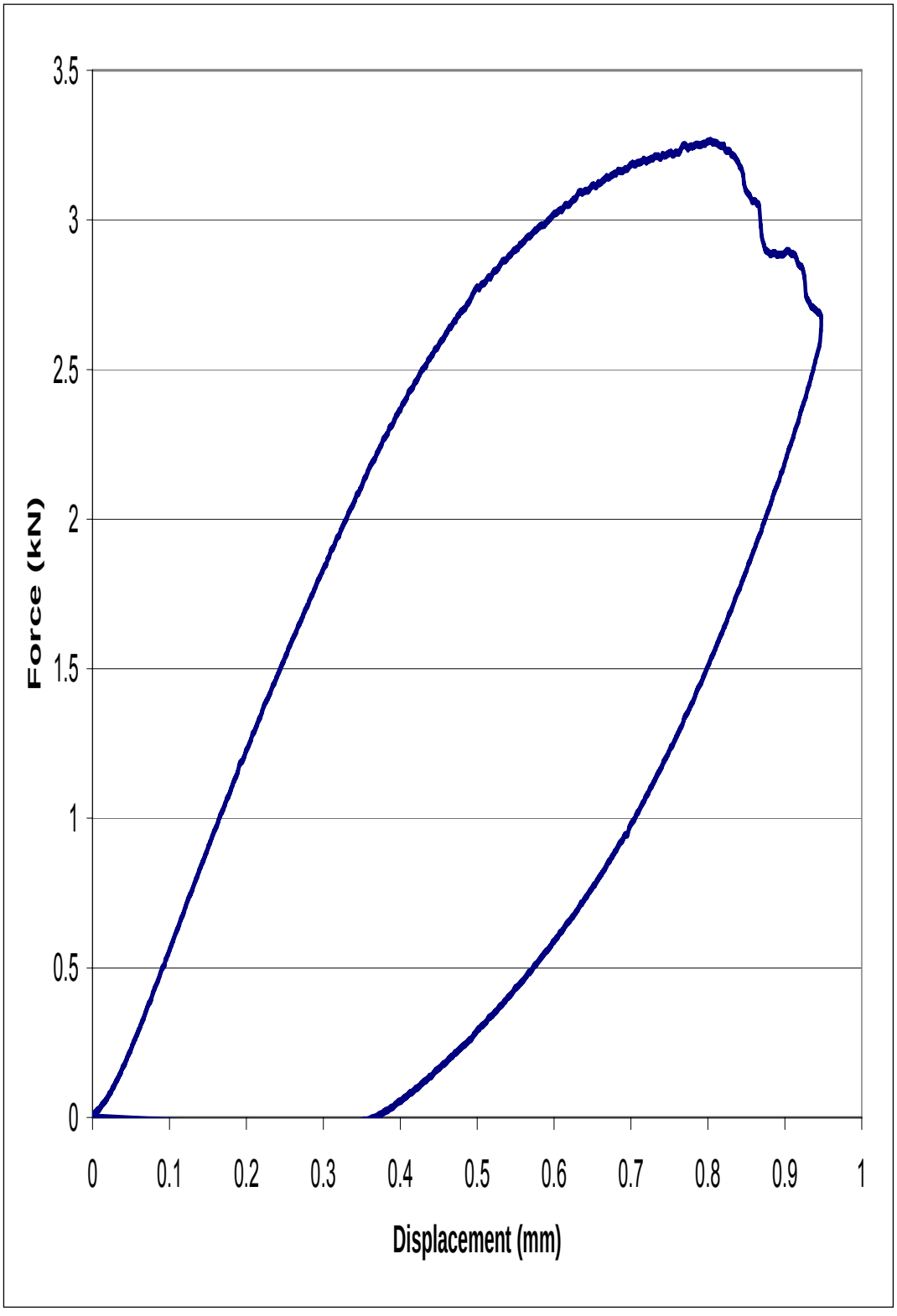

Figure E-17: SBS pultruded rod coupon 2 force vs. displacement curve

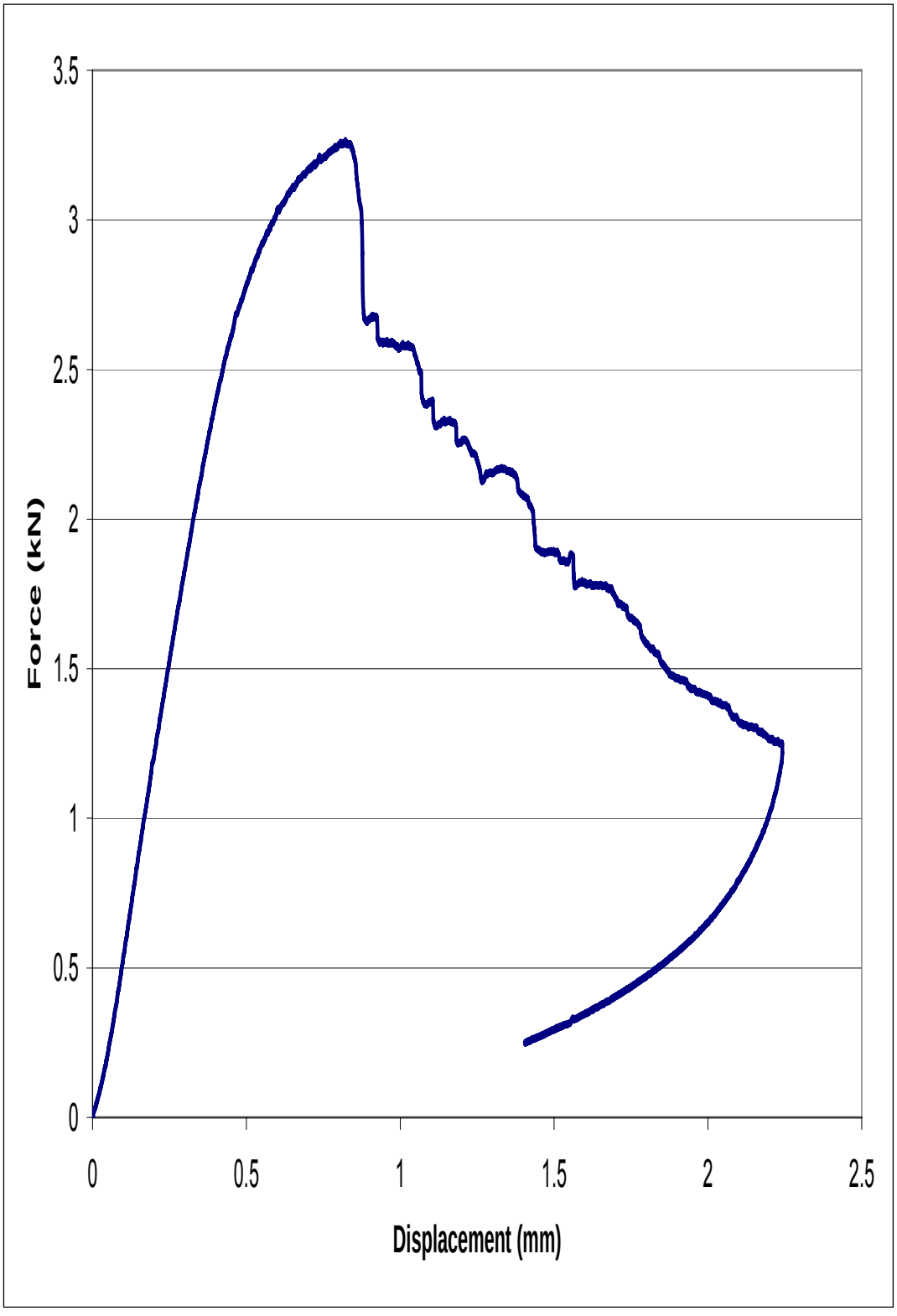

Figure E-18: SBS pultruded rod coupon 3 force vs. displacement curve

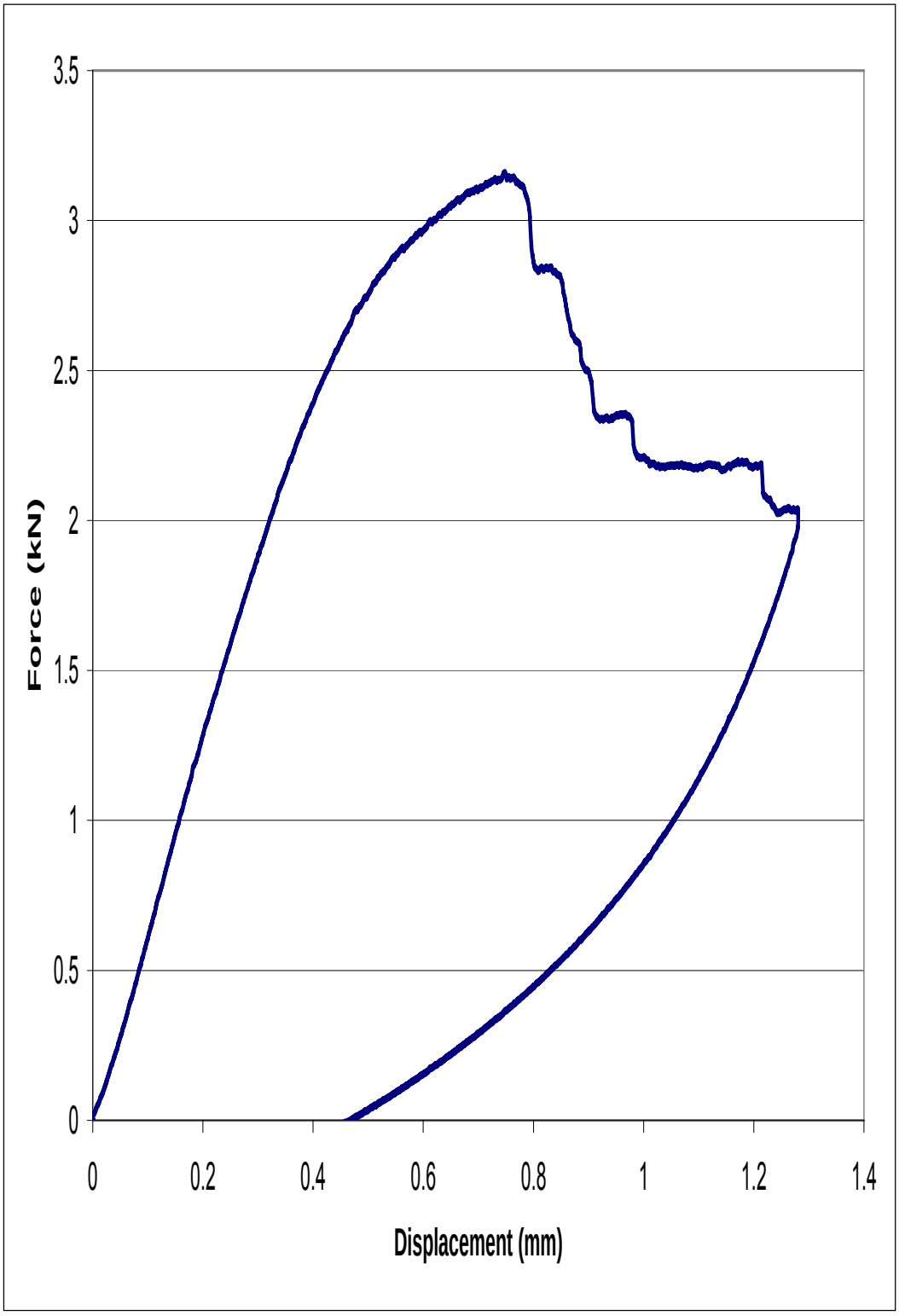

Figure E-19: SBS pultruded rod coupon 4 force vs. displacement curve

APPENDIX F

Pultruded Flat Tension Test Stress vs. Strain Curves

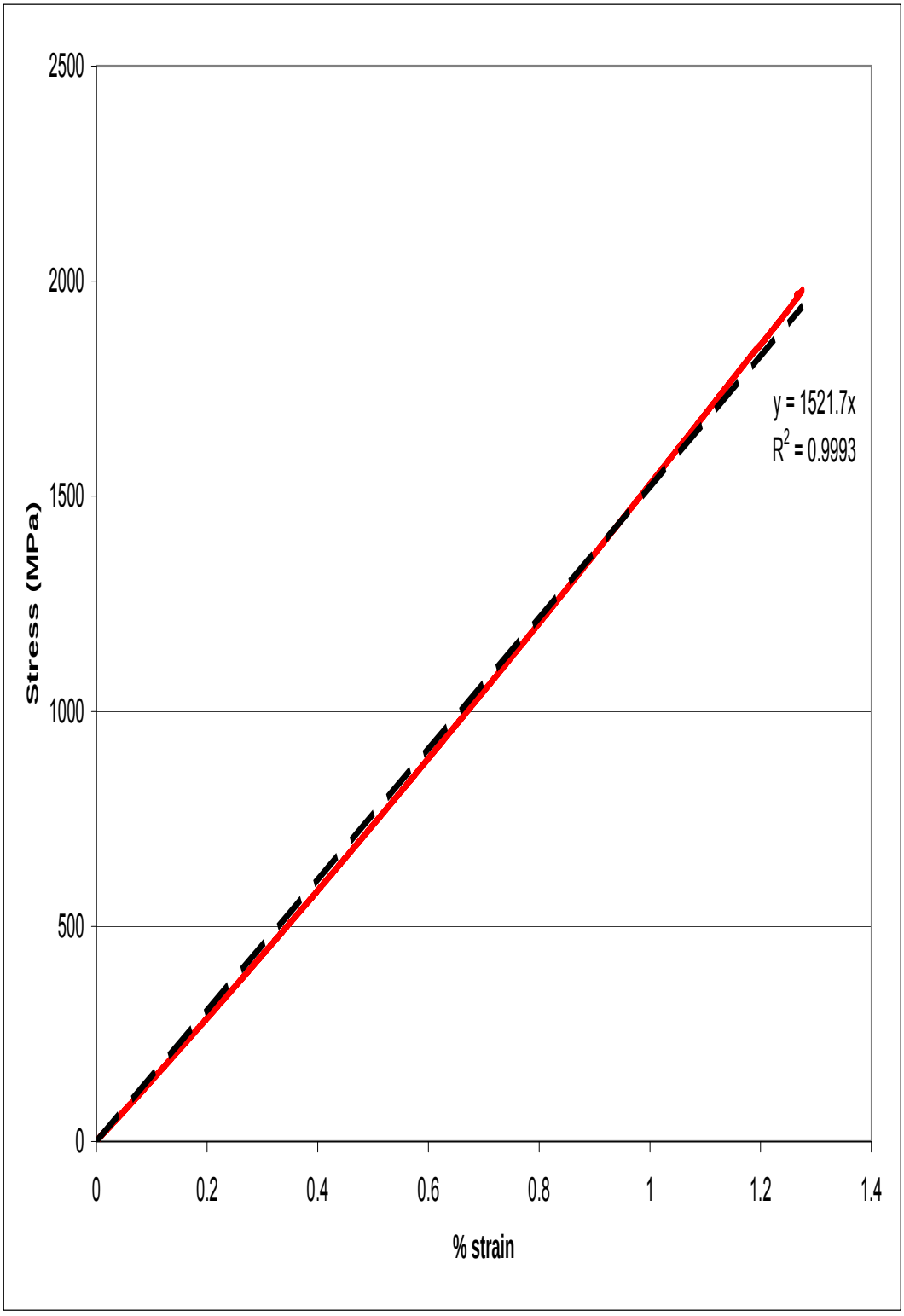

Figure F-1: Stress vs. strain curve of pultruded flat Zoltek 19-tow coupon 2

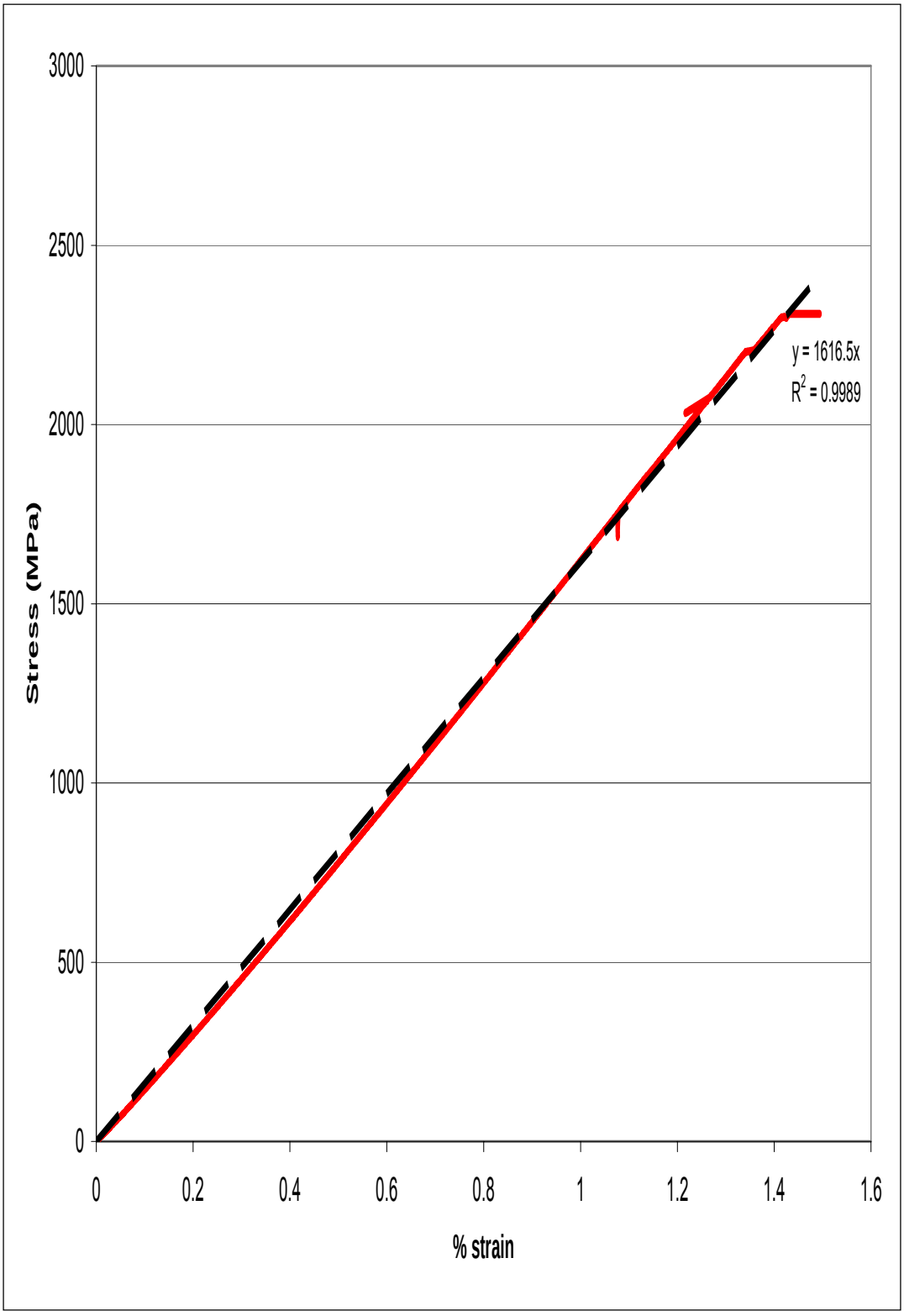

Figure F-2: Stress vs. strain curve of pultruded flat Zoltek 19-tow coupon 4

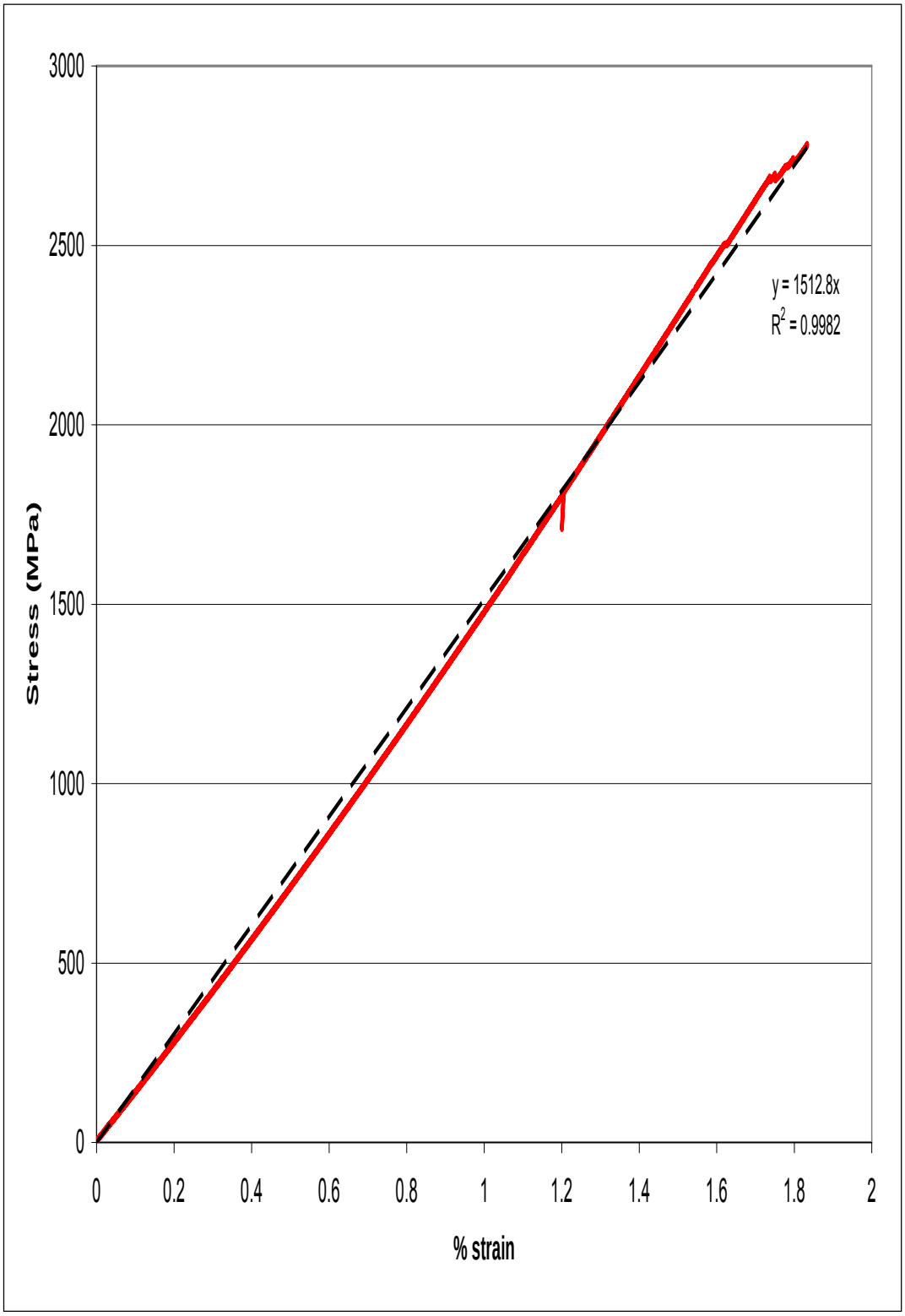

Figure F-3: Stress vs. strain curve of pultruded flat Toray coupon 1

APPENDIX G

Pre-interface Test SEM Surface Images

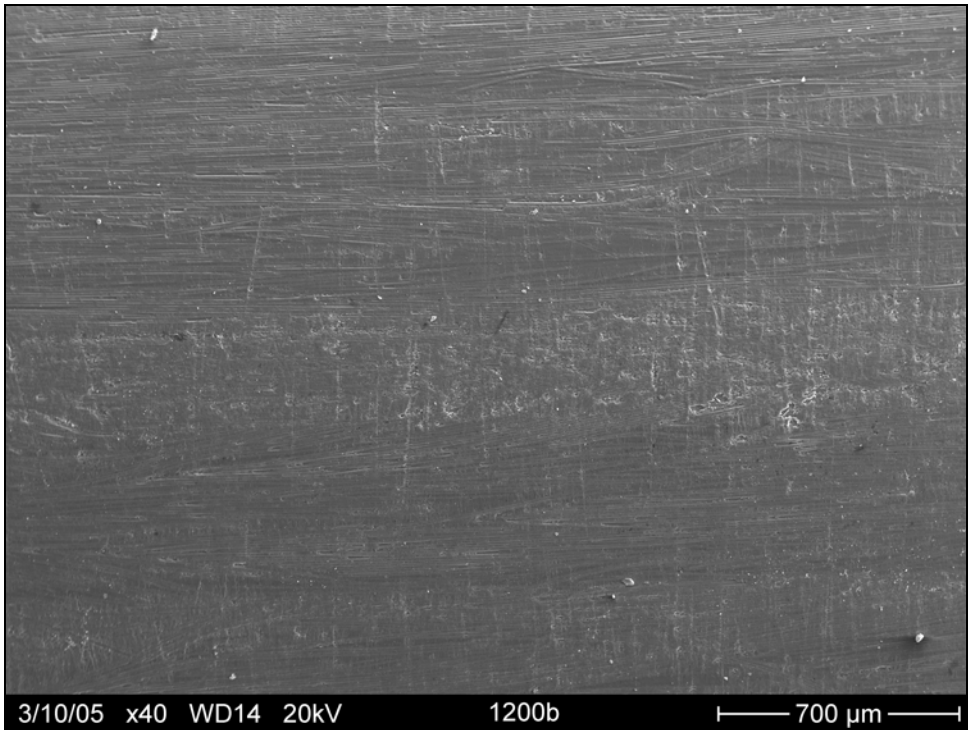

Figure G-1: Pre-interface tested rod surface after 1200 SiC grit abrasion treatment

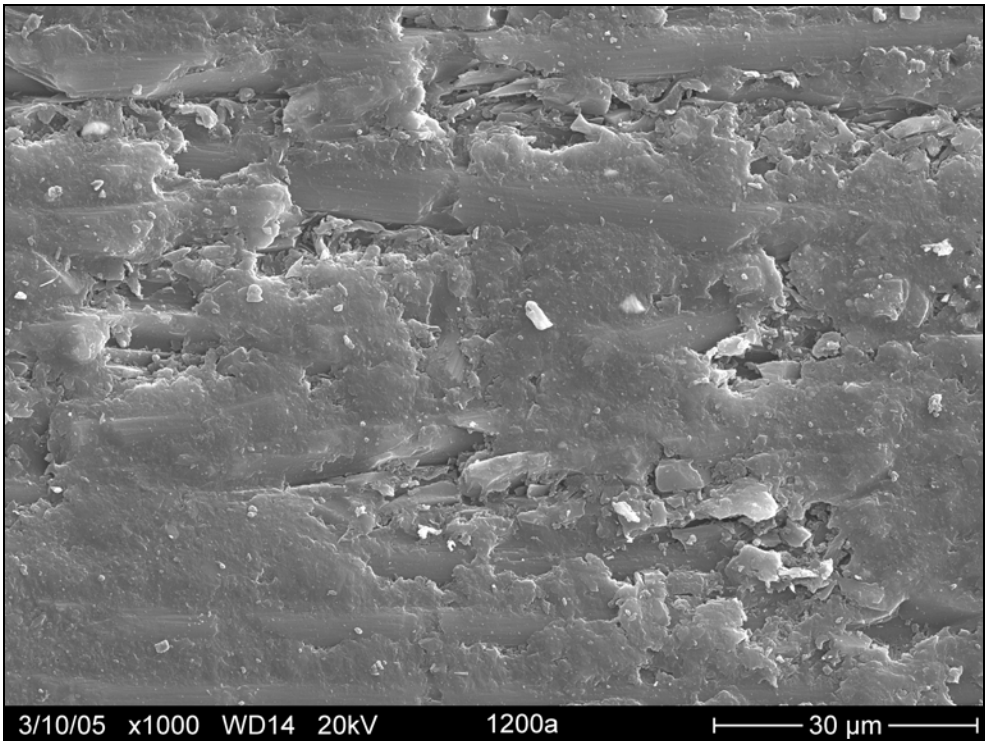

Figure G-2: Magnified view of rod surface after SiC 1200 grit abrasion treatment

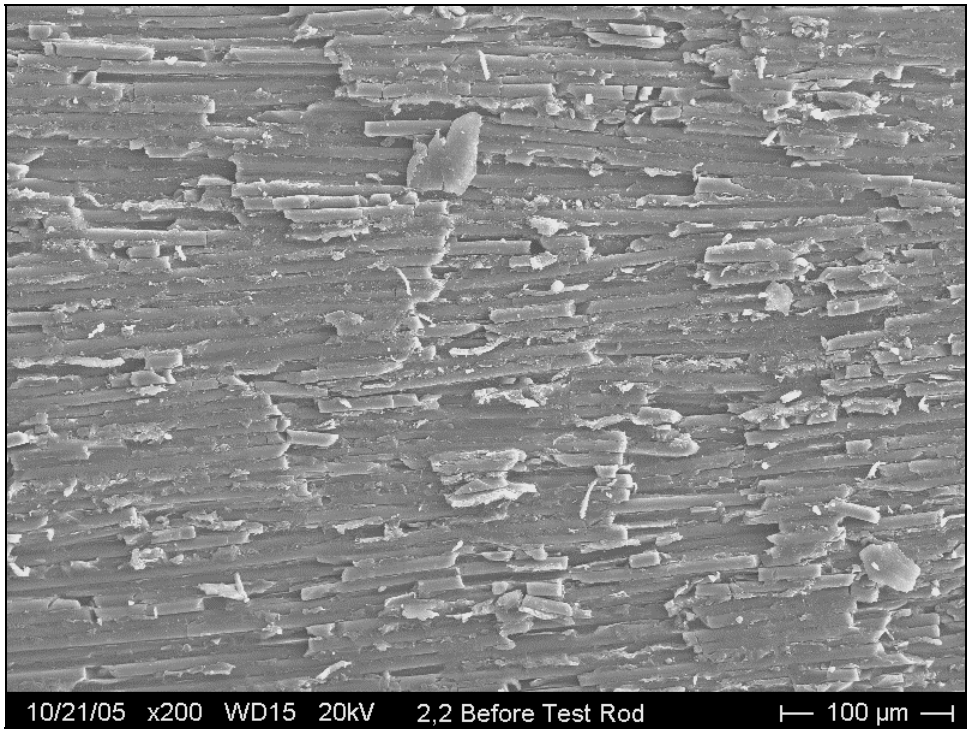

Figure G-3: Pre-interface tested rod surface after 2 kg/cm^2, 2 revolutions erosion treatment

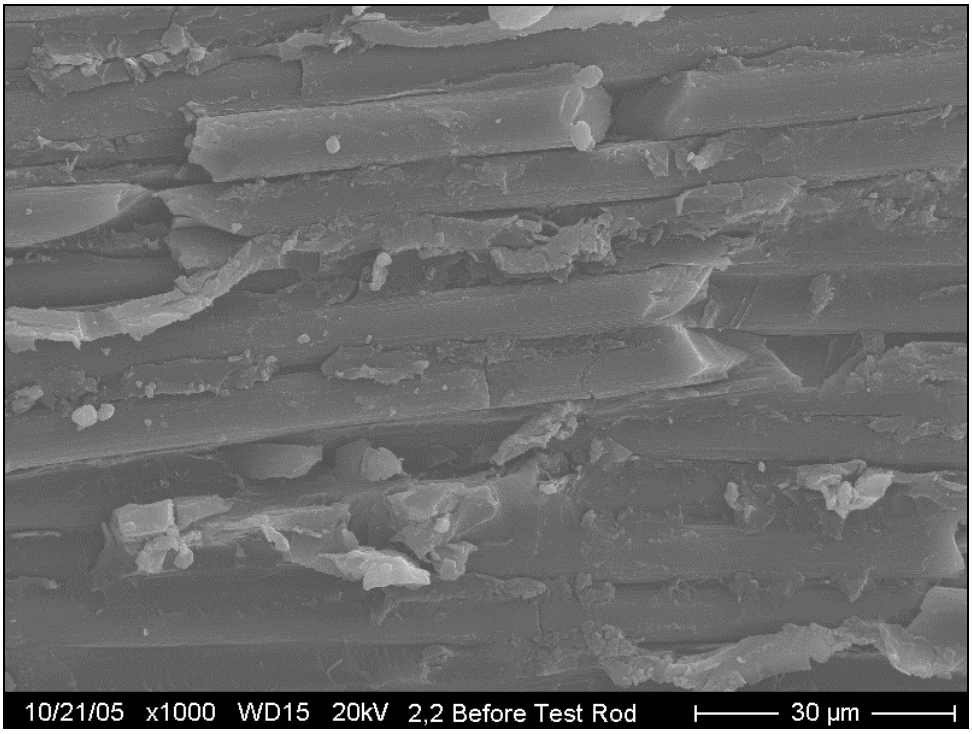

Figure G-4: Magnified view of rod surface after 2 kg/cm^2, 2 revolutions surface treatment

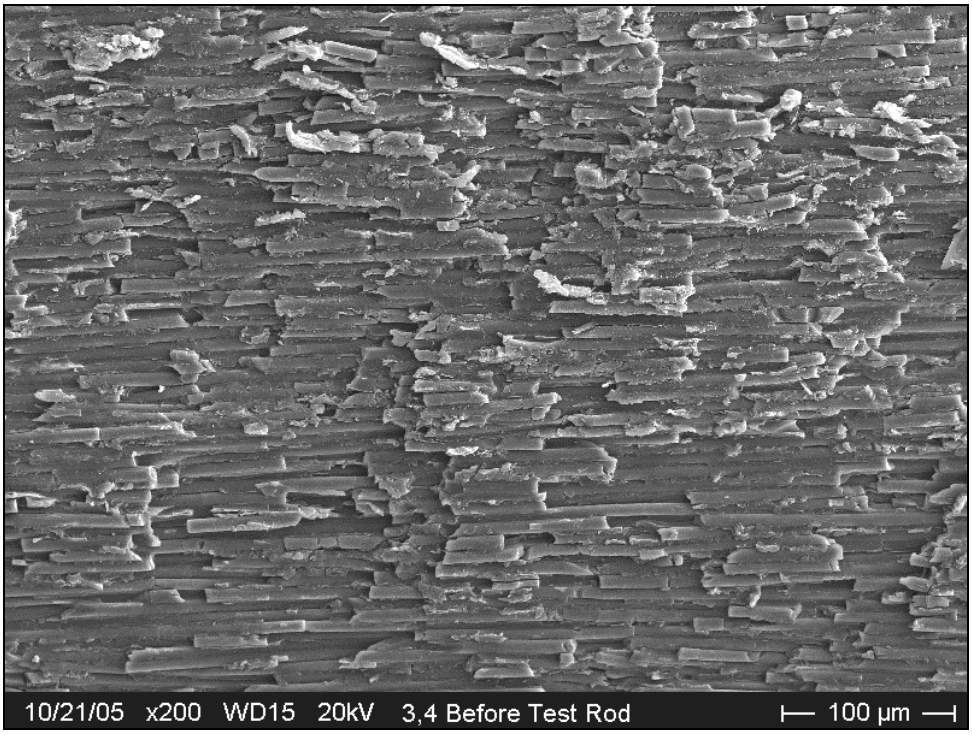

Figure G-5**:** Pre-interface tested rod surface after 3 kg/cm^2, 4 revolutions erosion treatment

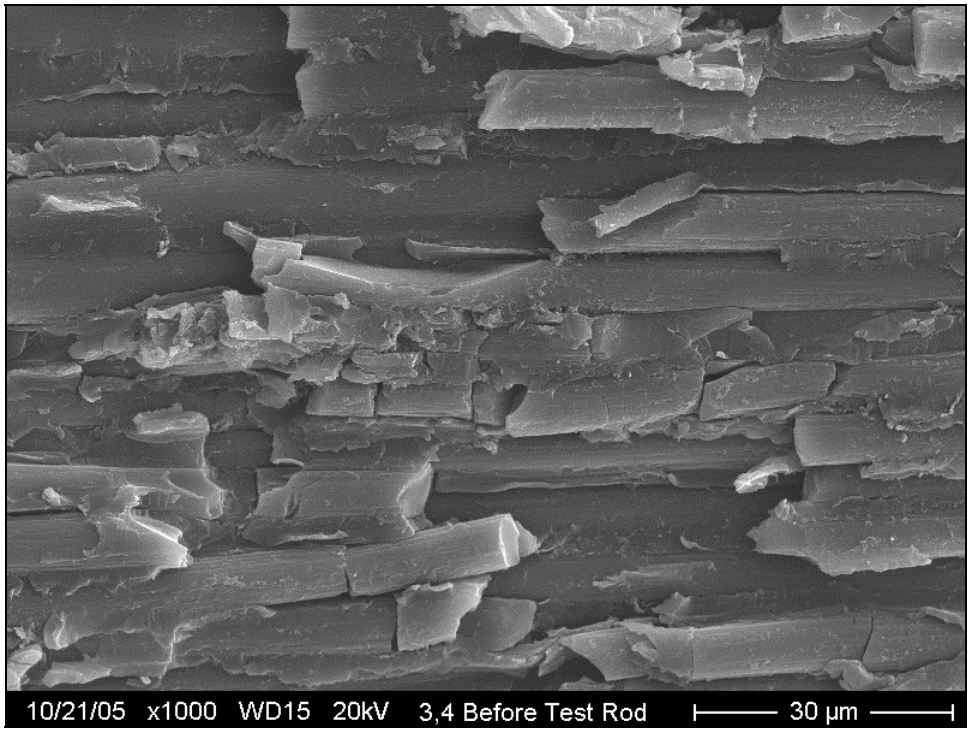

Figure G-6: Magnified view of rod surface after 3 kg/cm^2, 4 revolutions surface treatment

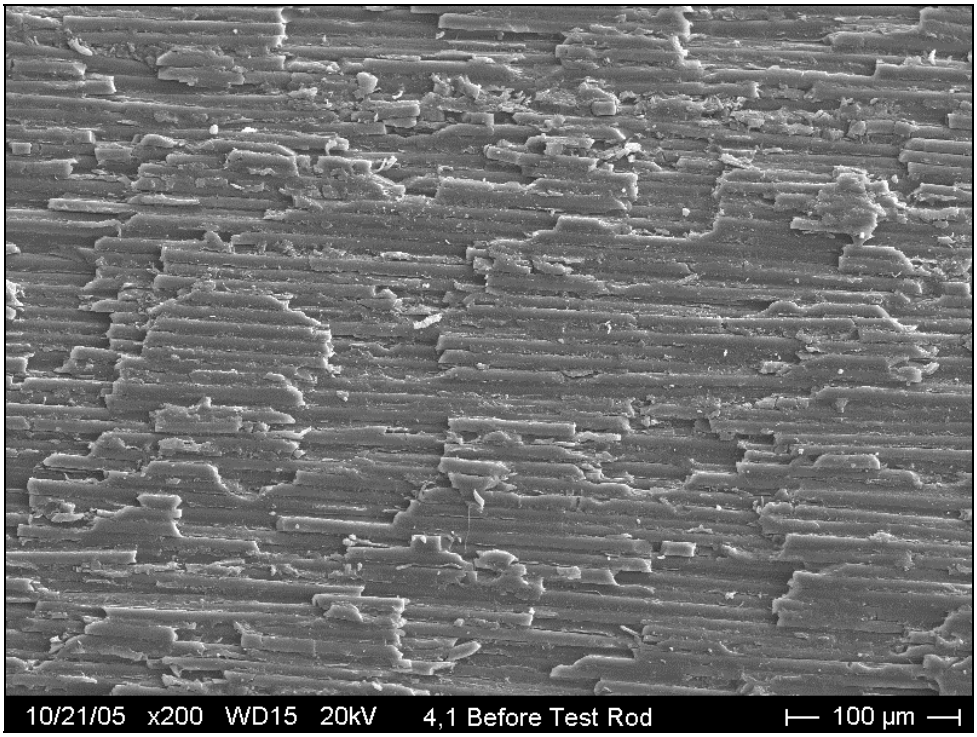

Figure G-7: Pre-interface tested rod surface after 4 kg/cm^2, 1 revolutions erosion treatment

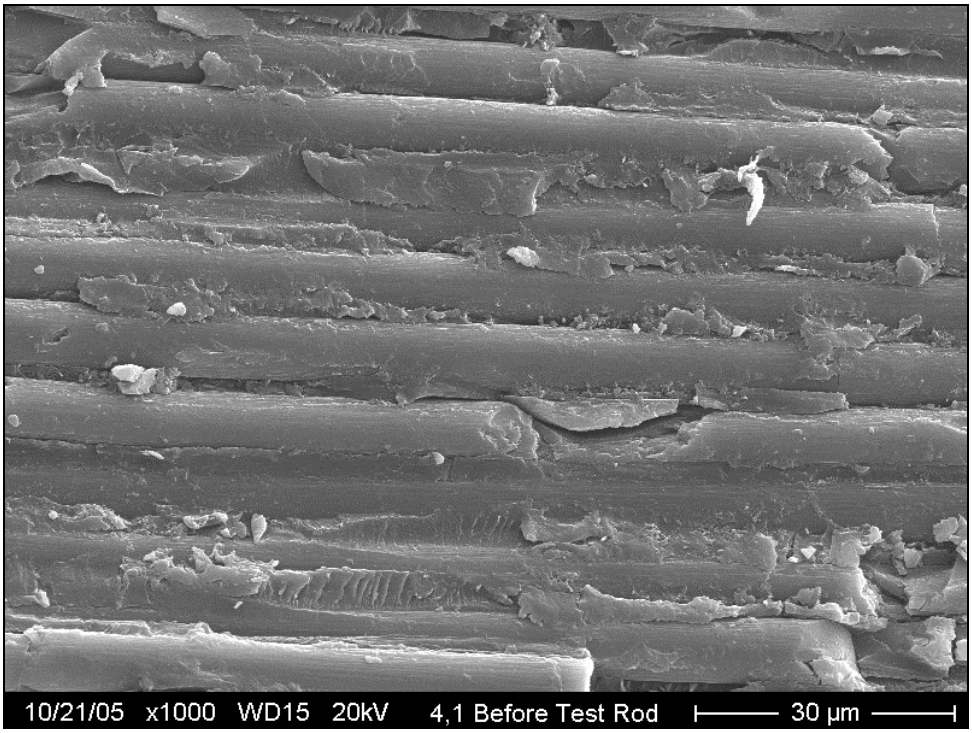

Figure G-8: Magnified view of rod surface after 4 kg/cm^2, 1 revolutions surface treatment

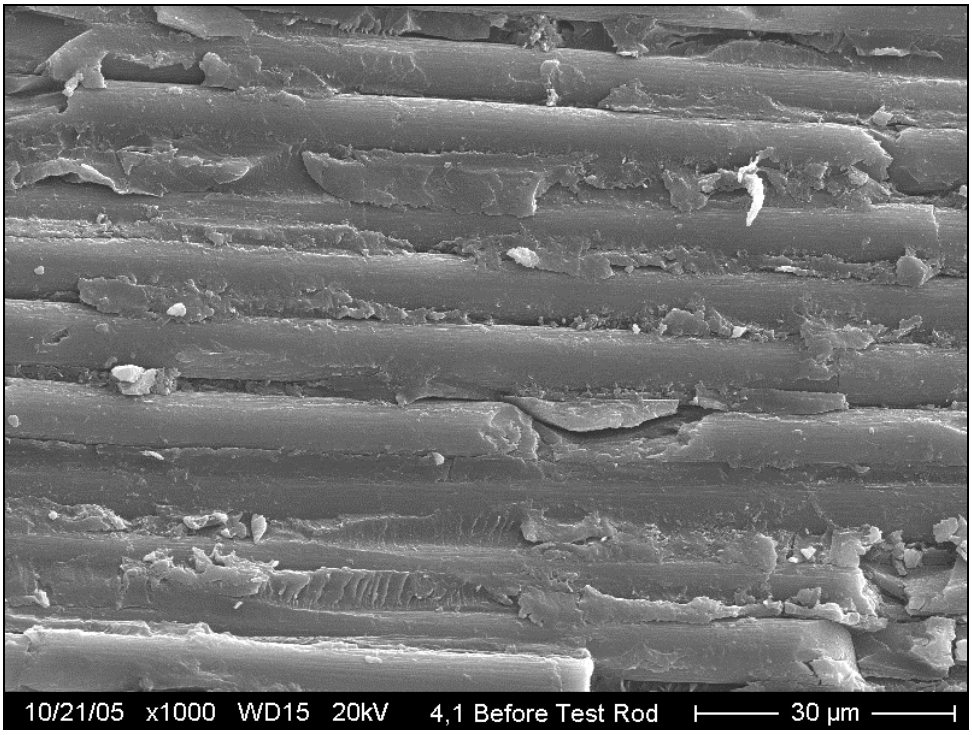

Figure G-9: Magnified view of rod surface after 4 kg/cm^2, 1 revolutions surface treatment

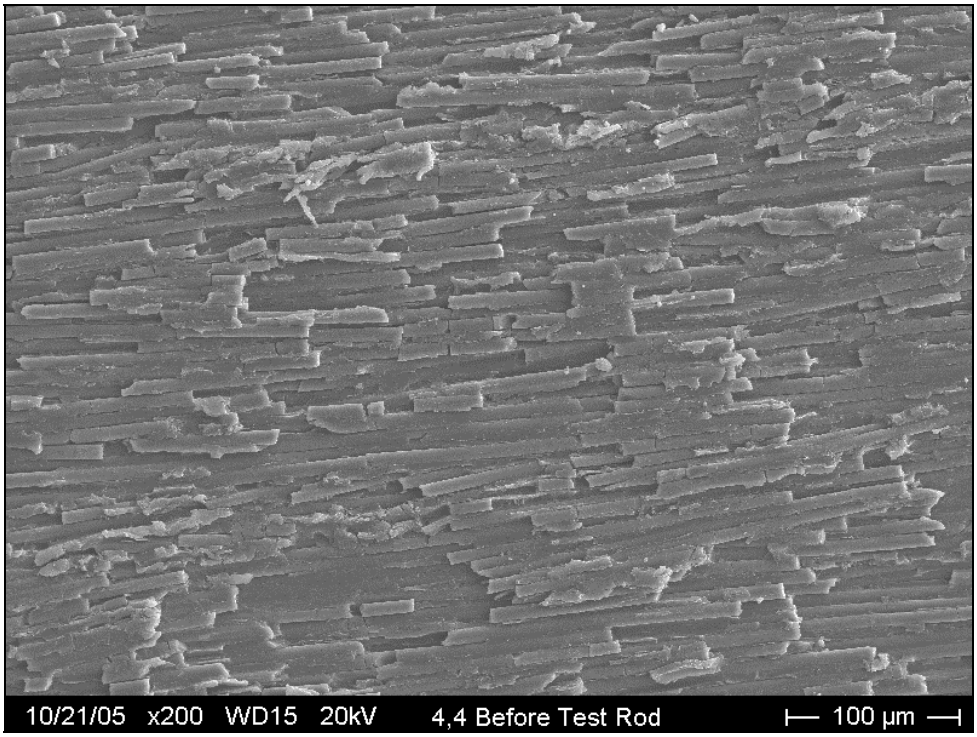

Figure G-10: Pre-interface tested rod surface after 4 kg/cm^2, 4 revolutions erosion treatment

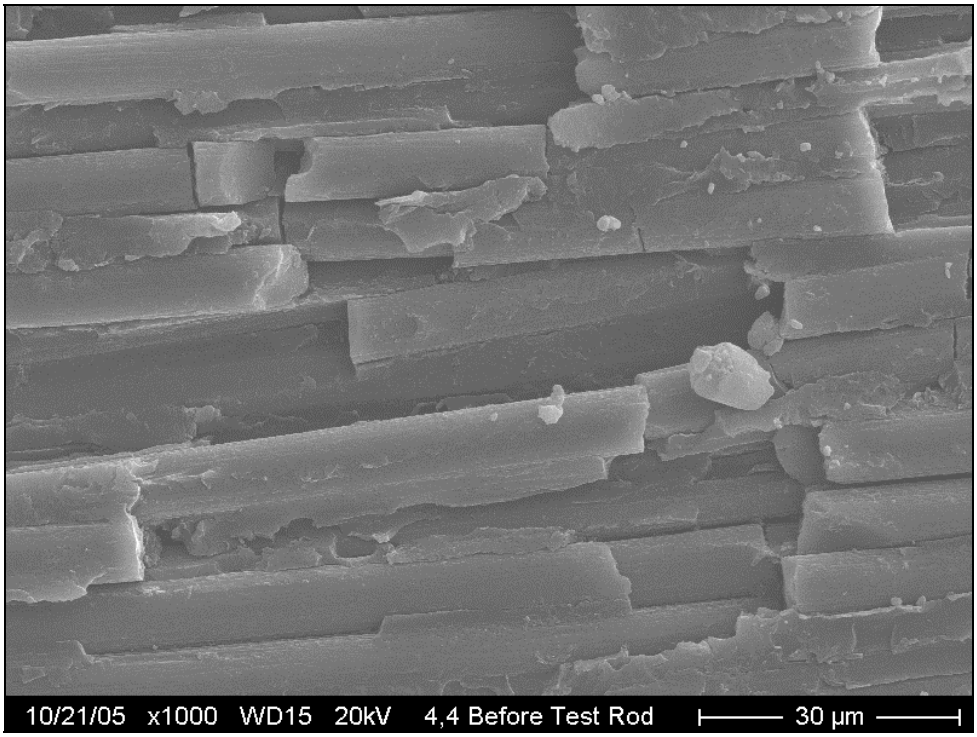

Figure G-11: Magnified view of rod surface after 4 kg/cm^2, 1 revolutions surface treatment

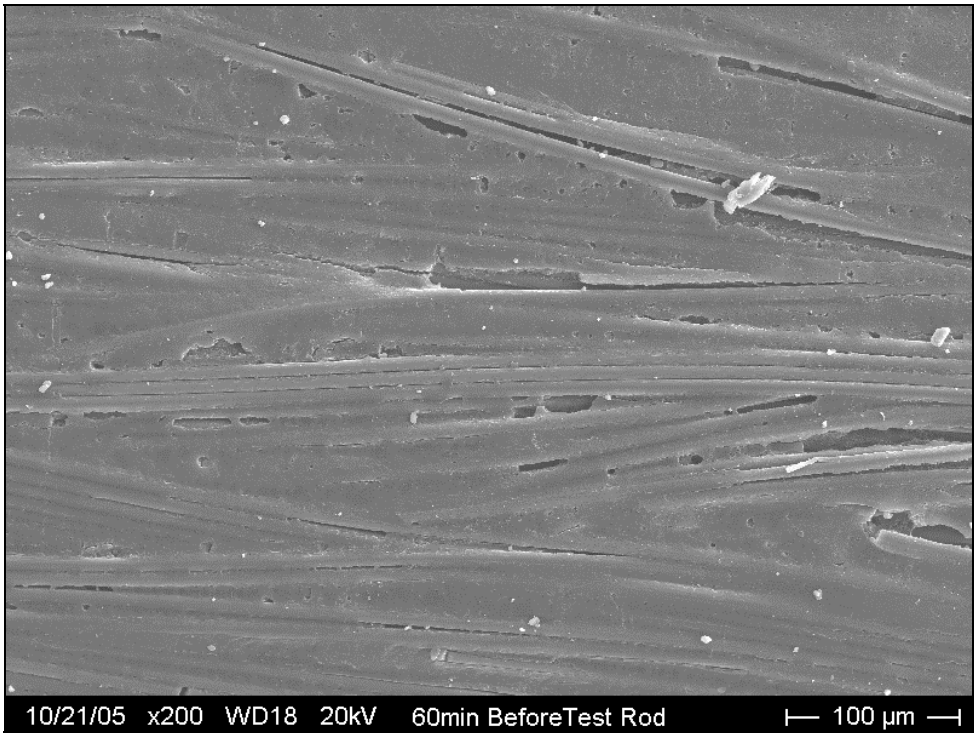

Figure G-12: Pre-interface tested rod surface after washed 60 min HNO_3 surface treatment

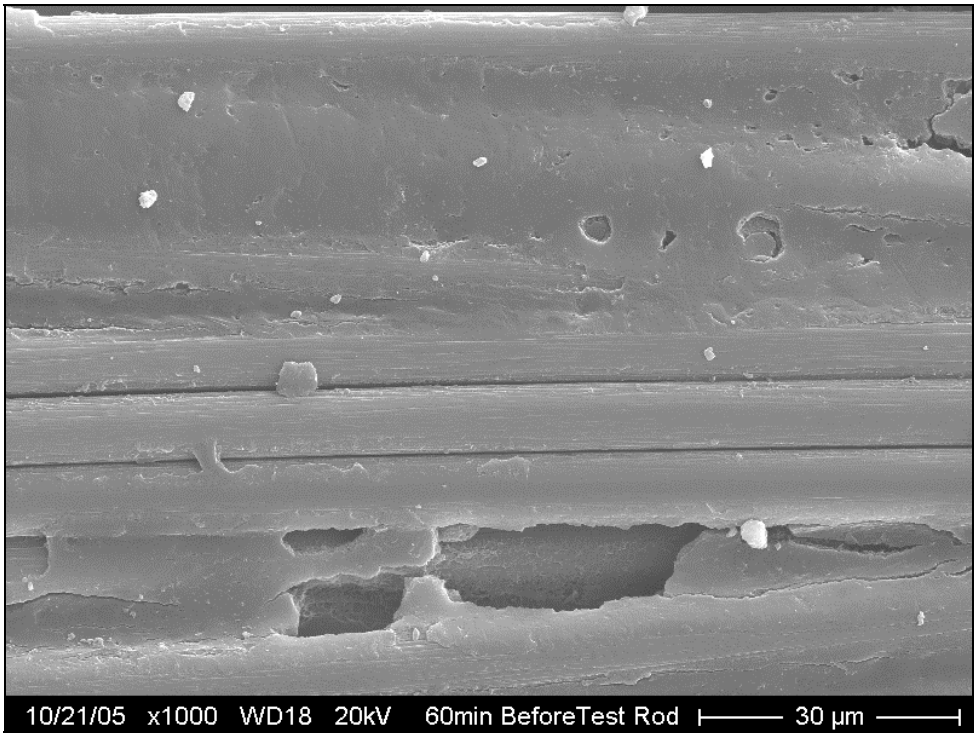

Figure G-14: Magnified view of rod surface after washed 60 min HNO_3 surface treatment

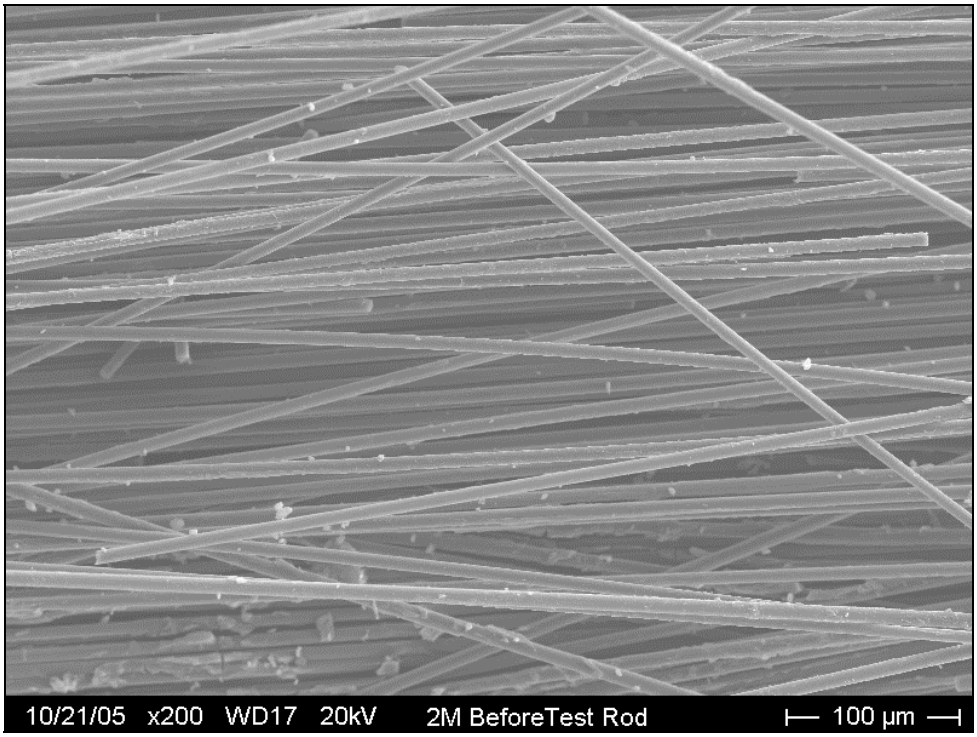

Figure G-15: Pre-interface tested rod surface after washed 60 min HNO_3 / 2M NaOH surface treatment

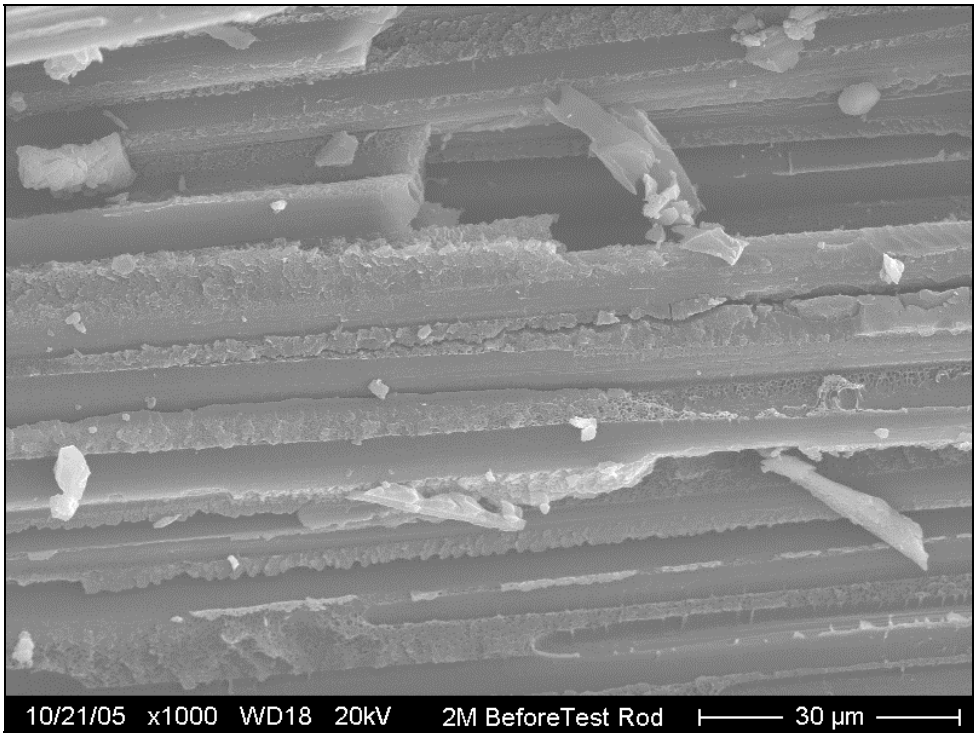

Figure G-16: Magnified view of rod surface after washed 60 min HNO_3 / 2M NaOH surface treatment

APPENDIX H

Post-interface Test SEM Surface Images

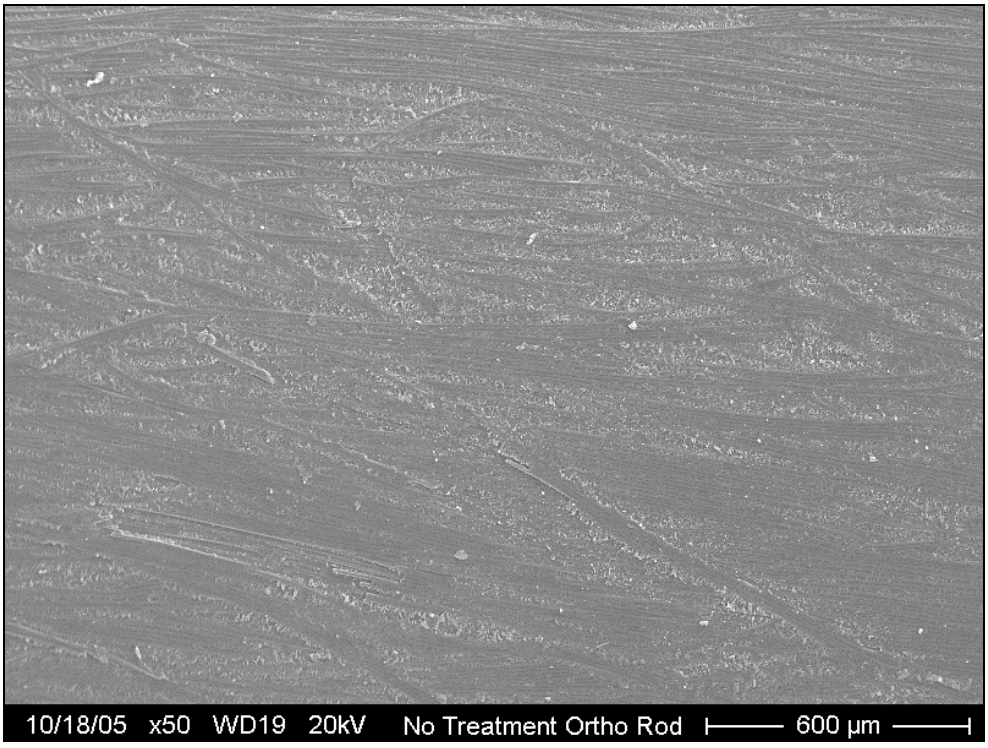

Figure H-1: Post-tested untreated rod with ortho spacing

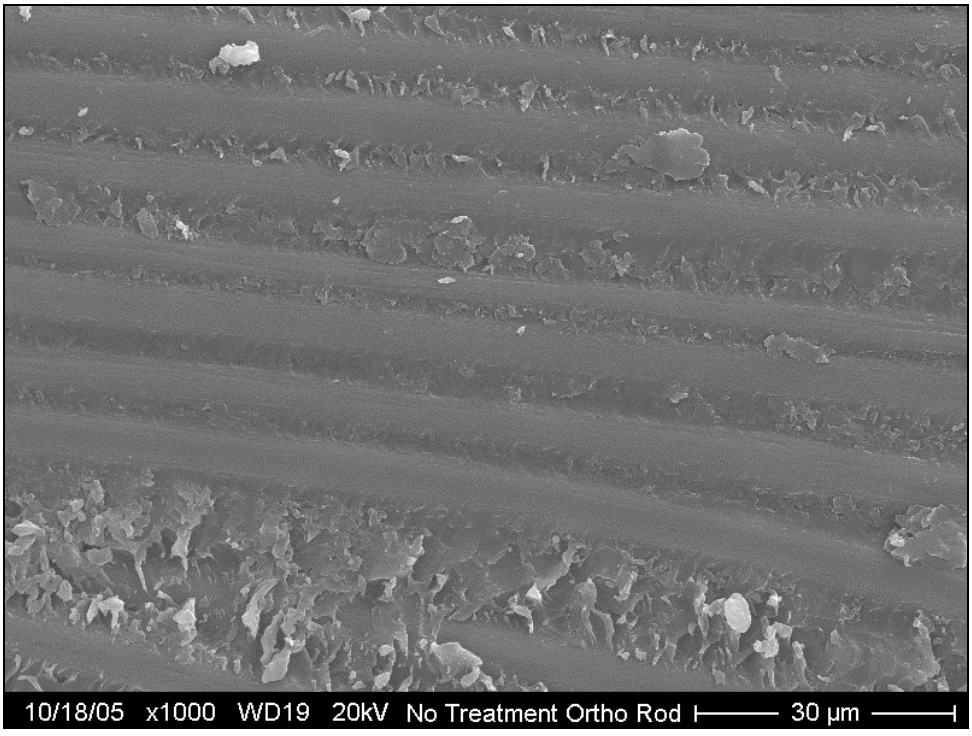

Figure H-2: Magnified view of post-tested untreated rod with ortho spacing

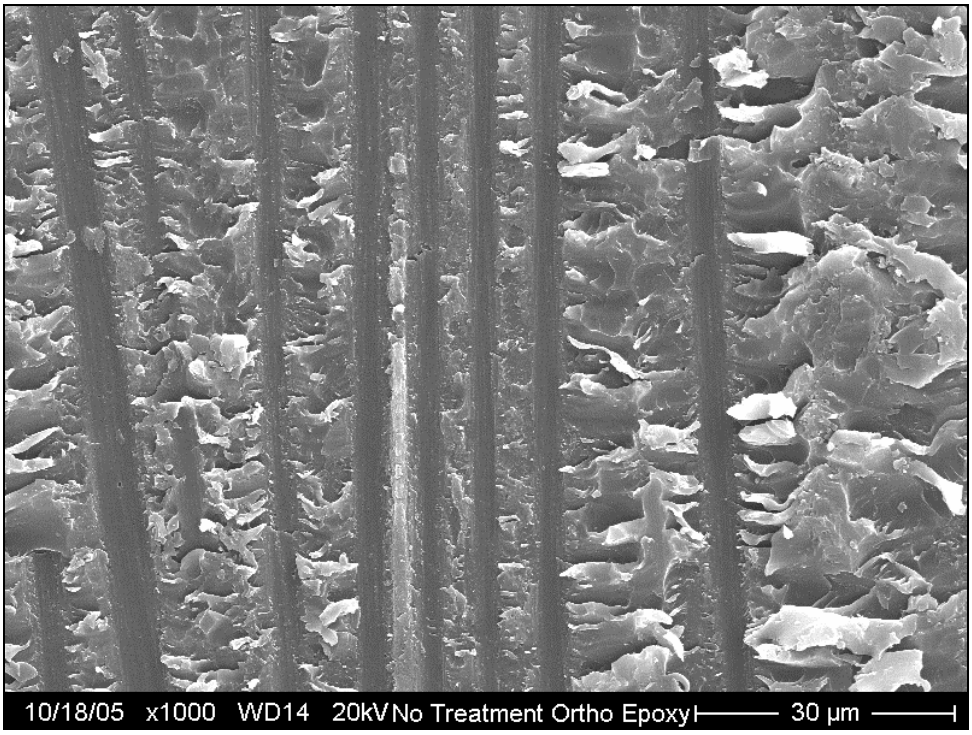

Figure H-3: Post-tested secondary epoxy interface surface of untreated rod with ortho spacing

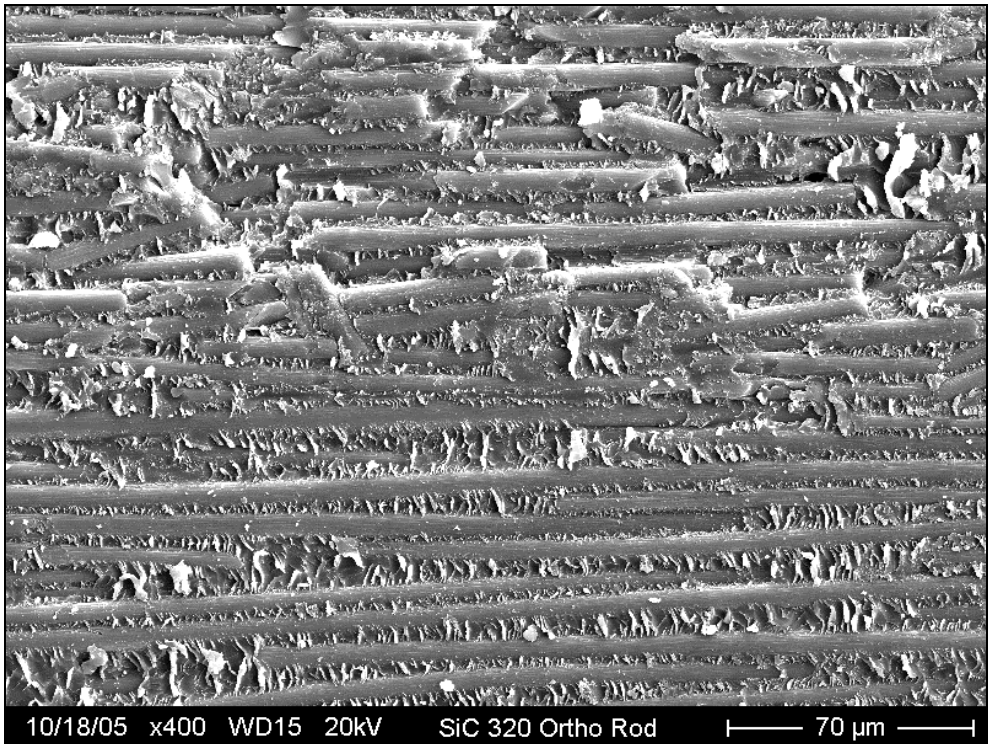

Figure H-4: Post-tested SiC 320 treated rod surface with ortho spacing

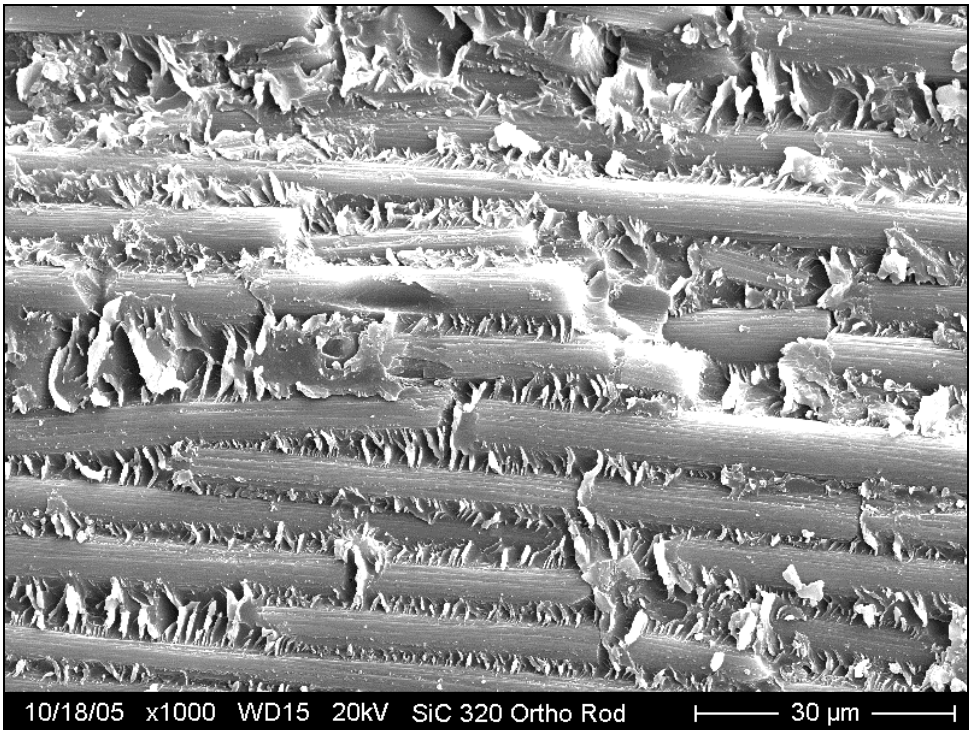

Figure H-5: Magnified view of post-tested SiC 320 treated rod surface with ortho spacing

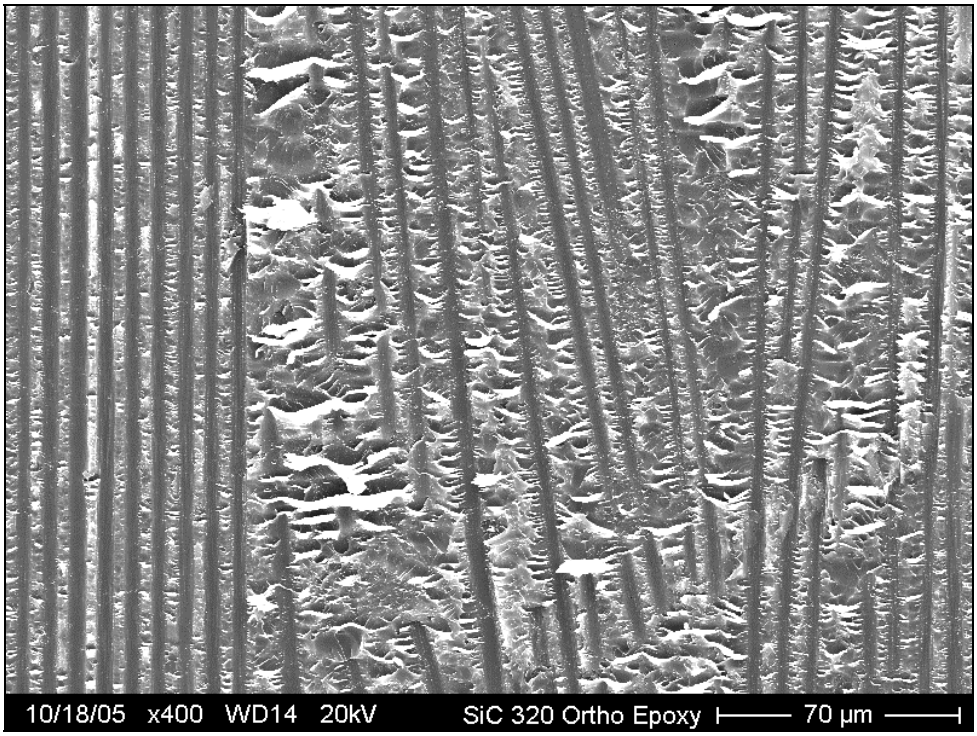

Figure H-6: Post-tested secondary epoxy interface surface of a SiC treated rod with ortho spacing

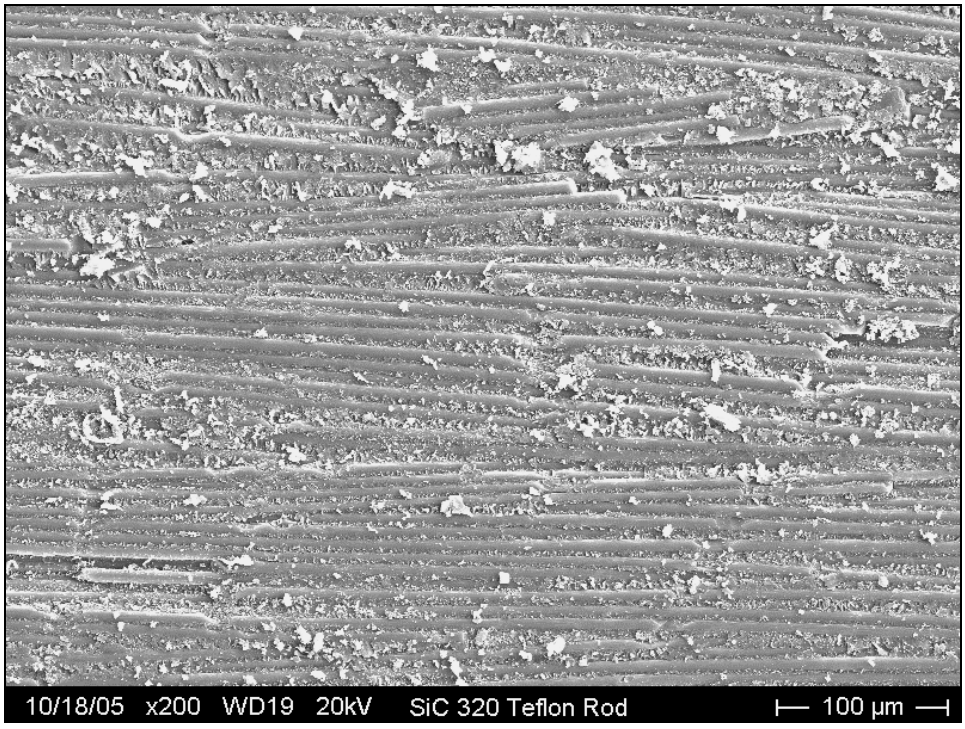

Figure H-7: Post-tested SiC 320 treated rod surface with Teflon spacing

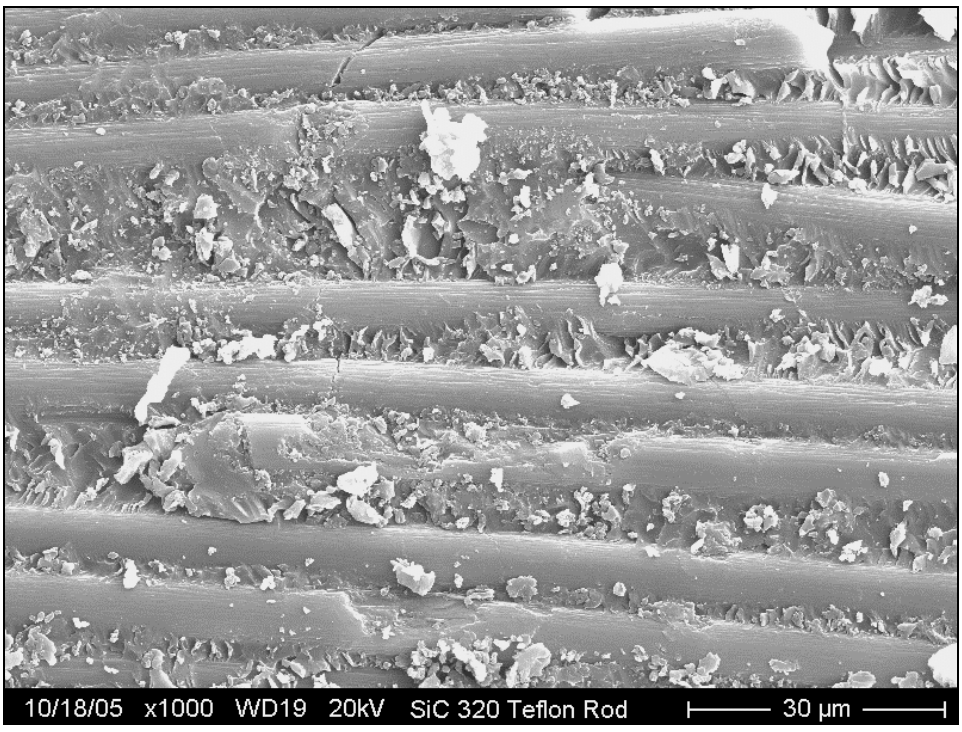

Figure H-8: Magnified view of a post-tested SiC 320 treated rod surface with Teflon spacing

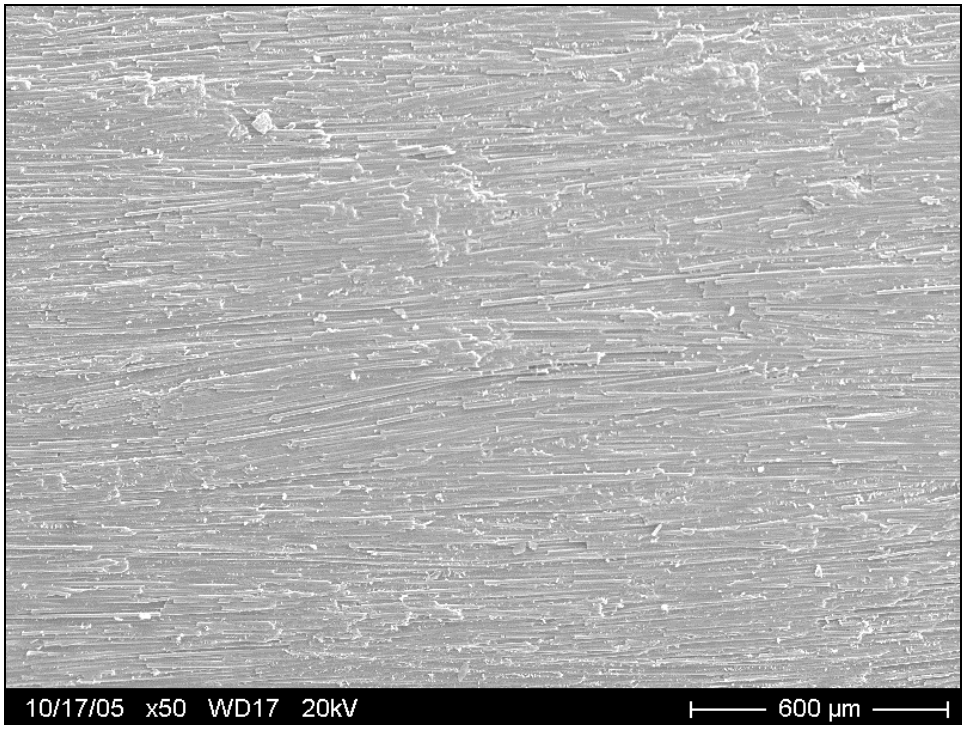

Figure H-9: Post-tested (2, 2) erosion treated rod surface

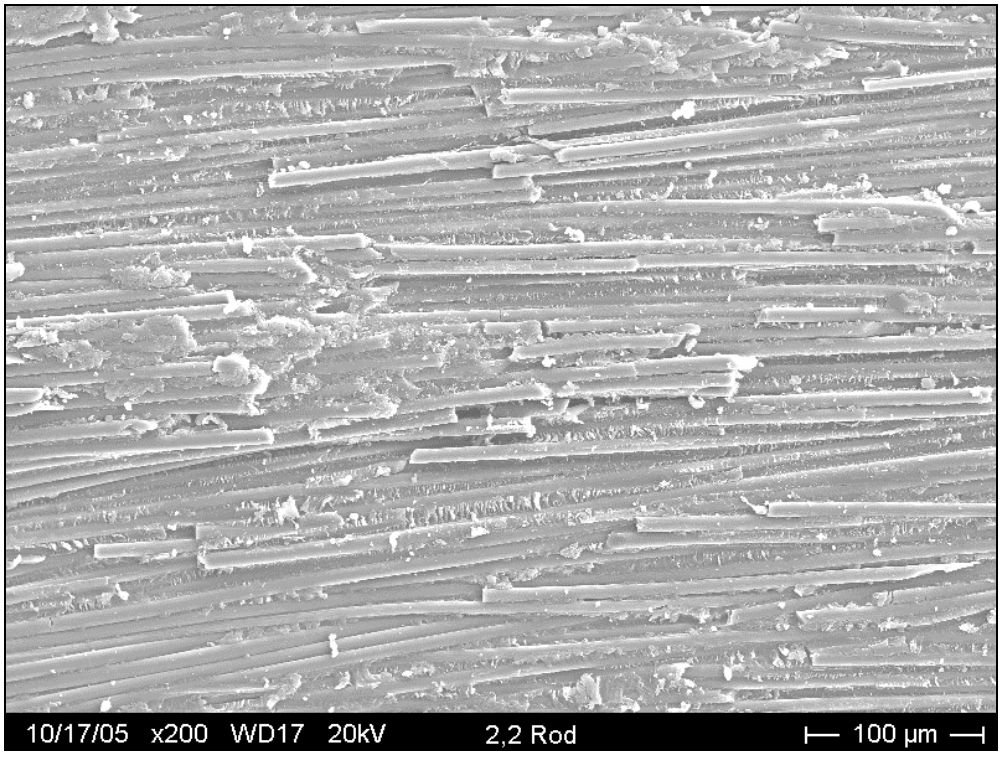

Figure H-10: Magnified view of (2, 2) erosion treated rod surface

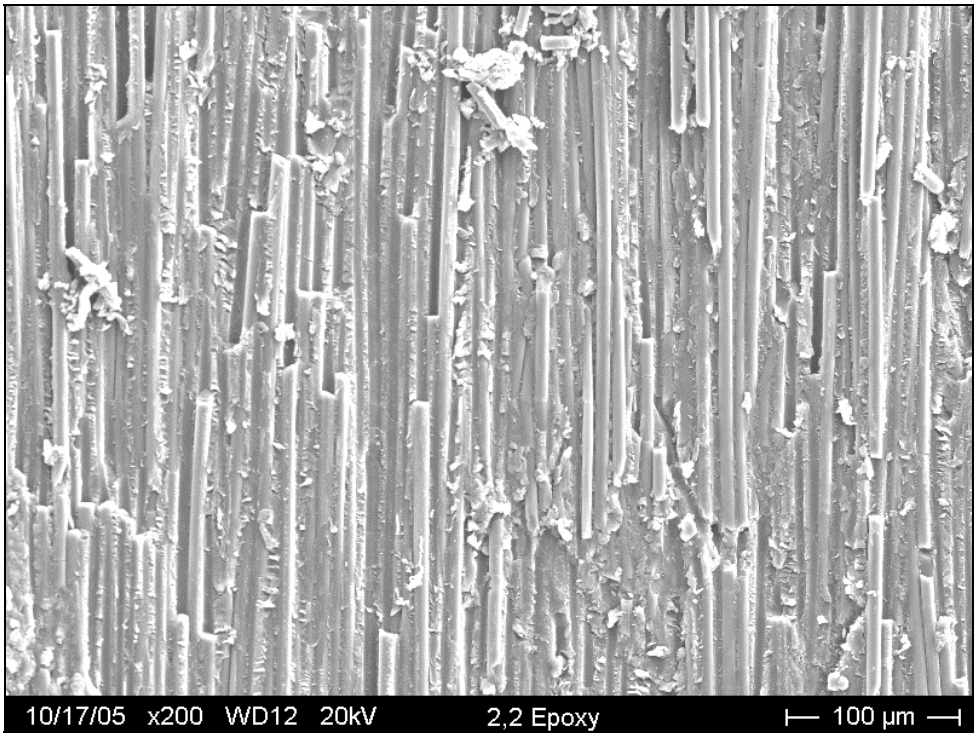

Figure H-11: Post-tested secondary epoxy interface surface from (2, 2) erosion treated rod

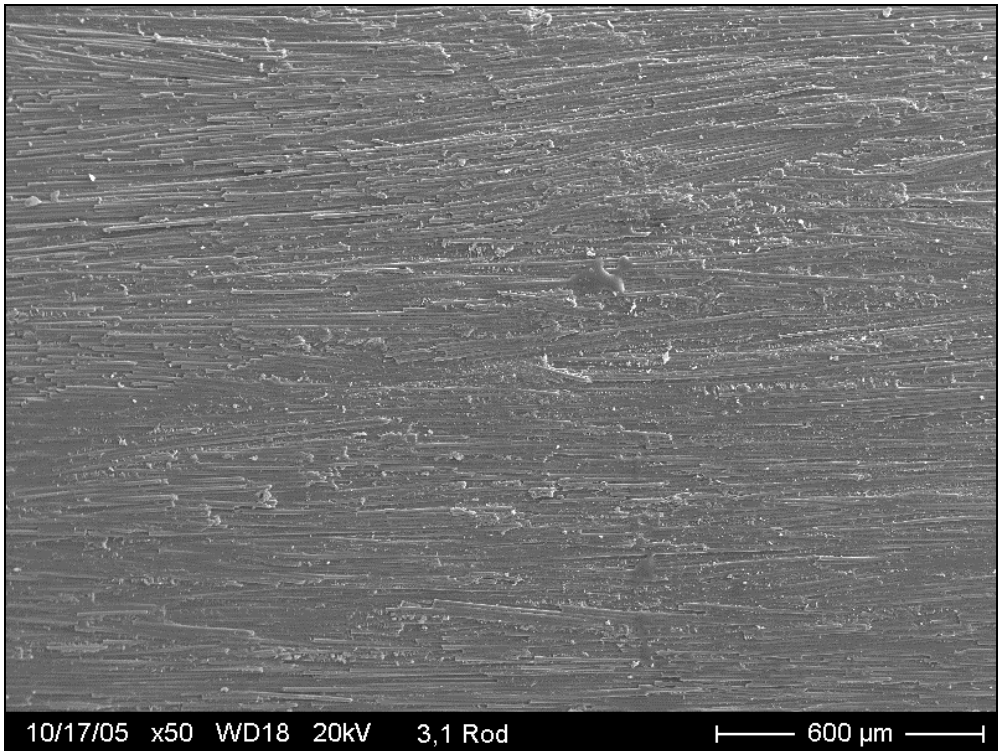

Figure H-12: Post-tested (3, 1) erosion treated rod surface

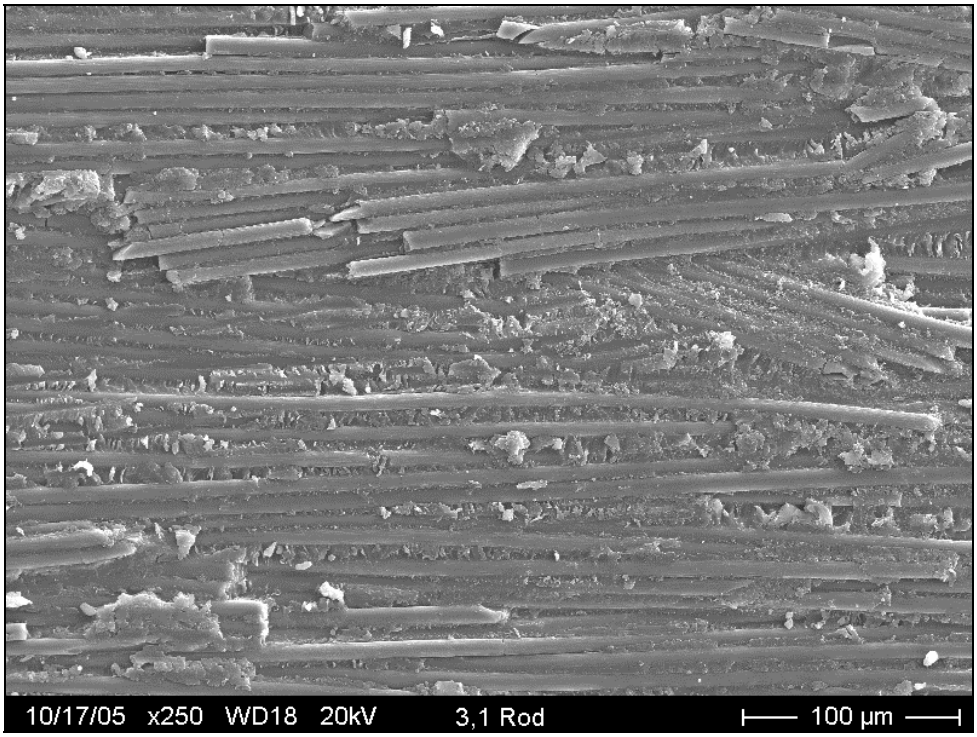

Figure H-13: Magnified view of (3, 1) erosion treated rod surface

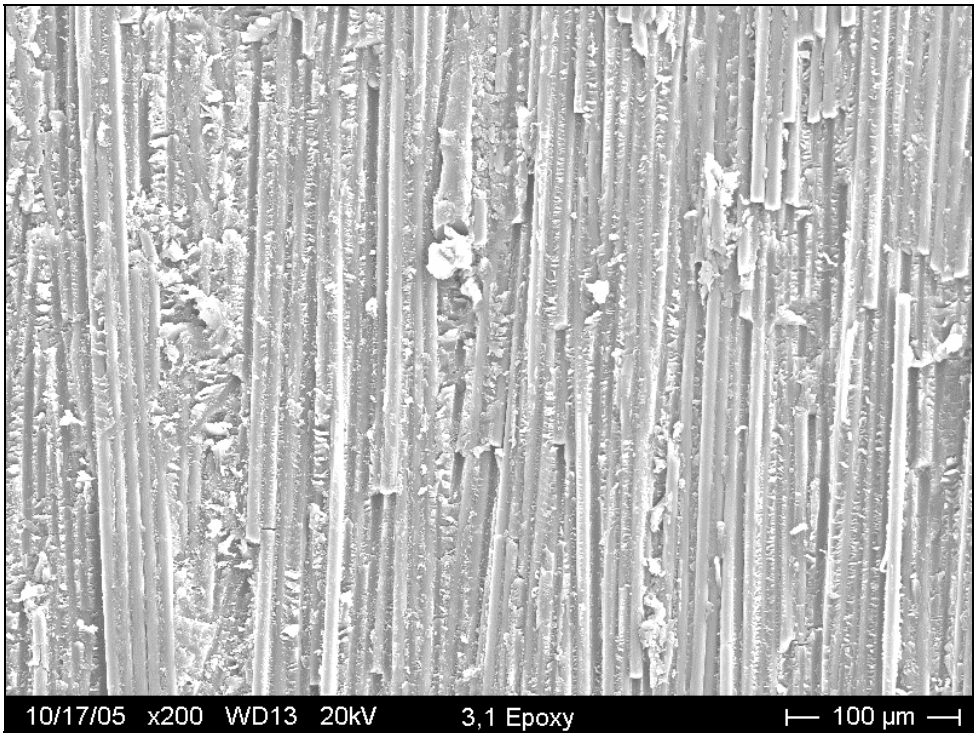

Figure H-15: Post-tested secondary epoxy interface surface from (3, 1) erosion treated rod

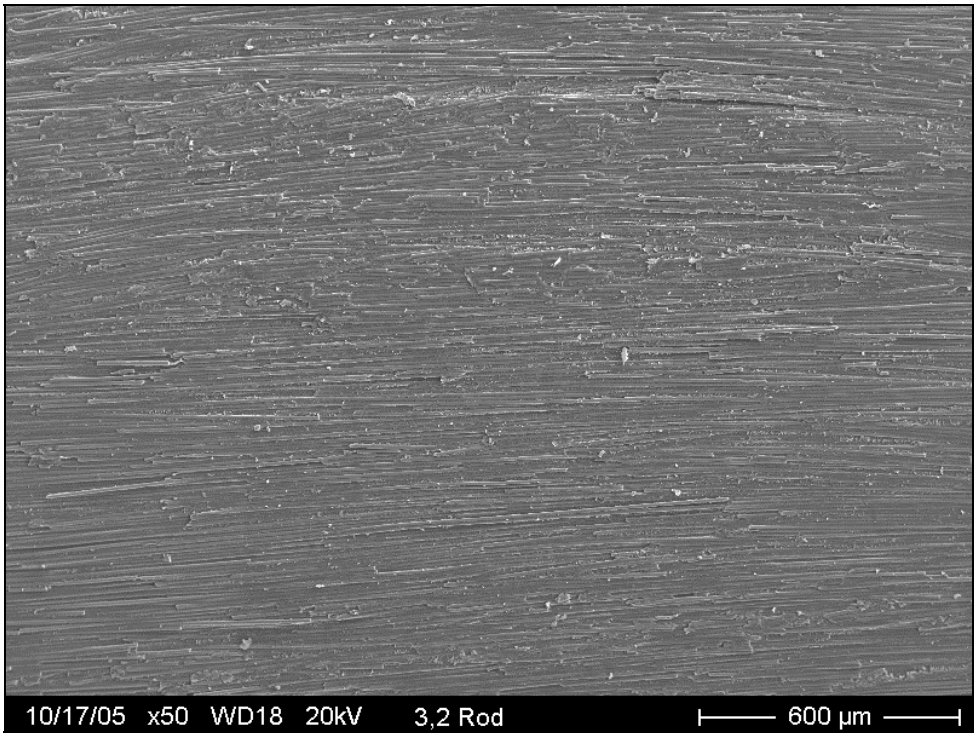

Figure H-16: Post-tested (3, 2) erosion treated rod surface

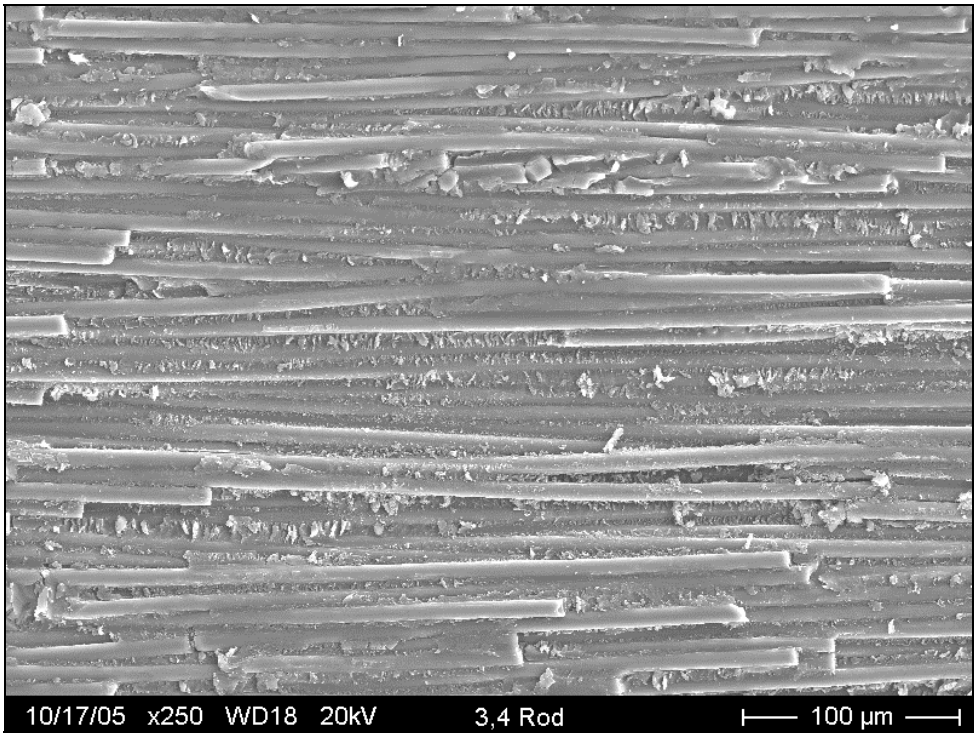

Figure H-17: Post-tested (3, 4) erosion treated rod surface

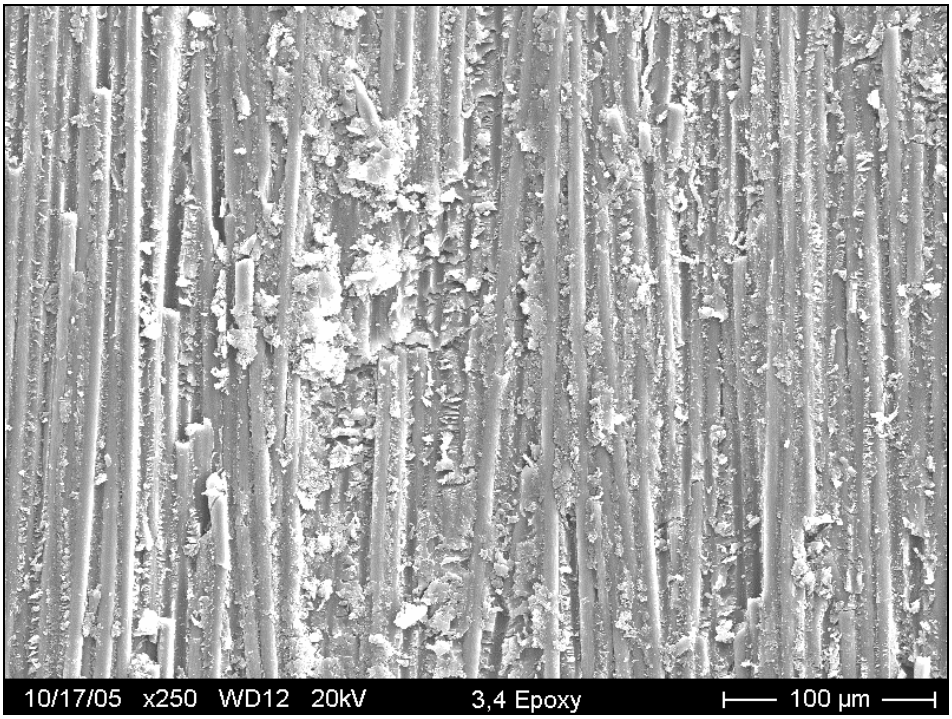

Figure H-19: Post-tested secondary epoxy interface surface from (3, 4) erosion treated rod

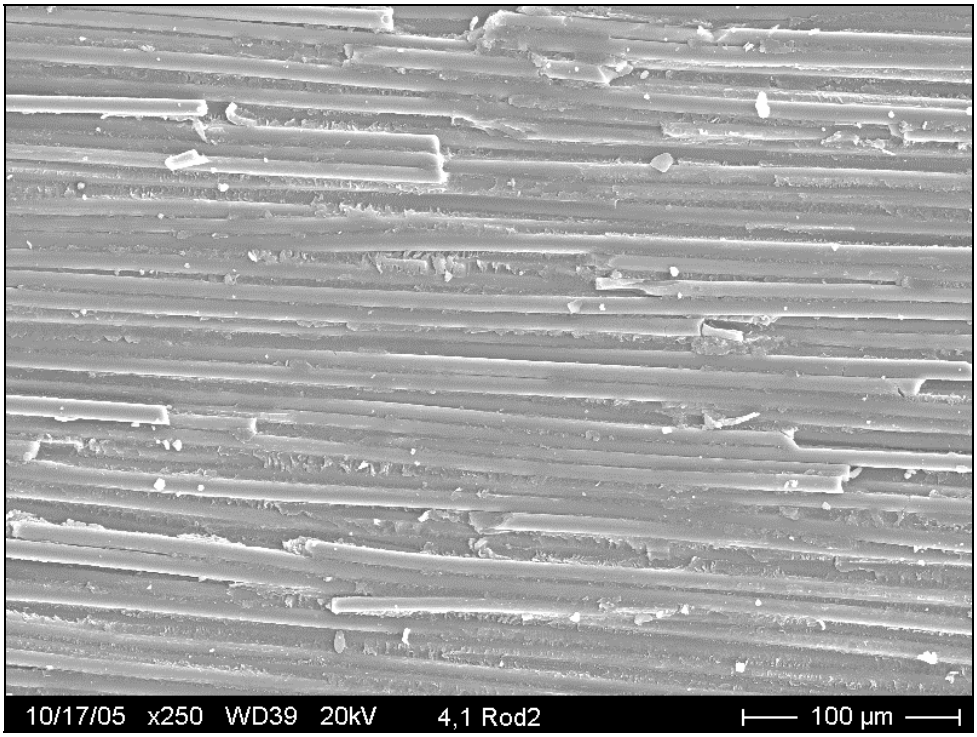

Figure H-20: Post-tested (4, 1) erosion treated rod surface

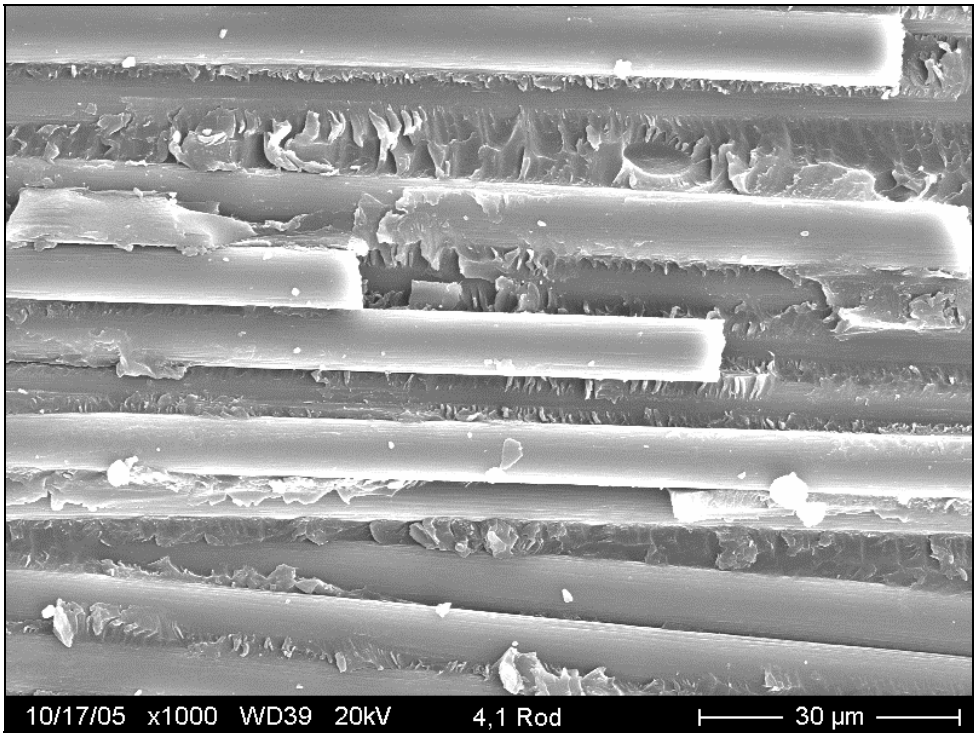

Figure H-21: Magnified view of post-tested (4, 1) erosion treated rod surface

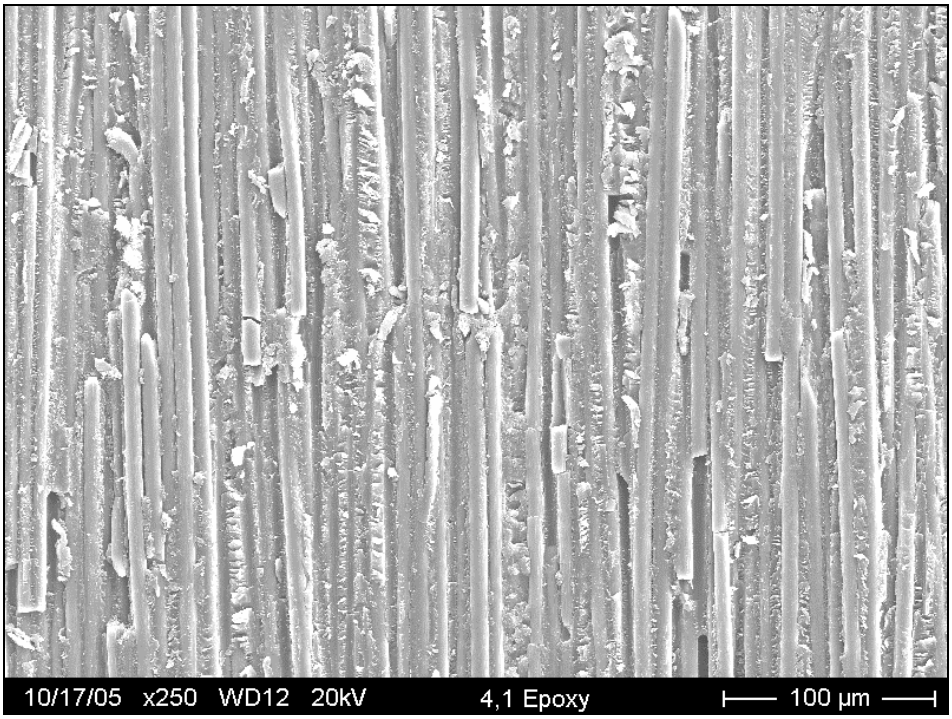

Figure H-22: Post-tested secondary epoxy interface surface from (4, 1) erosion treated rod

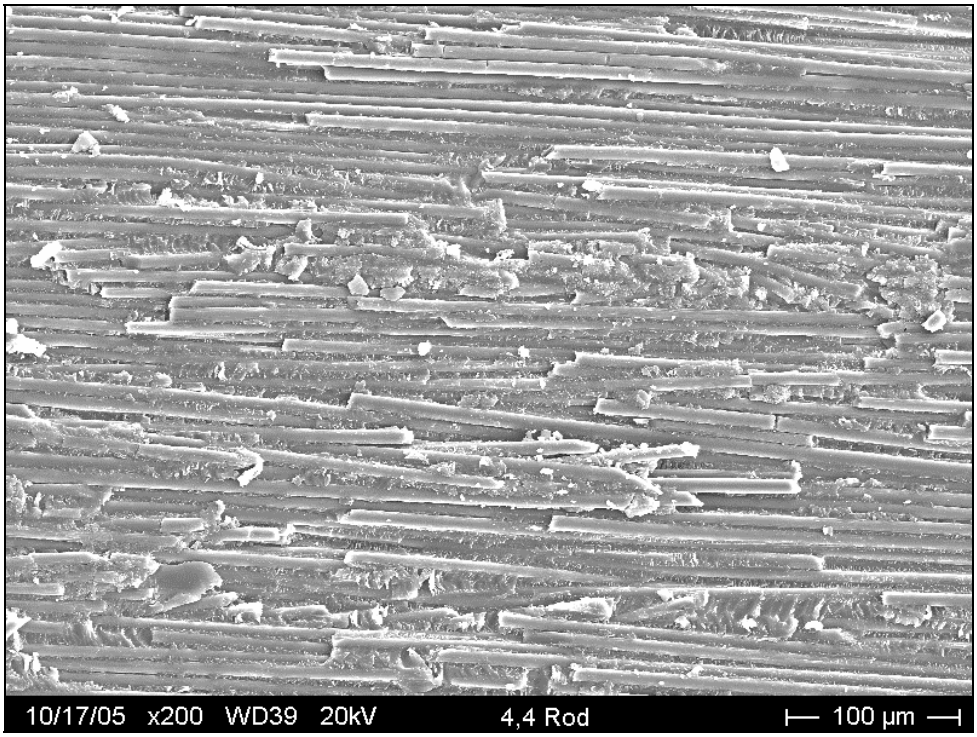

Figure H-23: Post-tested (4, 4) erosion treated rod surface

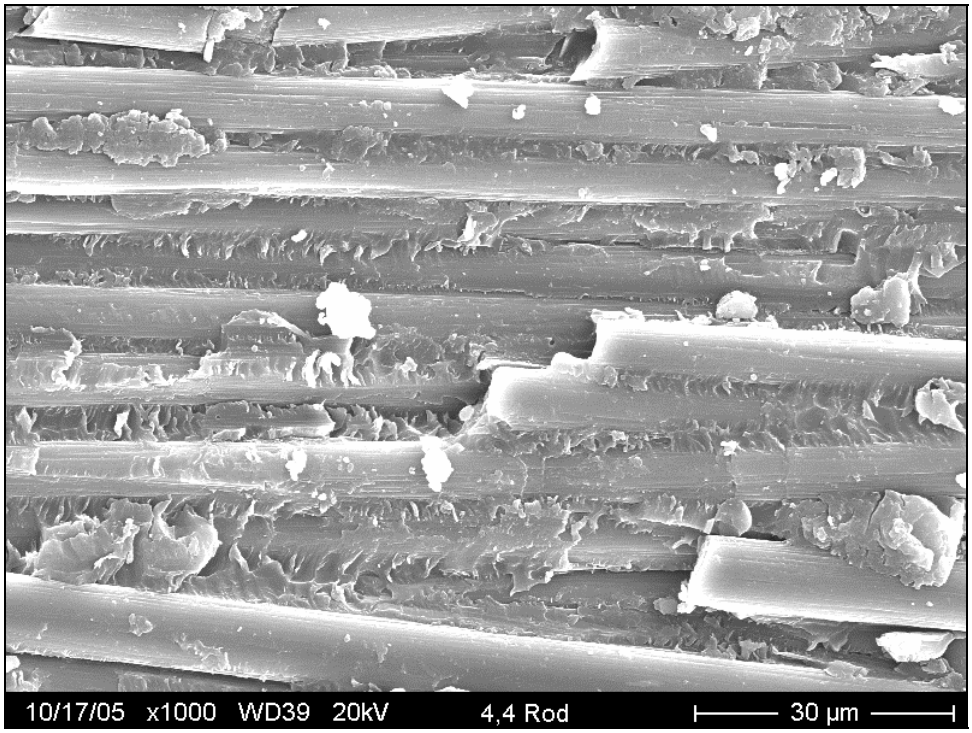

Figure H-24: Magnified view of post-tested (4, 4) erosion treated rod surface

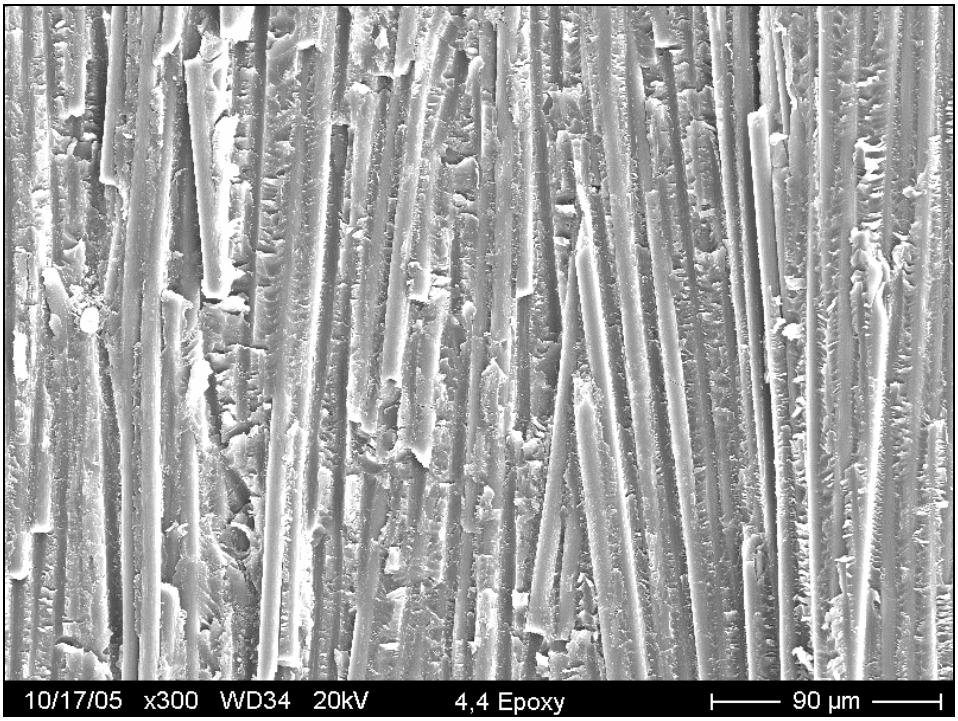

Figure H-25: Post-tested secondary epoxy interface surface from (4, 4) erosion treated rod

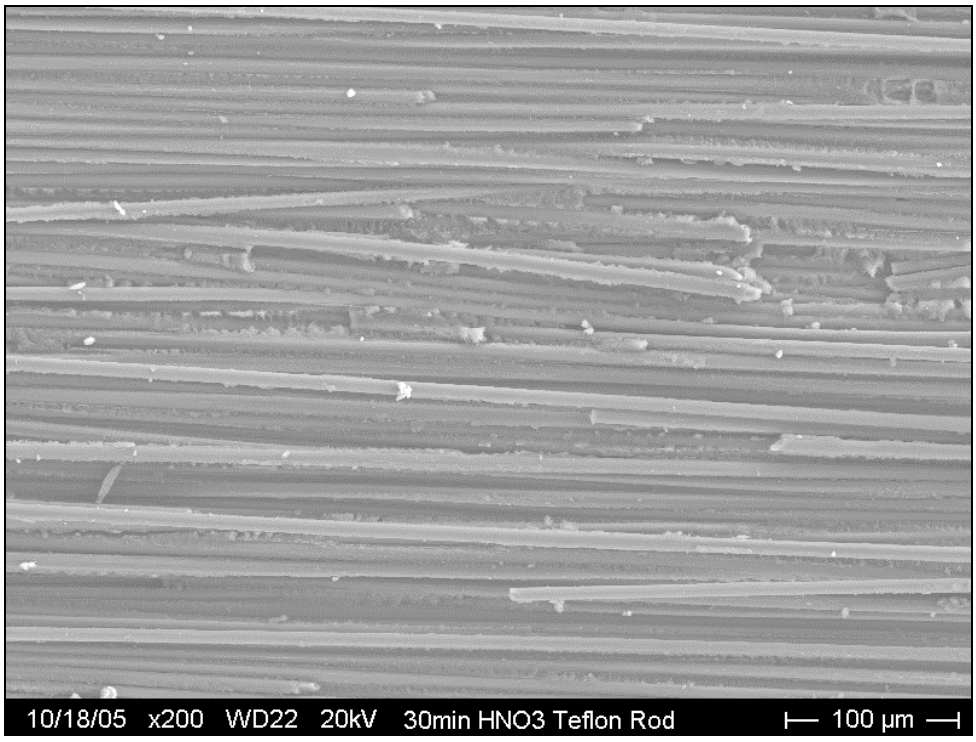

Figure H-26: Post-tested 30 min HNO3 treated rod surface

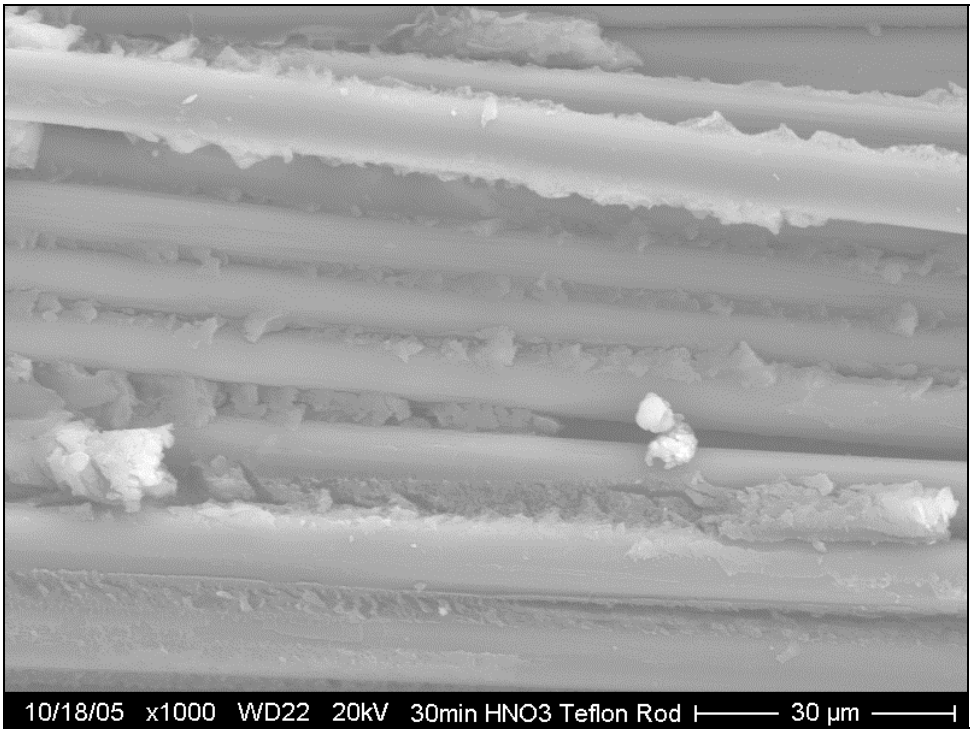

Figure H-27: Magnified view of post-tested 30 min HNO3 treated rod surface

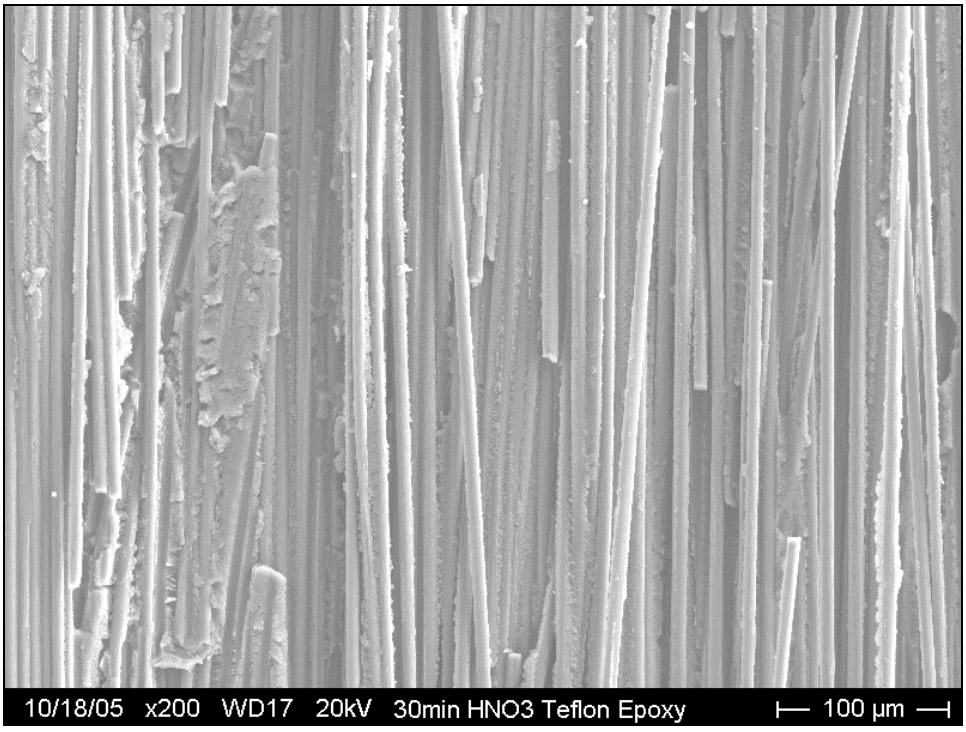

Figure H-28: Magnified view of post-tested secondary epoxy interface surface from 30 min HNO_3 treated rod

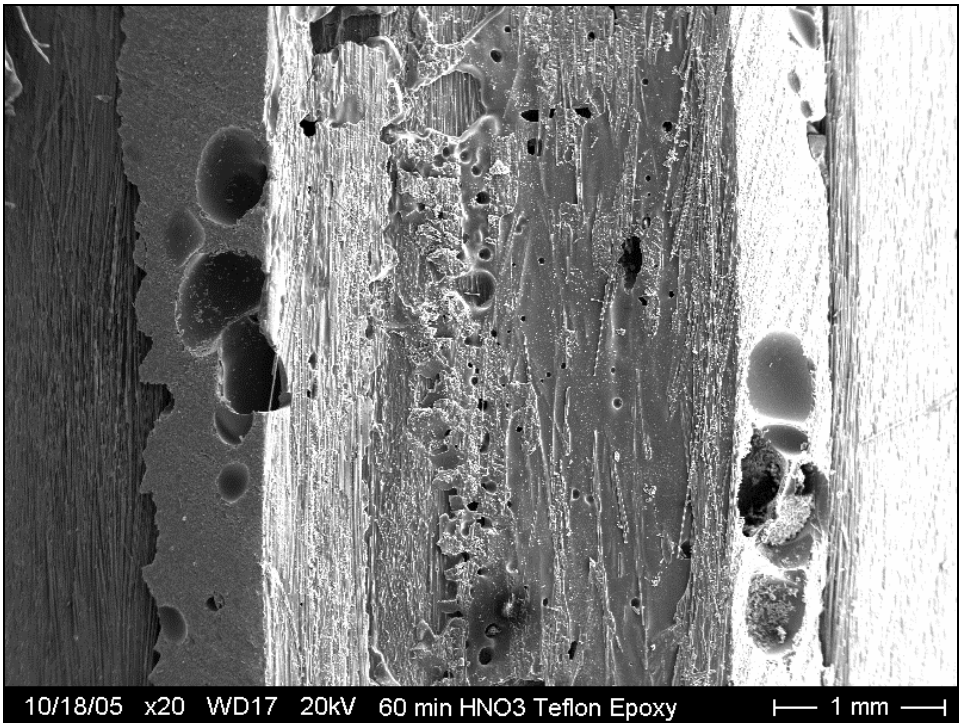

Figure H-29: Post-tested secondary epoxy interface surface from unwashed 60 min HNO_3 treated rod with Teflon spacing

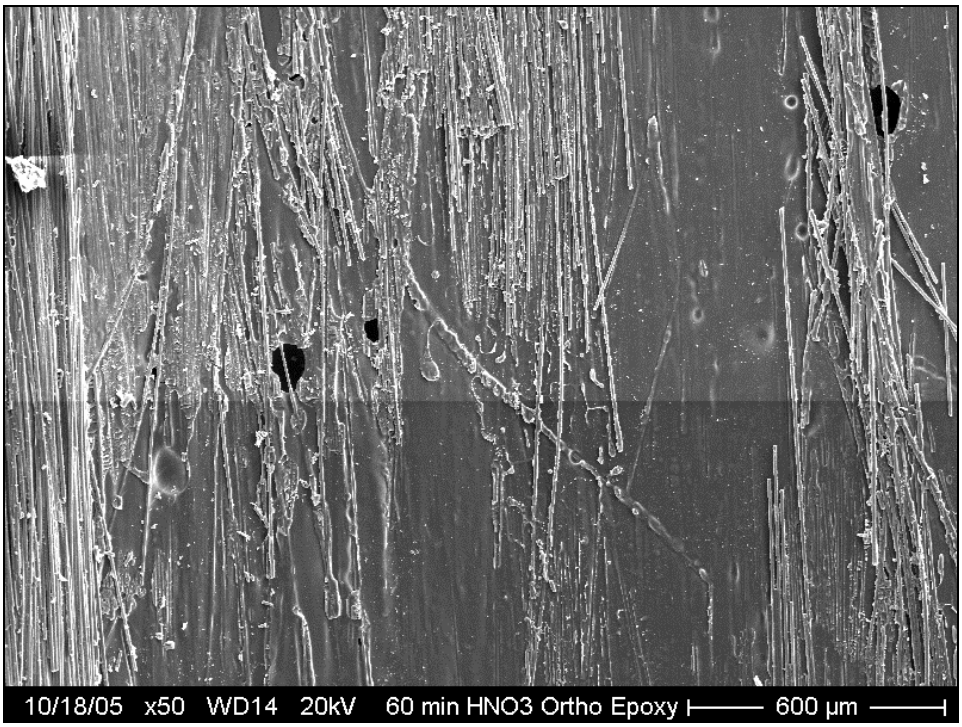

Figure H-30**:** Post-tested secondary epoxy interface surface from unwashed 60 min HNO_3 treated rod with ortho spacing

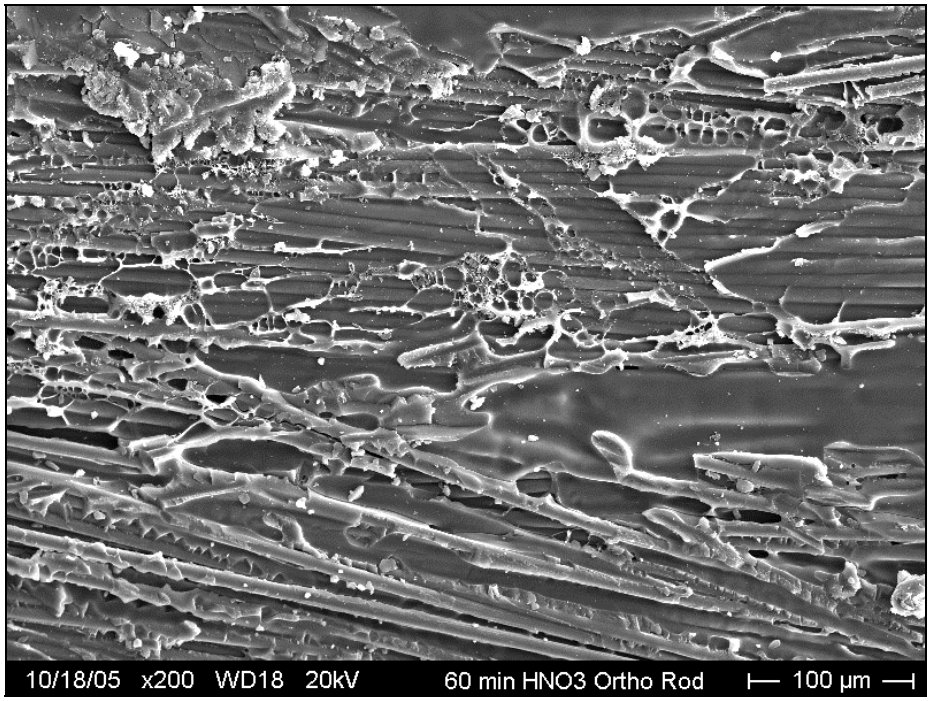

Figure H-31: Post-tested unwashed 60 min HNO_3 treated rod surface with ortho spacing

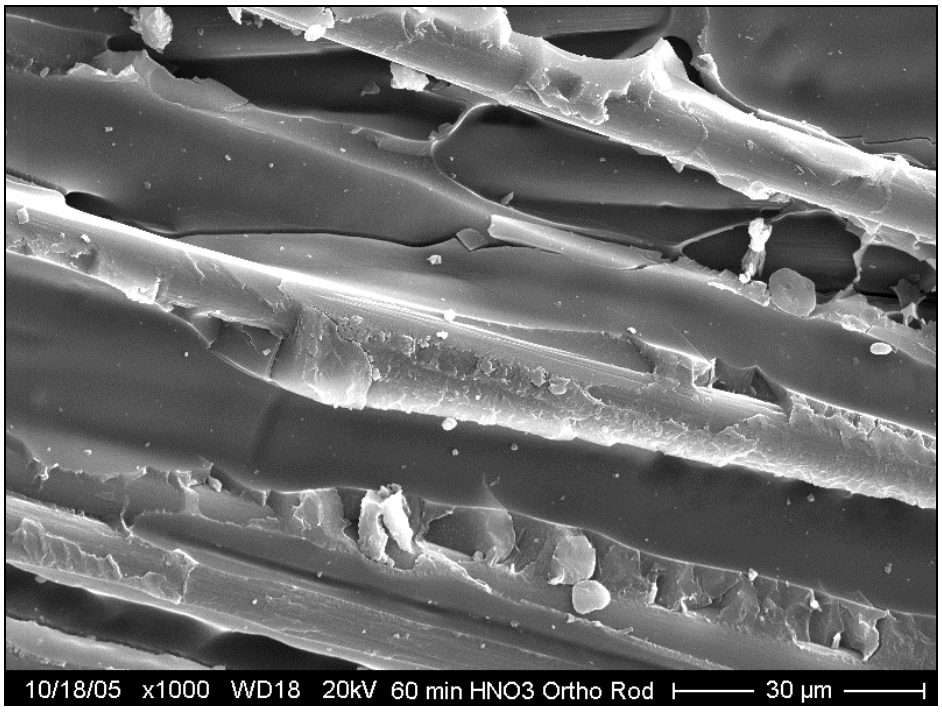

Figure H-32: Magnified view of post-tested 60 min unwashed rod surface with ortho spacing

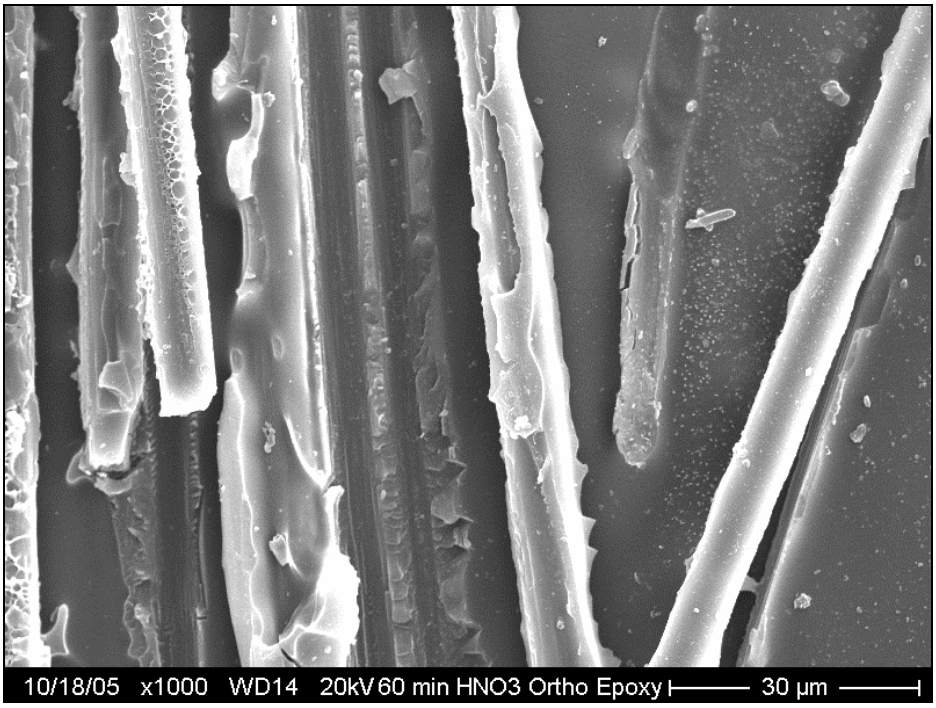

Figure H-33: Magnified view of post-tested secondary epoxy interface surface from unwashed 60 min HNO_3 treated rod with ortho spacing

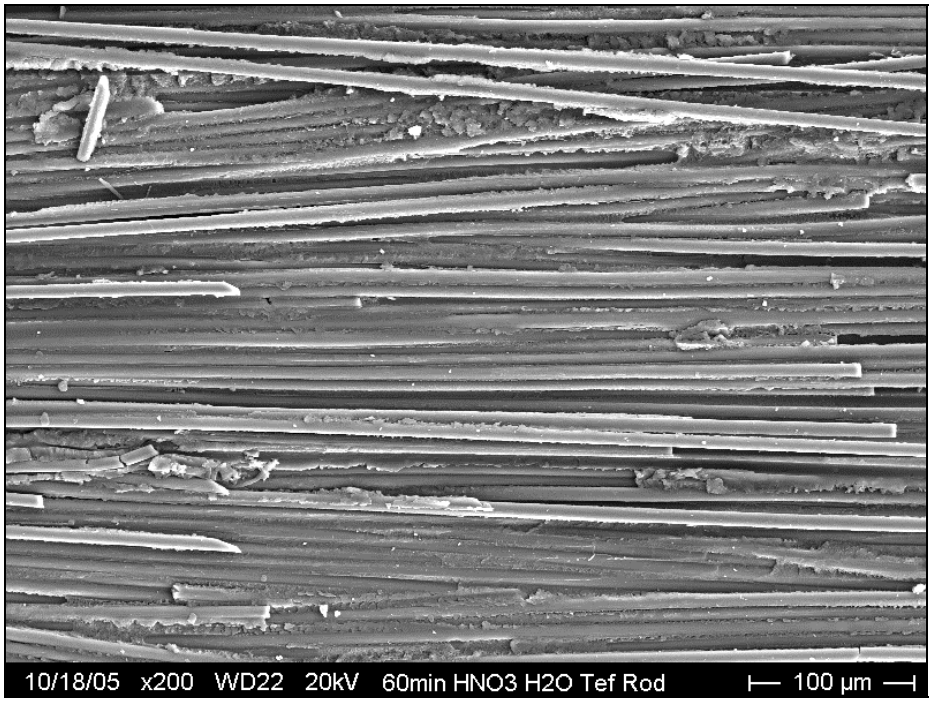

Figure H-34: Magnified view of post-tested secondary epoxy interface surface from washed 60 min HNO_3 treated rod with Teflon spacing

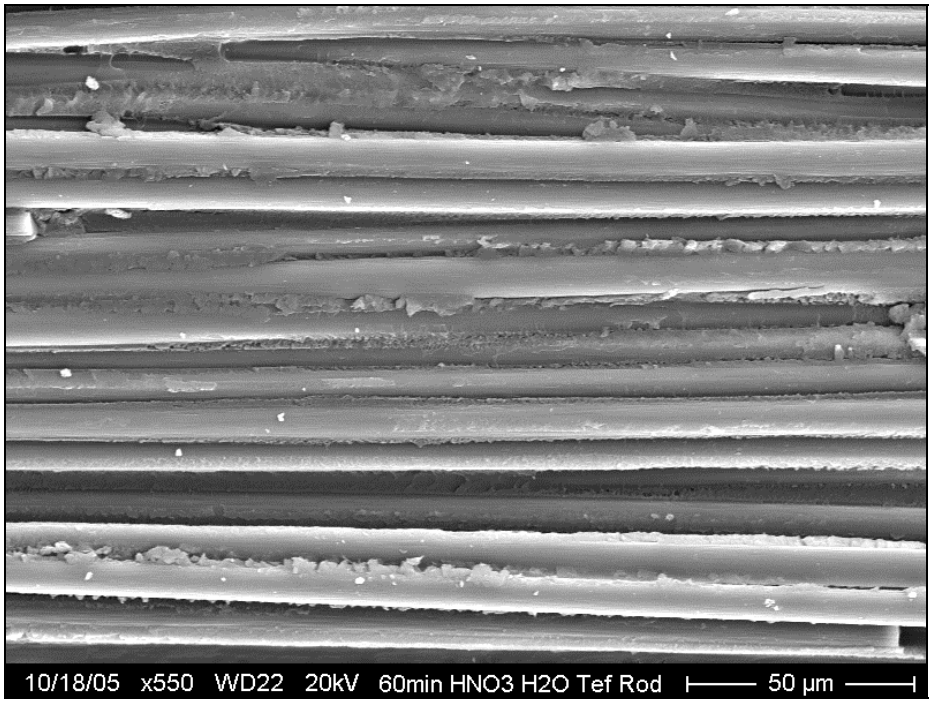

Figure H-35:Magnified view of post-tested washed 60 min rod surface

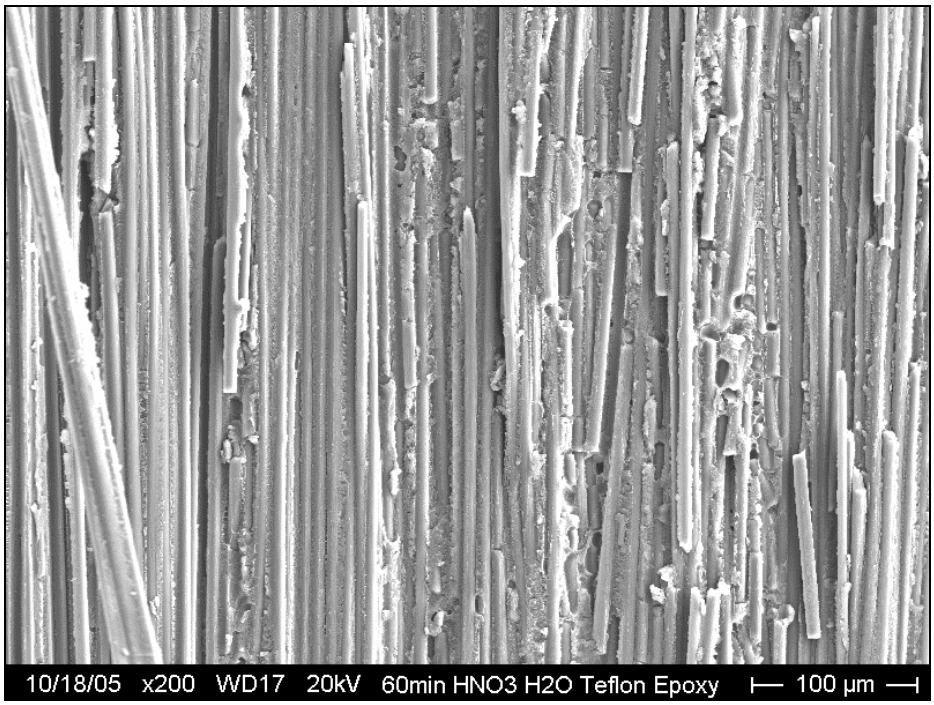

Figure H-36: Magnified view of post-tested secondary epoxy interface surface from washed 60 min HNO_3 treated rod with Teflon spacing

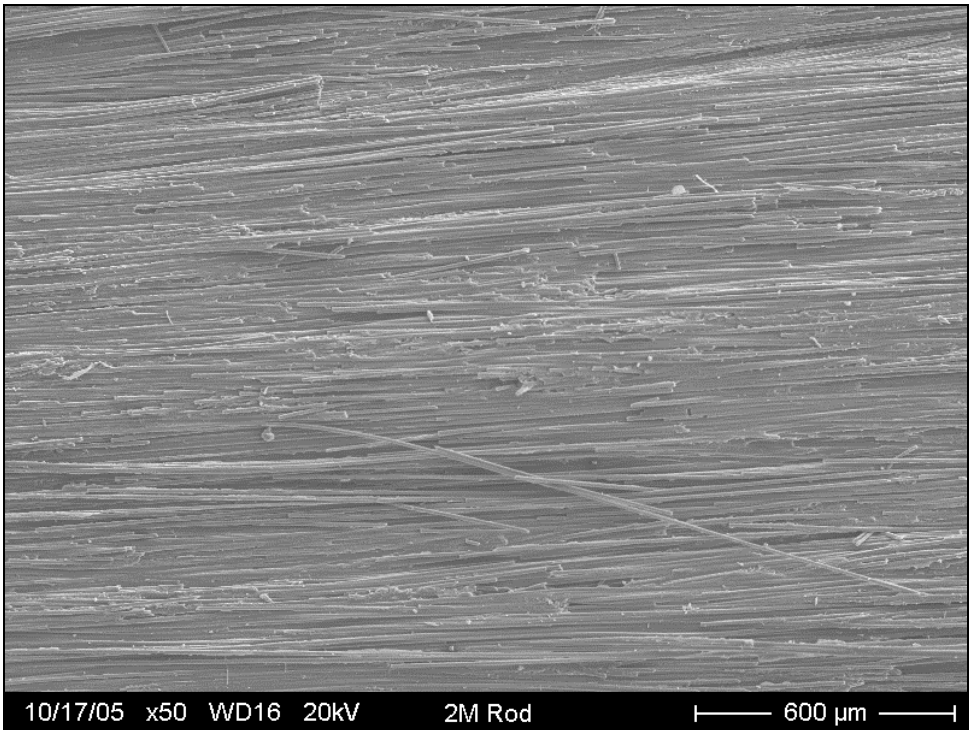

Figure H-37: Post-tested 60 min HNO_3 / 2M NaOH rod surface

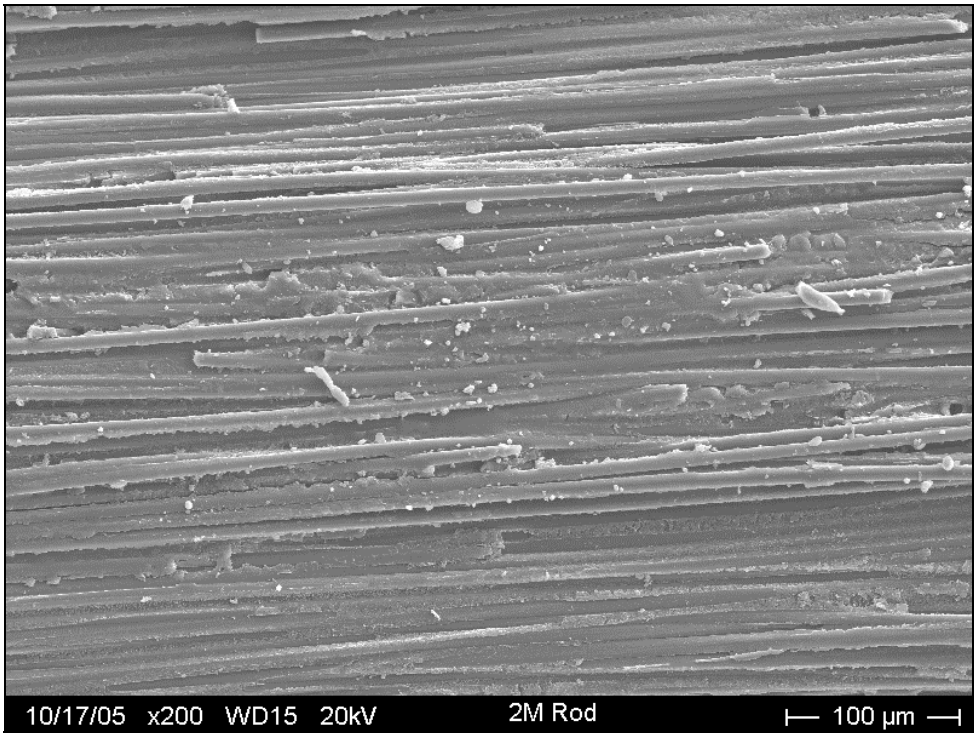

Figure H-38: Magnified view of post-tested 60 min HNO_3 / 2M NaOH rod surface

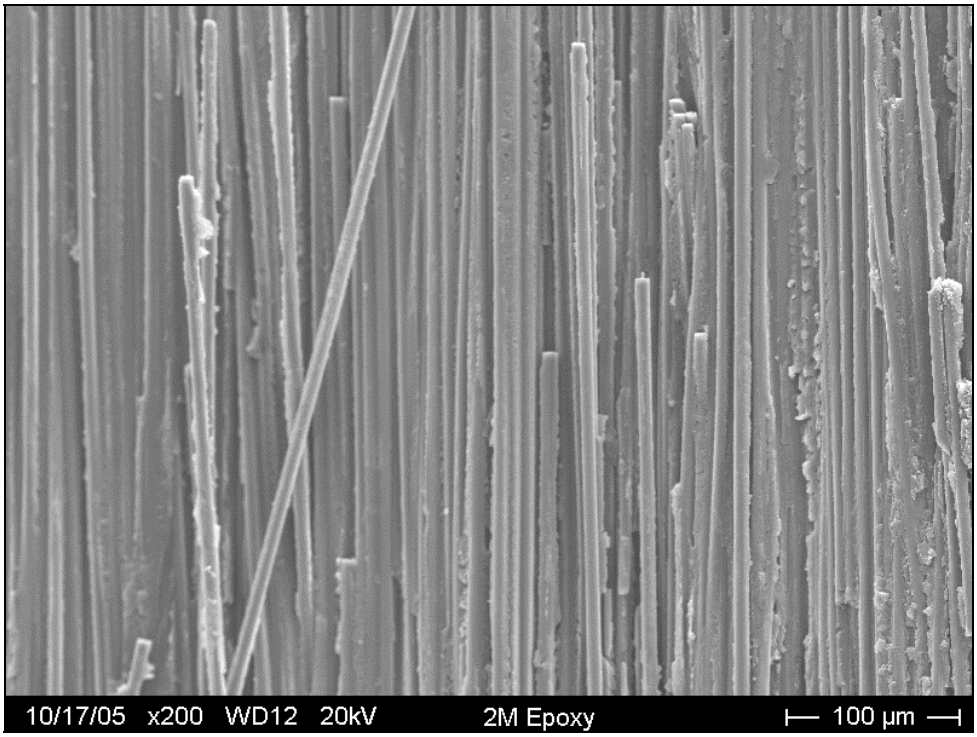

Figure H-39: Magnified view of post-tested secondary epoxy interface surface from washed 60 min HNO_3 / 2M NaOH treated rod